NAVAL POSTGRADUATE SCHOOL
Monterey, California

THESIS

MODAL ANALYSIS AND ACTIVE VIBRATION CONTROL OF THE NAVAL POSTGRADUATE SCHOOL SPACE TRUSS

by

Scott E. Johnson
John Vlattas

June 1998

Thesis Advisor: Brij N. Agrawal
Co-Advisor: Gangbing Song

Approved for public release; distribution is unlimited

REPORT DOCUMENTATION PAGE

Form Approved
OMB No. 0704-0188

1. AGENCY USE ONLY *(Leave blank)*	2. REPORT DATE	3. REPORT TYPE AND DATES COVERED
	June 1998	Master's Thesis

4. TITLE AND SUBTITLE
MODAL ANALYSIS AND ACTIVE VIBRATION CONTROL OF THE NPS SPACE TRUSS

5. FUNDING NUMBERS

6. AUTHOR(S)
Johnson, Scott E., and Vlattas, John

7. PERFORMING ORGANIZATION NAME(S) AND ADDRESS(ES)
Naval Postgraduate School
Monterey, CA 93943-5000

8. PERFORMING ORGANIZATION REPORT NUMBER

9. SPONSORING / MONITORING AGENCY NAME(S) AND ADDRESS(ES)

10. SPONSORING / MONITORING AGENCY REPORT NUMBER

11. SUPPLEMENTARY NOTES
The views expressed in this thesis are those of the author and do not reflect the official policy or position of the Department of Defense or the U.S. Government.

12a. DISTRIBUTION / AVAILABILITY STATEMENT
Approved for public release; distribution is unlimited.

12b. DISTRIBUTION CODE

13. ABSTRACT *(maximum 200 words)*

This thesis examines active control of the Naval Postgraduate School (NPS) Space Truss using a piezoceramic stack actuator. Preceding the development of an active control mechanism for the NPS space truss, modal testing was performed to identify the modal properties of the truss. An impact hammer provided excitation to the truss and accelerometers measured the truss' response. Two data acquisition systems were used independently to gather and analyze data. For active control, an active strut, consisting of a piezoceramic stack, a force transducer, and mechanical interfaces, was substituted in place of a critical diagonal strut and acted as a control actuator. The frequency response of the system was determined and a integral plus double-integral force feedback control law was designed and implemented. A linear proof mass actuator was employed to excite one of the truss' vibrational modes. The controller then suppressed the vibration along the length of the structure resulting in power attenuation on the order of 10 – 15 dB. Various combinations of velocity and position feedback gains were investigated in order to optimize the control action. Additional testing was performed to determine the controller's sensitivity over a frequency band.

14. SUBJECT TERMS	15. NUMBER OF PAGES
Active Vibration Control, Piezoceramic Actuators, Modal Testing, Modal Analysis	249
	16. PRICE CODE

17. SECURITY CLASSIFICATION OF REPORT	18. SECURITY CLASSIFICATION OF THIS PAGE	19. SECURITY CLASSIFI- CATION OF ABSTRACT	20. LIMITATION OF ABSTRACT
Unclassified	Unclassified	Unclassified	UL

NSN 7540-01-280-5500

Standard Form 298 (Rev. 2-89)
Prescribed by ANSI Std. 239-18

Approved for public release; distribution is unlimited

MODAL ANALYSIS AND ACTIVE VIBRATION CONTROL OF THE NAVAL POSTGRADUATE SCHOOL SPACE TRUSS

Scott E. Johnson
Lieutenant, United States Navy
B.S., Texas A&M University, 1991

John Vlattas
Lieutenant, United States Navy
B.S.M.E, University of Pennsylvania, 1991

Submitted in partial fulfillment of the
requirements for the degree of

MASTER OF SCIENCE IN ASTRONAUTICAL ENGINEERING

from the

NAVAL POSTGRADUATE SCHOOL
June 1998

Author: Scott

Scott E. Johnson

John Vlattas

Approved by: B. N. Agrawal

Brij N. Agrawal, Thesis Advisor

G. Song

Gangbing Song, Co-Advisor

G. Lindsey

G. Lindsey, Chairman
Department of Aeronautical/Astronautical Engineering

ABSTRACT

This thesis examines active control of the Naval Postgraduate School (NPS) Space Truss using a piezoceramic stack actuator. Preceding the development of an active control mechanism for the NPS space truss, modal testing was performed to identify the modal properties of the truss. An impact hammer provided excitation to the truss and accelerometers measured the truss' response. Two data acquisition systems, dSPACE and an Hewlett Packard spectrum analyzer, were used independently to gather and analyze data. For active control, an active strut element, consisting of a piezoceramic stack, a force transducer, and mechanical interfaces, was substituted in place of a critical diagonal strut and acted as a control actuator. The frequency response of the system was determined and an integral plus double-integral force feedback control law was designed and implemented. A linear proof mass actuator was employed to excite one of the truss' vibrational modes. The controller then suppressed the vibration along the length of the structure resulting in power attenuation on the order of 10 – 15 dB. Various combinations of velocity and position feedback gains were investigated in order to optimize the control action. Additional testing was also performed to determine the controller's sensitivity over a frequency band.

TABLE OF CONTENTS

LIST OF FIGURES

LIST OF TABLES

LIST OF ABBREVIATIONS

AC	Analog Current
ADC	Analog to Digital Converter
AL	Aluminum
CEM	Controls-Structure Integration Evolutionary Model
CSI	Controls-Structures Integration
DAC	Digital to Analog Converter
DC	Direct Current
ERA	Eigensystem Realization Algorithm
FEM	Finite Element Model
FFT	Fast Fourier Transform
FRF	Frequency Response Function
HP	Hewlett Packard
HVPZ	High Voltage Translators
IFFT	Inverse Fast Fourier Transform
LPACT	Linear Proof Mass Actuator
LVPZ	Low Voltage Translators
MAC	Modal Assurance Criterion
MDOF	Multiple Degrees of Freedom
NPS	Naval Postgraduate School
NRL	Naval Research Laboratory
PI	Physik Instrumente
PSD	Power Spectral Density
PZT	Lead Zirconate Titanate
SDOF	Single Degree of Freedom
SRDC	Space Research Development Center
SSAG	Space Systems Academic Group
TFE	Transfer Function Estimate

ACKNOWLEDGEMENTS

The author would like to gratefully acknowledge several individuals whose assistance has made the completion of this thesis possible. First to Dr. Albert Bosse and Dr. Fred Tasker of the Naval Research Laboratory, a special thanks for taking the time and effort out of a very busy schedule to aid us in our research. Your assistance has been invaluable. Our deepest gratitude to Dr. Brij Agrawal and Dr. Gangbing Song for their guidance and encouragement and for the opportunity to pursue an exciting and challenging area of research. In this academic pursuit, you have been our mentors.

Finally, and most importantly, I would like to take a moment and recognize my fiancée, Nicole Flynn. Niki, you have endured countless hours of aggravation throughout this endeavor and yet you have found it in your heart to forgive me and reciprocate with unwavering support and love. In no small part, this is also your thesis. My love always.

I. INTRODUCTION

A. BACKGROUND

As one stands on the doorstep of the twenty-first century, the commercial utilization and demand for space-based assets continue to increase at a dramatic rate. Coincident with this rise has been an increase in the performance requirements of these satellite systems. The communication and remote sensing systems being fielded today have pointing accuracies and attitude control requirements that are a significant increase over their predecessors. Integrating these stringent performances with the lightweight, flexible structures of the future provides challenges in the modeling, sensing, and control of these advanced space structures. Design methodologies and design-analysis tools must be developed to allow study of these design tradeoffs.

Large spacecraft normally employ truss-type structures such as those envisioned for the International Space Station. As these systems grow larger, their natural structural frequencies approach the operational control bandwidth of the spacecraft. The effect is to cause interaction between control and structures. Dynamic perturbations caused by crew movement, attitude adjustments, and thermodynamic loading in orbit can generate unacceptable levels of vibration. Remote sensors often require very precise pointing accuracies, which are not obtainable if sensors are subjected to even the smallest vibration. These perturbations must be eliminated or suppressed as rapidly as possible to minimize their impact on spacecraft payloads.

Passive and active damping techniques are employed to minimize spacecraft vibration. Passive damping normally involves visco-elastic materials that dissipate energy. Although efficient, in space applications where mass margin is a precious commodity, the mass penalty associated with a passive damping system is sometimes too great. The second method, active damping, is challenging to implement due to uncertainties in modeling the structural-dynamic characteristics of a spacecraft and developing the necessary closed-loop control laws. An accurate model of the dynamic

behavior of the spacecraft is essential before designing an active control system. This modeling can potentially be extremely difficult.

A popular actuator in the field of active vibration control is the piezoelectric actuator. Piezoceramic actuators offer an attractive means of producing forces in flexible structures. The devices are lightweight, simple, and compact. They have no moving parts and require only a supplied electrical voltage to function. Additionally, their bandwidth of operation is normally more than adequate for most applications and their frequency response is nearly instantaneous. Piezoelectric actuators can be bonded to a structure or substituted for a structural member as a stack of piezoceramics. An applied electric field to the piezoceramic actuator causes it to expand, and in so doing, apply force to the attached structure. The use of these active piezoceramic struts for vibration suppression has already been demonstrated for a number of specific space applications [Ref. 1-4]. Utilizing active piezoelectric struts as the actuators in a closed-loop feedback control law on large, flexible structures holds promise in the active-control of the structure's vibrational modes.

B. SCOPE OF THESIS

The Naval Postgraduate School (NPS) Space Truss simulates a flexible space structure. The truss consists of 12 cubic bays arranged in a T-configuration mounted to a base plate. To simulate the effects of a spacecraft disturbance on the truss a proof mass actuator is incorporated on the structure to excite the truss' vibrational modes. Two active bar elements consisting of a low-cost, commercially available piezoelectric actuator stack, a force transducer, and mechanical interfaces can replace truss members and act as load-carrying members as well as force actuators. By using the force transducer as a sensor, an integral plus double-integral force controller is used to suppress specific modal vibrations across the entire length of the truss. Ultimately, the NPS Space Truss will be a test-bed for active control of flexible space structures, and a platform that can be used to incorporate new control technology.

As a precursor to implementing active control on the NPS space truss detailed modal testing and analysis were conducted to verify the existing finite element model (FEM) of the truss [Ref. 5]. The testing methodology followed in Reference 5 is similar to research conducted at the Naval Research Laboratory (NRL). In attempting to determine the mode shapes of the NPS space truss, it was found that both the NPS and NRL data were not reliable. Since no reliable modal data exists on the bare[1] space truss, another series of modal tests were conducted in order to verify the bare truss characteristics.

The remainder of this thesis is organized as follows. Section II describes the NPS space truss experimental setup and modifications made to the truss to incorporate the proof mass actuator and piezoelectric active struts. Section III describes the experimental analysis and modal testing of the truss and Section IV the active control system development, implementation, and experimental results. Section V discusses our conclusions and further research possibilities.

[1] Bare refers to the fact that none of the active control equipment have been installed on the space truss.

II. THE NPS SPACE TRUSS

A. TRUSS DESCRIPTION

1. Background

The Naval Postgraduate School Space Truss is a derivative of the technology that evolved from an ongoing program of focused research at the NASA Langley Research Center for the development of Controls-Structures Integration (CSI) technology [Ref 6]. The CSI program was initiated as a means of expediting the development of technologies that integrate the stringent performance requirements of payload systems with the flexible space structures of the future. Since future space missions would include increased pointing accuracies, precise attitude control, and multiple-payload platforms, CSI was developed as a hands-on tool for exploring the integration of these technologies.

As a part of this development effort, NASA Langley fabricated a truss structure termed the CSI Evolutionary Model (CEM) [Ref. 7]. The CEM is a truss structure containing several wings with varying degrees of flexibility to study CIS technology. The central bus consists of a truss, 17 meters in length and divided into 62 cubic bays. The structure also includes an 11-bay laser tower and a 4-bay reflector tower. The truss is constructed of a series of node-ball joints and aluminum truss tubes with special end fittings to provide for easy manipulations of the structure.

The CEM configuration was designed and developed through a cooperative integrated design effort between the Langley CSI researchers and the manufacturer, AEC-Able Engineering of Santa Barbara California. Detailed analysis of the CEM structural components were conducted as part of the Phase 0 testing on the Langley truss [Ref. 8]. When the Naval Research Laboratory investigated truss candidates to serve as a baseline for conducting active vibrational control of a truss structure using smart structures [Ref. 1], the CEM was selected due to the extensive analysis conducted on the structure as part

of the CSI research program. The NPS Space Truss is a product of co-operative research between NRL and the SDRC. Material specifications for the truss components are identical to those Langley truss[2] and are available in Reference 8. Certain material specifications that are necessary prerequisites for the modal testing of Chapter III were validated at NPS [Ref. 5] and have been enclosed in Appendix A.

2. Space Truss Elements and Construction

The NPS Space Truss structure is composed of twelve cubic bays assembled from a combination of 161 elements that begin and terminate in aluminum node balls. The cubic bays are arranged in a T-configuration with the base of the structure hard-mounted to a plate. The structure is approximately 3.76 meters long, 0.35 meters wide, and 0.7 meters tall. The overall configuration and arrangement of the truss are depicted in Figure 1.

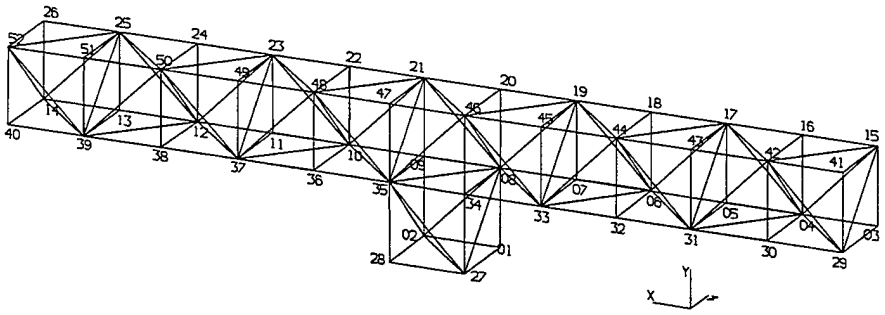

Figure 1. NPS Space Truss with Numbered Nodes

The twelve cubic bays are a combination of battens, longerons and diagonals. Longerons run down the length of the structure, battens compose the vertical elements, and diagonals run diagonally from one line of longerons to an adjacent line. Collectively, all of these elements will be referred to as struts. Each strut begins and ends at an aluminum node

[2] It should be noted that the Langley and NRL trusses contain node balls that are made of 304-steel, while the NPS space truss node balls are constructed of aluminum for reasons of cost. The material differences account for mass differences between the NPS and NRL trusses and variations in the natural frequencies of the two structures.

ball (Figure 2). Each node is a sphere approximately 38.7 mm in diameter, and contains eighteen connection points that interface with end assemblies of the truss struts and serve as mounting point for equipment during modal and active control testing. The numbering scheme depicted in Figure 1 is used to specifically designate individual nodes of the truss and is maintained as a standard throughout the entirety of the testing. Each strut begins and ends in an aluminum node ball and is also constructed of homogeneous aluminum. The struts themselves are assemblies made up of several components: the tube, outer sleeve, bolt, standoff, and nut (Figure 2). The tube is fastened to the outer sleeve with epoxy and then is fixed in place with a pin that is driven through the sleeve and tube.

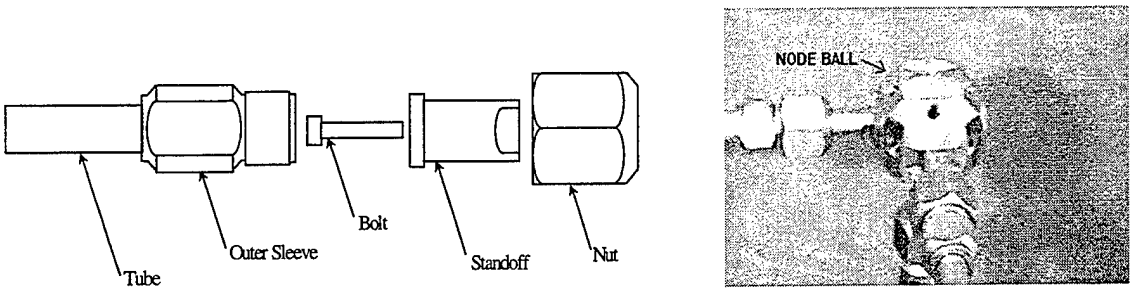

Figure 2. Strut Terminating End and Node Ball [After Ref. 9]

The NPS space truss is a precision structure that requires specific procedures for assembly and disassembly. Precision refers to the fact that the static truss experiences no internal loading, specifically that none of its strut members are under tension or compression. It is imperative that when conducting alterations to the truss configuration, the procedures outlined in Reference 5 are exactly followed. A failure to apply the correct torque to the structural members can place the entire structure under tension or compression thereby altering the modal characteristics of the truss. The modal testing and control law development in the upcoming sections is based on the characteristics of a balanced truss and could be adversely impacted by incorrect assembly techniques.

For the purposes of this thesis, the NPS space truss will be in one of two configurations: the bare configuration or modified configuration. These will hereafter be referred to as the bare or modified truss respectively. The bare truss is the configuration

that is used in the modal testing (Chapter III) of the structure and shown in Figure 1. The modified truss is the configuration that is used for the active control applications. In the modified truss (Figure 3), three of the bare truss' segments are replaced with specialized struts that perform the excitation and active control of the structure. These segments

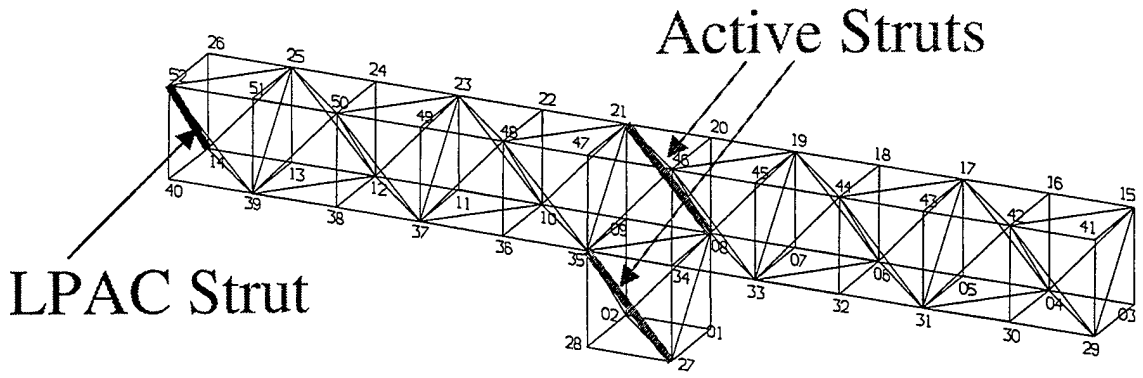

Figure 3. Location of Active and LPAC Struts

are the linear proof mass actuator (LPACT) strut, which holds a proof mass actuator to excite the truss, and two active control struts that contain piezoceramic stack that serve as the control actuators. The LPACT strut replaces the diagonal between nodes 52 and 14, and the active struts, the diagonals between nodes 27 and 35, and nodes 8 and 21. The specific struts are identified in Figure 3 above. The reasons for the placement of the struts at the given locations and detailed descriptions of these members and their capabilities are given in the following sections.

Incorporation of the LPACT and active struts into the NPS space truss significantly affects the mass and stiffness properties of the truss and as a result, its modal characteristics. In order to generate an accurate FEM of the bare and modified trusses it is necessary to include these mass differences. A detailed mass breakdown of the two different truss configurations is included in Table 17 of Appendix A and is used to develop the stiffness matrices that are incorporated in the truss MATLAB FEM code.

B. PROOF MASS ACTUATOR ASSEMBLY

1. LPACT Description and Assembly

Excitation of the modified truss is provided by a linear proof mass actuator (LPACT – Model Number CML-030-020-1) manufactured by Planning Systems Incorporated, Melbourne Controls Group. The specific operating characteristics of the linear precision actuator are described in Appendix B along with the LPACT natural frequencies and transfer function estimate. The LPACT electronics package provides signal conditioning for the accelerometers, rate feedback to dampen the structure, force feedback to add damping to the LPACT resonance, and user accessibility to the accelerometer and drive signals of each LPACT. Although, the principal use of the LPACT in this study is for truss excitation, the above features allow the user to measure and control the signals to and from the LPACTs. The LPACT can be used not only as an excitation source but also as an actuator for vibration control.

The concentrically mounted LPACT, shown in two views in Figure 4, is clamped onto a 7.0"cylindrical strut of 1.0" diameter. The LPACT will provide an output force of 3 lbs. From 10 to 1000 Hz. This bandwidth is more than sufficient for excitation of the truss since the first and second modes of the NPS space truss are at 15.0 and 18.0 Hz respectively. Attached to the bottom of the LPACT is a strut clamp with four flexible legs that provides a clamping interface to the central strut.

A gravity offload spring is used to center the LPACT (along the strut axis) within its flexures. The spring is placed between the bottom of the LPACT and the spring plate, which attaches via 4 screws to the bottom of the split-clamp nut. The spring position compensates for errors in the force magnitude due to flexure sag and magnetic circuit offsets. Flexure sag refers to the fact that the LPACT spring is modeled as a linear system when in reality it exhibits non-linear characteristics due to the orientation of the LPACT in gravity field. The overall effect of the error is that the effective resonance of

the LPACT body rises slightly due to this linearity. Additionally, during vibration when the LPACT travels through its maximum negative and positive positions, its mass distorts the magnetic field lines causing some leakage. In so doing, this magnet circuit offset introduces some error in the system force constant which may manifest itself in the force and rate feedback controllers provided by the electronics. Adjusting the spring height to accommodate angles of 0° to 45° between the strut and gravity minimizes these errors.

Each LPACT has two accelerometers that have been affixed with Permabond adhesive. The primary accelerometer, which is co-located with the LPACT's primary force, is mounted to a ring attached to the central strut (hard mounted to the space truss) of the LPACT. The secondary accelerometer is mounted on the proof-mass of the actuator. Both of these mounting locations are shown in Figure 4. The primary accelerometer can be used to measure structural vibration at the location of the LPACT, and can also be used to close the "rate loop" to add damping to the attached structure. The secondary accelerometer can be used to provide a sense of force output from the actuator, and can be used to close a force loop around the actuator in order to add damping to its flexure mode. The secondary accelerometer allows the user too directly measure the output force from the LPACT:

Output force = Proof-Mass Acceleration * Mass of LPACT.

The outputs of both the Primary and Secondary Accelerometers are available for measurement and control.

2. LPACT Electronics Characteristics

The LPACT electronics consists of a single enclosure that controls the functionality of each LPACT as follows:

a) Provides signal conditioning and amplification of all accelerometers.

b) Allows closure of a force loop for each LPACT: feeding back an estimate of the proof mass's velocity (by integrating the secondary accelerometer)

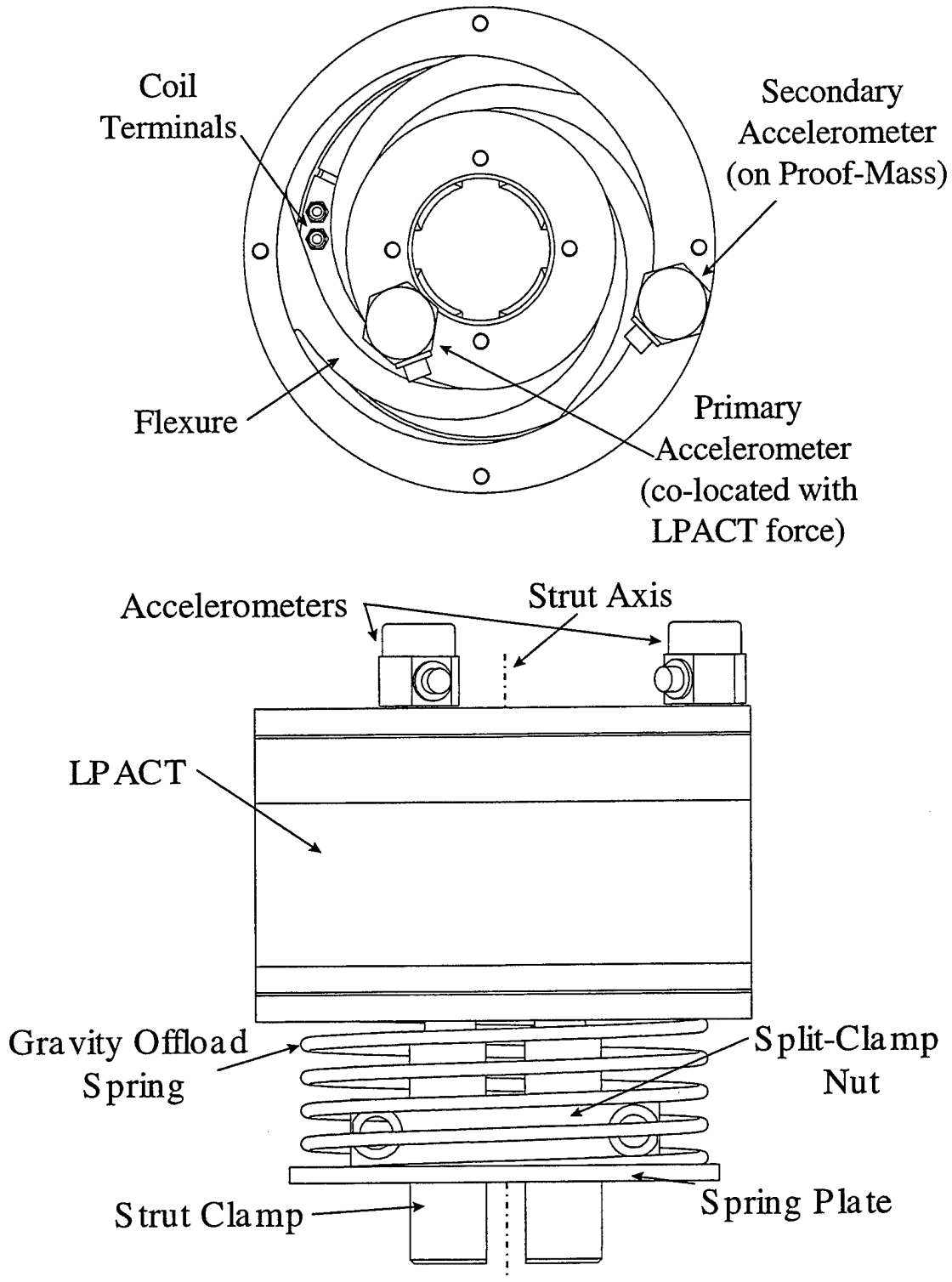

Figure 4. LPACT Top and Side View [From Ref. 10]

to provide damping to the LPACT's flexure resonance.

c) Allows closure of a rate loop for each LPACT: feeding back an estimate of the attached structure's velocity (by integrating the primary accelerometer) to provide increased structural damping to the structure.

d) Applies current to the LPACT coil from a command consisting of summation of 1) user input command, 2) force loop command and 3) rate loop command.

e) Provides user access to the conditioned accelerometer outputs, and the voltage command to the servo amp of the LPACTs.

The table below shows the connectivity of the cable assembly to the LPACT. Marking the black coax cable (#1 and #2) helps distinguish between the two assemblies and serializes each cable. Figure 5 shows the front and rear panels of the enclosure. The main power switch for the electronics is located on the front panel along with a light that indicates whether the LPACT is on or off. An analog current (AC) receptacle is located on the rear panel, which is fused at 6 amp.

Cable Assembly cable	**connect to LPACT Electronics (all on rear panel)**	**connect to LPACT Component**
Black Coax	'To Coil' (banana plug to BNC adapter)	6" Blue Pigtail from coil (BNC)
Blue Coax marked with Red Tape	'From Secondary Accelerometer' (BNC)	Secondary Accelerometer on Proof Mass (microdot)
Blue Coax	'From Primary Accelerometer' (BNC)	Primary Accelerometer on Co-Locate Ring (microdot)

Table 1. LPACT Electronics Connectivity Guidelines [From Ref. 10]

For each LPACT there are three switches located on the front panel: one to enable/disable the LPACT amplifier, another to enable/disable the force loop, and a third

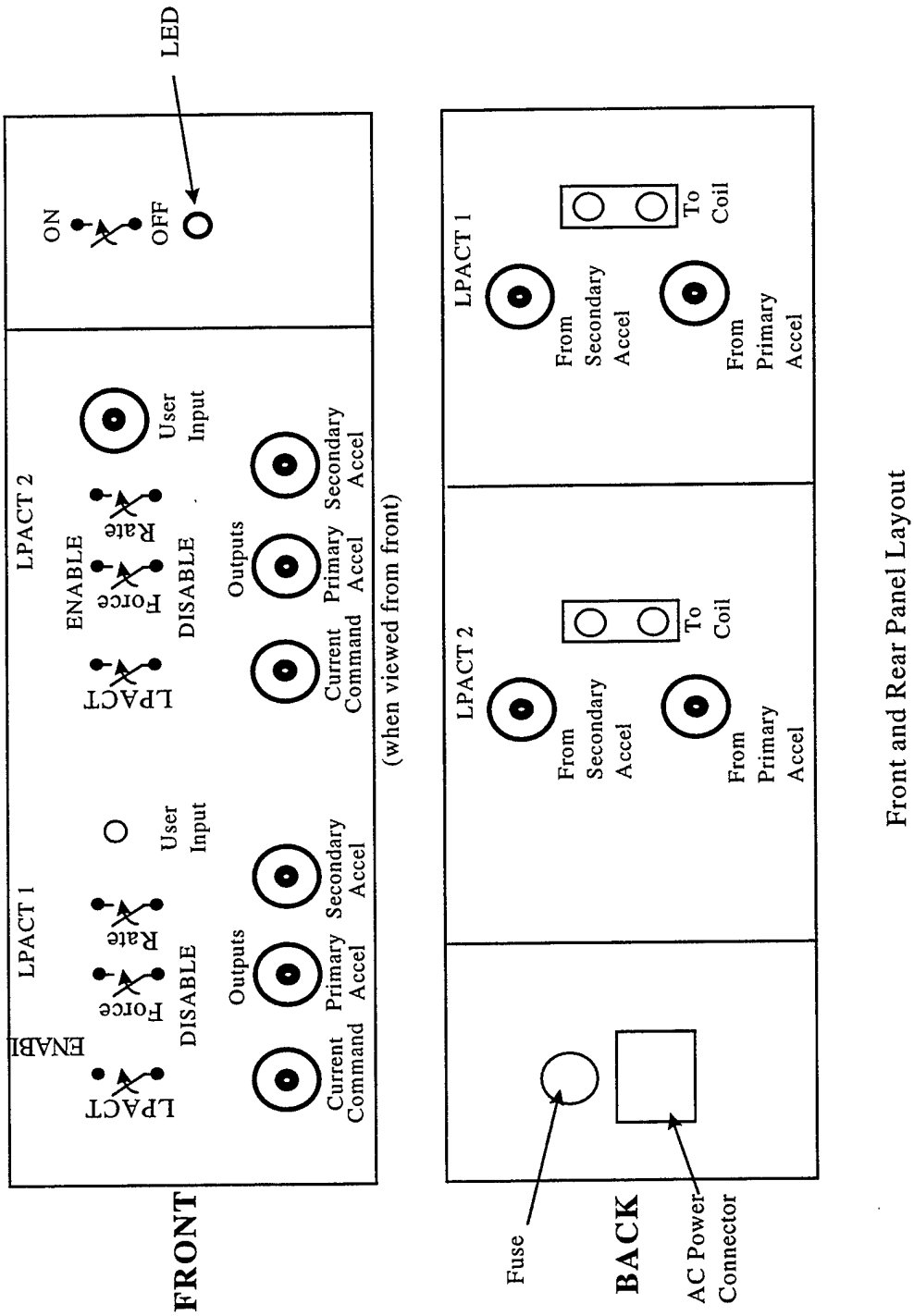

Figure 5. LPACT Control Electronics Rear Panel [From Ref. 10]

to enable/disable the rate loop. There are also four connectors on the front panel, of which one is for the user to input their commands. The others are outputs for the user to measure the primary accelerometer, the secondary accelerometer, and the LPACT command signals. The LPACT coil and accelerometer cables connect to the rear panel. The LPACT coil connects to the banana jack labeled LPACT coil. The primary and secondary accelerometer inputs are labeled 'From Primary Accelerometer' and 'From Secondary Accelerometer' respectively.

The enclosure houses several printed circuit boards, power supplies, and interconnecting wiring. Each LPACT has two associated printed circuit boards: 1) a 'Pre-Amp and Loop' board for conditioning the LPACT's accelerometers and implementing its force and rate loops, and 2) a 'Servo Amp' board for converting voltage commands to current to be applied to the LPACT's coil. The user may change the gain and filter settings of the force and rate loop by selecting the switch settings on the appropriate LPACT 'Pre-Amp and Loop' board (as described in the following sections). The 'Servo Amp' board is not adjustable by the user.

To introduce how the electronics interacts with the LPACT and the space truss, a simplified, system-level block diagram is shown in Figure 6. The rate and force loops are in the feedback path.

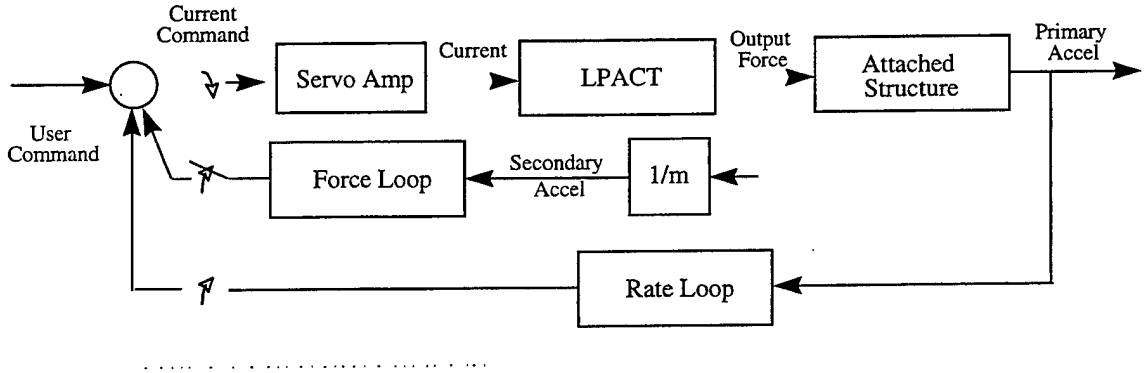

Figure 6. System Level Block Diagram [From Ref. 10]

3. Installation of LPACT and Design Modifications to the NPS Truss

One purpose of a truss in spacecraft design is to provide added area for the mounting of spacecraft sensors. Normally, these sensors will be attached to the remote ends of a truss in an effort to isolate them from the influences of other spacecraft instrumentation. In this configuration, the opposite end of the truss will be cantilevered to the spacecraft. This rigid connection between the spacecraft bus and truss provides a path that propagates disturbances into the truss structure. To simulate this geometrical relationship, the LPACT is located at one end of the space truss to excite the various modes of the truss.

The LPACT is attached to the end bay of the truss on the outside diagonal element. The diagonal element was chosen, vice a longeron, to impart force in both the x and y-axis. Installing the LPACT strut onto the truss changes the stiffness properties of the truss elements. Due to the weight of the truss alone, the bottom longerons, oriented in the x direction, are under compression while the top longerons are under tension. The additional mass of the LPACT will further affect these elements. Since the gravity vector is perpendicular to the truss' x-axis, the location of the LPACT in the y-axis is irrelevant. This effect is unavoidable regardless of the element that is replaced. However, the location of the LPACT in the z-axis is relevant. If the LPACT were installed on an off center vertical longeron, the weight of the LPACT would produce a torsion along the length of the truss. Therefore, the properties of the truss are position sensitive to the location of the LPACT in the z-axis. In an effort to minimize the impact of installing the LPACT, the LPACT should be placed on the diagonal, and the LPACT's center of mass should be co-located with the diagonal geometric center.

To ensure mass symmetry, the LPACT proof mass was centered on the truss end-bay diagonal element. The LPACT was centered between the two nodes of the diagonal by designing the connecting rods to center the LPACT central strut on the truss diagonal, and then adjusting the strut clamp so as to place the center of mass of the entire assembly at the center of the diagonal. To determine the LPACT's center of mass, a scale device

was constructed as shown in Figure 7. An eight-foot segment of monofilament line was attached to a hang-type scale and suspended from the ceiling. One end of the LPACT strut was suspended from the scale and a stationary mount supported the other. By using the relationship,

$$X_{cm} = (x_1 \cdot m_1 + x_2 \cdot m_2)/m_1 \cdot m_2 \qquad (2.1)$$

alternating the side of the strut to which the scale was suspended, and adjusting the LPAC strut clamp, the center of mass was positioned in the middle of the LPACT strut.

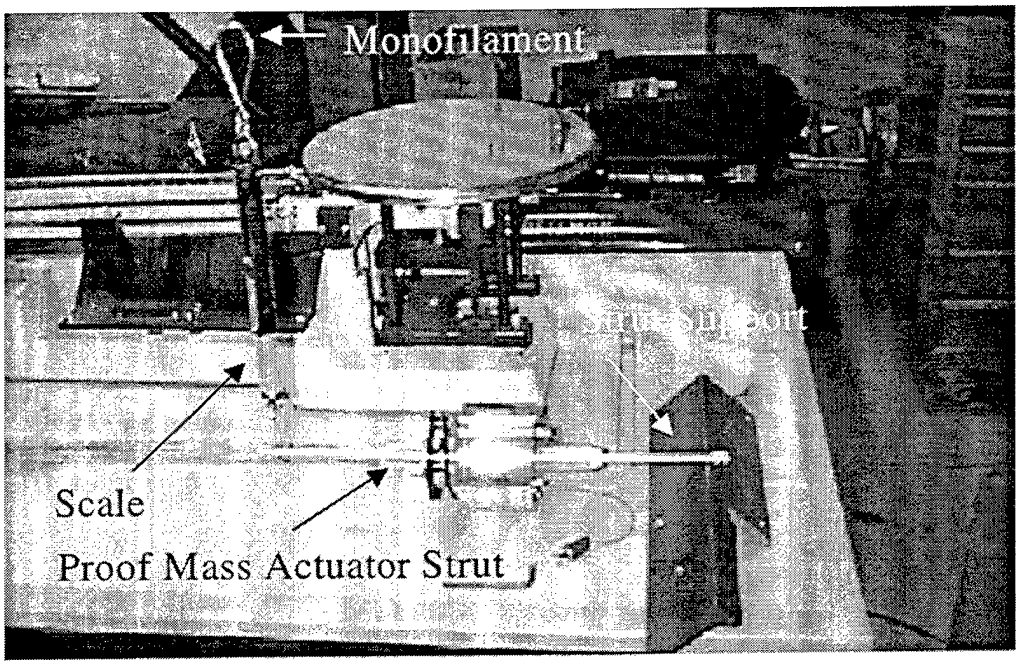

Figure 7. Determination of Center of Mass of LPACT Strut

The two connecting rods, which interface between the LPACT and the space truss, were fabricated at the NPS machine shop. Prior to the design and machining of the connecting rods, the length of the LPACT assembly listed in Reference 10 was verified by the NPS machine shop. Overall length of the LPACT/connecting rod assembly is extremely important since the truss diagonal element length is 15.994 ± 0.001 inches.[3] If

[3] The dimensioning tolerances used by the NPS machine shop in manufacturing the interface struts for the LPACT and active elements are tighter than those used by AEC-ABLE engineering during the initial design of the structure. AEC-ABLE's design tolerance for the truss struts was +/- .010" while the NPS machine shop designed to .0005". This is reflected in the design drawings of Appendix C and resulted in some problems during the installation of the active struts.

this assembly does not equal 15.994", the other elements, which connect to the node balls, which hold the LPACT strut will be put in tension or compression. As negligible as these stresses might be, they could significantly affect the dynamic characteristics of the space truss. The final design specifications for the LPAC connecting rods are displayed in Appendix C.

The Naval Research Laboratory constructed their LPACT connecting rods out of 304-grade steel [Ref. 1]. The material was chosen for its high stiffness and strength properties. Machining this high-grade steel, however, is a difficult and time-consuming task, and for this reason, aluminum 6061-T6 (AL-6061-T6) was used to manufacture the NPS connecting rods. The concern in employing AL-6061-T6 is the strength of the threads that engage into the nut assembly attached to the node ball. After extensive installation and removal of the LPAC strut during the active control testing it was noted that the threads on the interface struts had worn. It is recommended that future struts be made out of 303 or 304-grade steel.

The technical drawings for the LPACT interface struts are enclosed in Appendix C. Each connecting rod has a bolt tapped into one end that couples to the LPACT central strut. The connecting rod can then be screwed into the central LPACT strut that is supplied by the manufacturer with .25-20 tapped holes. The opposite end of the connecting rod is machined with 9/16-24 threads, which engages the nut assembly attached to the truss node ball. The installed LPACT is shown in Figure 8. As a final note, the truss assembly procedures detailed in Reference 5 should also be applied to installation and removal of the LPAC strut from the truss.

C. THE ACTIVE STRUT ASSEMBLY

1. Introduction

Although the specifics of the truss active control system will be discussed in detail in Chapter IV, it is necessary to introduce some of these concepts in order to understand

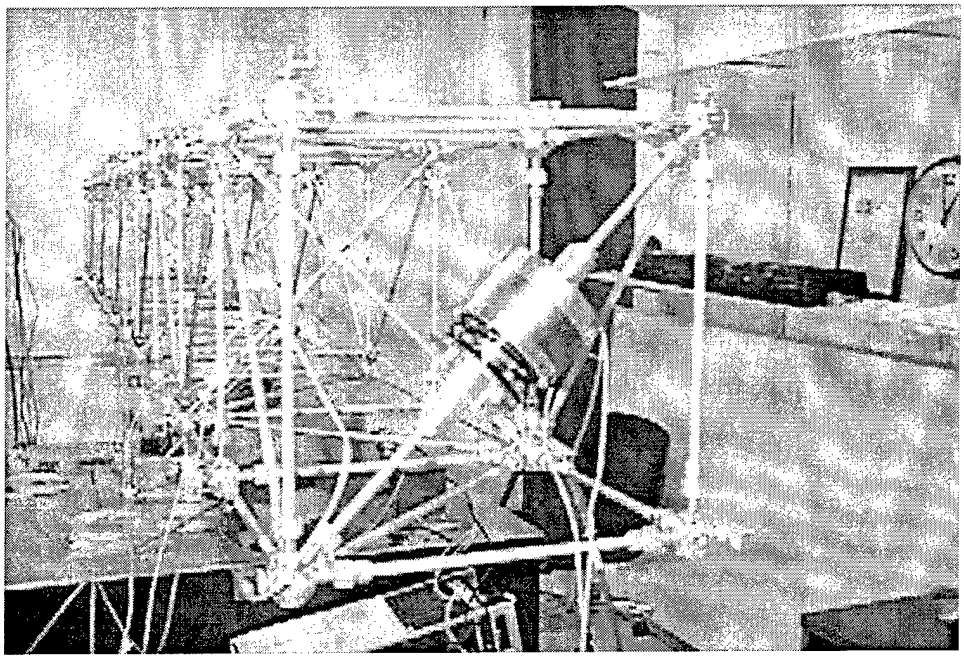

Figure 8. LPACT Mounted on NPS Space Truss

the components that make up the two active struts that are incorporated into the NPS space truss. The generic architecture of a closed-loop active control system is displayed in Figure 9. The ingredients necessary for performing closed-loop active control on a structure are threefold:

(1) A sensor that measures the state of the structure based on any input and converts it into a form useable by the system controller;

(2) A controller that analyzes the output response of the system relative to a reference signal and provides an actuating signal to control the response of the structure; and

(3) The actuator that receives the actuating signal from the controller and converts this signal into an actual physical output that alters the response of the system.

In the NPS space truss, two of the above three components (the sensor and actuator) are physically incorporated in the active strut assembly making the two active struts essential elements for the success of the active control applications. The active

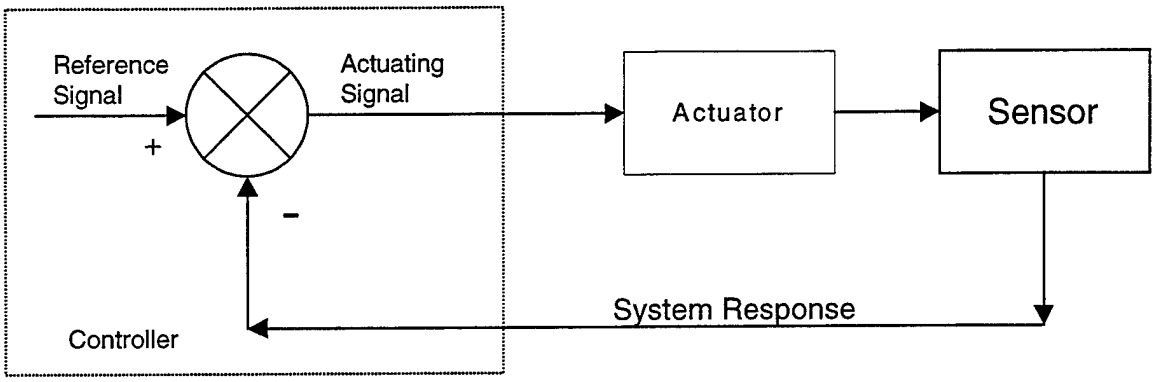

Figure 9. Closed Loop Active Control System

struts (Figure 10) are individually composed of a PCB Piezotronics force sensor, a Physik Instrumente (PI) piezoceramic stack actuator, a flexible tip, and two truss interface rods. All these elements thread together to form an integrated active strut that provides vibration suppression to the truss structure based on sensor input.

2. Fundamentals of Piezoelectric Strut Operation

The centerpiece of the active strut is the piezoceramic stack manufactured by Polytec PI of Hamburg, Germany. If unconstrained, this device converts the controller's actuating voltage into a physical displacement. The translators used for the control applications are electrically controllable actuators that belong to a class of active sensors that function on the basis of the piezoelectric effect. These piezotranslators allow precise movements from the sub-nanometer to the millimeter range with extreme accuracy.

The Curie brothers discovered the piezoelectric effect in 1880. The basis of the principle explains the ability of certain crystalline materials to generate an electrical signal proportional to an externally applied mechanical force. The phenomenon has been termed the 'direct' effect and is based on an asymmetric crystal arrangement in the material. These materials have a cubic crystal lattice structure above a certain temperature threshold (Curie temperature) and a tetragonal lattice below. When the material transitions from the cubic to the tetragonal phase, through the application of an external force electric dipoles are induced on the lattice. The electrical dipoles induced

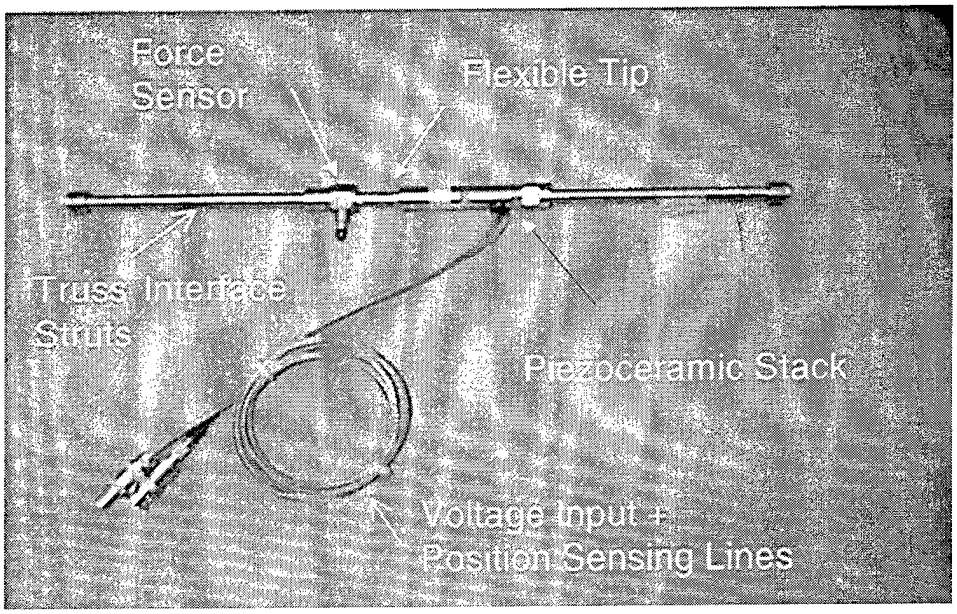

Figure 10. Active Strut Assembly

on the crystal surface and the voltages thus generated exceed a threshold that is measurable by an external apparatus. Conversely, when an electric field is applied to these materials the crystalline structure changes shape producing dimensional changes in the material. This 'indirect' effect manifests itself in a mechanical force applied to a constrained body. The piezoelectric translators used in our active struts take an externally applied voltage and transform it into a force applied axially along the diagonal assembly.

Piezoelectricity occurs naturally in some crystalline materials and can be induced in other polycrystalline materials through a process known as "poling". The poling process changes the dimensions of a ceramic element. The crystal lattice structure may be poled by the application of a large electric field, usually at high temperature. After the process is complete, a voltage lower than the poling voltage changes the dimensions of the material as long as it is applied. A voltage with the same polarity will cause additional expansion along the poling axis and contraction along the lateral axes. Application of a voltage of opposite polarity causes the ceramic to shrink along the poling axis (3-axis). Figure 11 shows the typical coordinate system used to represent a poled piezoelectric.

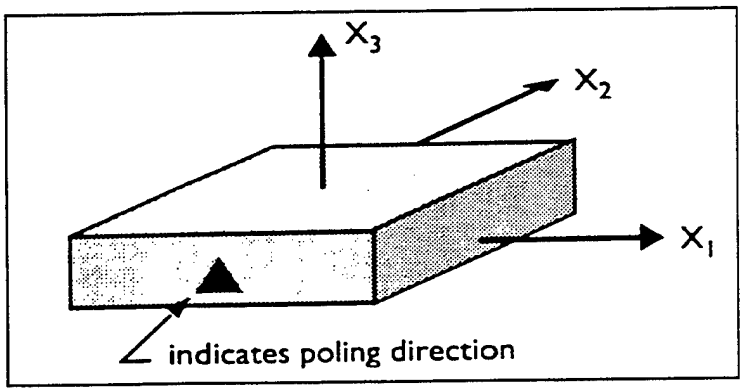

Figure 11. Poling Directions for a Piezoceramic Material

The direct piezoelectric effect has been used extensively in sensors such as accelerometers. Use of the converse effect had been restricted to ultrasonic transducers until recently. Barium titanate, discovered in the 1940s, was the first widely used piezoceramic. Lead zirconate titanate (PZT), discovered in 1954 [Ref. 11], has now largely superseded barium titanate because of its stronger piezoelectric effects. Researchers in the area of structural control have taken notice of the very desirable features of piezoelectric actuators for use in structural control applications. Piezoceramics are compact, have good frequency response, and can be easily incorporated into structural systems. Actuation strains on the order of 1000 μstrain have been reported for certain PZT materials. Strains are non-dimensional ratios of the change in length to the original length for a given impetus. Piezoceramics produce strains that are to some degree, linearly related to the applied electric field making them very attractive for structural control applications.

There are several methods to model the constitutive behavior of piezoelectric materials. The most popular is the macromechanical approach that provides the relationship between the electrical and mechanical effects in a manner that can be applied to typical isotropic or orthotropic materials. For piezoelectric materials, the following linear relation can describe the interaction between the electrical and mechanical variables:

$$S_i = s_{ij}^E T_j + d_{mi} E_m$$
$$D_m = d_{mi} T_i + \varepsilon_{mk}^T E_k \tag{2.2}$$

The mechanical variables are the stress, *T,* and the strain, *S*, and the electrical variables are the electric field, *E,* and the electric displacement, *D*; *s* is the compliance, *d* is the piezoelectric constant and ε is the permitivity. The first equation describes the converse piezoelectric effect, and the second equation describes the direct effect. The stress and strain are second order tensors, while the electric field and electric displacement are first order.

The equations above written explicitly in matrix form are:

$$\begin{bmatrix} S_1 \\ S_2 \\ S_3 \\ S_4 \\ S_5 \\ S_6 \\ D_1 \\ D_2 \\ D_3 \end{bmatrix} = \begin{bmatrix} s_{11}^E & s_{12}^E & s_{13}^E & 0 & 0 & 0 & 0 & 0 & d_{31} \\ s_{12}^E & s_{11}^E & s_{13}^E & 0 & 0 & 0 & 0 & 0 & d_{31} \\ s_{13}^E & s_{13}^E & s_{33}^E & 0 & 0 & 0 & 0 & 0 & d_{33} \\ 0 & 0 & 0 & s_{55}^E & 0 & 0 & 0 & d_{15} & 0 \\ 0 & 0 & 0 & 0 & s_{55}^E & 0 & d_{15} & 0 & 0 \\ 0 & 0 & 0 & 0 & 0 & s_{66}^E & 0 & 0 & 0 \\ 0 & 0 & 0 & 0 & d_{15} & 0 & \varepsilon_1^T & 0 & 0 \\ 0 & 0 & 0 & d_{15} & 0 & 0 & 0 & \varepsilon_1^T & 0 \\ d_{31} & d_{31} & d_{33} & 0 & 0 & 0 & 0 & 0 & \varepsilon_3^T \end{bmatrix} \begin{bmatrix} T_1 \\ T_2 \\ T_3 \\ T_4 \\ T_5 \\ T_6 \\ E_1 \\ E_2 \\ E_3 \end{bmatrix} \tag{2.3}$$

Where S_1 through S_3 are the normal strains, S_4 through S_6 are the shear strains, T_1 through T_3 are the normal stresses, T_4 through T_6 are the shear stresses, D_1 through D_3 are the electric displacements and E_1 through E_3 are the electric fields associated with the given coordinate system.

The piezoelectric constants of most interest from a structural standpoint are the *d* constants. These constants relate the strain developed in the material to the applied electric field. The higher the value of these constants the more desirable. The d_{33} constant relates the strain in the 3-direction to the electric field in the 3-direction. Similarly, the d_{31} and d_{32} constants relate the strain in the 1 and 2-directions to the electric field in the 3-direction. The electric field is voltage applied across the piezoelectric divided by its thickness. It is important to point out that d_{33} is usually positive and d_{31}

and d_{32} are negative. This means that a positive field (i.e., a field applied in the poling direction) will produce a positive mechanical strain in the 3-direction and a negative strain in the 1 and 2-directions.

For structural applications, piezoceramic actuators arranged in a stacked configuration (Figure 12) have been found to be the most effective. In this design, the active part of the actuator consists of a stack of thin ceramic disks. Between each stack,

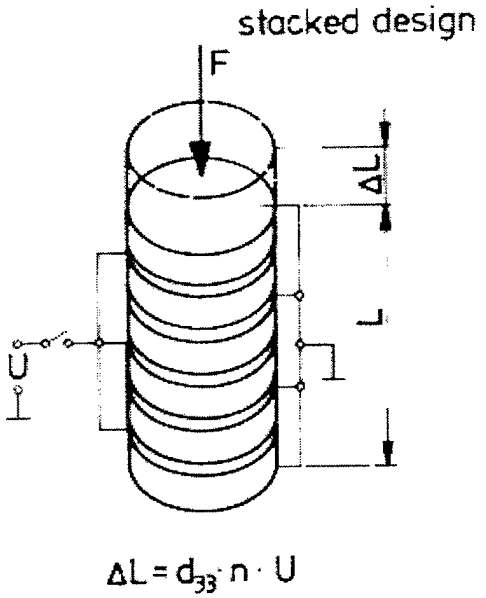

Figure 12. Stacked Piezoceramic Design [From Ref. 12]

flat metallic electrodes are entrained that feed into the operating voltage. Each ceramic disk lies between two electrode surfaces, one of which is connected to the control voltage and the other to ground. The piezoelectric effect in these actuators is linearly dependent on the externally applied electric field. An electric-field strength of up to 2 kV/mm [Ref. 12] is necessary for maximum expansion. The layer thickness of the ceramic material used determines the control voltage. The P-848.30 model translators employed in our testing have a 1-mm thickness. In general, translators supplied by Physik Instrumente have ceramic layers between 0.1 and 1 mm thickness with corresponding control voltages ranging from 100 V (low voltage translators, LVPZ) to 1000V (high voltage translators, HVPZ) respectively. The model P-843.30 piezoceramic actuator used in our

experimentation has a maximum operating voltage of 100 V.

For a piezoceramic stack actuator, the free displacement of the translator is defined by,

$$\delta_F = U \cdot n \cdot d_{33} \tag{2.4}$$

where δ_F, is the free displacement, U, is the voltage potential applied across each of the ceramic disks, n, is the number of ceramic disks in the translator, and d_{33} is the poling direction. The stiffness of the piezoceramic stack is defined as,

$$k_a = \frac{E_a \cdot A_a}{L} \tag{2.5}$$

We can model the active struts that are integrated into the NPS space truss as a piezoceramic stack placed in series with a spring, where the spring in our system is a representation of the interface struts, the flexible tip and the PCB force sensor. If the spring-stack system is fixed at both ends, the displacement of the system written in terms of the compressive force on the system and the stiffness of the components becomes,

$$\delta_F = \frac{F}{k} + \frac{F \cdot L}{E_a \cdot A_a} \tag{2.6}$$

where F is compressive or tensile force resulting from the expansion or contraction of the actuator, k, is the effective stiffness of the spring system, and L, is the length of the piezoceramic stack. By equating 2.4 and 2.6 and solving for F, it is found that the force exerted by the actuator onto the space truss is

$$F = \frac{U \cdot n \cdot d_{33}}{\left[\frac{F}{k} + \frac{F \cdot L}{E_a \cdot A_a}\right]} \tag{2.7}$$

3. Piezoelectric Strut Operating Characteristics

The expansion characteristics of the PI Piezoelectric Translation Model P-843.30 are derived from the manufacturer's data displayed in Table 19 of Appendix B [Ref. 12]. The nominal operating voltage range of the P-843.30 is 0 to +100 volts with a maximum expansion of 45.00 microns at an ambient temperature of 23 degrees Celsius. The

maximum pushing and pulling loads generated by the actuator are 800 and 300 Newtons respectively.

The P-843.40 has two electrical interfaces. The first is a voltage input that applies an operating voltage of 0-100V to the piezoceramic disks. The second provides expansion data for the piezo when used in conjunction with a PI digital display. The expansion data is supplied by a strain gauge that is attached internally to the piezoceramic stack. The gauge is one of the components of a Wheatstone bridge and would normally be supplied with a constant voltage by the digital display. As the piezo expands, the strain gauge's resistance changes and the output current of the Wheatstone bridge increases or decreases proportional to the displacement of the piezo. Although this interface is not used in our control applications, this feature has utility in control system design. This position information could be used in the design of a positive-position feedback control system or integrated with our force feedback control system using a complimentary filter.

Since the piezo ability to transform a voltage signal into actual physical expansion is the critical element in the active control experiments of the NPS space truss it was deemed necessary to verify the expansion characteristics of the piezos prior to their installation into the active struts. The experimental arrangement in Figure 13 was used for verification of the piezo's expansion characteristics. The Model P-843.30 piezo was mounted to a right-angle test stand. The test stand orientation was chosen to eliminate the effects of the gravity vector on the displacement of the actuator. If the piezo were tested in a vertical orientation (expansion in the vertical direction), the gravity vector would oppose the piezo motion and adversely impact the results. In the horizontal position, the cross product of the gravity vector and the direction of the expansion and contraction are zero. Since bending of the piezo was considered negligible due to its short length and large stiffness, the free end of the piezo was not supported during this testing.

The motion of the free end of the piezoceramic actuator is measured using a Kaman Eddy Current Sensor. Specific characteristics of the sensor are available in Reference 13 and have been summarized in Appendix B for completeness. The sensor,

supported by its own test stand, is placed approximately .005 inches away from the moving end of the piezo. A thin, conductive piece of metal (Aluminum) is attached to the end of the piezoceramic actuator using petrol wax. When an AC current flows through the sensor coil, an electromagnetic field is generated around the sensor. As the conductive end of the actuator moves through this field, the sensor induces a current flow that is transformed into a voltage through the bridge network that is part of the sensor's electronics box. The resultant voltage is measured using a Hewlett Packard (HP) 54601A digital oscilloscope and is directly proportional to the displacement.

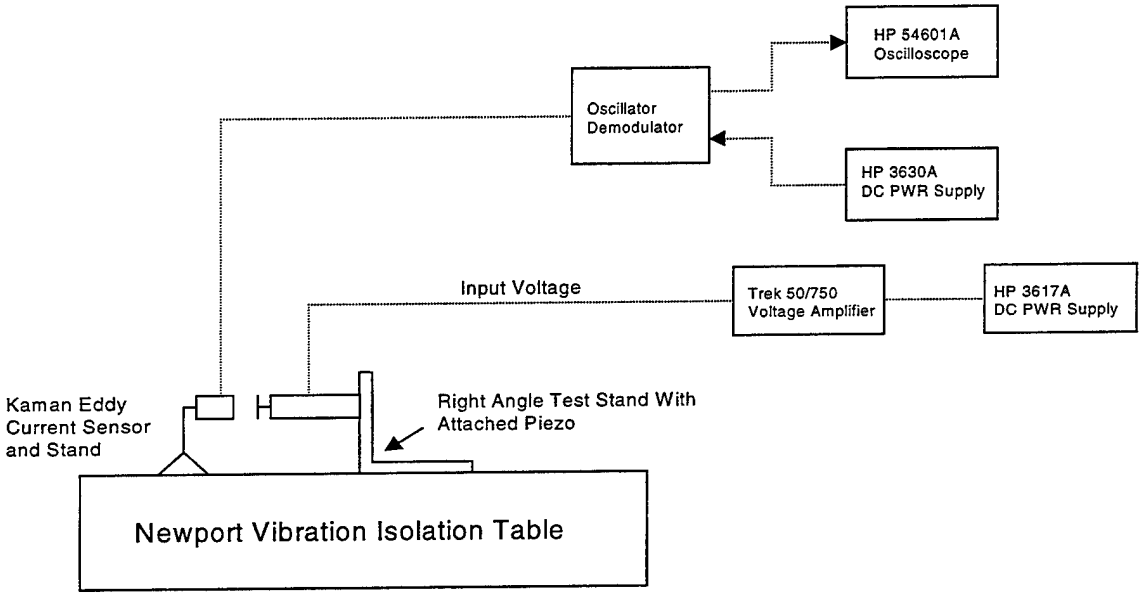

Figure 13. Experimental Setup for Verifying Piezo Expansion Characteristics

Once testing has commenced it is imperative that the test stand not move relative to the piezoelectric device otherwise the data will be inaccurate. The sensor-output voltages can be converted to a physical displacement using the manufacturer calibration data provided in Appendix B. Both of the piezoelectric actuators utilized in the control applications were tested from 0 to 100 volts with a step size of 10.0 volts. The voltage source was a HP-3617A digital current (DC) power supply. This power supply is amplified to the correct input voltage using a Trek 50/750 Voltage Amplifier. Table 3 summarizes the test results and Figure 14 displays the resultant expansion and contraction curves relative to the manufacture's calibration data.

An examination of the data displayed in Figure 14 reveals a close correlation between the experimental testing of the piezoceramic struts and the calibration data supplied by the manufacturer. The program that displays the data is included in Appendix D. Errors can be attributed to the fact that the input signal sent to the piezos

HP-E3630 Voltage (V)	Piezo Input Voltage (V)	Piezo Actuator #1 - SN 82686			Piezo Actuator #2 - SN 82687		
		V_{avg} - Trial 1	V_{avg} - Trial 2	V_{avg} - Trial 3	V_{avg} - Trial 1	V_{avg} - Trial 2	V_{avg} - Trial 3
0.000	0	2.505	2.159	2.107	2.010	1.892	1.866
0.666	10	2.407	2.090	2.034	1.951	1.830	1.800
1.333	20	2.282	2.001	1.948	1.867	1.752	1.717
2.000	30	2.134	1.905	1.864	1.772	1.655	1.619
2.666	40	1.988	1.805	1.753	1.660	1.553	1.525
3.333	50	1.850	1.682	1.644	1.534	1.438	1.405
4.000	60	1.693	1.569	1.526	1.402	1.325	1.299
4.666	70	1.558	1.455	1.417	1.280	1.220	1.190
5.333	80	1.428	1.342	1.300	1.156	1.105	1.075
6.000	90	1.300	1.222	1.188	1.045	1.002	0.975
6.666	100	1.175	1.117	1.087	0.937	0.901	0.870
6.000	90	1.229	1.168	1.138	0.997	0.956	0.928
5.333	80	1.300	1.237	1.205	1.060	1.028	1.000
4.666	70	1.380	1.319	1.285	1.140	1.100	1.073
4.000	60	1.461	1.403	1.373	1.228	1.187	1.160
3.333	50	1.552	1.490	1.462	1.319	1.280	1.252
2.666	40	1.657	1.594	1.560	1.416	1.382	1.353
2.000	30	1.767	1.696	1.668	1.534	1.494	1.460
1.333	20	1.891	1.824	1.785	1.652	1.605	1.580
0.666	10	2.016	1.942	1.907	1.771	1.733	1.702
0.000	0	2.157	2.077	2.034	1.898	1.866	1.825

Table 2. Experimental Verification of Manufacturer's Expansion Data

was adjusted by hand. In so doing, the time that the piezo was left at a specific input voltage varied from test to test resulting in small positioning errors that can be seen in the data. If these tests were to be repeated it is recommended that the test be automated using the dSPACE data collection system. In each of the three curves in Figure 14, the lower curve represents the expansion of the piezo and the upper, the contraction. It should also be noted that in the two test cases, the contraction curve does not return to zero at the end of the testing. The reason for this is the hysteresis in the system. During the testing it was observed that during each voltage measurement, the output voltage read

on the oscilloscope would slowly drift down. Given enough time to drift, the piezo would eventually reach a level of zero expansion.

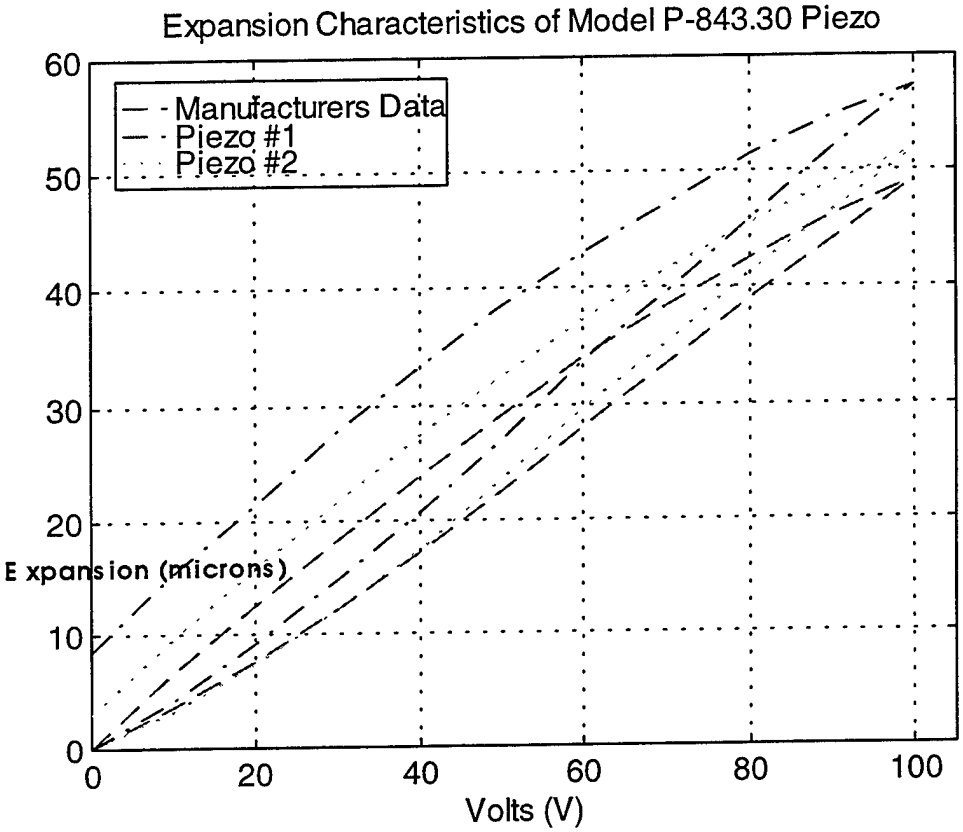

Figure 14. Piezo Model P-843.30 Expansion Characteristics

4. PCB Piezotronics Force Sensor

The second critical component of the active strut is the sensor. The sensor is required to feed the system response of the truss to the controller. Knowledge of the type of control system that will be used during the active testing is necessary since sensors are designed to detect one specific parameter (i.e. displacement, strain, or acceleration) and must be tailored to the requirements of the active control system. Initially, two types of control systems force feedback and positive position feedback were considered. The fact that previous research [Ref. 1 and 3] had shown that force feedback could be used successfully in active control truss structures made this attractive. Once the decision was

made to go with a force feedback control system, it was necessary to incorporate a force sensor into the active strut assembly. After a review of commercially available sensors, the PCB Piezotronics Model 208B02 was selected.

The Model 208B02 is designed to measure axial compressive and tensile forces. The sensor is equipped with internal mounting holes with uniform 10-32 threads that allow an interface with the other active strut components. The dynamic range of the sensor is between 100-lb. compression and 100-lb. tension. The maximum forces that it can endure are between 1000-lb. of compression and 500-lb. of tension. Additional information on the PCB force sensor can be found in Reference 14.

As in the case of the piezoceramic actuators, the importance of the sensor in the active control system made it necessary to test whether the force sensors were operating properly prior to the installation of the active struts into the space truss. Reference 14 provides calibration data for both of the PCB force sensors. The calibration data correlates the output voltage of the sensor with a given compressive or tensile force. To verify the calibration data, known weights were suspended from the two active struts. By hanging a known weight from the strut, a tensile force of known magnitude was applied to the force sensor. The voltage output of the force sensor was compared to the output of the calibration curves for the weight in question to see verify the proper operation of the devices. In both cases, three weights were applied to each of the active struts and each correlated to the calibration data provided by the manufacturer.

5. Active Strut Design and Installation on the NPS Space Truss

To proceed with the active control applications the PI piezoceramic actuator and PCB force sensor had to be incorporated into an active strut and installed into the NPS space truss. To meet its active control function and to protect the piezoceramic assembly during operation, certain design requirements for the active strut had to be met. First, the strut has to provide a means for removing moments that could be transmitted from the truss to the piezoceramic struts during expansion and contraction. Second, the active strut has to be designed so that the piezoceramic actuator was under some preload in

order to operate properly as part of the active-control system. Lastly, the strut must provide an interface between the truss and the sensor/actuator assembly.

The PI piezoceramic struts are extremely sensitive to applied moments. Although the actuators are encased in a stainless steel shell, the ceramic material inside the metal casing is as fragile as glass. Moments and shear forces that are applied to the top piece can damage the ceramic disks inside. The piezoceramic actuator mounting guidelines that are detailed in References 12 and 15 state that the translators should not be mounted rigidly at both ends and that no bending moments should be applied to the apparatus. Any applied load should act down the axis of the strut through the end-piece mounting points. If this is not possible then a special mount design should be utilized. Although the arrangement of active struts in the truss and the positioning of the translators within the struts appeared to allow only forces in the axial direction, a PI flexible tip was incorporated into the design to eliminate any moments that would be generated during the active control applications. The PI flexible tip is designed to give the translator flexibility. It was positioned in between the end-piece of the translator and the PCB force sensor.[4] The whole assembly was then incorporated into the truss using the two interface struts.

Preload can be supplied to the active strut via mechanical and electrical means. Mechanical preload involves designing the strut length so that it is slightly longer than the spacing between the node balls thus ensuring that the active strut would be in compression. This has the advantage of ensuring that a preload in the system, but the disadvantage is that it could result in long term deformation of the truss. An electrical preload entails placing a bias voltage on the piezoceramic actuator causing it to expand and thereby place a preload on the strut. The advantage here is that a preload would be applied only when the active control system was operating and eliminate the constant

[4] A specially designed adapter was obtained from PCB Piezotronics to interface between the force sensor and the flexible tip. Since PI of Germany designs the flexible tips their dimensions utilize metric threads while the force sensors are supplied with 10-32 to 10-32 interfaces. A special 10-32 to 5-mm thread had to be obtained to allow a solid connection between the tip and the force sensor.

application of forces on the truss.

Although appealing, an electrical preload could not be made to work due to the geometric and manufacturing constraints of the system. The overall length of the active strut was designed to 15.994 +/- .001 inches to match the original manufacturer's design. Recall that the operating range of the piezoceramic actuator was from 0 to 100 Volts. An applied voltage of 50 Volts would result in an expansion of only .0007 inches which is less than the manufacturing tolerance of the active strut making it ineffective as a means of providing preload. Additionally, the temperature in the laboratory causes the truss to expand and contract. Dimensional changes in the truss, caused by fluctuating temperatures, were of the same magnitude as the expansion of the piezoceramic actuator caused by the application of a bias voltage.

Mechanical preload for the active strut was provided by a series of shims that were manufactured by the Space Systems Academic Group (SSAG) machine shop. The shims were of varying thickness, ranging from .001" to .005". During the active strut installation, shims were placed between the end of the interface struts and the standoff that is fastened to the node balls. By placing shims into the structure, the active strut was placed under constant compression. As many shims as possible were placed at the interface to ensure that temperature fluctuations in the laboratory did not take the active strut out of preload. A total of .009" of shims were inserted into the truss during the installation of active strut #1 (between nodes 35 and 27). The PCB force sensors were employed during installation to verify that the active strut had been placed under compression. An increase in PCB sensor voltage indicates application of a compressive force.

Incorporation of the active struts into the NPS space truss is made possible through the design of two interface struts. The interface struts are milled out of 303-steel bar stock and have been designed to center the sensor/actuator on the diagonal. The material was chosen for its high stiffness and strength and low coefficient of thermal expansion. Each of the two interface struts in the active strut assembly has a slightly different design since each interfaces separately with the PCB force sensor and PI

Piezoceramic stacks. The technical drawings for the struts are enclosed in Appendix C.

A final mention must be made regarding incorporation of the active strut assembly into the space truss. The procedures for the installation of struts into the truss detailed in Reference 5 should be followed but extreme care must be taken when torquing the nuts to 70 ft-lbs. When torque is applied to the active strut during installation, this torque travels down the length of the strut and applies torque to the tip of the piezoceramic stack. During the installation of the second active strut, excessive torque was applied to stack causing irreparable damage to internal ceramics. It is imperative that during installation, a second wrench be used on a position between the torque wrench and the piezoceramic stack to offset the applied torques and prevent them from damaging the piezos.

D. LASER DIODE ASSEMBLY

1. Qualitative Requirement

The vibration of the space truss is not normally visible to the naked eye. It was determined that a method to qualitatively evaluate the effects of the control system on the structure would be a useful tool during the active-control experimentation. A laser-diode assembly (Figure 15) was designed to amplify the vibrations of the truss and display them on the laboratory wall. By designing the mounting elements with sufficient flexibility, the appendage, when mounted on the truss would vibrate synonymously with the truss. The laser diode, mounted on the flexible appendage, would vibrate with the truss and the spot beam projected onto the laboratory wall would give an indication of the motion of the structure.

2. Laser-Diode Assembly Design and Installation

The laser-diode assembly is composed of three parts. The first is a rod element that interfaces between the laser diode and the truss. The rod element has the necessary

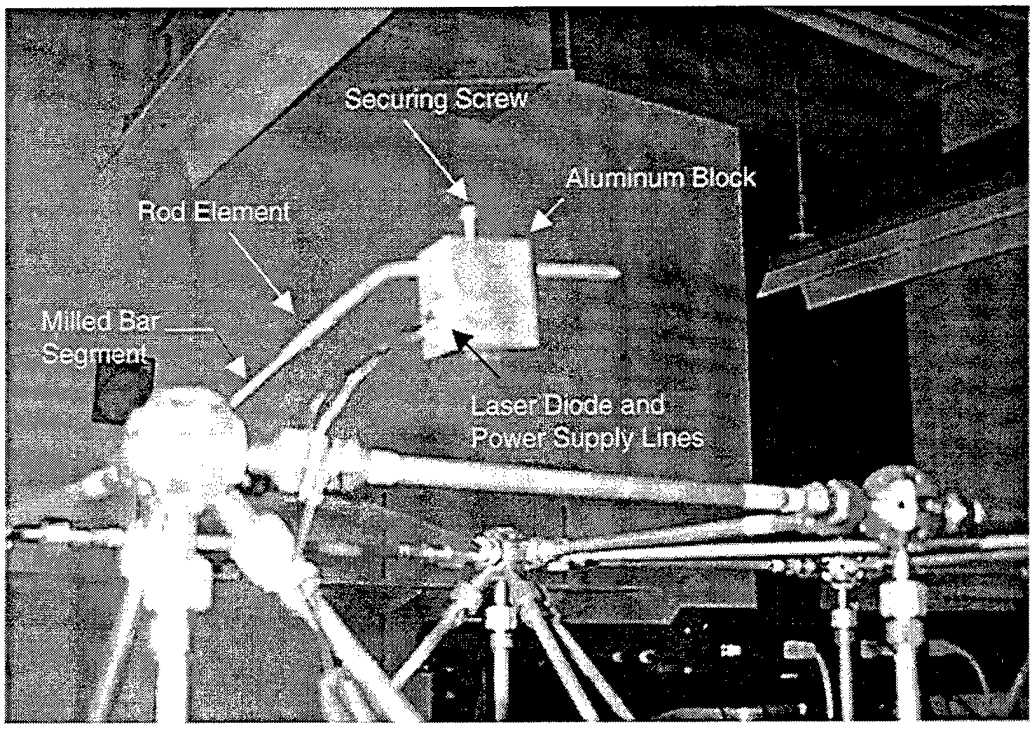

Figure 15. Laser Diode Assembly

flexibility to convey the truss vibration to the laser. The second element is an aluminum block that serves as a mounting point for the laser diode. Lastly, the laser diode projects the pinpoint beam on the laboratory wall.

The bar segment is an 8"-long, ¼"-diameter, stainless steel rod. One end of the rod contains a .328" long segment with .164-32 UNC threads that allow it to screw into any of the truss node balls. A one-inch segment of the rod is milled to a 1/8" diameter to give the bar its required flexibility. A one cubic inch aluminum block is attached to the bar segment. A ¼"- diameter hole is drilled through the length of the block to allow it to slide back and forth along the length of the rod segment. Adjusting the position of the aluminum block along the length of the rod changes the fundamental frequency of the laser-diode assembly and prevents resonant motion of the structure. This allows a qualitative picture of the amount of vibrational motion present in the space truss. Once the block is placed in the desired position a securing screw can be tightened to fix the assembly. A second 5/8" hole is drilled through the aluminum block and serves as a mounting point for the laser diode. The diode is secured to the aluminum block using

petrol wax.

The laser diode projects a laser spot beam on the lab wall that is synonymous with the motion of the truss. It is a 1-mW, 635-nm, laser-diode, Model PLC6351FW supplied by Lasermate Corporation of Walnut, CA. The laser is powered by a Hewlett Packard E3615A DC power supply. Maximum power applied to the laser should not be greater than 5 Volts, with 2-4 Volts being the optimum operational range and continuous use for periods greater than two hours are not recommended due to heat dissipation problems.

III. MODAL TESTING AND ANALYSIS OF THE NPS SPACE TRUSS

A. BACKGROUND

1. Principals of Modal Testing

The objective of conducting modal testing and analysis on a structure is twofold: (a) Determination of the structure's vibration levels, and (b) Verification of theoretical models and predictions. The latter, is the most common application and serves as an important tool in engineering design. Vibration modes measured during testing are compared with corresponding modes produced by a finite element model. The validation of a theoretical model is necessary so that the response of a structure to more complex excitations such as "shock" may be predicted with a degree of confidence.

To validate the theoretical model, modal tests provide estimates of a structure's frequency response function (FRF), which is used to identify the system's natural frequencies and can be used to determine descriptions of the mode shapes (eigenvectors). Also of consideration is the determination of the structure's damping ratios. Predicting the damping ratios from a theoretical model is nearly impossible and therefore correlation to testing results is not practical.

A comprehensive modal analysis strategy incorporates three distinct stages that are displayed in Figure 16.

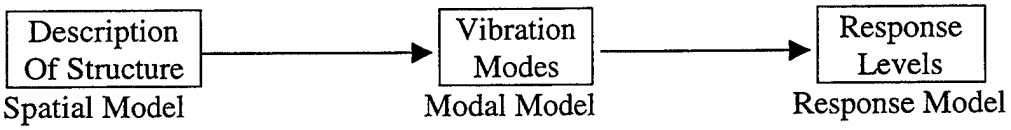

Figure 16. Structural Analysis Procedure [After Ref. 16]

The "spatial model" defines the physical characteristics of the structure. This typically includes the structure's *mass*, *stiffness*, and *damping* properties. The "modal model" is the result of performing a modal analysis on the spatial model and describes the

structure's unforced modal behavior. Included within the "modal model" are the natural frequencies, the corresponding mode shapes of those frequencies, and their associated damping ratios.

The third element of the process is the development of the "response model." Generally, this is of greatest value to the researcher since it provides an insight into a structure's reaction to a given excitation. Many methods are available to excite a structure. An impulse excitation is used for this research. The structure's reactions are most often described in terms of the FRF, which identifies the structure's response for a frequency spectrum of interest.

Modal testing is the mechanism employed in pursuance of the development of the "response model," and is governed by the basic relationship [Ref. 16]:

$$\boxed{\text{Response}} \quad = \quad \boxed{\text{Properties}} \quad X \quad \boxed{\text{Input}}$$

This relationship describes a structure's response as a function of its properties and a forcing function. If two of the variables are known, the third can be determined. Measuring only the structure's response is insufficient since a particularly large response cannot be determined to be a function of only the input or the resonance of the structure. The excitation and response are measured simultaneously allowing the use of the above basic relationship to determine the truss' properties.

2. Theoretical Background

Obtaining test data that may be used to verify a theoretical model was a primary goal of this research. The theoretical model describes the vibrational characteristics of the subject structure, specifically the natural frequencies and their associated mode shapes. Before testing, a review of how a theoretical model computes these characteristics should be investigated.

Realistically, most structures cannot be modeled as systems with only a single

degree-of-freedom (SDOF). Today's elaborate structures, like the NPS Space Truss, are complex bodies that consist of multiple-degrees-of-freedom (MDOF). Assuming that the truss behaves like a linear system, it can be modeled by the superposition of multiple SDOF systems. The complexity of the system increases exponentially with the number of the DOF so only a two-DOF system (Figure 17) will be presented. Ignoring damping, the coupled equations of motion that describe the dynamics of the two-DOF system are:

$$m_1\ddot{x}_1(t)+(k_1+k_2)x_1(t)-k_2x_2(t)=0 \tag{3.1a}$$

$$m_2\ddot{x}_2(t)-k_2x_1(t)+k_2x_2(t)=0 \tag{3.1b}$$

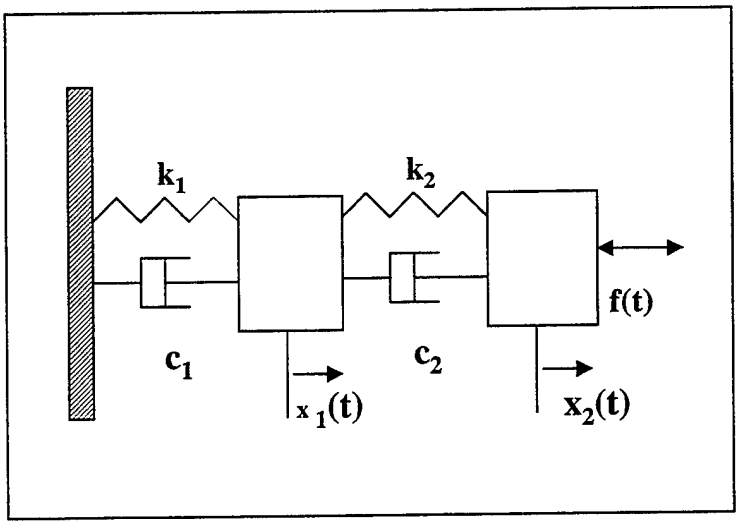

Figure 17. 2-DOF System

Letting $k_{11}=k_1+k_2$, $-k_2=k_{12}=k_{21}$, and $k_{22}=k_2$, equation (3.1) can be written in matrix form:

$$\begin{bmatrix} m_1 & 0 \\ 0 & m_2 \end{bmatrix}\begin{Bmatrix} \ddot{x}_1 \\ \ddot{x}_2 \end{Bmatrix}+\begin{bmatrix} k_{11} & k_{12} \\ k_{12} & k_{22} \end{bmatrix}\begin{Bmatrix} x_1 \\ x_2 \end{Bmatrix}=0 \tag{3.2}$$

Assuming a solution of the form:

$$\begin{Bmatrix} x_1 \\ x_2 \end{Bmatrix}=\begin{Bmatrix} u_1 \\ u_2 \end{Bmatrix}f(t) \tag{3.3}$$

implying that $\frac{x_1}{x_2}$ is time independent. Substituting equation (3.3) into (3.1), we obtain:

$$m_1 u_1 \ddot{f}(t) + (k_{11} u_1 + k_{12} u_2 f(t) = 0 \tag{3.4a}$$

$$m_2 u_2 \ddot{f}(t) + (k_{12} u_1 + k_{22} u_2) f(t) = 0 \tag{3.4b}$$

A solution exist if

$$-\frac{\ddot{f}(t)}{f(t)} = \frac{k_{11} u_1 + k_{12} u_2}{m_1 u_1} = \frac{k_{12} u_1 + k_{22} u_2}{m_2 u_2} = \lambda \tag{3.5}$$

and provided a solution exists for

$$\ddot{f}(t) + \lambda f(t) = 0 \tag{3.6}$$

equation (3.4) becomes

$$(k_{11} - \lambda m_1) u_1 + k_{12} u_2 = 0 \tag{3.7a}$$

$$k_{12} u_1 + (k_{22} - \lambda m_2) u_2 = 0 \tag{3.7b}$$

Let $\lambda = \omega^2$ and allowing the solution to equation (3.4) be in the form of

$$f(t) = C\cos(\omega t - \phi) \tag{3.8}$$

where C is an arbitrary constant, ω is a non-arbitrary frequency, and ϕ is the phase angle. From equation (3.7) we obtain

$$(k_{11} - \omega^2 m_1) u_1 + k_{12} u_2 = 0 \tag{3.9a}$$

$$k_{12} u_1 + (k_{22} - \omega^2 m_2) u_2 = 0 \tag{3.9b}$$

Written in matrix form equation (3.9) becomes

$$\begin{bmatrix} k_{11} & k_{12} \\ k_{12} & k_{22} \end{bmatrix} \begin{Bmatrix} u_1 \\ u_2 \end{Bmatrix} = \omega^2 \begin{bmatrix} m_1 & 0 \\ 0 & m_2 \end{bmatrix} \begin{Bmatrix} u_1 \\ u_2 \end{Bmatrix} = 0 \tag{3.10}$$

Determining the non-trivial values of ω^2 is the classical eigenvalue problem. A solution for ω^2 exist only if

$$\det \begin{bmatrix} k_{11} - \omega^2 m_1 & k_{12} \\ k_{12} & k_{22} - \omega^2 m_2 \end{bmatrix} = 0 \tag{3.11}$$

The two-DOF system's characteristic equation is

$$m_1 m_2 \omega^4 - (m_1 k_{22} + m_2 k_{11}) \omega^2 + k_{11} k_{22} - k^2{}_{12} = 0 \tag{3.12}$$

Recalling that $\omega^2 = \lambda$, equation (3.12) becomes a second order equation that corresponds

to two DOF. The solution of equation (3.12) is

$$\omega_1^2 = \frac{m_1 k_{22} + m_2 k_{11}}{2 m_1 m_2} - \frac{1}{2}\sqrt{\left(\frac{m_1 k_{22} + m_2 k_{11}}{m_1 m_2}\right)^2 - \frac{k_{11}k_{22} - k^2{}_{12}}{m_1 m_2}} \tag{3.13a}$$

$$\omega_2^2 = \frac{m_1 k_{22} + m_2 k_{11}}{2 m_1 m_2} + \frac{1}{2}\sqrt{\left(\frac{m_1 k_{22} + m_2 k_{11}}{m_1 m_2}\right)^2 - \frac{k_{11}k_{22} - k^2{}_{12}}{m_1 m_2}} \tag{3.13b}$$

where ω_1 and ω_2 are the natural frequencies of the system and each is associated with its own modal vector or mode shape. Let

$$\omega_1 \Rightarrow \begin{bmatrix} u_{11} \\ u_{21} \end{bmatrix} \equiv \{u\}_1 \tag{3.14a}$$

$$\omega_2 \Rightarrow \begin{bmatrix} u_{12} \\ u_{22} \end{bmatrix} \equiv \{u\}_2 \tag{3.14b}$$

The second subscript refers to the corresponding natural frequency. Rearranging equation (3.9)

$$\frac{u_{21}}{u_{11}} = -\frac{k_{11} - \omega_1^2 m_1}{k_{12}} = -\frac{k_{12}}{k_{22} - \omega_1^2 m_1} \tag{3.15a}$$

$$\frac{u_{22}}{u_{12}} = -\frac{k_{11} - \omega_2^2 m_1}{k_{12}} = -\frac{k_{12}}{k_{22} - \omega_2^2 m_1} \tag{3.15b}$$

equation (3.8) can be decomposed into two parts, each associated with a natural frequencies.

$$f_1(t) = C_1 \cos(\omega_1 t - \phi_1) \tag{3.16a}$$

$$f_2(t) = C_2 \cos(\omega_2 t - \phi_2) \tag{3.16b}$$

The motion at any time can be obtained as the superposition of the two modes, principally

$$\{x\} = \{x\}_1 + \{x\}_2 = C_1\{u\}_1 \cos(\omega_1 t - \phi_1) + C_2\{u\}_2 \cos(\omega_2 t - \phi_2) \tag{3.17}$$

or in matrix form:

$$\{x\} = [u]\{f(t)\} \tag{3.18}$$

where $[u]$ is the system's modal matrix, consisting of the two modal vectors. Experimentally identifying the natural frequencies and mode shapes that describe the

space truss can be used to validate the system model.

B. THE NECESSITY FOR RE-TESTING

Testing of the space truss was conducted as part of the research in Reference 5. After a comprehensive analysis of the results and a review of the testing conditions, several potential improvements were identified and re-testing the truss was determined to be prudent. The data collected during the research conducted in Reference 5 could not be used to produce accurate mode shapes of the truss.

The first improvement identified concerns the length of time for which data was collected during each impact test. When analyzing test data, the minimum frequency resolution obtainable is inversely proportional to the test duration and is defined by

$$\Delta f = 1/t_{test} \tag{3.19}$$

where Δf is the frequency resolution and t_{test} is the time duration of the test. The memory required to store data for each impact test is a function of the test duration and the sampling frequency. The impact testing conducted in Reference 5 utilized the dSPACE data acquisition hardware and eight accelerometers. For dSPACE to acquire data on all eight accelerometers (24 channels) and sample quickly enough to "capture" the impact magnitude the test duration was limited to 0.5 seconds. The reason for the short test duration is due to the limited 512K storage capacity of dSPACE. Equation (3.19) dictates that the minimum frequency resolution that could be obtained for this data is 2 Hz. The FEM of the truss developed by NRL [Ref. 9] shows that the first and second modes are less than 2 Hz apart. Even if ideal data were collected, the use of a 0.5 sec test duration would make the first two modes indistinguishable.

The second improvement was a re-design of the impact thumb screws. A review of the testing conditions revealed that the impact thumb screws used as impact points were in direct contact with the thumbscrews upon which the accelerometers were mounted, resulting in an energy short. In essence, the accelerometer was the impact point rather than a point on the truss. When properly performed, the energy from an impact is

cleanly transmitted into the truss and the accelerometers measure the resulting oscillation. If even a partial fraction of the impact energy is directly transmitted to the accelerometer at impact the resulting data will be corrupted. Eliminating the energy short was accomplished by grinding down a small portion of the impact thumb screws until there was no longer contact with the accelerometer thumb screws.

Modifying the dSPACE system configuration from that used during testing conducted in Reference 5 was identified as a third improvement. The dSPACE configuration during the original testing prevented the system from correctly measuring the magnitude of the impact force. Determining an accurate transfer function estimate between the input and the output is obviously a function of the quality of the data. During the initial modal testing of the NPS space truss (dSPACE experiments), the true peak magnitude of the hammer impulse was not captured (Figure 18). Due to memory limitations, the user must compromise between sampling frequency and the duration of data acquisition. Data collection is triggered when the impact hammer signal exceeds a pre-set threshold trigger value. Capturing a value that triggers data collection is a function of sampling frequency. Using a very high sampling frequency (10 kHz) will ensure that the hammer signal is sampled at some value over the trigger. This high sampling frequency, however, will result in a shorter test duration and will result in poor frequency resolution. The dSPACE sampling frequency was too low during the testing conducted in Reference 5 and as a result the true hammer impact magnitude was not captured. This oversight most likely introduced some error during data analysis, specifically when using the MATLAB command "TFE" which estimates the transfer function of system based on the input and output response [Ref. 17].[5]

A Hewlett Packard oscilloscope was employed to manifest this improvement. The dSPACE system setup was not changed and the oscilloscope was used to capture the hammer peak magnitude during testing. The true magnitudes read from the oscilloscope

[5] MATLAB contains a toolbox function, "TFE", that estimates the transfer function between a known system input and the observed system output, using Welch's averaged periodogram method.

during testing are recorded in Appendix E for each trial. Before analyzing the data, the trigger value stored by dSPACE was simply replaced with the true impact magnitudes read off the oscilloscope. The substitution results in a more accurate analysis, especially

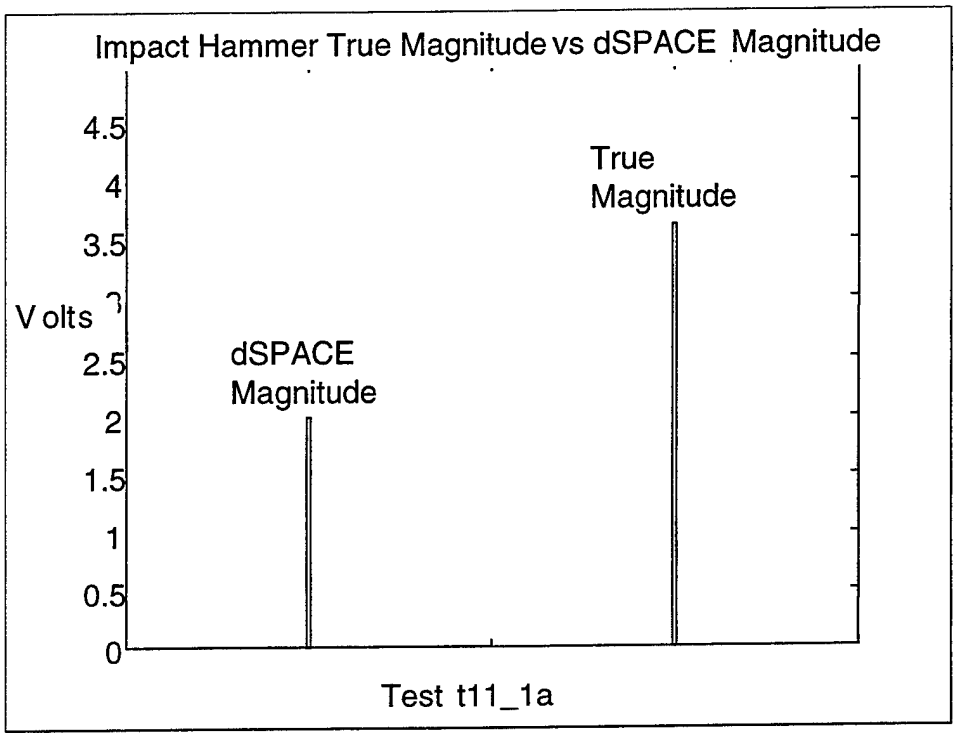

Figure 18. Impact Hammer True Magnitude vs. dSPACE Magnitude

when comparing the system input to the system response.

A final improvement was switching the type of tip used on the impulse hammer. Tips constructed of varying materials impart different amounts of power into different frequency bandwidths. Softer tips will inject more power into the lower frequencies while harder tips inject more power into the higher frequencies. As an illustration, striking the truss with a rubber mallet produces results that are dramatically different from the results produced by striking the truss with a ball-ping hammer. Although the initial dSPACE testing was conducted with a hard plastic tip, prior to the testing that employed the HP-35665A, the correlation between the hammer tip and the power spectrum was identified. As a result, during the most recent series of modal tests, a soft rubber tip was attached to the impact hammer.

C. dSPACE EXPERIMENTAL SETUP

1. Overall System

Testing the NPS space truss is governed by the relationship that the system response is a function of the system properties and system input. In the case of the NPS space truss, the response and the input can be physically measured. From these two measurements, the truss' properties (in our case, the natural frequencies, damping ratios and eventually the mode shapes) are determined, and compared with the FEM calculated properties.

Four accelerometers are employed to measure the truss response. Associated equipment includes the following: a Kistler 12-channel signal conditioner for the accelerometers, a PCB Piezotronics signal conditioner for the impulse hammer, a PC based analog-to-digital (AD) data acquisition system (dSpace™), an oscilloscope, and a host computer. An impulse hammer provides system input. In the experimental setup (Figure 19), a separate signal conditioner (one channel) was used with the impulse force hammer that is also connected to the dSpace system.

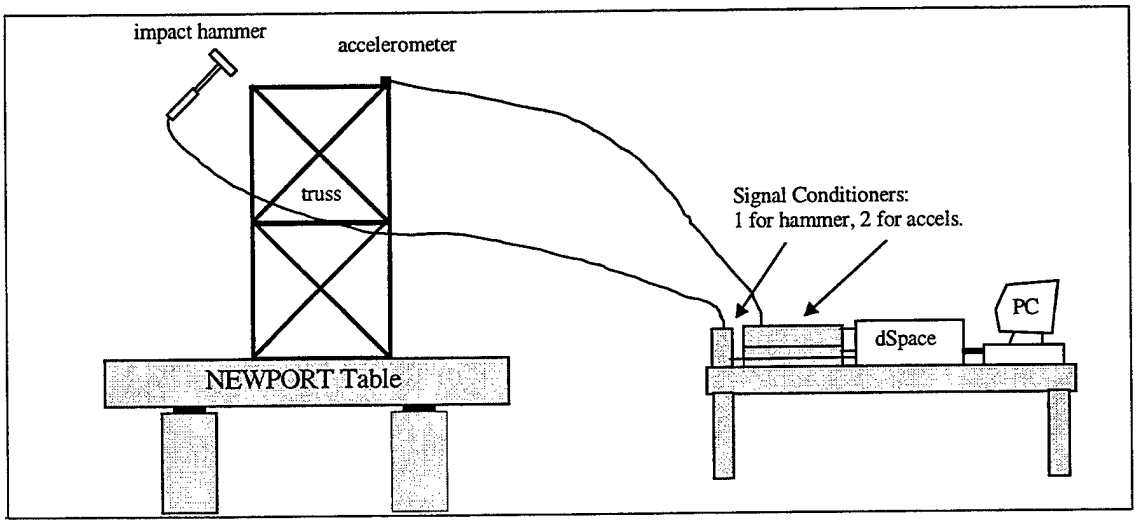

Figure 19. dSpace Experimental Setup

The NPS Space Truss is mounted on a Newport Vibration Control System Table.

The Newport's 1000-lb. tabletop is floated on a cushion of N_2 during testing. Each of its four pedestal legs contains a piston which, when charged, floats the table. The advantage of using such a mounting platform is that it filters out unwanted disturbance vibrations. Specifically, disturbances in the frequency range above 12 Hz are attenuated by more then 99% by the table [Ref. 18]. The Kistler accelerometers are highly sensitive measuring devices with sensitivity ranges from 100-500 mV/g [Ref. 19]. Any outside disturbance could corrupt the collected data.

Because of dSPACE's memory limitations and frequency resolution issues, only four accelerometers were used during this round of testing. To obtain the FRF at every node, the accelerometers were moved to a different set of nodes between each test. The detailed location of every accelerometer for each test is contained in Appendix E. Ultimately, the experiment was conducted twelve times, each time measuring the response at four different nodes. Upon completion of testing, all the nodal data matrices are superimposed to generate a global picture of the truss' response. Rather than randomly selecting the nodes to be tested, a systematic method of accelerometer placement was conceived. Commencing at the far end of the truss, the accelerometers were placed on the four extreme nodes (3, 15, 29, and 41) in the plane perpendicular to the truss's global x-axis. After testing each accelerometer configuration, the four accelerometers were moved down bay to the next four nodes. The position of the accelerometers relative to each other did not vary when changing the test configuration.

The final element of the modal testing relationship is the input that was provided via an impulse force hammer. By striking the impact node such that the force is distributed equally along all three axes, the truss is excited through its range of natural frequencies. Two nodes were selected as impulse hammer targets: node 41 and node 24 (Figure 20). Nodes 41 and 24 were chosen in order to excite the truss' entire range of frequencies equally. Node 41 is located on the extreme end of the truss where the first mode shape will have its greatest amplitude (nodes 15, 52, and 26 would work equally well). Node 24 is located midway down the length of the truss, where the higher mode shapes have their greatest amplitude.

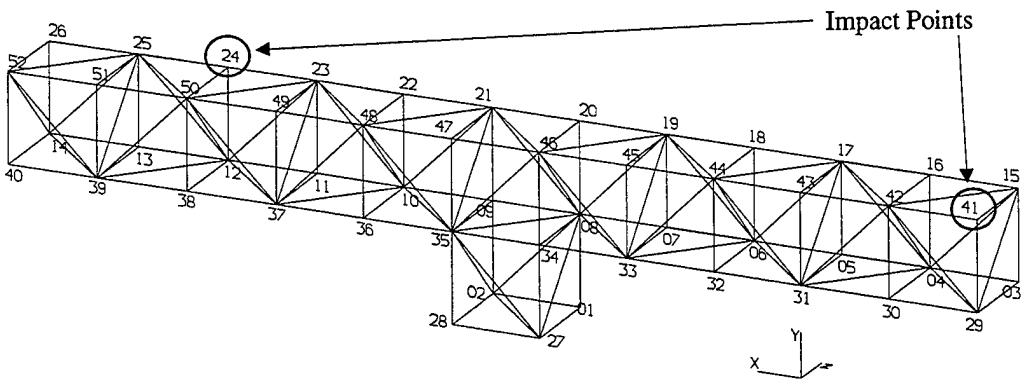

Figure 20. Impact Node Locations

The four accelerometers used in the modal testing of the NPS Space Truss were purchased in February, 1996. They arrived with current calibration certificates, stating that they their calibration would remain within an acceptable tolerance level for at least one year from the date of delivery [Ref. 19]. The PCB® Piezotronics impulse hammer used in the testing was last calibrated August 30, 1989 [Ref. 20]. A simple re-calibration method was devised and implemented in order to acquire accurate modal data.

2. Method of Excitation

Many methods of exciting the truss are available to the user and each method has advantages and disadvantages. Numerous issues need to be considered when selecting the method of excitation: the objective of the testing, the assets available, and the time available to conduct the testing are just a few of these considerations. Two major categories of excitation exist: steady state and transient. Steady-state methods consist of an input that is maintained until enough data points are acquired whereas transient methods consist of an input that is instantaneous and possesses a limited frequency content. A few of the steady state methods include: slow-stepped sinusoidal sweep, stepped sinusoidal, periodic, and random. Two commonly employed excitations in the transient category are the chirp and impact methods. A review of the equipment available at the NPS Space Research Development Center (SRDC) limited the method of excitation

to three options: Steady-state random noise, transient "linear rapid frequency sweep," and a transient instantaneous impact delivered by an impulse hammer.

The first to be considered is the steady-state random method. A random input, in the form of "white" (all frequencies) or "pink" (energy level decays with increasing frequency) noise can be used to excite the truss. Noise is available from most signal generators and can be input into the structure via devices such as an LPACT or piezoceramic strut. Though this method has merit, the requirement of attaching an actuator to the structure dramatically changes the mass and stiffness properties of the truss and therefore alters the structure's modal characteristics. Attempting to acquire modal data on the bare unmodified truss is obviously impossible if an actuator is attached and this method of excitation was disregarded.

Next, is the transient "linear rapid frequency sweep" method. This method is attractive because it provides a flat modulus spectrum and high frequency cutoff rates at the starting and stopping frequencies [Ref. 21]. Additionally, the test time normally involved once the test set-up is completed is relatively short. Once again, an excitation device must be attached to the structure and imposes the same problem discussed with the random method.

An "instantaneous" impact by an impact hammer is a popular form of structural excitation. Although this type of test places greater demands on the analysis phases of testing, it is the easiest to implement and most deterministic. Most importantly, no modifications to the truss are necessary. For these two reasons an impact excitation was selected. Despite its simplicity, this method does have a few drawbacks that are discussed below.

A hammer impulse resembles a half-sine shape. The shape of the time-domain impulse, when transformed into the frequency domain, consist of a nearly constant force over a broad frequency range. By varying the time pulse amplitude and duration, the frequency content can be tailored to excite certain bandwidths with varying magnitudes. Figure 21 is an illustration of the time signal that a hammer blow produces and its corresponding frequency content.

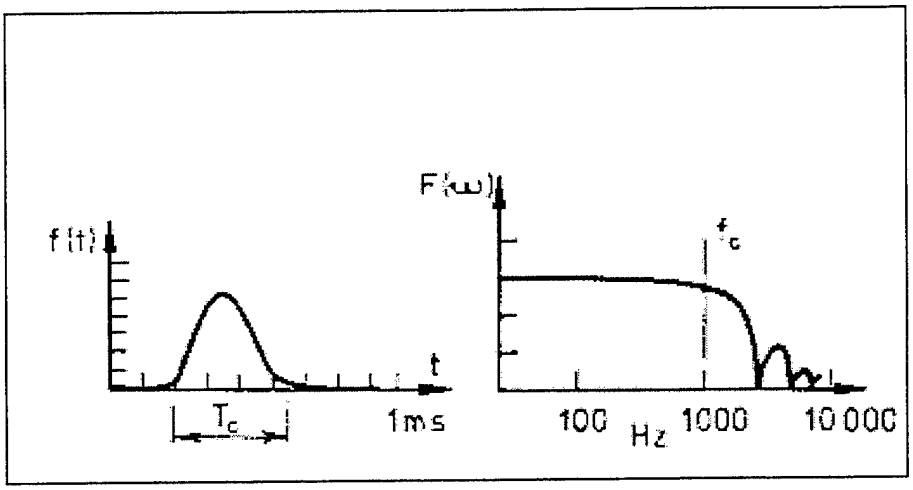

Figure 21. Impact Profile (Time and Frequency Domain) [From Ref. 16]

The hammer's size, length, material and velocity at impact determine the amplitude and frequency content (wave shape) of the force impulse. The frequency content is generally determined by the material of which hammer's tip is and the hammer's mass and velocity at impact determine the FRF's energy content.

A quartz force sensor mounted on the striking face of the hammer measures the hammer's response. The sensing element functions to transfer the impact force into an electrical signal for display and analysis. It is composed of rigid quartz crystals and contains a built-in micro-electronic unity gain, isolation amplifier. The striking end of the hammer has a threaded hole for a variety of impact tips. The tips transfer the force of the impact to the sensor and protect the sensor face from damage. The tip choice can be tailored to achieve specific testing requirements.

Impacting different structures and materials has little or no effect on the impulse hammer's force profile. Figure 22 displays the relative impact force profiles that result from striking structures constructed of various materials. Generally speaking, however, the hammer tip affects the impulse frequency content and the hammer mass affects the signal energy level. Frequency content and energy level are interrelated so both will be affected by different hammer configurations. Hammer velocity at impact affects both

quantities. In general, massive structures with lower stiffness require the use of an additional mass which is in the form of the mass-extender and soft impact tips to adequately excite the lower frequencies [Ref. 20]. Before testing, various combinations of hammer tips and extenders should be examined. Analyze the results for frequency content and insure that the reasonably flat portion of the spectrum is sufficient to cover the structural resonances of interest.

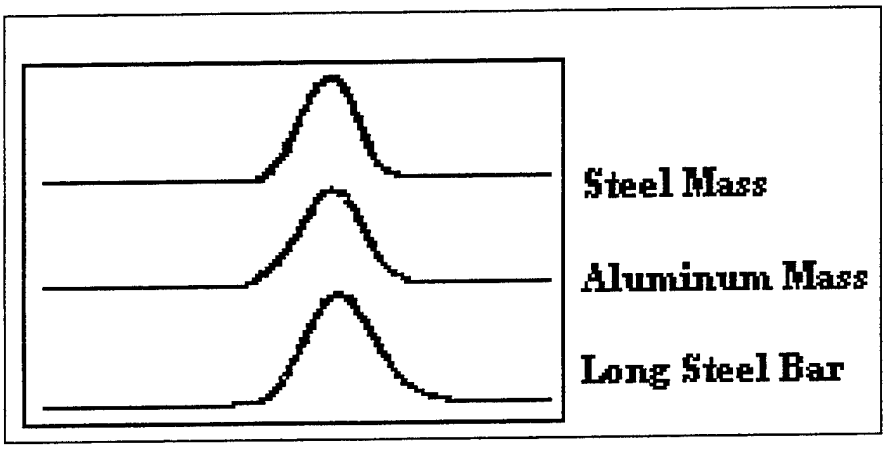

Figure 22. Impact Force Profile [From Ref. 20]

The PCB impact hammer is supplied with three different tips, each manufactured from different material, steel, aluminum, and plastic, and each having a different degree of stiffness. Different impact tips dramatically alter hammer's force signal. The force signals produced by the three tips are shown in Figure 23. A stiffer tip produces a very discrete signal in the time domain which, when transformed, contains a wider frequency bandwidth and is ideal when exciting a structure's higher frequencies. A softer tip produces a signal that is longer in duration and results in the impact energy being concentrated in the lower frequencies. The research conducted in Reference 5 employed a relatively stiff impact tip that was unsuitable for the testing considering the truss' lower first few natural frequencies. This is one of the reasons why the decision was made to retest the NPS space truss. The softest tip available, the red-colored tip, was employed for the follow-on testing.

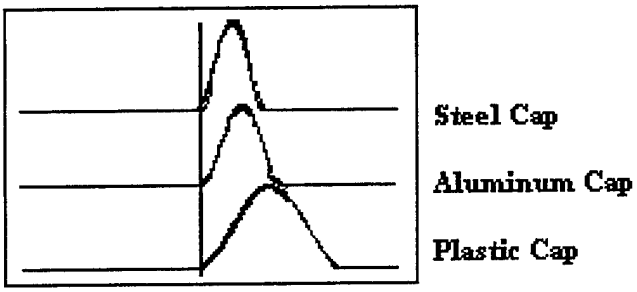

Figure 23. Impact Force Profile of Hammer Tips [From Ref. 20]

3. Impulse Hammer Calibration

In order to estimate the transfer function between the impact node and the surrounding nodes, the input provided by the impulse hammer must be accurately known. To do so we must have an accurate relationship that relates the voltage sensed by the impact hammer when striking the truss to the actual force imparted onto the truss during the impact. In order to find this relationship, a calibration experiment was conducted to determine its sensitivity (k_f).

The sensitivity of the PCB® Piezotronics Impulse Force Hammer used in the space truss modal testing was experimentally determined August 11, 1997 [Ref. 5]. An evaluation of the test procedure revealed some limitations that may have resulted in data that had a higher than expected standard deviation. Additionally, since the custody of the hammer was transferred and subsequently operated after the initial testing, the hammer was re-calibrated.

The test set-up and procedures were identical to that used in Reference 5. The test employed a suspended precision test mass (755.6 g block of aluminum), a calibrated Kistler accelerometer, the PCB® Piezotronics impulse hammer, a signal conditioner, the dSpace data acquisition system, and a host computer with analysis software (Table 3.3). The block, hammer, and accelerometer arrangement are displayed in Figure 24.

The impulse hammer calibration uses the basic Newtonian equation for force:

$$F = ma \tag{3.20}$$

The impulse hammer imparts a force onto the mass. Upon impact, the piezo crystal

Item	Model & Serial #	Calibration value	Mass
Kistler accelerometer	Model # 8690C50 S/N C112865	10.132 g/V where g=9.807 m/s^2	11.2 g
PCB® Piezotronics Impulse Force Hammer	Model # 086B01 S/N 4144	(see test results)	N/A
Aluminum test mass	N/A	N/A	755.6 g (bare), 767.4 g (w/ accel. and adhesive)
Accel. signal condit.	Model # 5124A S/N C74930	N/A	N/A
PCB® Piezotronics Signal Conditioner	Model # 484B S/N 2086	N/A	N/A

Table 3. dSpace Equipment Inventory

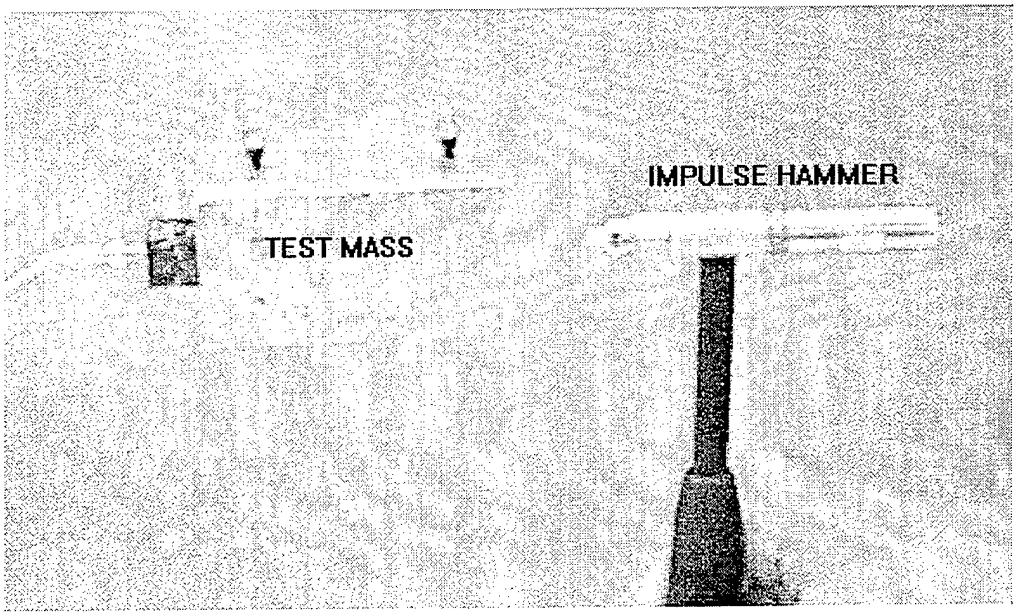

Figure 24. Impulse Hammer Calibration

inside the hammer produces a voltage that is proportional to the magnitude of the impact force. The acceleration is measured in all three axes by a tri-axis Kistler accelerometer. Ultimately, we have equation (3.20), and one unknown, F. To effectively employ Newton's equation, we add the necessary conversion factors to come up with equation (3.21a).

$$k_f \cdot V_f = m \cdot k_a \cdot V_a \tag{3.21a}$$

Rearranging the terms in equation (3.21a) yields the hammer's calibration value or sensitivity

$$k_f = \frac{m \cdot k_a \cdot V_a}{V_f} \tag{3.21b}$$

where: $k_f \equiv$ calibrated hammer sensitivity in N/V

$m \equiv$ test mass (=767.4 grams)

$k_a \equiv$ accelerometer calibration (=10.132 g/V)

$V_a \equiv$ accelerometer voltage reading

$V_f \equiv$ impulse hammer voltage reading

Care should be taken to strike the hanging mass so that it accelerates only in one direction. Additionally, the impact point should be in the center of the block so that no rotation/moment is imparted into the mass. Since the mass is suspended from a height of 15 feet, centrifugal acceleration can be neglected along the direction of the impact vector. Air resistance is also neglected.

Fifty successful tests were conducted. The MATLAB program *hammer.m* was written to calculate the sensitivities based on the relationship presented in equation (3.21b) and is included in Appendix F. While conducting each test, acceleration was measured in all three axis. Ideally, acceleration of the mass should only be in the x-axis. If the x or z-axis acceleration exceeded 15 percent of the y-axis acceleration, the test was disregarded. The testing performed in Reference 5 did not monitor the x or z-axes and resulted in a higher standard deviation. Because the standard deviation calculated during this testing is lower, the final calculated impulse hammer sensitivity is presumed to be more precise. Prior to each test, any swinging of the mass was damped by hand, and the mass itself was leveled using an ordinary carpenter's torpedo level. Table (4) contains the detailed results of the tests, the associated filenames, and the directories in which the data files are saved. The final sensitivity is 9.847 N/V with a standard deviation of 0.8982%.

Directory: Ham.3-5 Test Date: 8 March 1998									
filename	**k_f**	**filename**	**k_f**	**filename**	**k_f**	**filename**	**kf**	**Filename**	**k_f**
cal1.mat	10.052	cal11.mat	10.587	cal21.mat	10.446	cal31.mat	11.367	Cal41.mat	8.712
cal2.mat	9.684	cal12.mat	8.174	cal22.mat	9.022	cal32.mat	8.883	Cal42.mat	10.829
ca3.mat	9.629	cal13.mat	11.992	cal23.mat	9.448	cal33.mat	9.328	Cal43.mat	9.227
ca4.mat	10.663	cal14.mat	8.775	cal24.mat	10.814	cal34.mat	9.085	Cal44.mat	9.192
cal5.mat	9.649	cal15.mat	9.621	cal25.mat	7.996	cal35.mat	10.053	cal45.mat	10.318
cal6.mat	10.504	cal16.mat	10.878	cal26.mat	10.414	cal36.mat	9.577	cal46.mat	8.987
cal7.mat	10.077	cal17.mat	11.220	cal27.mat	11.429	cal37.mat	9.850	cal47.mat	9.750
cal8.mat	10.358	cal18.mat	10.963	cal28.mat	9.708	cal38.mat	8.232	cal48.mat	8.808
cal9.mat	10.042	cal19.mat	9.603	cal29.mat	8.298	cal39.mat	8.938	cal49.mat	9.944
cal10.mat	10.104	cal20.mat	10.244	cal30.mat	10.164	cal40.mat	10.591	cal50.mat	10.129
								ave:	9.847
								std dev:	.8982%

Table 4. Impulse Hammer Calibration Test Results

4. Accelerometer Setup

Pertaining to this research, accelerometers were used to measure the truss response during modal testing. The proper placement and setup of the accelerometers are of considerable significance. Kistler accelerometers, model 8690C50, were used in the modal testing. Model 8690C50 has a 50 g maximum sensitivity range (g = 9.807 m/s^2). The SRDC possesses a model 8690C10 accelerometer that has a 10 g maximum sensitivity range. Since only four accelerometers were employed during the modal testing, the 50 g accelerometers were chosen for testing throughout to maintain consistent testing conditions and to avoid signal overloads when the accelerometers were mounted on nodes near the impact node. The eight accelerometers purchased by the Naval Postgraduate School arrived with current calibration certificates, stating that their calibration would remain within an acceptable tolerance level for at least one year from the date of delivery. The calibration expired February 27, 1998 [Ref. 19].

The preferred mounting adhesive for the Kistler model 8690C10 and C50 accelerometers is the Kistler supplied Petro Wax from Katt & Associates in Zoar, Ohio. [Ref.19]. Before applying the wax adhesive, clean the flat surface of the thumbscrew with ordinary alcohol. Attach the accelerometer by applying a thin (~0.1 mm) layer of wax to the flat surface of the thumb screw and attaching the accelerometer to this layer with firm finger pressure and an alternating twisting motion. Once the accelerometer is attached, connect the cable. Immediately after connecting the cable, use a "ziplock"-type fastener to fasten the accelerometer cable to a truss strut. The cable should be fastened to the truss approximately four to five inches from the accelerometer connection. This protects the accelerometer from falling and damaging itself should the wax adhesive fail. Figure 25 shows an accelerometer mounted to node 41 as well as the attached impact thumbscrew. After being mounted, the accelerometer was leveled using a simple carpenter's torpedo level to align the accelerometer along the three axes.

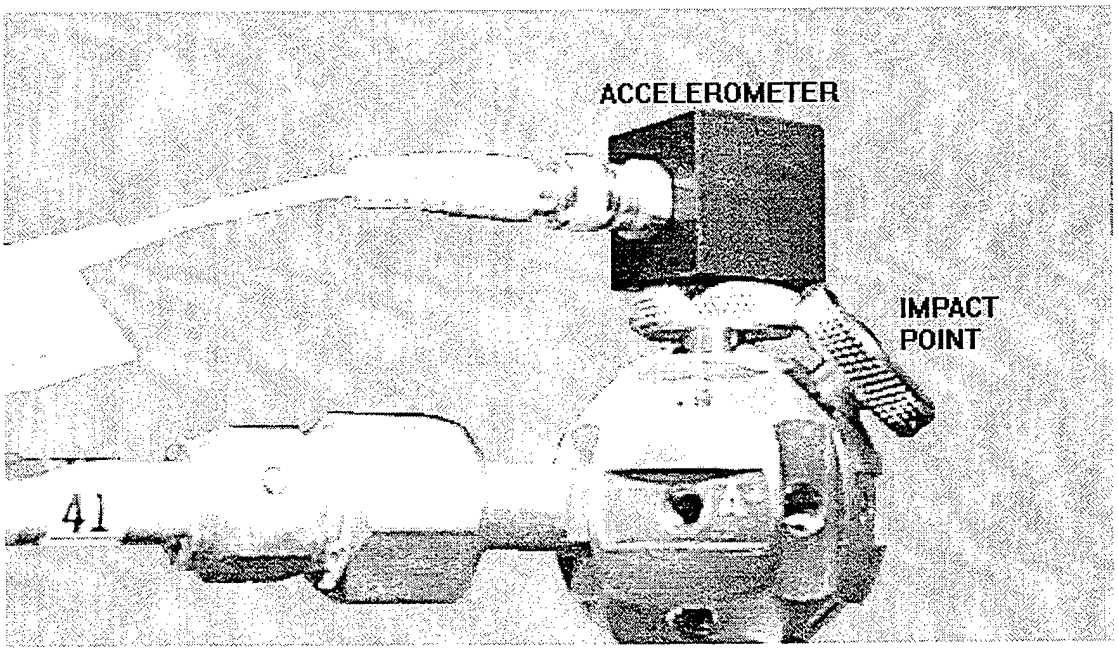

Figure 25. Accelerometer Placement (w/ Impact Point)

The type of data sought determines the accelerometer placement. In order to obtain a global set of data all nodes of the truss should be tested. Using only four

accelerometers will require twelve separate configurations in order to test the 48 nodes[6]. The various accelerometer configurations are discussed in Section D below and are detailed in Appendix D.

It should be noted that during testing, the accelerometer axis orientation was different from that of truss axis orientation. Both the truss and the accelerometers have a conventional right-handed coordinate system. The electrical connectors on the accelerometers prevent mounting them in a manner that aligns their axis with the axis of the truss. It will be import to remember this while analyzing the data. The transformation between the coordinate systems is:

Accelerometer	Truss
+ x	+ x
+ y	- z
+ z	+ y

Using the above template, the global orientation between the truss coordinates, accelerometer coordinates, and dSPACE output channels is displayed in Table (5). The cable number, which identifies an input cable, is attached to a specific accelerometer during each test.

5. Electronics Setup

There are several pieces of electronic equipment used during the dSPACE modal testing. The accelerometers are connected to a Kistler twelve-channel couplers (or signal conditioners), model 5124A. These signal conditioners include a current regulator, buffer amplifier and decoupling network that removes the DC bias and passes the dynamic signal as output [Ref. 22]. Three separate acceleration signals are generated by each accelerometer, corresponding to the x, y, and z axes. Each signal is carried on its own wire from the accelerometer to the signal conditioner. Each accelerometer connection cable consists of four internal wires that carry a signal: x-axis, y-axis, z-axis, and the

[6] The four nodes fixed to the base plate are not tested.

cable	channel #	truss axis	accel. axis
1	1	x	x
	2	-z	y
	3	y	z
2	4	x	x
	5	-z	y
	6	y	z
5	7	x	x
	8	-z	y
	9	y	z
6	10	x	x
	11	-z	y
	12	y	z
n/a	25	(hammer)	

Table 5. Accelerometer – Truss Alignment

ground. The signal conditioner amplifies the three separate signals which are fed into dSpace (the Analog to Digital (AD) data acquisition system) via ordinary coaxial cables (one per axis, or three per accelerometer). The accelerometer signals occupy channels one through twelve on the AD connection board. The impulse hammer is connected to its own signal conditioner. The output of the hammer signal conditioner is split by a co-axial splitter and fed into dSpace and into an oscilloscope. Ultimately, thirteen channels are fed into dSpace (12 from the accelerometers and one from the impulse hammer). Finally, dSpace is connected to a desktop PC that displays the acquired data and saves the data as *.mat* files for further analysis.

D. dSPACE DATA COLLECTION

A total of 240 tests were conducted during modal testing of the NPS Space Truss. The data files from these tests, saved as *.mat* files, are located on the dSpace interface computer (desktop PC) in the directory *c:\andberg\truss`I\impact*. A detailed list of the filenames and the dates on which the testing were conducted is located in Appendix E. Each test is a collection of data over the thirteen channels.

The dSpace System was configured for a 5 kHz sampling frequency over a period of 3.0 seconds. Recall, that the data acquisition duration was the primary reason for re-

testing the NPS Space Truss. Previous testing acquired data for a period of 0.5 seconds limiting the FRF resolution to only 2.0 Hz. Setting the acquisition duration to 0.3 seconds yields a FRF resolution of 0.333 Hz. Utilizing the Nyquist criteria, a 10kHz sampling frequency will allow frequencies up to 5 kHz to be detected. For each test, data collection was initiated when the hammer output attained a predetermined trigger level, which was set to 0.2 mV. This filters out any weak, hammer impacts, and kept the computer from recording data until after the truss had been excited.

Before the commencement of testing ensure that the oscilloscope is powered on and that one of the impulse hammer leads is fed into the "channel 1" port on the face of the oscilloscope. Setting the oscilloscope to 1.0 Volt/division and 500 μsec/division provides the best display of the impulse hammer signal. Enabling the "Auto-store" feature holds the signal on the oscilloscope display. After each impact, the oscilloscope y-axis cursor is used to identify the peak magnitude of the impulse, these results are displayed in Appendix E.

After turning on the signal conditioners each channel's line must be tested by pressing the Front Panel Line-Test button. A green LED indicates a good condition whereas a red LED indicates that either, the cable is damaged, there is an bad connection, and/or the accelerometer itself is damaged.

To initiate dSpace, turn-on the dSpace host PC, turn on dSpace, invoke MATLAB and change directories to *c:/andberg/dspace*. At the MATLAB prompt type *newmode*. When the SIMULINK block diagram appears, go to the "code" pull-down option and select "generate real time" (Figure 26). This will open a DOS window, generate the code, and report "download succeeded", unless there is an error. At this point, close the DOS window, minimize the SIMULINK window, and execute the program *trace_40w.exe*, whose icon is in the Microsoft Toolbar. Within the TRACE window go the "file" pull-down option and select "load", load file *newmode.trc*. Again in the "file" pull-down option select "open", and open experiment file *4mode.exp*.

To begin collecting data, the impulse hammer should strike an impact point on the truss. It is important that the impact vector be equally distributed along all three axis of

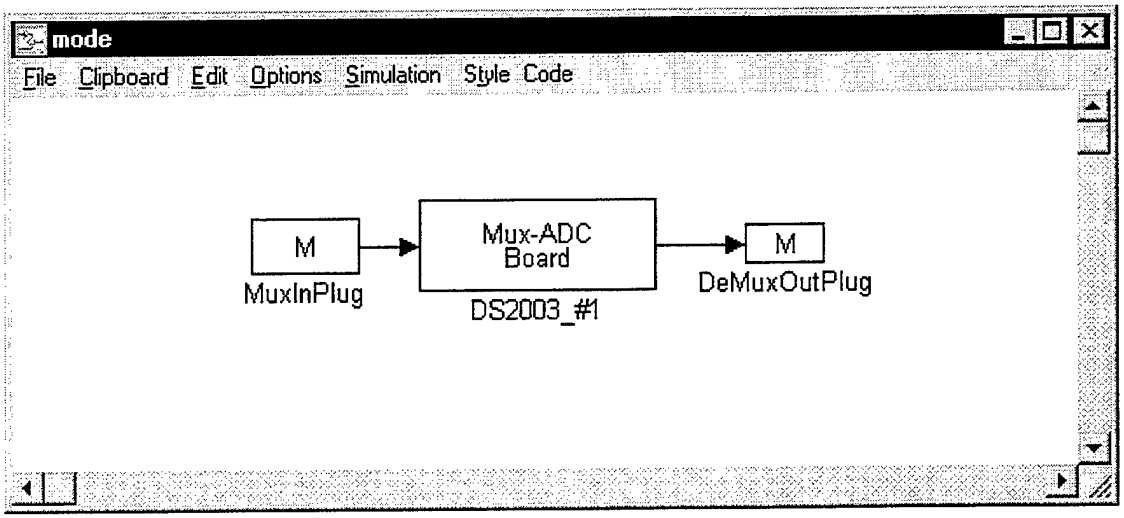

Figure 26. SIMULINK Window: *newmode.m*

the truss (Figure 27). The overall input, provided by the impulse hammer was decomposed into x, y, and z components. These simple coordinate transformations into the truss coordinate system are express in the following equations:

$$\text{x axis input value} = \cos^2(45^\circ) \text{ x (Hammer Input)} \quad (3.33a)$$

$$\text{y axis input value} = \sin(45^\circ) \text{ x (Hammer Input)} \quad (3.33b)$$

$$\text{z axis input value} = \cos(45^\circ) \text{ x } \sin(45^\circ) \text{ x (Hammer Input)} \quad (3.33c)$$

The truss' x and z-axes are scaled the by a factor of 0.5 and the truss's y-axis is scaled by a factor of 0.707. Each impact with the hammer should produce a clean spike as displayed on the TRACE software. If multiple impacts are detected the test should be disregarded. Read from the oscilloscope, accepted impacts ranged from 1.75 V to 5.00 V. If the impact magnitude fell outside this range the test was disregarded. Periodically the hammer would fail to trigger dSPACE and likewise these tests were disregarded. The same individual should apply the impact hammer for each test for consistency. After each test it is important to damp the truss by gently holding a strut for a few seconds. Also, a periodic check of the accelerometers' alignments with the carpenter's level will prevent the possibility of corrupted data from a miss-aligned accelerometer.

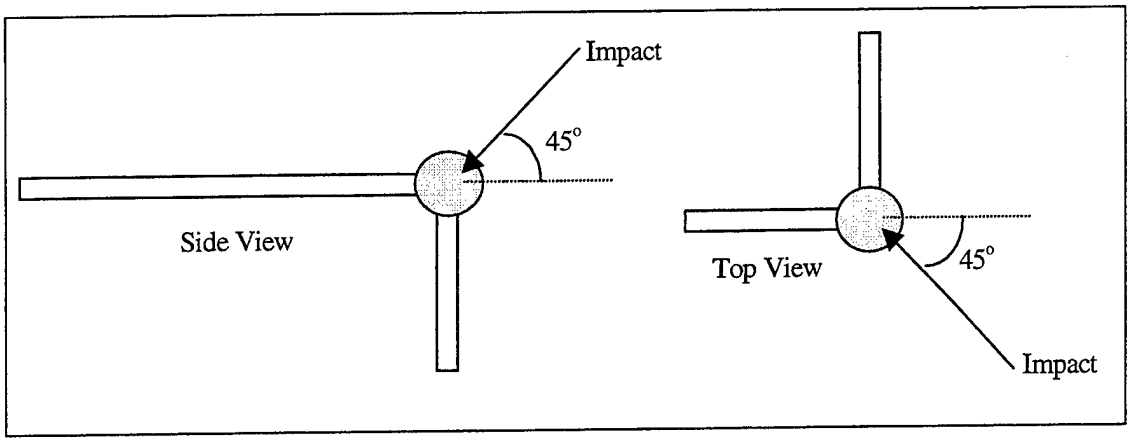

Figure 27. Impulse Hammer Impact Alignment

Commencing at one end of the truss, an accelerometer was placed on nodes 3, 15, 29, and 41. Ten tests at each impact node were conducted for this accelerometer configuration. After testing each accelerometer configuration, the four accelerometers were moved down one bay to the next four nodes. The position of the accelerometers relative to each other did not vary when changing test configurations. All twelve bays were tested resulting in a grand total of 240 test. Averaging ten tests minimized the possibility of bias towards a particular axis or the introduction any other anomalous effects.

E. dSPACE DATA ANALYSIS

The first step in analyzing the dSPACE modal data was to develop a MATLAB code that allowed the user to process and display the accelerometer data while taking into consideration the inherent sensitivities of the accelerometers as well as the impulse hammer impact scaling. Two programs were developed to perform these functions, *tfeavga.m* and *tfeavgb.m* (Appendix G). Each program is associated with the impact node used during testing: *tfeavga.m* processes data collected for node 41 impacts and *tfeavgb.m* for node24 impacts. There are no functional differences between the two programs.

Both programs use the *tfe.m* (Transfer function estimate) function available in the MATLAB Signal Processing Toolbox [Ref. 17]. The program will find a transfer function estimate, T_{xy}, given an input signal vector, x, and output signal vector, y. The resulting transfer function, which is the quotient of the cross spectrum of x and y and the power spectrum of x, is given in equation (3.34) [Ref. 17: p. 2-218]:

$$T_{xy}(f) = \frac{P_{xy}(f)}{P_{xx}(f)} \tag{3.34}$$

During modal testing, the input is taken from channel 25, the impulse hammer, and the output comes from the twelve, accelerometer channels.

Unlike the research conducted in Reference 5 where each set of data was processed individually, multiple tests were conducted for each accelerometer configuration and the data averaged. Averaging the data in the frequency response (FRF) domain is not possible because the phase (the imaginary portion) can not be accounted for. To average the data the power spectral density (PSD) was computed. When constructing the PSD, the phase information is discarded leaving only the amplitude information, which can be averaged

Executing *tfeavga.m* or *tfeavgb.m* overlays the transfer function estimates for the x, y, and z axes on the same plot. The test results for nodes 41, 44, 49, and 52 are presented in Appendix H, all data files are contained in the SRDC and the plotted data of all the nodes are contained on the thesis processing station in the directory *c:/truss-control/dspace/data*. The natural frequencies identified are shown in Table 6.

dSPACE		
Mode Number	ω_n(rad/s)	frequency (Hz)
1	859.87	15.00
2	1031.85	18.00
3	1929.55	33.66
4	1986.88	34.66
5	3706.62	64.66
6	4394.52	76.66
7	4929.94	86.00
8	5770.32	100.66
9	7452.23	130.00
10	7700.45	134.33

Table 6. NPS Space Truss Natural Frequencies (dSPACE)

For several different reasons, minimal analysis was performed on the dSPACE data. First, the primary emphasis of the modal testing was to create a file that contained the mode shapes of the truss and use the X-Modal software to animate the mode shapes. The experimental analysis software "X-Modal" was selected because it can generate the mode shape file when provided the experimental data and then graphically animate each mode[7]. Using X-Modal requires the data to be in Universal-58 format. Converting the dSPACE *.mat* files into a Universal-58 format that is compatible with X-Modal is a complex and time consuming process.

Similar modal testing research was conducted at the Naval Research Laboratories [Ref. 1]. Initially NRL used dSPACE, but after preliminary testing it was judged to be inadequate due to the limited dynamic range of the system and the injection of noise into the data stream. Lastly, dSPACE's limited memory capacity was identified as a significant handicap and further research using this system was not pursued. If dSPACE is elected to be used again for modal testing, increasing the memory capacity needs to be considered. More memory can be purchased from the manufacturer, but because it is "static" memory the expense is significant.

---

[7] The mode shape file was created using IDEAS software, but X-Modal was still used to display the mode shapes.

F. HEWLETT PACKARD 35655A EXPERIMENTAL SETUP

Analysis of the data obtained using dSPACE emphasized the need for a more reliable data acquisition system, principally a system that is designed specifically for signal analysis. Manipulating the dSPACE data was labor intensive and analysis of the data was difficult. Ultimately the Hewlett Packard 35665A was selected. The HP-35665A is specifically designed for signal analysis and its data handling protocol is extremely efficient. Disregarding the fact that the HP-35665A is also a two-channel signal analyzer, the memory capacity and the user-friendly operating features are much more attractive than the dSPACE system.

1. Overall System

The Hewlett Packard 35665A Dynamic Signal Analyzer is a two-channel FFT spectrum/network analyzer with a frequency range that extends from nearly DC to just over 100 kHz. The HP-35665A is most commonly employed to provide measurement solutions in vibration, acoustics, and control systems. Although the HP-35665A is primarily a frequency-domain analyzer it can be employed to make time-domain and amplitude-domain measurements. Signal characterization in the frequency domain is an important contrast to the more traditional oscilloscope – an instrument that characterizes signals in the time domain. The oscilloscope normally displays a parameter (usually amplitude) versus time compared to the spectrum analyzer that compares the same parameter versus frequency [Ref. 23].

2. Accelerometer Setup

The accelerometer placement and setup during modal testing using the HP-35665A is identical to that of dSPACE, with a few exceptions. The differences include the number of accelerometers used during each test, the absence of dummy masses, and the selection of the accelerometer's sensitivity. The mounting, alignment, and coordinate axis alignment procedures are identical to the procedures described in Section C,

Subsection 4.

Because the HP-35665A is only a two channel signal analyzer, testing was time consuming and laborious. Channel 1 was occupied by the impact hammer to provide input into the system and trigger data collection, and channel 2 was occupied by one axis of the accelerometer. Rather than analyzing all three axis of four nodes during each test as in the dSPACE testing, only one axis of one node is being analyzed during each test.

Initially, this generated concerns regarding the introduction of error due to inconsistencies associated with the moving and realigning the accelerometer multiple times to allow testing of the entire structure. However this is a misconception, regardless of how many accelerometers are employed during testing, each accelerometer requires alignment. Secondly, conducting 312 test vice 48 will not produce inconsistencies since the results generated by the signal analyzer are a function of the input relative to the output. Therefore variations in the magnitudes of each impact will not affect the validity of the data. Regardless, all nodes should be tested simultaneously. This is reaffirmed by the research conducted at the Naval Research Laboratories. Using a Hewlett Packard multi-channel signal analyzer, NRL tested all nodes simultaneously.

Employing a single accelerometer during each test has some advantages. Since multiple accelerometers were no longer used, the dummy masses simulating the accelerometers used in previous testing were not required during testing with the signal analyzer. When attached to the truss, the total mass of eight accelerometers is significant and not compensating the unsampled nodes with dummy masses would result in flawed data. The mass of a single accelerometer, however, is negligible and the associated error is insignificant. As a result, the truss was tested with only one accelerometer and closely approximated a true "bare" truss. Since the mass properties of the finite element model did not include the mass of the accelerometers, employing only one accelerometer during testing will decrease the divergence of the experimental model to the analytical model.

The next step in preparing the NPS Space Truss for modal analysis is accelerometer placement and setup. Because the HP-35655A was limited to analyzing one axis during each test, the same accelerometer was used throughout testing to maintain

consistency and minimize the introduction of errors that could result from using different accelerometers. Accelerometers mounted on the extreme end nodes experience the greatest accelerations because the first two mode shapes contain the most energy at these nodes. To avoid overloading the accelerometer when mounted on the ends of the truss during testing the less sensitive 50g accelerometer was selected.

All three axes of each node (excluding the four base nodes) were tested in order to obtain a global picture of the truss' response and resulted in a total of 288 tests being conducted. Employing only one accelerometer was time consuming and labor intensive, therefor each node was tested only once. If this testing is to be re-performed a more capable multi-channel spectrum analyzer should be used to perform the testing. This would not only be much quicker but also present fewer opportunities for the introduction of error.

The same accelerometer axis orientation employed in the dSPACE testing was used. It is worth noting again that the accelerometer axis coordinates are different than the truss coordinates. It will be extremely important to remember this while analyzing the data especially when preparing files for use with the "X-Modal" software.

3. Electronics Setup

Unlike the modal testing utilizing dSPACE, the electronics setup employed with the HP-35665A is relatively simple. The tri-axis Kistler accelerometers are still the fundamental device used for measurement during testing. Since the HP-35665A is a two channel analyzer only one axis of a mounted accelerometer can be analyzed during each test. The dSPACE system is a PC based data acquisition system and requires a digital to analog (DAC) signal converter. Although the HP-35655A is also a digital system, it possesses its own DAC and as a result eliminates the need for a supplementary DAC. Accelerometer voltage outputs pass thru the Kistler signal conditioner and are fed directly into the signal analyzer via an ordinary coaxial cable. Similarly, the impulse hammer is connected to its own signal conditioner, which in turn is fed into the signal analyzer. Figure 28 illustrates the experimental arrangement used for the HP-35665A modal

testing.

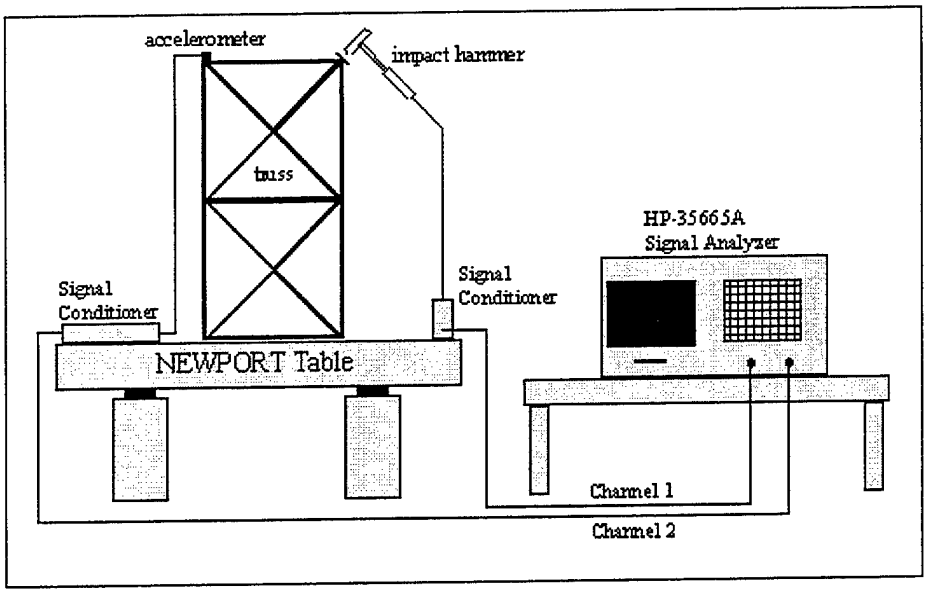

Figure 28. HP-35665A Experimental Setup

Configuring the HP-35665A for the impact modal tests is described in a step-by-step format in the equipment operator's guide (Reference 24). To avoid difficulties that may be encountered when using the HP-35665A and to shorten the learning curve for the user that wishes to reproduce the testing or perform similar testing, the steps involved in configuring the equipment are discussed in more detail below:

Step 1: Turn on the spectrum analyzer.

The 1/0 (power) switch is on the front panel of the machine. Depress the "1" side of the switch.

Step 2: Connect the impact hammer to the analyzer.

Connect the BNC cable from the hammer signal conditioner into the "Channel 1" BNC port on the front of the machine.

Step 3: Connect the accelerometer to the analyzer.

Connect the BNC cable from the accelerometer signal conditioner into the

"Channel 2" BNC port on the front of the machine.

Step 4: Preset the analyzer.

Presetting returns most of the analyzer settings to their default positions.

>Press [**Preset**][8] and press [DO PRESET].

Step 5: Define the analyzer instrument mode.

This configures the analyzer to make two channel measurements. Network measurements (such as impact testing) can only be made in two channel mode.

>Press [**Inst Mode**] and press [2 CHANNEL].

Step 6: Define the analyzer's frequency bandwidth.

The HP-35665A obviously has a finite memory capability and therefore can analyze only a limited amount of data during each test. Three parameters, frequency bandwidth [SPAN], resolution [RESOLUTION], and duration of data collection [RECORD LENGTH] are all inter-related and are a function of the amount of memory the analyzer possesses. A very narrow bandwidth can be analyzed with very high resolution with the test duration lasting for tens of seconds or a wide bandwidth may be analyzed with very high resolution with data being collected for approximately 0.5 seconds. Remember that collecting data for only a half second will provide an unacceptable frequency resolution of 2 Hz. Resolution is defined by the number of lines of data that are collectively analyzed during the Fourier analysis. The fewer the number of lines analyzed, the more

[8] A bolded, bracketed command (ie. **[Xxxx]**) refers to the actual buttons on the machine face, while the [XXXX] refers to the "ghosted" options displayed on the machine display.

accurate the results. Therefore, a 400 line resolution is more accurate than 800 line resolution. Recall that frequency resolution is inversely proportional to the test duration. If the test duration is 2 seconds then the frequency resolution will be 0.5 Hz. Likewise if the testing duration is 0.25 seconds the frequency resolution will be 4 Hz.

The objectives of the testing will dictate what each of these parameters should be. The key is to identify the optimal combination of the three above parameters. For the space truss modal testing these parameters were set as follows: [SPAN] = 200 Hz, [RESOLUTION] = 800 Lines, and [RECORD LENGTH] = 4 Seconds.

The frequency bandwidth may be entered by pressing [**Freq**] on the front face of the machine and then entering the desired value from the key pad or by using an attached keyboard. Additionally, the frequency bandwidth may be varied by pressing the [↓] or [↑] or by turning the knob on the front face of the analyzer left or right to achieve the desired setting.

Step 7: Select the Display Format.

When initially powered on, the HP-35665A only displays the magnitude plot. To view both magnitude and phase, two traces are needed.

>Press [**Disp Format**] and press [UPPER/LOWER].

Step 8: To Display frequency response on trace A.

>Press [**Meas Data**] and press [FREQUENCY RESPONSE].

Step 9: To Display frequency response on trace B.

By pressing [**Active Trace**] the working trace will flip between trace A and trace B.

>Press [**Active Trace**] and press [FREQUENCY RESPONSE].

Step 10: Define Trace B coordinates.

The analyzer now displays dB magnitude on trace A and phase on trace B.

>Press [**Trace Coord**] and press [PHASE].

Step 11: Define channel 1 (Impact Hammer) input range.

The analyzer has 40 pre-programmed input ranges, ranging from –51 dBVrms to +27 dBVrms in 2 dB increments. The user can set the input range manually, or can use the analyzer's autoranging feature. If autoranging is on, the analyzer automatically selects a less-sensitive range if the signal exceeds the current input range. To make the best measurement possible, the user should carefully consider the method used to set the input range, by setting the range manually or using autorange. The maximum and minimum ranges are display below in Table 7.

Maximum Input Range (+27dBVrms) and its Maximum Values in equivalent units			
DBVrms	dBV(peak)	Vrms	V(peak)
+27 dBVrms	+30.01 dBV(peak)	+22.39 Vrms	+31.66 V(peak)
Minimum Input Range (-51dBVrms) and its Minimum Values in equivalent units			
DBVrms	dBV(peak)	Vrms	V(peak)
-51 dBVrms	-47 dBV(peak)	+2.818 mVrms	+3.986 mV(peak)

Table 7. Minimum Input Range Digital Signal Analyzer

When autoranging is on, the analyzer continuously monitors the amplitude of the input signals and, if necessary, automatically selects the input range. If the input signal increases enough to exceed the current input range, the analyzer changes to a less-sensitive scale. If the measurements are averaged and autoranging occurs, the analyzer will initiate a new series of averages. Autoranging for the HP-35665A is an "autorange up" feature. When the measurement is started the analyzer sets the input to the most sensitive range and

automatically steps up through less-sensitive input ranges until the input channel is no longer overloaded.

The input range may also be entered manually. This is the ideal method when the user wishes to preserve the dynamic range and ensure the best possible measurement. Ideally, the signal peak should fall in the upper half of the input range. If the input range is set too low (more sensitive than necessary), the analyzer's input circuitry will introduce distortion into the measurement. If the input range is set too high (less sensitive than necessary) however, the resulting loss of dynamic range will introduce additional noise, and in some cases causes the low-level frequency components to be obscured by the increase in the noise floor.

If the input signal exceeds the current input range, or exceeds +27 dBV if autoranging is enabled, an overload condition will be displayed. An overload condition will be indicated by the **Ov1** or **Ov2** status messages as well as the **OVLD** status message that may appear at the bottom of the trace display. The analyzer's response to an overload condition varies. If autoranging is enabled, an overload condition simply causes the analyzer to change to a less-sensitive input range, unless the maximum input range is already selected. In some cases, the **OVLD** message remains on the display even when there is no longer an overload condition. This indicates that the overload condition has affected the measurement in progress.

Determining the impact hammer input range is a simple procedure. The hammer signal is fed from the PCB signal conditioner to a HP-54601A, four-channel oscilloscope. The oscilloscope's auto-store feature is used to retain the voltage trace from the impact hammer on the oscilloscope display. The settings on the oscilloscope that optimized the display were a **TIME/DIV** setting of 5 msec/division and a **VOLT/DIV** setting of 1 volt/division. A series of 20 impacts was executed and the traces held on the oscilloscope. By examining these traces the average hammer peak voltage was calculated to be 1.5 volts, or 1.7609

dBVpeak. This value was entered into the HP-35665A for the channel 1 input. The machine defaults up to 2.0103 dBVpeak, the next pre-set input range.

>Press [**Input**] and press [CHANNEL 1 RANGE].

>From the keyboard, type 2.0103, press [dVBpk].

Step 12: Define channel 2 input range.

A similar procedure is followed to determine the channel-2 input range. The same accelerometer that was used during modal testing (serial number C112868) was attached to node 3 of the space truss. The signal from the accelerometer was fed thru the Kistler signal conditioner, and into the four-channel oscilloscope. The oscilloscope auto-store feature was enabled, the **TIME/DIV** setting was 5 msec/division, and the **VOLT/DIV** setting was 1 volt/division. A series of 20 impacts was executed and the voltage traces held on the oscilloscope display. The accelerometer output voltages are sinusoidal and exponentially decay in nature, therefor only the initial peaks on the display were considered. The average, initial (first), accelerometer peak voltage was calculated to be .3 volts, or -5.22879 dBVpeak. This value was entered into the HP-35665A for the channel 2 input. Again the machine defaults up to –3.9897 dBVpeak (.67 volts), the next pre-set input range.

>Press [**Input**] and press [CHANNEL 1 RANGE].

>Press [+/-] and type –3.9897, press [dVBpk].

Step 13: Define data acquisition trigger.

This step will instruct the analyzer to identify channel 1 as the data acquisition trigger.

>Press [**Trigger**] and press [CHANNEL 1 TRIGGER].

Step 14: Define trigger threshold level.

The threshold level identifies the minimum channel 1 voltage level that triggers data acquisition.

>Press [TRIGGER SETUP].
>Type 5 on the keyboard and press [PERCENT].

Step 15: Define channel 1 delay.

This step instructs the analyzer to begin the measurement 1.0 ms before the trigger signal, allowing capture of the leading edge of the impact hammer signal.

>Press [+/-] and type 1.9513 and press [ms].

Step 16: Define channel 2 delay.

This step instructs the analyzer to begin the measurement 1 ms before the trigger signal matching channel 1.

>Press [+/-] and type 1.9513 and press [ms].

Step 17: Define channel 1 (Impact Hammer) force window.

A window is a time-domain weighting function applied to an input signal. It is a filter used to remove signals that are not periodic (therefore spurious) within the input time record. This makes the input time record appear to be periodic, usually by forcing the amplitude to zero at both ends of the time record.

Ideally, the impulse delivered from the impact hammer should be a delta function, exciting all frequencies equally. The impact, however, is not infinitely discrete in the time

domain and is more accurately described by a half-wave of sinusoid and therefore a *Force* window is applied to the impact hammer input.

The *Force* window passes the first part of the time record and sets the last part to a fixed value (Figure 29). The user specifies the width of the window, thus controlling where the fixed level begins. The width that is specified determines how much of the signal is passed. Note that the width must be narrower than the duration of data acquisition (time record) for the force window to be effective. The force window is ideal for impact testing because it removes residual oscillations in lightly damped systems. The HP-35665A allows the force window to be used simultaneously with the *Exponential* window that is applied to channel 2. This allows the user to superimpose the windows when conducting measurements employing both channels and is ideal when measuring properties of mechanical structures during impact testing.

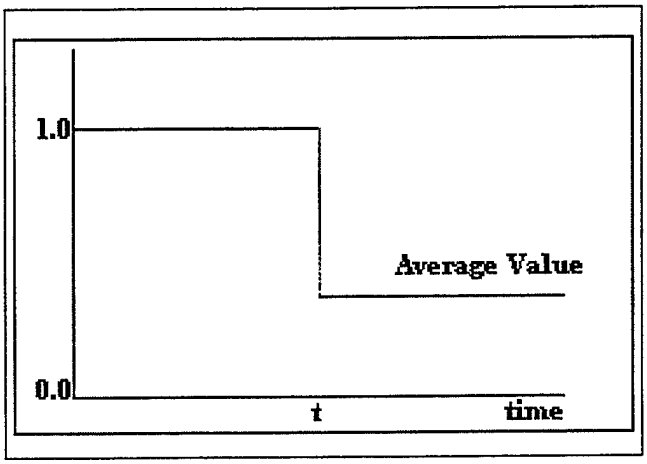

Figure 29. Force Window

When using the force window, the width of the impact force is required. Following the same procedure and equipment setup used to determine the input ranges, the force width was determined. Displaying the impact hammer impulse on the oscilloscope, the total impulse duration and peak voltage can be observed. The half power of the peak voltage (3 dB drop) was calculated and the corresponding time is interpolated from the impulse trace. In essence, a half power top hat window was created.

Interpolating off the oscilloscope display, the force width was determined to be 20 mseconds.

>Press [**Window**] and press [FORCE EXPO].

>Toggle to [CHANNEL 1 **FORCE** EXPO] .

>Press [FORCE WIDTH], type 20, and press [mS].

Step 18: Define channel 2 (Accelerometer) exponential window.

The *Exponential* window attenuates the input signal exponentially at a rate that is determined by a specified time constant. Values between 0.1 mico-second and 9.99×10^6 seconds may be entered. The exponential window is ideally suited for lightly damped systems that do not decay within one time record. Generally the time constant should be set to one-fourth of the time record for the window to be effective. Since the duration of the data acquisition (time record) is four seconds the time constant is one. If a Force window is applied to channel 1 and an Exponential window is applied to channel 2, the data for channel 1 is multiplied by both the Force and the Exponential windows (Figure 30).

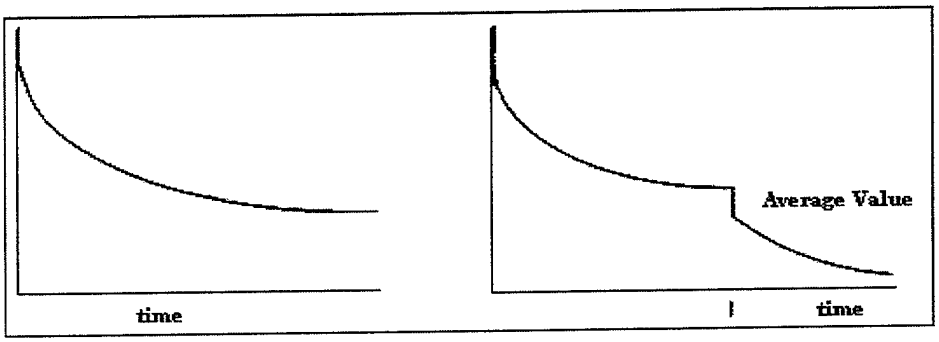

Figure 30. Exponential Force Window

>Press [**Window**] and press [FORCE EXPO].

>Toggle to [CHANNEL 2 FORCE **EXPO**]

>Press [EXPO DECAY], type 1, and press [SEC].

To save the test data the HP35655A is equipped with 3.5 inch floppy disk drive. The data can be directly transferred from the machine to a normally formatted disk for storage. Saving the data is uncomplicated and the procedure is as follows. After the completion of each test ensure that a formatted disk is inserted into the analyzer's drive.

> Press the [**Disk/Util**] button located on the face of the analyzer.

>Press [SAVE DATA]

>Press [SAVE TRACE]

>Press [INTO FILE].

The user will be prompted to input a file name. The file name may be entered by two different methods. First, each character on the keypad is assigned a alphabetical equivalent, once this letter assignment is decoded the filename can be entered. Or secondly, and the easiest method, a keyboard can be attached to the analyzer and the file name can simply be typed in, of course followed by the enter key.

G. HP-35665A DATA COLLECTION

A total of 288 tests were conducted during the course of modal testing. All data files collected were saved as *.dat* files (Hewlett Packard Standard Data Format) and were loaded onto 1 GB floppy disks (ZIP disks) which are maintained in the NPS Dynamics Laboratory. A complete listing of the data filenames is located in Appendix I. Each test is a collection of data for one axis of one node.

The HP-35665A was configured as described in Section F, Subsection 3. A few key parameters are worth noting again. The bandwidth analyzed was 200 Hz, the sampling duration was 4.0 seconds providing a 0.25 Hz frequency resolution, and the sampling line resolution was 400 lines. Provided the HP-35665A is properly configured for impact testing, striking the truss with the impulse hammer will trigger data

acquisition. For modal testing of the NPS Space Truss, the trigger level was set to 0.2 mV (impact hammer voltage).

The test procedures for the HP-35665A are similar for those of the dSPACE system. After turning on the signal conditioners and making sure that the accelerometers are securely connected to them, each channel's line must be tested by pressing the Front Panel Line-Test button. A green LED indicates a good condition whereas a red LED indicates that either the cable is damaged, there is an bad connection, and/or the accelerometer itself is damaged. To initiate HP-35665A data analysis simply press the **[Start]** button on the front of the machine at which time the message "waiting for trigger" will appear in the upper left hand corner of the screen. To begin collecting data, the impulse hammer should strike an impact point on the truss. Ensure that the impact vector be equally distributed along all three axes of the truss as described in Section D. The HP-35665A was configured to collect and average a series of three impacts, which should minimize the possibility of any bias towards a particular axis.

H. HP-35665A DATA ANALYSIS

1. Data Conversion

When saved, the data is formatted in the Hewlett Packard Standard Data Format and is appended with ".dat". It is necessary to convert this data to a familiar format. Provided with the analyzer is a set of utilities diskettes. Specific programs contained on the utilities diskettes convert the data from Standard Data Format to other formats. Formats of interest are those compatible with the MATLAB and X-Modal software, *.mat* and the Universal-58 *.unv* format respectively.

To perform the data format conversions the utilities program and the data files to be converted need to be in the same directory. The utilities program, *sdftoml*, converts data from the SDF format to the MATLAB *.mat* format. The created files will automatically have the suffix *.mat* appended unless otherwise specified by the user.

Similarly the utilities program, *sdftounv.m*, converts the SDF formatted data to a Universal-58 format. Universal-58 is a universally accepted data format utilized by most higher level data analysis systems, including the experimental X-Modal software. From within the DOS window, the syntax to perform the data conversions:

SDFTOML <sdf file name> <new mat file name> [/X]
SDFTOUNV <sdf file name> <new mat file name> [/X]

[/X] simply outputs the X-axis data points.

Attempting to go through all 288 data files individually and convert them from the SDF format to the MATLAB and Universal-58 formats would be a difficult task. The program *sdfconv.m* was written specifically to perform the conversion of these data files. A copy of *sdfconv.m* is located on the working PC in the directory *C:\Truss_Control\Programs*, and can also be viewed in Appendix J. *sdfconv.m* loads all files, converts them to the appropriate format, and retaining the same name saves the newly formatted file with the *.mat* or *.unv* suffix. The newly created files are placed into the directory the user is currently working in.

When saving data, the file name indicated the node being tested, the axis being tested, and the impact point. The naming convention is of the form "*i(node)(axis)(impact point).mat*". The impact node naming convention is consistent with reference 5, "*a*" refers to node 41 and "*b*" refers to node 24. For illustration, the file *i32xa.mat* contains test data for the x-axis of node 32 and the impact node was node 41. A complete listing of the data files is located in Appendix I.

Executing the HP35665A utilities program, SDFTOML, creates the variables: "o2i1x" and "o2i1". The variable "o2i1x" is simply a column vector of incremented discrete frequencies. The total frequency bandwidth and the interval are a function of the resolution and frequency span settings of the HP-35665A. Determining the required settings is discussed in Chapter III, Section F, Subsection 3. The variable "o2i1" contains the complex FRF data that correlates to each of the frequency elements contained in the

variable "o2i1x". Complex data notation is convenient since it contains both magnitude and phase information. Presentation of the data is performed using the program *mat_plot.m*, plotted data for nodes 41, 44, 49, and 52 is displayed in Appendix K. All data and plots are available on the thesis processing station in the directory *c:/truss_control/hp/data*. This program plots the magnitude of the FRF data, "o2i1", as a function of frequency. Likewise the phase can also be plotted.

2. Mode Shape Animation

The goal of the modal testing was to create a file that contained the truss' mode shapes and then graphically animate the modes of the truss. The "X-Modal" software was identified as an efficient tool that animates the mode shapes. Two processes exist to animate the modes using X-Modal. Regardless, both methods require that the structure's geometry data file to be loaded into the work-session. The first method involves loading the FRF data and performing a parametric estimation or "Quick Fit". This method is relatively accurate and using a curve-fitting technique produces a display of the selected mode shapes. Using a mouse, a modal frequency on the FRF magnitude display is selected and consequently the modal vibration of the truss is displayed. This is not the preferred method since operator discretion and skill are factors. The second method is the most desirable route since the mode shapes are displayed based on only the loaded mode shape data and not on operator discretion or skill. This method involves actually downloading the mode shape data file and then displaying the mode shapes for each mode.

The Universal-58 format is field specific and is exploited by the X-Modal software to associate the data contained in each file with the corresponding node and axis tested and the impact node. X-Modal has reserved specific fields in the data files to identify the tested node, the tested axis and the impact nodes. When the data file is first created, these fields are assigned a general value of 1. These reserved fields have been highlighted below in Figure 31. Referring to Figure 31, the first field, 10, identifies the node tested, field 1 identifies the axis, and field 41 identifies the impact node. The axis

field has three possible values, 1, 2, or 3 which identify the x, y, and z axes respectively. The impact node field has only two possible values, 41 or 24.

```
    -1
    58
Freq Resp

08-Apr-97 23:30:00
NONE                                    Chan  2   Chan  1
This is row  1 col  1 from matrix   1 that is  1 rows by  1 cols by  1025 bins
    4         1    1         0 NONE              10    1 NONE              41   1
         5       801         1  0.0000E+000  2.5000E-001  0.0000E+000
        18    0    0    0 Freq Resp            Hz
         0    0    0    0 Chan  2              V
         0    0    0    0 Chan  1              V
         0    0    0    0
 -1.8880E-001  0.0000E+000  7.5070E+001 -1.3161E+002  2.2815E+001 -7.9189E+001
  1.0350E+001 -5.4870E+001  6.4542E+000 -4.0958E+001  5.2856E+000 -3.3389E+001
```

Figure 31. Universal-58 Data File Header

Since a corresponding file describes the truss' geometry only these values may be entered otherwise the results will be erroneous. Also great care must be taken when entering the field values, since misplacing the data will inhibit the file from being compiled. If the value entered into the field is two digits, the second digit needs to be in the same position as the original default value. Following the convention described, the fields in the data files were corrected and then merged together to form one large global file, *unvdata.unv*. This single file is located on the working PC in the directory *C:\Truss_Control\Programs*.

Utilizing a created mode shape file is the preferred method for animating the modal vibrations of the truss. X-Modal and IDEAS are both capable of building the mode shape file from the test data. Dr. Albert Bosse, Naval Research Laboratories Washington D.C. assisted in the generation of the mode shape file, *shape.unv*, using IDEAS. After creating the mode shape file, the file was loaded into X-Modal so the mode shapes could be animated.

Before a FEM can be validated against testing data, the data itself must be examined for accuracy. Graphically animating the mode shape data, although rudimentary, is a simple precursory method of inspecting the data. This process, at a minimum, can immediately identify flawed data. If the mode shape data is flawed, the animated motion of the truss will be irregular and discontinuous. If the animated mode

shapes visually appear to be valid and no anomalies are apparent then the data should be further analyzed in detail. One technique is ensuring the mode shapes satisfy the Modal Assurance Criterion (MAC) discussed below. Unfortunately, using the test data, the animated modes of the truss were visibly flawed and these results correlate with the results obtained after applying the MAC to the data. Using IDEAS, the natural frequencies and their associated damping ratios were identified and displayed in Table 3.8.

Hewlett Packard 35665A			
Mode Number	ω_n(rads/sec)	Freq (Hz)	ζ
1	1196.377701	15.3801	1.5554%
2	1418.087295	18.2303	3.0735%
3	2380.900605	30.6078	3.2664%
4	2683.804667	34.5018	1.5702%
5	5171.048401	66.4767	0.5042%
6	6153.899741	79.1118	0.4537%
7	6934.394987	89.1455	0.2785%
8	7927.934313	101.9180	0.9119%
9	8030.458081	103.2360	0.3442%
10	9692.463267	124.6020	0.7863%

Table 8. NPS Space Truss Natural Frequencies (HP-35665A)

3. Modal Assurance Criterion (MAC)

Mode shape vectors, if computed correctly, are orthogonal. This property can be used to validate the accuracy of a FEM. The mode shapes of a FEM should be orthogonal, but should also be orthogonal to the mode shapes created from testing data (assuming the testing data is accurate).

Consider the modal vectors

$$\{u\}_1 = \begin{Bmatrix} u_{11} \\ u_{21} \end{Bmatrix} = \begin{Bmatrix} u_1 \\ u_2 \end{Bmatrix}_1 \tag{3.24a}$$

$$\{u\}_2 = \begin{Bmatrix} u_{12} \\ u_{22} \end{Bmatrix} = \begin{Bmatrix} u_1 \\ u_2 \end{Bmatrix}_2 \tag{3.24b}$$

Using equation (3.12), equation (3.24) can be rewritten in the form

$$\{u\}_1 = u_{11}\begin{Bmatrix} 1 \\ \dfrac{-(k_{11}-\omega_1{}^2 m_1)}{k_{12}} \end{Bmatrix} \tag{3.25a}$$

$$\{u\}_2 = u_{12}\begin{Bmatrix} 1 \\ \dfrac{-(k_{11}-\omega_2{}^2 m_1)}{k_{12}} \end{Bmatrix} \tag{3.25b}$$

From equation (3.25)

$$\{u\}^T{}_2[m]\{u\}_1 = u_{11}u_{12}\begin{Bmatrix} 1 \\ \dfrac{-(k_{11}-\omega^2{}_1 m_{1)}}{k_{12}} \end{Bmatrix}^T \begin{bmatrix} m_1 & 0 \\ 0 & m_2 \end{bmatrix} \begin{Bmatrix} 1 \\ \dfrac{-(k_{11}-\omega^2{}_1 m_1}{k_{12}} \end{Bmatrix} \tag{3.26}$$

$$= u_{11}u_{12}m_1 + \frac{m_2}{k_{12}{}^2}(k_{11}-\omega^2{}_1 m_1)(k_{11}-\omega^2{}_2 m_1)$$

Substituting $\omega^2{}_1$ and $\omega^2{}_2$ from equation (3.13) into equation (3.26) gives

$$\{u\}^T{}_2[m]\{u\}_1 = 0 \tag{3.27}$$

Both modes $\{u\}_1$ and $\{u\}_2$ must satisfy the following equations:

$$[k]\{u\}_1 = \omega^2{}_1[m]\{u\}_1 \tag{3.28a}$$

$$[k]\{u\}_2 = \omega^2{}_2[m]\{u\}_2 \tag{3.28b}$$

Multiplying equation (3.28a) by $\{u\}^T{}_2$ gives

$$\{u\}^T{}_2[k]\{u\}_1 = \omega^2{}_1\{u\}^T{}_2[m]\{u\}_1 \tag{3.29}$$

Substituting equation (3.27) into equation (3.29) provides

$$\{u\}^T{}_2[k]\{u\}_1 = 0 \tag{3.30}$$

Therefore the modal vectors, $\{u\}_1$ and $\{u\}_2$, are orthogonal with respect to the stiffness matrix.

Because the elements of each modal vector are ratios of each other, it can be shown that the modal vector once normalized satisfies

$$[\bar{u}]^T[m][\bar{u}] = 1 \tag{3.31}$$

Let

$$[\bar{u}] = [u][\bar{m}]^{-1/2} \tag{3.32}$$

where

$$[\bar{m}]^{-1/2} = \begin{bmatrix} \dfrac{1}{\sqrt{m_1}} & 0 \\ 0 & \dfrac{1}{\sqrt{m_2}} \end{bmatrix}$$

then

$$[\bar{u}]^T [m][\bar{u}] = [\bar{m}]^{-T/2} [u]^T [m][u][\bar{m}]^{-T/2} = [\bar{m}]^{-T/2} [m][\bar{m}]^{-1/2} = [I] \tag{3.33}$$

Based on the procedure just prescribed, the program *macplot.m* was written to validate the accuracy of mode shape data. *macplot.m* and the associated programs that it calls, when executed, are contained in Appendix L. *macplot.m*, the associated programs, and the mode shape data files are located in the directory *c:/truss_control/truss/Unv_files/* on the working PC in the NPS Smart Structures laboratory. Each time a new mode shape file is analyzed the program *macplot.m* has to be modified. When executed, the line of code that loads the mode shape file needs to be tailored to reflect the name of the mode shape file to be analyzed. Upon inspection of the program, the line to be modified is readily apparent.

The mode shape file, *shape.unv*, was created from the FRF data acquired during modal testing of the NPS truss and *macplot.m* was modified to load *shape.unv*. Executing *macplot.m* generates a mesh graph which essentially plots equation (3.33). The results, presented in Figure 32, clearly show the presence of relatively large off diagonal elements, which indicate that the test data is not accurate. The mode shape file, *dshape.unv*, was created from data acquired during modal testing of the Naval Research Laboratory's truss. The data used to construct the mode shape file, *dshape.unv*, is known to be relatively high quality data, and the resulting analysis of *dshape.unv* is shown in Figure 33. As expected, the off-diagonal elements are orders of magnitude lower that the main diagonal elements.

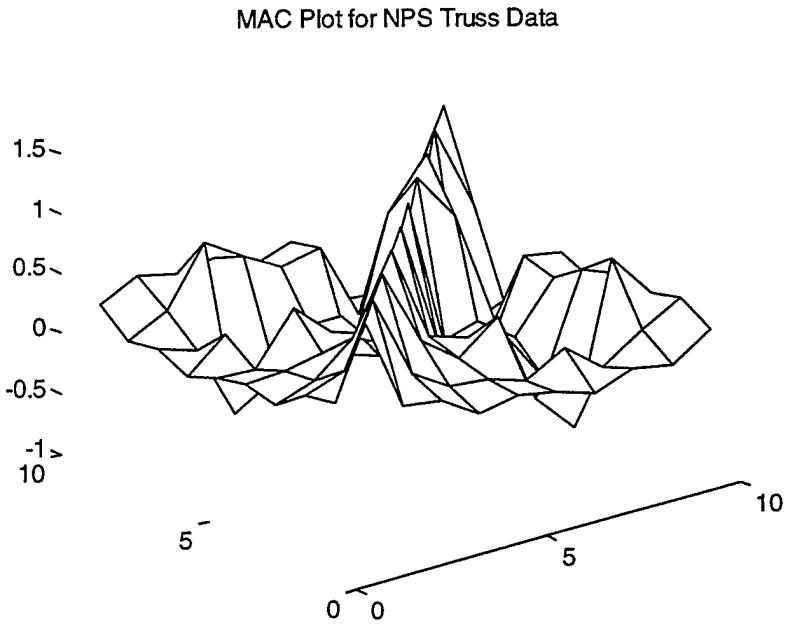

Figure 32. NPS Space Truss Mode Shape Orthogonality

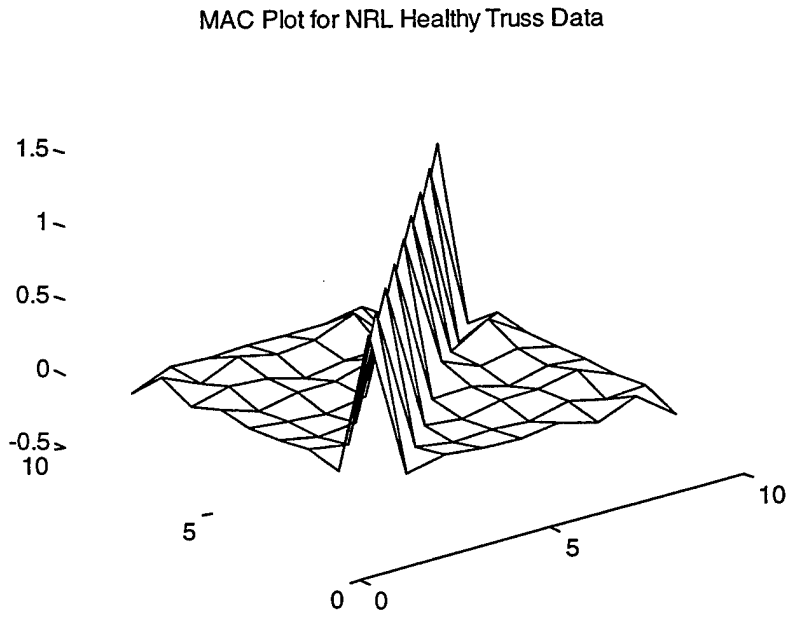

Figure 33. NRL Space Truss Mode Shape Orthogonality

I. X-MODAL

1. Overview

X-Modal is an experimental modal analysis software package developed at the University of Cincinnati, Structural Dynamics Research Lab (UC-SDRL) in conjunction with Boeing. The primary function of this software package is to provide a flexible environment for analyzing data acquired for the purpose of experimentally determining the modal parameters of a structure. This flexible environment involves a unique data management structure as well as a user programming capability. X-Modal does not acquire FRF data but utilizes FRF data acquired from any data acquisition system as long as the data can be provided in Universal File format. X-Modal provides a graphical user interface (GUI) in parallel with a command driven interface to provide users with any type of programmatic interaction desired. X-Modal utilizes MATLAB to provide user programmability as well as to implement all the major modal parameter estimation algorithms documented in the literature.

Currently, X-Modal requires a Hewlett-Packard (HP) 700 Series Workstation with the following hardware specifications: 32 Mb RAM, 75 Mb Disc Memory, and 100 Mb of Swap memory. The X-Modal software package is written in the C (98%) and Fortran (2%) programming languages under HP-UX Unix environment. Currently the following software specifications are required: HP-UX (Rev. 9.01 or later), MATLAB(Rev. 4.2c or later), and X11R5 Window System with Motif (Rev. 1.2). Documentation and on-line help is provided electronically from within X-Modal via the GNU "Ghostview" utility. Paper copies can be processed by copying the Encapsulated Post Script (EPS) files to any Post Script or Encapsulated Post Script, Level II printer.

2. LOG-ON Procedures

Logging into X-Modal is a relatively simple exercise. As mentioned above the user needs to be on a Hewlett Packard machine, these are located in the Aerospace

Engineering computer lab in Haligan. After logging on the user must link to the NRL site, the syntax is:

telnet finite.nrl.navy.mil

The user will be prompted for a username and password. After successfully linking to the remote site the environment for using X-Modal must be set and then X-Modal can be executed. The syntax to perform this is:

setenv DISPLAY=userterminal.nps.nps.navy.mil:0.0

export DISPLAY

X-Modal

The X-Modal GUI will appear. Next load the truss geometry file and mode shape file. X-Modal is menu driven, open the *file* pull down and load the file *nps_geometry.unv*. Following the same procedure load the mode shape file *id1_shape.unv*. To animate the modes open the *animate* pull down and select *dynamic*. The user will be prompted for the mode number. Entering the desired number will display a graphical animation of the truss' motion.

IV. CONTROL SYSTEM DESIGN AND IMPLEMENTATION

A. FREQUENCY RESPONS OF THE ACTUATOR-SENSOR SYSTEM

Prior to designing the active controller it is necessary to identify the specific modal frequencies of the active control system, whose input is the piezoceramic actuator and whose output is the force sensor. Isolating first and second modes is critical since the integral force feedback controller to be used targets specific modal frequencies [Ref. 1 and 3]. The frequency response function measured in this section is the output voltage of the PCB force sensor relative to the actuator voltage, both of which are located on the active strut. This measurement was performed after all the active control components were installed on the structure.

The frequency response function of the actuator/sensor system was obtained using the HP-35665A digital signal analyzer. Pink noise, generated by the signal analyzer, was applied to the piezoceramic actuator through a Trek voltage amplifier. The response of the system was measured by the PCB force sensor and fed back to the signal analyzer via a signal conditioner. The signal analyzer compared the input relative to the output and generated a frequency response function for the actuator/sensor system. The experimental setup for this experiment is displayed in Figure 34.

The magnitude/phase plot is displayed in Figure 35 and the frequency response of the actuator and sensor assembly is displayed in Figure 36. To design the active controller the first two peaks (1^{st} and 2^{nd} natural frequencies) of the frequency response are considered. The active strut was positioned between nodes 27 and 35 for the active control testing. This strut experiences the greatest modal strain energy for the truss' second mode as identified by the truss characterization work in References 1 and 9. By examining the frequency response and magnitude-phase plots, the frequency associated with active strut 1 was determined to be 16.75 Hz (90-degree phase lag). A controller's best performance is when there is a ninety-degree phase lag between the system response

and the actuating signal. 16.75 Hz was selected because of the associated 90-degree lag.

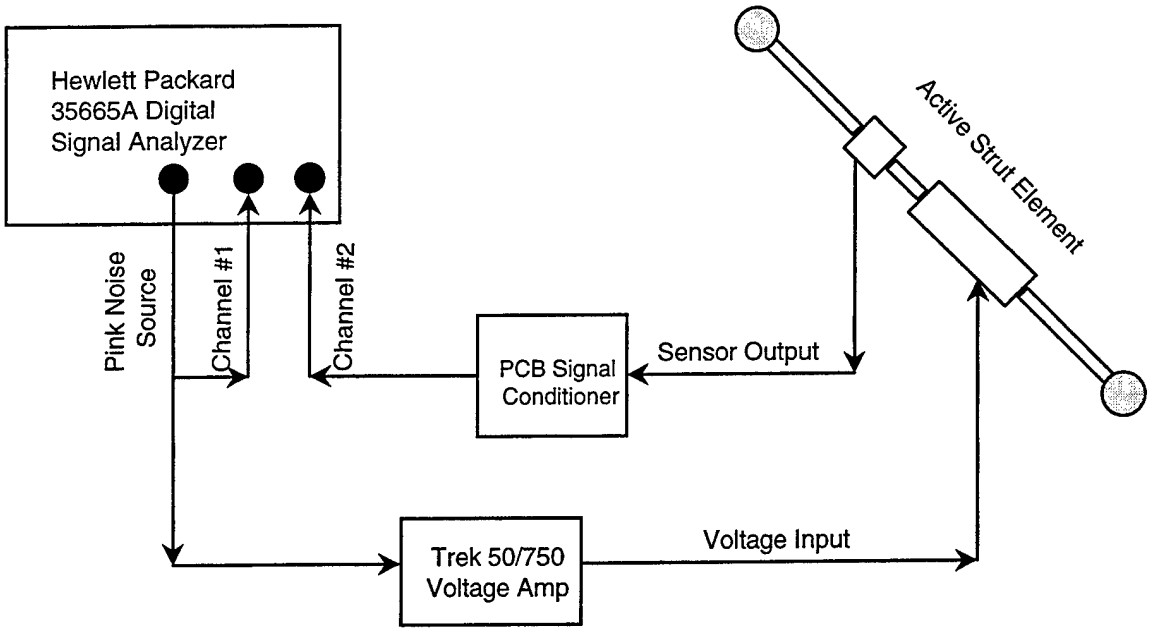

Figure 34. Experimental Setup – System Frequency Response

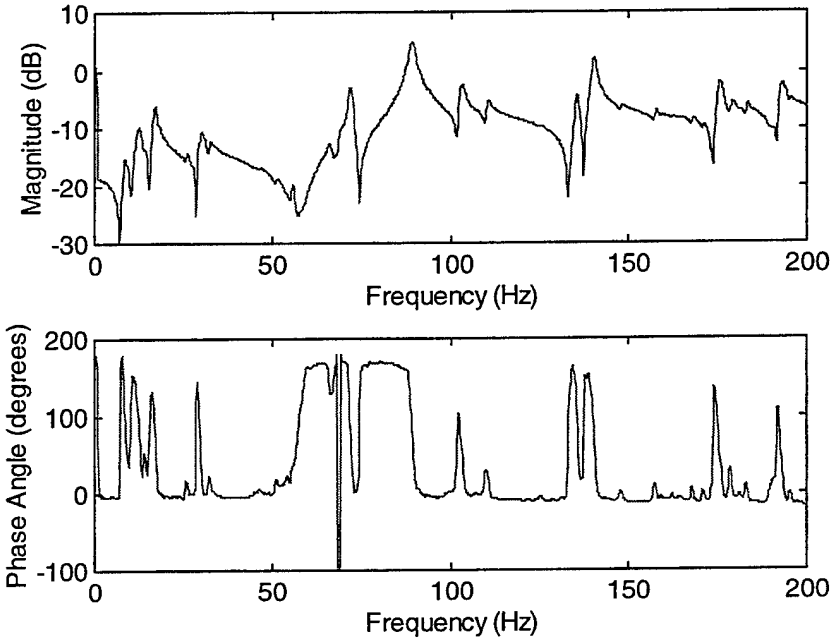

Figure 35. Frequency Response Magnitude and Phase Plot

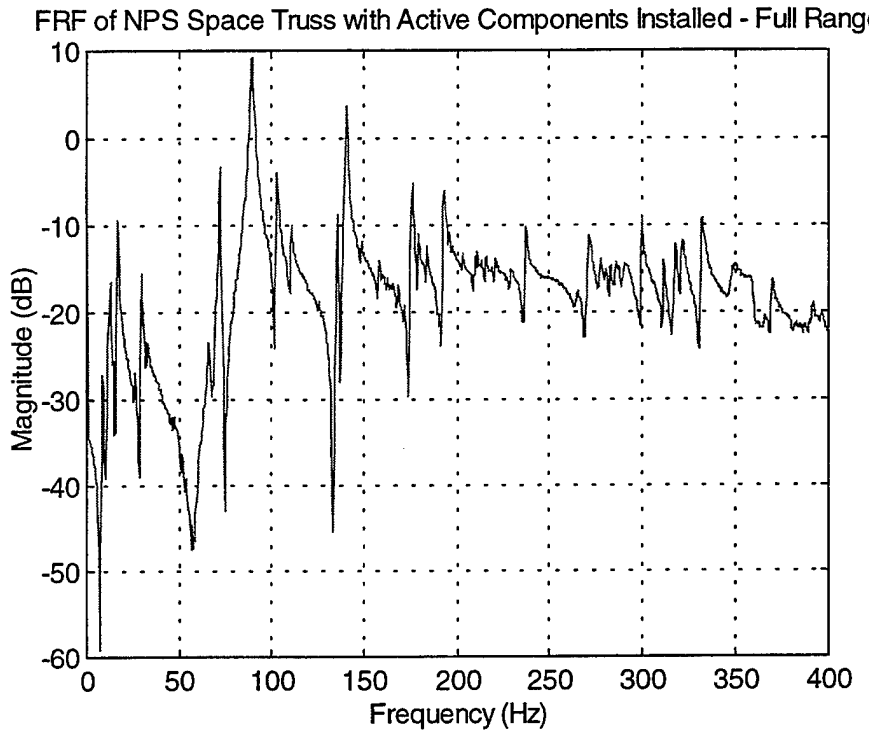

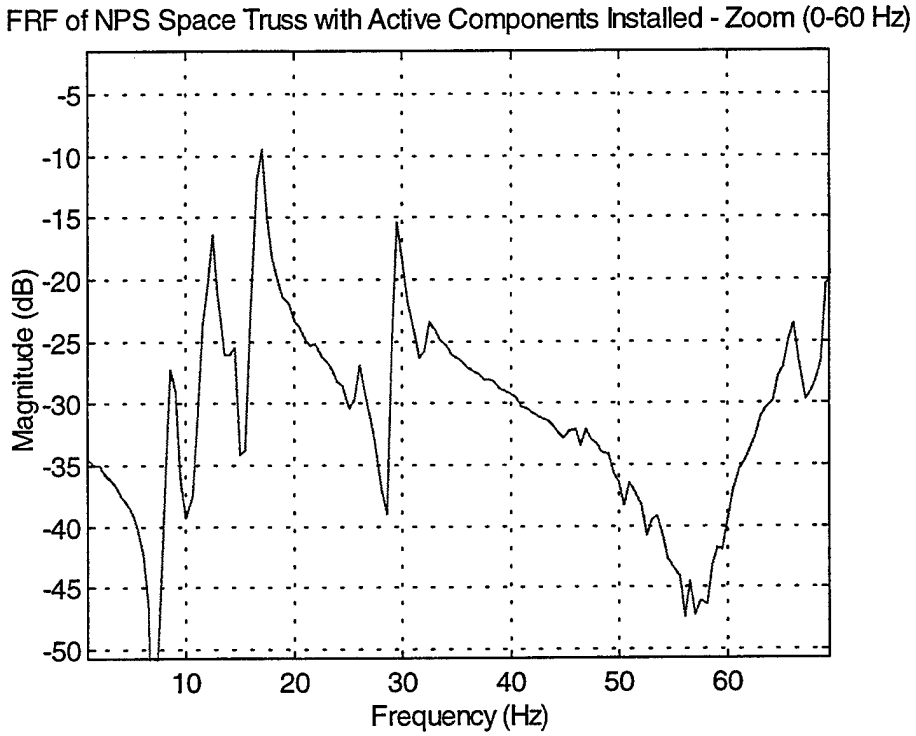

Figure 36. Frequency Response Function - Active Strut #1

B. ACTIVE CONTROL EXPERIMENTAL SETUP

The experimental setup for the active control experiment is displayed in Figure 37. The active control experiments were conducted to evaluated the effectiveness of the controller to changing gain parameters and the effectiveness of the controller to shifting frequencies. The experimental arrangement can be broken up into three parts: the components that excite the truss (LPACT strut, signal generator), the components that are part of the control mechanism (dSPACE, active strut) and the components that sense the response of the truss (dSPACE, accelerometers, and laser diode). It is clear that dSPACE plays a critical role in this experimentation and as a result, the dSPACE electronics package and its associated software are discussed in the following section.

The LPACT strut carries out the excitation of the truss. The connections between the LPACT and its control unit are via the interfaces located on the backside of the control module and were described in detail in Chapter II, Section B. The input to the LPACT strut is via an HP-33120 signal generator. The output of the signal generator is connected to the "user input" connection on the front side of the control unit. The force and rate loops for the LPACT were disabled for all control testing. The settings for the signal generator were dependent on the type of control testing. For the evaluation of gain parameters, a sinusoidal signal of 50 mV peak-to-peak amplitude and 16.75 Hz was input into the truss; and for the evaluation of the controller's sensitivity to frequency, a sinusoidal signal with 50 mV peak-to-peak amplitude was input while the frequencies were shifted.

The controller's actuating signal originates in the dSPACE (DS-1003) digital signal processor. The output signal is passed through a Trek 50/750 voltage amplifier and then into the PI piezoceramic actuator. At the start of this experimentation, some concerns were expressed that the Trek model voltage amplifier might prove too noisy for the control applications. The researchers at NRL [Ref. 1] initially used a Trek but discarded it in favor of a Burleigh amplifier because of the high-frequency noise it

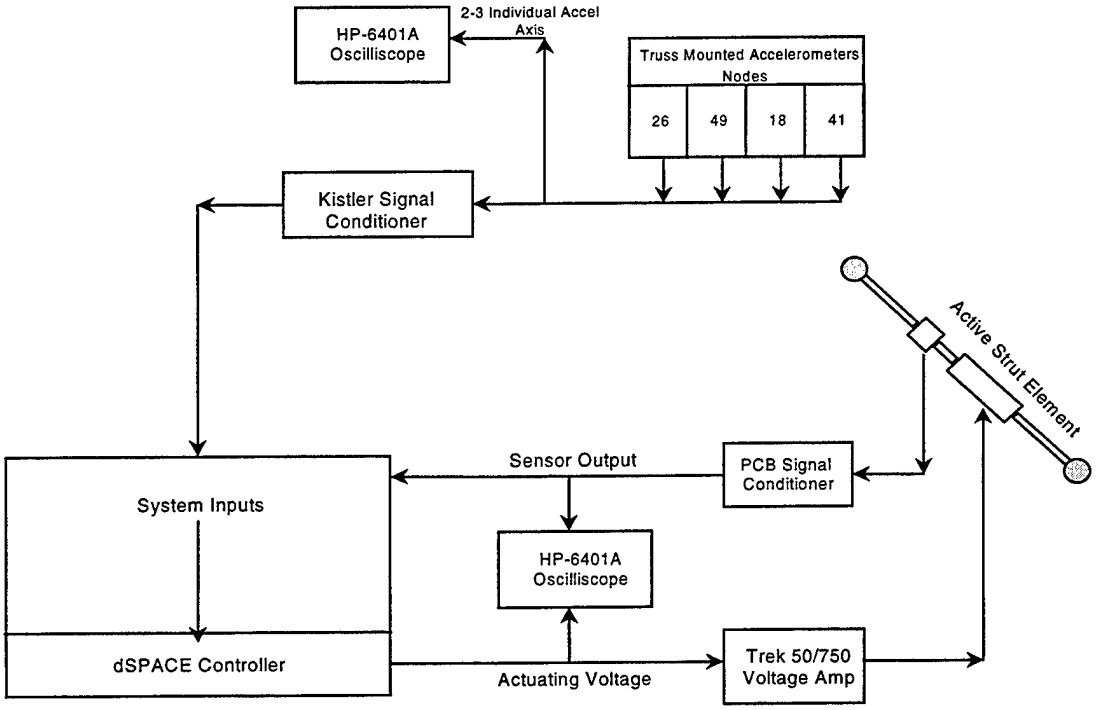

Figure 37. Active Control Experimental Setup

injected into the system. The control response in these experiments did not seem to be affected by the use of the Trek, but Burleigh model amplifiers were researched and are included with the Trek information that is part of Appendix B in the event they may be required in the future.

The PCB force sensor measured the response of the system to the excitation of LPACT strut and the expansion and contraction of the PI piezoceramic stack. The output of the sensor was passed through a PCB Piezotronics Model 484B signal conditioner and then into one of the input channels (Plug 1) for the dSPACE digital signal processor. The signal conditioner is set to a DC bias of 11 Volts.

The voltage outputs of the force sensor and the dSPACE actuating signals were monitored using a HP-54601A oscilloscope. The actuating voltage should not be measured downstream of the Trek 50/750 since this is high voltage and would damage the oscilloscope. The performance of the controller was monitored so as to protect it and the equipment from damage in the event that the system goes unstable during the testing.

The sensor input was placed in channel #1 and the actuating voltage was monitored in channel #2. Optimal settings for the HP were 500-mV/div and 50 msec and 2.0-V/div and 50 msec for channel #1 and #2, respectively. When the controller is operating (Controller download from Simulink has succeeded) the actuating signal should exhibit a 3.3-Volt bias on the oscilloscope. This bias is the voltage applied to the piezoceramic stack actuator to place it at the midpoint of its expansion in order to give the active strut some mechanical preload. Additionally, it serves as an indicator for whether the dSPACE system and the controller are operating properly.

The last part of the experimental setup was used to measure the truss response. The truss response is measured through the active strut force sensor and with four Kistler accelerometers that are mounted across the truss. Accelerometers were mounted at nodes 26 and 41 because they were located at the extreme ends of the truss and represent the points that will experience the maximum displacement for the first and second mode shapes of the truss. Likewise, two more accelerometers were located at nodes 18 and 49, where the third and fourth mode shapes have the most power. The accelerometers were used to monitor the amount of vibration present on the structure before and after the implementation of the active controller.

The accelerometers were mounted in the same fashion as described in Chapter III. The connecting cables run through the Kistler multi-channel signal conditioners and into the input channels for dSPACE. All three axes of each accelerometer were connected and monitored by the dSPACE system. The plug arrangement was the same for all the active control experiments and is displayed in Table 10. The z-axes of the node-41 and 26 accelerometers were also monitored using a second HP oscilloscope. Monitoring is conducted to verify the effects of the control action at the nodes where the amplitude of vibration is the greatest.

The truss motion was monitored using the laser diode assembly mounted at nodes 15 or 51. These nodes are selected because truss motion is greatest at these points. The laser pinpoint is projected on the laboratory and gives a real-time view of the truss motion. The mounted laser diode gives an excellent, qualitative assessment of

whether or not the controller was damping the truss' motion. The diode is powered by a HP-3615A DC power supply set between 2.5 and 4.5 Volts.

Active Control Experimentation	
dSPACE Plug Arrangement	
ADC Plug Number	Sensor Measured
Plug 1	Force Sensor
Plug 2	Node 41 - X-Axis
Plug 3	Node 41 - Y-Axis
Plug 4	Node 41 - Z-Axis
Plug 5	Node 18 - X-Axis
Plug 6	Node 18 - Y-Axis
Plug 7	Node 18 - Z-Axis
Plug 8	Node 49 - X-Axis
Plug 9	Node 49 - Y-Axis
Plug 10	Node 49 - Z-Axis
Plug 11	Node 26 - X-Axis
Plug 12	Node 26 - Y-Axis
Plug 13	Node 26 - Z-Axis

Table 9. Active Control dSPACE ADC Plug Inputs

C. CONTROL SYSTEM DESIGN

1. Controller Design in Simulink

Truss active control is implemented through a integral force-feedback control law. Experimentation by the NASA Langley and the Naval Research Laboratory has displayed success in the active control of space structure using integral force feedback [Ref. 1 and 4]. Additionally, integrated force feedback was selected because it is inherently stable [Ref. 4], performance can be easily established, and implementation is relatively simple. A block diagram of the closed-loop control hardware of the NPS truss is displayed in Figure 38. The truss controller was designed in Simulink on the SRDC dSPACE desktop PC and is composed of a bandpass filtered force feedback control law. The controller design is shown in Figure 39. All the Simulink controller designs have been saved on the dSPACE, desktop PC in the *C:/Matlab/Bin/Truss98* directory under the filename *iictrl.m.*

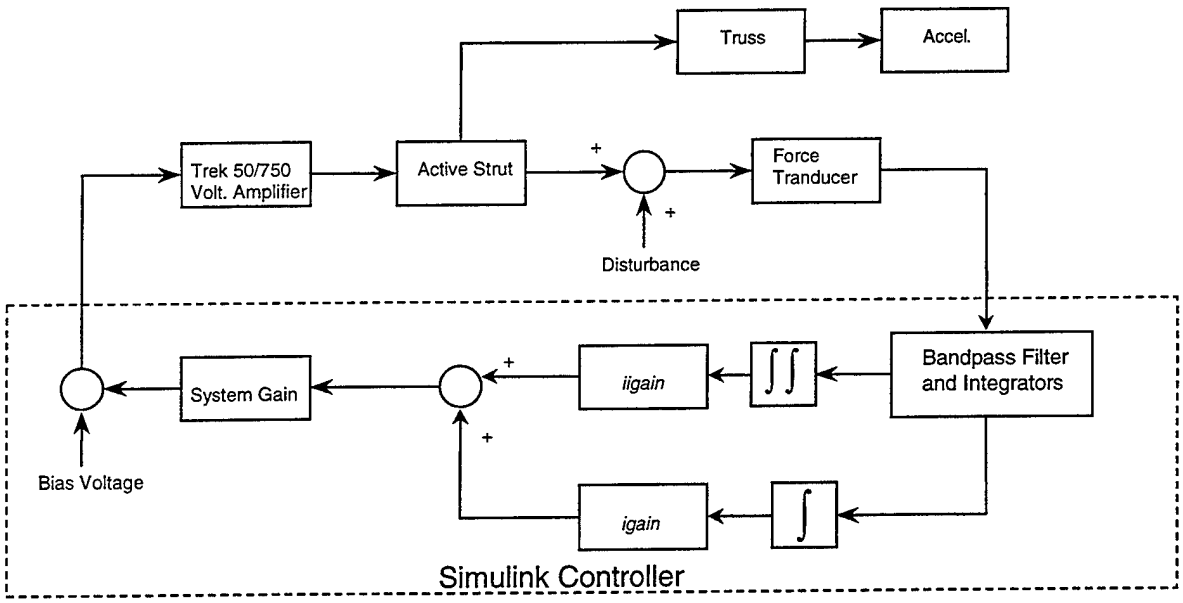

Figure 38. Block Diagram of Truss Closed-Loop Control Hardware

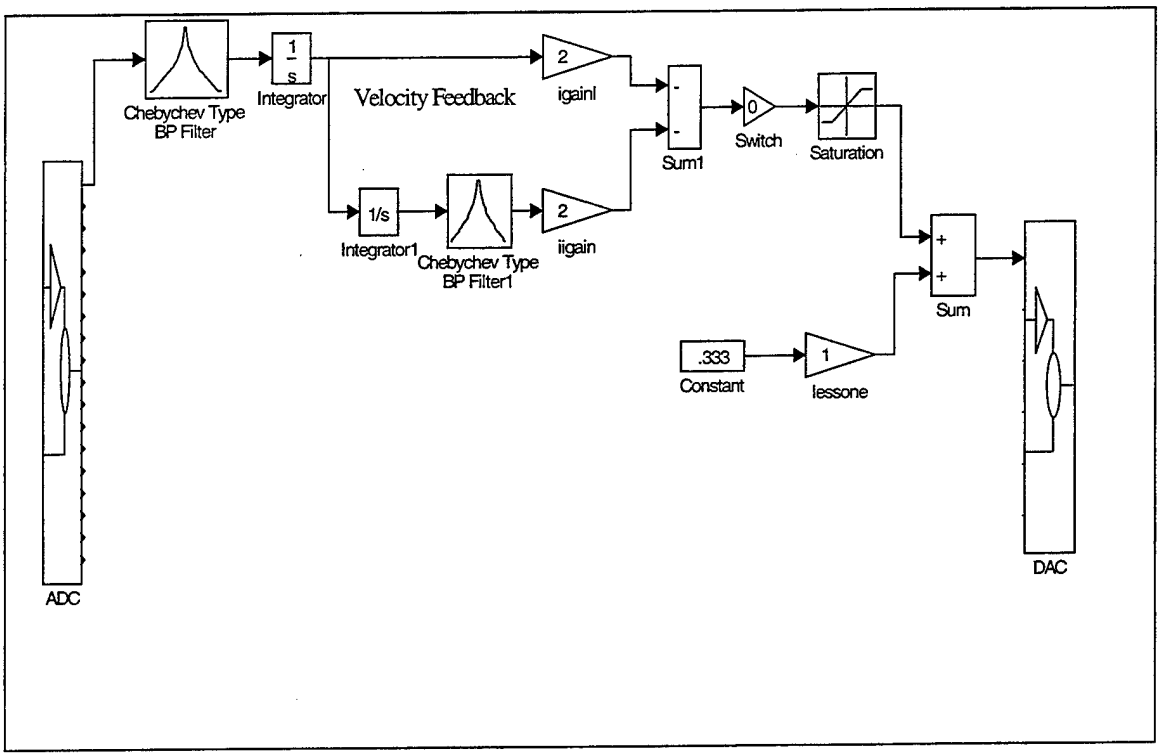

Figure 39. Single Strut Controller in Simulink

The controller is composed of two feedback paths: *igain* and *iigain*. Both paths are summed and passed through a saturation filter that prevents possible damage to the piezoceramic stack once the signal is amplified by the Trek 50/750, voltage amplifier. The output signal is then combined with a positive .333 Volt bias that provides a mechanical preload for the active strut after amplification with the Trek 50/750.

The bandpass filters in the design were inserted to prevent the amplification of DC current at low frequencies and random noise at high frequencies. Both bandpass filters are centered at 16.75 ± 1.5 Hz, which is the frequency that was identified in the frequency response testing as having a 90-degree phase lag for the truss' second mode shape. Part of the active control testing evaluates the effect of altering this frequency on the controller performance.

Due to the use of bandpass filters in the controller design, the performance of the double-integral force feedback controller has a high sensitivity to the targeted natural frequencies of the system. After the insertion of the active components the truss' modal frequencies shifted. Due to this slight shift in the natural frequency of the second mode, the bandpass filter was no longer centered on the targeted frequency. Although the bandpass filter was only 1.48 Hz off, the phase lag was no longer the ninety degrees necessary for optimum controller performance and was ineffective in controlling the truss vibration. Once the correct frequencies were identified and the bandpass filter centered on this frequency, the controller was able to achieve a fifty- percent power reduction for that center frequency.

The incorporation of a second active strut that is targeted against the first modal frequency of 12.25 Hz would have an identical controller. When installed, both struts operate independent of each other and therefore the controllers are independent of each others control action. Figure 40 is included as a guideline for future researchers.

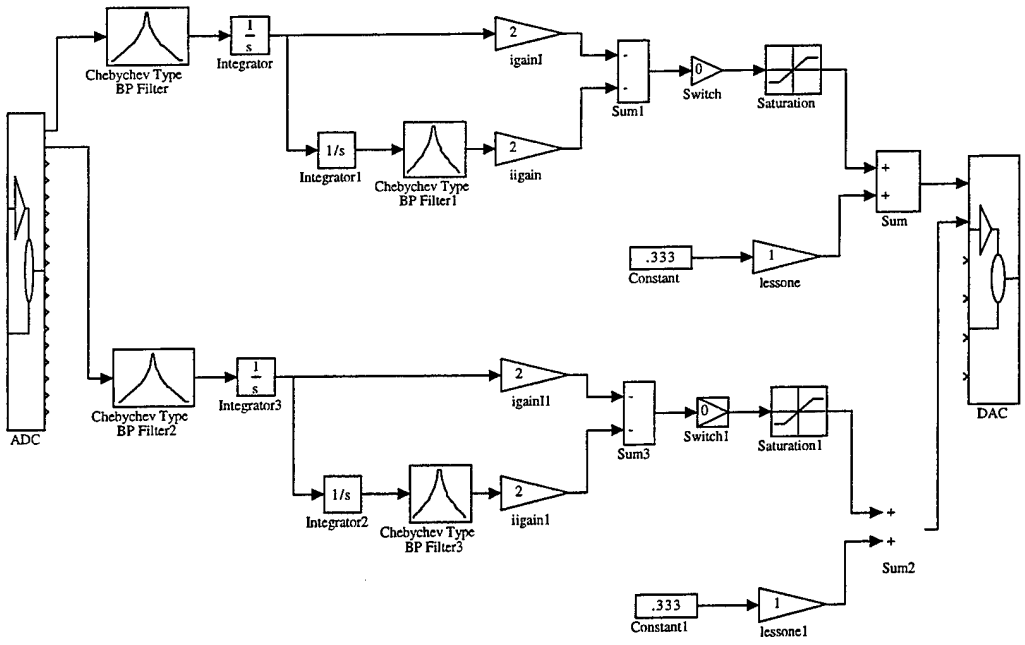

Figure 40. Two Strut Controller in Simulink

2. Control System Implementation Using dSPACE

The system used to implement the active control of the NPS space truss was the dSPACE real-time control and data acquisition system and its associated software. The system provides real-time control, real-time data acquisition and quasi-real time adjustment of the active control parameters (i.e. velocity and position feedback gains). Figure 41 is a schematic of the control system implementation. What follows is a description of this system and how it was used in the active control experimentation.

The actual controller for the space truss was designed in Simulink on the dSPACE desktop PC. When the controller is ready for use it is downloaded to the dSPACE digital signal processor by selecting the "Generate and Build Real Time" command from the "CODE" pull down menu in the Simulink window (Figure 26). This will open a DOS

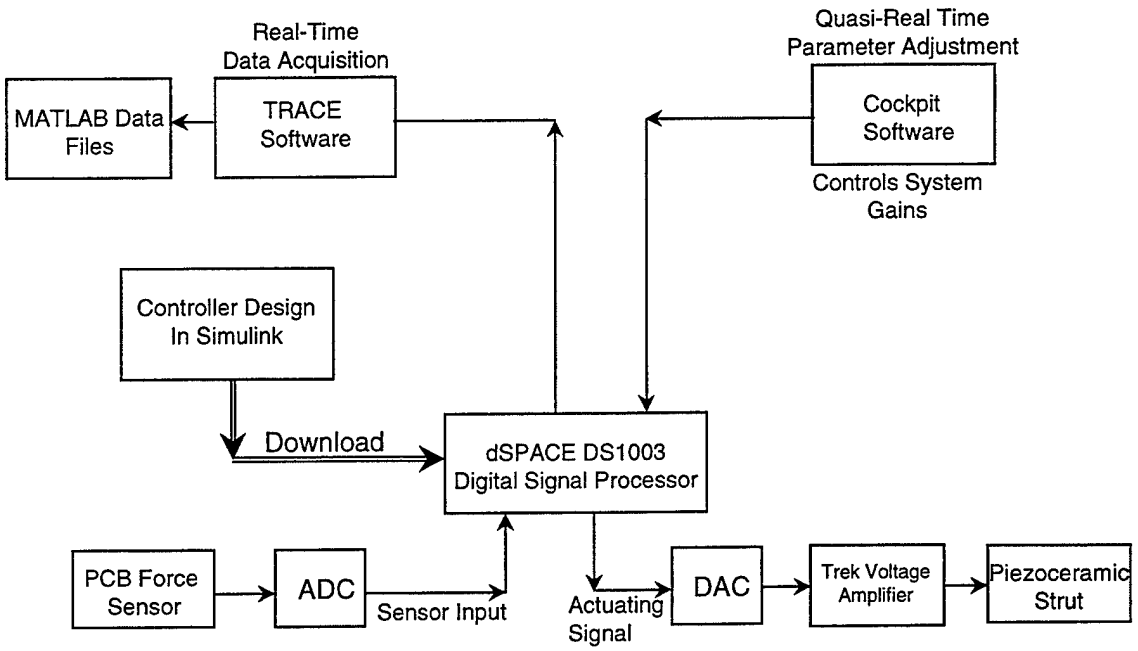

Figure 41. dSPACE Electronics Arrangement

window, generate the coded instructions for the dSPACE digital signal processor, and report "*download succeeded*", unless there is an error. This command sequence implements the controller on the dSPACE digital signal processor. At this point, the control system is running.

Control system input is received from the PCB force sensor via a PCB signal conditioner. The signal enters (Plug 1) via an analog to digital converter (ADC) and then is processed by the controller that has been downloaded from Simulink. The digital signal processor generates an actuating signal, which is passed on to the Trek voltage amplifier through a digital to analog converter (DAC). Both the ADC and DAC are hardware components of the dSPACE system and are equipped with software components that can be used in Simulink.

The dSPACE system has two associated software packages that can be used in conjunction with the control applications. The first of these is the TRACE software. TRACE provides the user the ability to conduct real-time data acquisition of sensors that are plugged into the ADC. In the active control experimentation, data was collected on

Plugs 1-13 (Table 10) and saved in MATLAB format using a TRACE file. All TRACE files designed for use with the active controller are located in the *c:/matlab/bin/truss98* directory.

The files in question are *iictrl.exp* and *iictrl.trc*. To implement the TRACE file in conjunction with the active controller the Simulink model of the controller must have already been downloaded to the digital signal processor using the procedure described above. Once this has been accomplished the TRACE file can be implemented by executing the program *trace_40w.exe* located on the Microsoft Toolbar. Within the TRACE window, go to the "FILE" pull-down option, select "load", and load file *iictrl.trc*. Again in the "FILE" pull-down option, select "open", and then open experiment file *iictrl.exp*. This program will display the data inputs into the 13 plugs as well as three signals that are internal to the controller.

To initiate data acquisition press "start." The time duration for all the active control experiments was twenty seconds. The first five seconds of each experiment was the uncontrolled response of the truss. After five seconds, control action was initiated by turning on the Trek 50/750 voltage amplifier and applying current to the piezoceramic stack. Data was collected for the remaining fifteen seconds of the experiment. The data is then saved in MATLAB format (*.mat*) using the "save" command that is located under "FILE" pull-down menu. All our active control files are saved in the *c:/matlab/bin/truss98/expdata* directory. Eighteen sets of data were taken and are analyzed in Section D of this chapter. The graphs of some of the data are included for reference in Appendix M.

The second piece of software provided with the dSPACE system is the COCKPIT. COCKPIT gives the user the ability to adjust controller parameters such as the system integral force feedback and double-integral feedback gains in quasi-real time. To initiate the COCKPIT software, execute the program *Cockpt40.exe* located on the Microsoft Toolbar. Within the COCKPIT window, go to the "FILE" pull-down option, select "load trace file", and load file *iictrl.ccs*. The program window will appear with several slide bars that allow the user to control the velocity, position and system gains. Pressing the

"start" button in the upper left-hand corner of the display window, initiates COCKPIT and allows quasi-real time control of the aforementioned parameters. Moving the slide bar in the control window now changes the actual gain values. The program allows rapid execution of test protocols since it eliminates the need to return to the Simulink window to change gain parameters.

D. ACTIVE VIBRATION CONTROL RESULTS

A total of eighteen different tests were conducted with the integral plus double-integral force feedback controller. The testing was divided into two parts: an evaluation of different gain parameters and analysis of the controller's sensitivity to alteration of the frequency at which its bandpass filters were centered. For each trial, the truss response was measured using the four truss-mounted accelerometer arrangement described in Section B of this chapter. For each trial, the time data was collected using the TRACE software and saved in *.mat* format in the *C:/Matlab/Bin/Truss98/ExpData* directory.

The format of each test was identical. All trials were twenty seconds in duration. At the commencement of each trial no actuating signal was being applied to the controller. The dSPACE signal processor was operating at all times but application of the actuating signal to the piezoceramic stack was controlled by powering the Trek 50/750 voltage amplifier on and off. The TRACE software was allowed to collect data on the uncontrolled for five seconds. At the five-second point the Trek 50/750 voltage amplifier was powered on and an actuating signal was applied to the structure. The TRACE software continued collecting data on the truss response for fifteen seconds after the initiation of control action. Fifteen seconds was judged as sufficient time for any transients to die out and allow the system to achieve steady state.

The active control data was analyzed and is partially displayed in Appendix M. This compilation includes the time data of the force sensor and the accelerometer data for nodes 41 and 26. This nodal data is the most significant since these are two of the nodes with greatest amplitude for the first and second mode shapes of the truss. The *.mat* data files are plotted using the *graph.m* MATLAB code (Appendix N). The degree of control

response is evaluated by graphing the power spectral densities of the controlled versus uncontrolled data for each of the trial using the *psdplot.m* MATLAB code (Appendix O). All the aforementioned graphs are displayed in Appendix M.

1. Evaluation of Active Control Gain Parameters

Ten different combinations of velocity, position, and system gain parameters were tested. The specific test configurations (gain values) along with the results are detailed in Table 11. The gain values were adjusted to determine which set of parameters optimized the performance of the controller. The time data was collected using the TRACE software and evaluated using the MATLAB codes of Appendix N and O. The power spectral density comparison for the best case is displayed in Figure 43.

The best results were those of trial 10 that resulted in a power reduction of 14.817 dB. The time response for this trial is displayed in Figure 42. An analysis, however, of the time data for this case reveals that the system is on the verge of going unstable. When the truss was disturbed with control system running the system went unstable. As a result, although showing a smaller power reduction of only 13.854 dB, trial 8 (with velocity, position and system gains, set at 300, 100 and 2, respectively) has been identified as the optimal controller performance.

Adjustments of Velocity, Position and System Gain				
Data Set Name	Velocity Gain	Position Gain	System Gain	Power Reduction (dB)
Trial2	300	0	1.75	11.609
Trial3	200	0	1.75	8.746
Trial4	100	0	1.75	5.368
Trial5	0	100	1.75	0.323
Trial6	250	0	1.75	0.000
Trial7	300	100	1.75	11.397
Trial8	300	100	2.00	13.854
Trial9	300	100	2.25	12.938
Trial10	300	100	2.50	14.817

Table 10. Active Control Trials – Variations in Gain Parameters

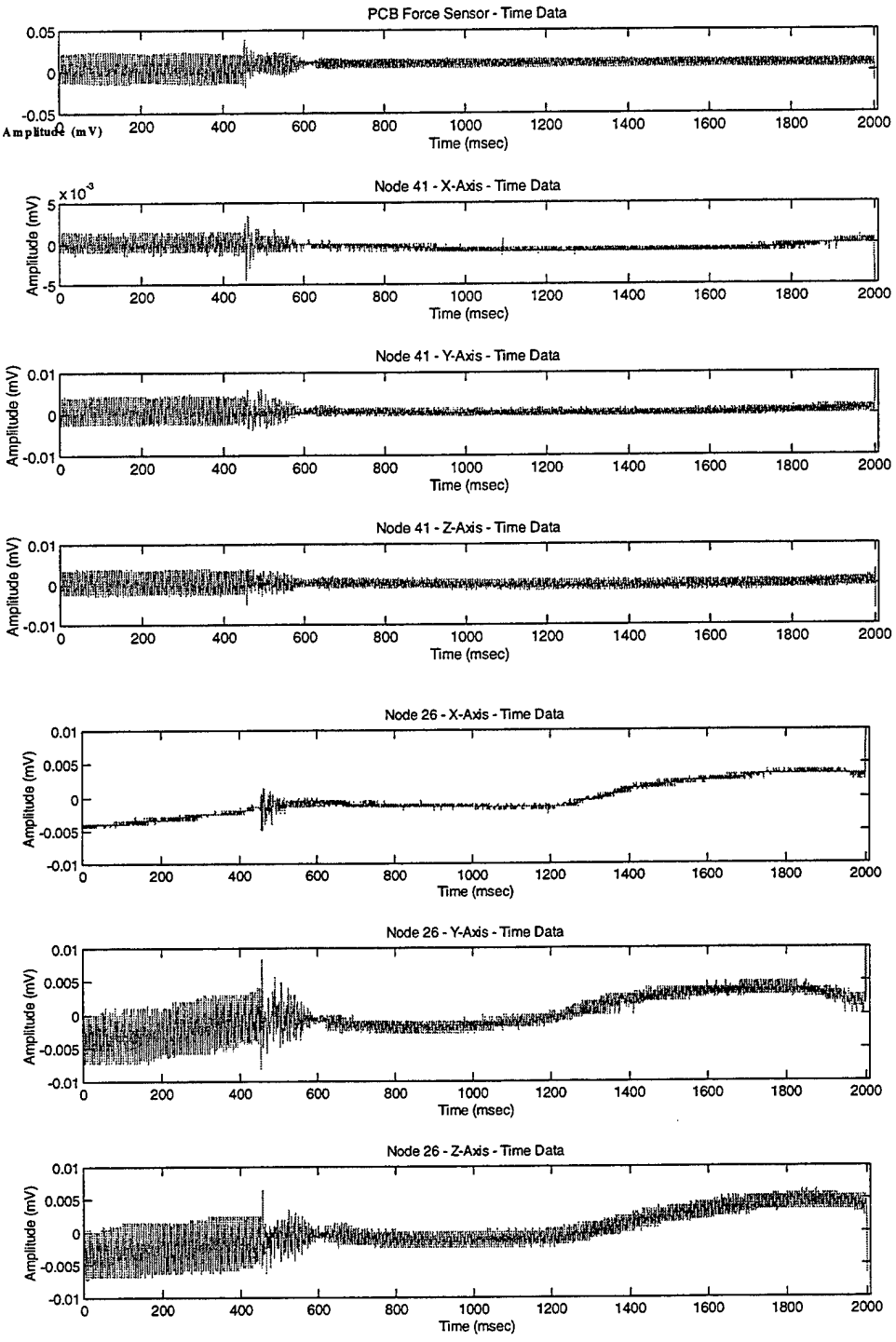

Figure 42. Active Control Testing – Trial 8 – Node 26 and 41 Response

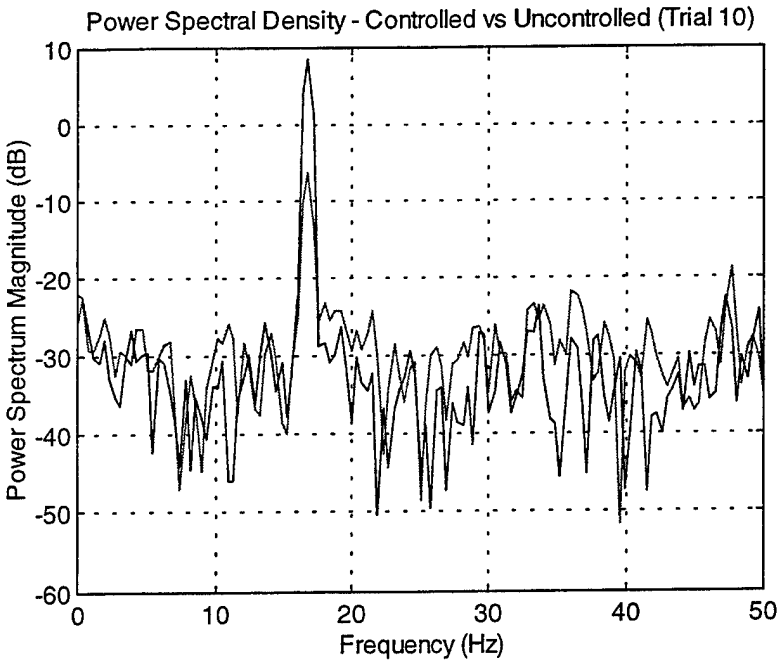

Figure 43. Best Case Active Control – Power Reduction of 15 dB

2. Sensitivity of Controller to Frequency

The second set of control testing evaluated eight alternatives to the center frequency (16.75 Hz) of the bandpass filter that was used in the first set of tests. Shifting the center frequency of the filter results in a change in the phase lag between the controller and the actuator-sensor system and as a result alters the performance of the controller. The range of frequencies tested was from 16.0 to 17.5 Hz and the resultant phase lag was from 25 to 180 degrees. The aim was to identify the frequency that resulted in the best controller performance. The test results are detailed in Table 12.

The controller's best performance was at a frequency of 16.85 Hz. This resulted in an increase in vibration supression of 12.01%. All of the frequency tests were compared against the parameters of trial 7 (control) of the previous testing. An evaluation indicates an increase in controller performance in the range between 16.75 and 17 Hz.

Adjustments of Bandpass Central Frequency Velocity Gain = 300, Position Gain = 100, System Gain = 2			
Data Set Name	BandPass Central Frequency (Hz)	Power Reduction (dB)	Percentage Reduction/Increase From Trial7 Perf (%)
Trial11	17	8.8336	-22.494
Trial12	17.25	6.652	-41.63
Trial13	17.50	5.178	-54.57
Trial14	16.50	12.265	7.61
Trial15	16.25	7.024	-38.37
Trial16	16.00	0.000	N/A
Trial17	16.65	12.513	9.78
Trial18	16.85	12.766	12.01

Table 11. Active Control Trial – Variations in Bandpass Frequency

E. DEVELOPMENT OF SYSTEM STATE-SPACE REPRESENTATION

From the frequency response magnitude and phase data obtained by the HP-35655A, analyses were performed to extract information that can aid in the development of an active control model of the NPS space truss. The following section details the analysis that was used to extract natural frequencies and damping ratios for the individual modes of the actuator-sensor system. Building on this analysis, a state-space model for the actuator-sensor system can be extracted from the data and therefore, the associated system transfer function, poles and zeros, and an associated root-locus diagram can be obtained.

Obtaining a state-space representation of the actuator-sensor system is a goal of this analysis. From this state-space representation the open-loop transfer function of the truss can be obtained along with the associated pole-zero and root-locus models. It should be noted that this analysis could generate the characteristic properties of the actuator-sensor system. The open loop transfer function and poles-zero models that are developed are those of the modified truss system. This analysis does provide a system transfer function that can be combined with a model of any controller to obtain a global transfer function that is representative of the entire system.

State-space realization from experimental data is attributed to work performed by Ho and Kaman [Ref. 25] in the 1960s. Ho and Kaman introduced the concepts of minimum realization theory that allowed the construction of the state-space representation of a linear system from noise-free data. The approach was later modified and extended [Ref. 26] for the identification of modal parameters from noisy data. This technique, known as the Eigensystem Realization Algorithm (ERA), is used here in a modified form to formulate the state-space representation of the space truss.

Before applying the above technique, certain quantities such as the observability and controllability matrices of a system need to be defined since they are an integral part of the system realization methodology that makes up the ERA. The development of these matrices is detailed in References 27 and 28, but is summarized here for completeness. The equations of motion for a finite-dimensional, linear-dynamic system are a set of n_2 second-order differential equations, where n_2 is the number of independent system coordinates. Let M, ζ, and K be the mass, damping, and stiffness matrices, respectively. The state equations can then be expressed in matrix notation as

$$\mathrm{M}\ddot{\omega} + \zeta\dot{\omega} + \mathrm{K}\omega = f(\omega,t) \tag{4.1}$$

where the ω represents the generalized vectors of acceleration, velocity and position and $f(\omega,t)$ is the forcing function over the period of interest at specific locations on the structure. Equation (4.1) can be rewritten as a first-order system of differential equations in a number of ways, but a particular useful reformulation is of the form:

$$A_c = \begin{bmatrix} 0 & \mathrm{I} \\ -M^{-1}K & -M^{-1}\zeta \end{bmatrix}, \quad x = \begin{bmatrix} \omega \\ \dot{\omega} \end{bmatrix} \tag{4.2a}$$

$$B_c = \begin{bmatrix} 0 \\ M^{-1}B_2 \end{bmatrix}, \quad f(\omega,t) = B_2 \cdot u(t) \tag{4.2b}$$

where A_c is a state matrix and B_2 is a $\mathrm{n}_2 \times r$ input "influence matrix" that characterizes the locations and the types of inputs, and r is the number of inputs into the system. Using this formulation equation (4.1) can be rewritten as

$$\dot{x} = A_c \cdot x + B_c \cdot u \tag{4.3}$$

If the response of the system is measured by m output quantities in an output vector, $y(t)$, that is measured by sensors such as accelerometers, strain gauges, force sensors, etc., the output can be written in matrix form as

$$y = C_a \cdot \ddot{\omega} + C_v \cdot \dot{\omega} + C_d \cdot \omega \tag{4.4}$$

where C_a, C_v, and C_d are the output influence matrices for acceleration, velocity and displacement. These matrices describe the relationship between the ω vectors and the measured output vector, y. If one solves for omega double-dot in equation (4.1) and substitutes the quantity into equation (4.4), the resultant equation becomes:

$$y = C_a \cdot M^{-1} \cdot [B_2 \cdot u - \zeta \cdot \dot{\omega} - K \cdot \omega] + C_v \cdot \dot{\omega} + C_d \cdot \omega \tag{4.5a}$$

or

$$y = C \cdot x + D \cdot u \tag{4.5b}$$

where

$$C = \left[C_d - C_a \cdot M^{-1} \cdot K \quad C_v - C_a \cdot M^{-1} \cdot \zeta\right] \qquad D = C_a \cdot M^{-1} \cdot B_2$$

Equation (4.3) and (4.5a) represent the continuous-time model of a dynamical system. The discrete-time representation of the above equations is expressed below:

$$x(k+1) = Ax(k) + Bu(k) \tag{4.6}$$

$$y(k) = Cx(k) + Du(k) \tag{4.7}$$

where x, u and k are the state, control and output vectors respectively. The matrices [A_c, B_c, C, D] and [A, B, C, D] are used to determine systems response to any input.

From Reference 27 the solution at time, t_f, to equation (4.3) is of the form

$$x(t_f) = e^{A_c(t_f - t_o)} \cdot x(t_o) + \int_{t_o}^{t_f} e^{A_c(t_f - \tau)} \cdot B_c \cdot u(\tau) d\tau \tag{4.8}$$

for $t \geq t_o$. The solution to the discrete-time representation, equation (4.6), for time $t_f = p\Delta t$ where Δt is the sampling time is

$$x(p) = A^p x(0) + \sum_{i=1}^{p} A^{i-1} B u(p-i) \tag{4.9}$$

or in matrix form

$$x(p) = A^p x(0) + \begin{bmatrix} B & AB & A^2B & \cdots & A^{p-1}B \end{bmatrix} \cdot \begin{bmatrix} u(p-1) \\ u(p-2) \\ u(p-3) \\ \vdots \\ u(0) \end{bmatrix} \tag{4.10}$$

we set the two matrices in equation (4.10) equal to

$$Q_p = \begin{bmatrix} B & AB & A^2B & \cdots & A^{p-1}B \end{bmatrix} \quad \text{and} \quad P_p = \begin{bmatrix} C \\ CA \\ CA^2 \\ \vdots \\ CA^{\alpha-1} \end{bmatrix} \tag{4.11}$$

In system identification theory, the Q_p and P_p matrices are termed the generalized observability and controllability matrices [Ref. 27 and 28]. In both cases, the properties defined by these specialized matrices determine the observability and controllability of a system. A state of a system is said to be controllable if the state can be reached from any initial state in a finite time through some control action. Likewise, a system is observable if knowledge of the input, u, and output, y, over a finite time interval completely determines the state, x. Both of these matrices play an integral role in the Eigensystem Realization Algorithm.

A "realization" is a computation of the A, B, and C matrices that are defined in equation (4.11). A system has an infinite number of realizations, which predict the same response from an individual input. "Minimum realization" develops a model containing the smallest state-space dimensions among this infinite number of realizations. The ERA method produces a series of minimized matrices that are derived from the discrete time data. In the case of the space truss this data is provided by the frequency response data that was collected by the HP-35655A digital signal analyzer. A complete knowledge of the A, B, and C matrices will define the state-space model of the actuator-sensor system that is both observable and controllable. The computational steps of ERA used in this development are adapted from Reference 27 and displayed in Figure 44. The computational steps of the ERA are realized in the MATLAB code, *active.m,* which is

included in Appendix P. The following paragraphs are description of the ERA approach along with some observations on peculiarities in the data may have affected the quality of the analysis.

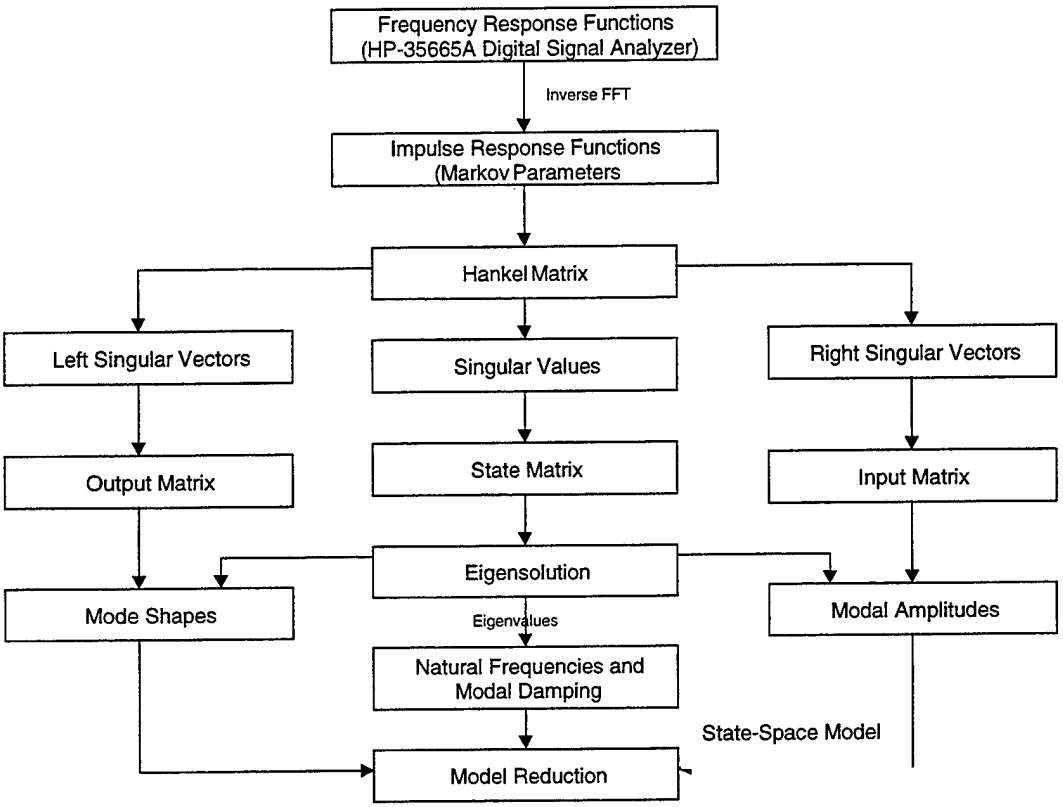

Figure 44. Flowchart for Modified ERA Analysis

To use the ERA, a set of discrete-time data is required. The data collected on the HP-35655A is in the frequency domain. Taking the inverse fast-fourier transform (IFFT) of the HP data obtains a series of complex data of which the real portion is an impulse-time representation of the data. This impulse response is displayed in Figure 45.

Taking the IFFT of the frequency response data is not, however, without error. The HP-35655A has aliasing and does not fully record all the spectral lines of the frequency response, in this particular case, only 800 of the 2048 are displayed in Figure 36. This data is vital when generating the time response. For this analysis, to offset the "lost" data zeros were inserted into the missing spaces prior to implementing the IFFT. This procedure will inject some error into the regenerated time data and will have a minor

effect on the data quality and resultant state-space representation. The procedure by which zeros replace the missing data is documented in the MATLAB code of Appendix P. The frequency response data will have to be collected again upon the installation and testing of the second active strut. At this time, it is important to select the feature on the HP-35655A that keeps all the spectral lines. This will eliminate any future error when the IFFT is generated.

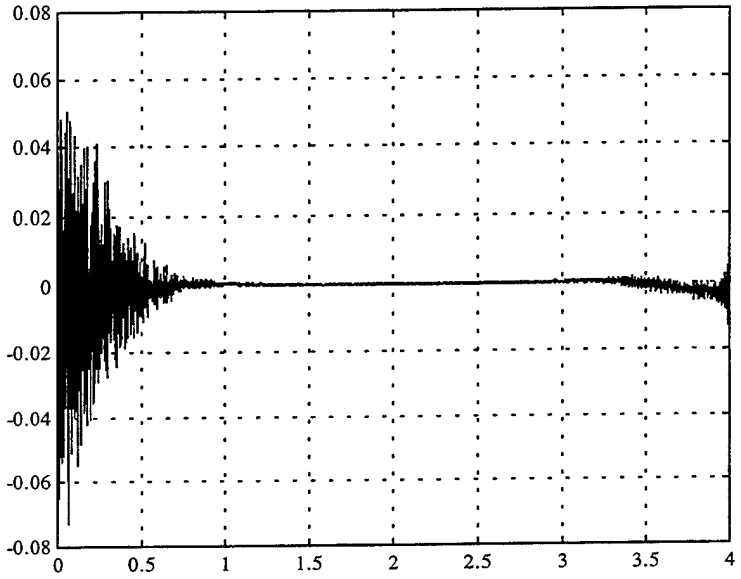

Figure 45. Impulse Response Generated From FRF of Actuator/Sensor Assembly

Once an impulse time response of the actuator-sensor system has been obtained, the ERA can be implemented. The first step is to place the time data into a reduced hankel matrix. The generalized hankel matrix is of the form:

$$H(i-1) = \begin{bmatrix} Y_k & Y_{k+1} & \cdots & Y_{k+\beta-1} \\ Y_{k+1} & Y_{k+2} & \cdots & Y_{k+\beta} \\ \vdots & \vdots & \ddots & \vdots \\ Y_{k+\alpha-1} & Y_{k+\alpha} & \cdots & Y_{k+\alpha+\beta-2} \end{bmatrix} \tag{4.12}$$

where the Ys are the Markov parameters of the form:

$$Y_o = D, \quad Y_1 = C \cdot B, \quad Y_2 = C \cdot A \cdot B, \quad \cdots, \quad Y_k = C \cdot A^{i-1} \cdot B \tag{4.13}$$

The *A, B, C,* and *D* are the matrices defined in equation (4.6) and (4.7), and are obtained from the real part of our time-domain matrix. Selecting an arbitrary number of points where we have an impulse response signal then generates the reduced hankel matrix. In this particular case, after an examination of Figure 45, the first 200 points of the time-domain data was utilized in the generation of the hankel matrix.

The ERA then conducts a singular value decomposition (SVD) on the hankel matrix to determine the optimal modal vectors [Ref. 27, p. 342]. The resultant SVD matrix is the same size as the hankel matrix, but has "ranked" the elements as a means of displaying which are most likely modal frequencies of the system. The singular values of the sensor-actuator system are displayed in Figure 46. A simplistic description of this process is to say that each "significant" singular value in Figure 46 represents a specific modal frequency for the sensor-actuator system.

In the case of the sensor-actuator system, "significant" is defined as non-zero, therefore from Figure 46, we determine that there are thirty modal frequencies for our system between 0 and 200 Hz. The elements that define these modal frequencies now become the observability and controllability matrices for our system and are used to derive the overall system state matrix. The MATLAB command, *svd.m*, generates the observability and controllability matrices as follows:

$$[u,s,v]=svd[h] \tag{4.14}$$

where *u* and *v* are the observability and controllability matrices respectively. From the observability and controllability matrices it is now possible to define the state matrix, *A*. Remember that the observability matrix for the is of the form:

$$X=\begin{bmatrix} C \\ CA \\ CA^2 \\ \vdots \\ CA^{m-1} \\ CA^m \end{bmatrix} \tag{4.15}$$

Equation (4.15) shows that the state matrix, *A*, is entrained in the observability matrix.

Some simple matrix manipulation is used to extract the state matrix. First, the observability matrix into is decomposed into two separate matrices, *u1* and *u2*.

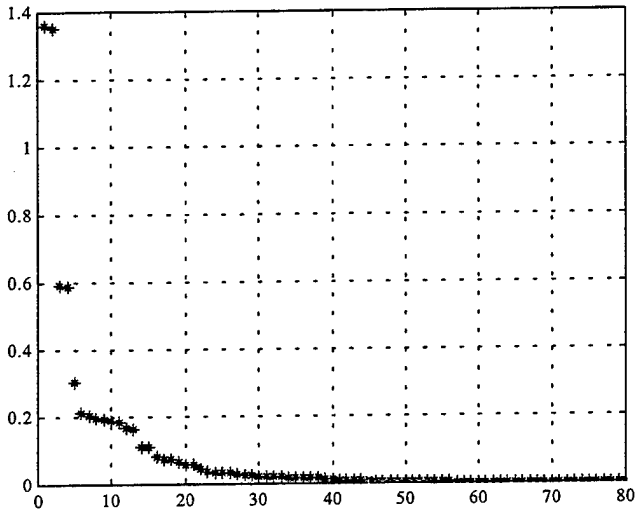

Figure 46. System Singular Values

$$u_1 = \begin{bmatrix} C \\ CA \\ CA^2 \\ \vdots \\ CA^{m-1} \end{bmatrix} \qquad u_2 = \begin{bmatrix} CA \\ CA^2 \\ \vdots \\ CA^{m-1} \\ CA^m \end{bmatrix} \tag{4.16}$$

Then by noting that:

$$u_1 \cdot A = u_2 \tag{4.17}$$

the state matrix can be obtained by taking the inverse of u_1 and multiplying by u_2.

$$A = [u_1]^{-1} \cdot [u_2] \tag{4.17}$$

The ERA now uses the eigenvalues of the state-matrix to determine the natural frequencies and associated damping ratios of the system. The *active.m* analysis code uses the MATLAB function (eig_fr) to pull out the natural frequencies and damping ratios from the individual elements of the state matrix. The code was developed with the assistance of Dr. Fred Tasker of the Naval Research Laboratory. The code is included

below for reference along with its derivation. Reference 29 provides clarification on the specific format of certain MATLAB functions. The variables called into the function are the elements of the state matrix (D1) and the time increment (delt). These variables are used in the experimental determination of the impulse response.

```
function [fre1,zet1] = eig_fr(D1,delt)
nmod2 = size(D1,1);
for i = 1:nmode2
        alpha1 = 0.5 * log (D1(i). * conj(D1(i))/delt;
        beta1 = atan2(imag(D1(i),real(D1(i)))/delt;
        om1(i) = sqrt (alpha1^2 + beta1^2);
        fre1(i) = om1(i)/(2*pi);
        zet(i) = -alpha/om1(i);
end
```

Recall that the definition of the eigenfunction in complex form is:

$$z_i = e^{\lambda_i \cdot \Delta t} \tag{4.18}$$

$$\lambda_i = \left(-\zeta_i \cdot \omega_i + j \cdot \omega_i \cdot \sqrt{1-\zeta_i^2}\right) \tag{4.19}$$

Substituting equation (4.18) into (4.19):

$$z_i = e^{\lambda_i \cdot \Delta t} = e^{\left(-\zeta_i \cdot \omega_i + j \cdot \omega_i \cdot \sqrt{1-\zeta_i^2}\right)\Delta t} \tag{4.20}$$

which can be written as:

$$z_i = e^{-\zeta_i \cdot \omega_i \cdot \Delta t} \cdot e^{j \cdot \omega_i \cdot \sqrt{1-\zeta_i^2} \cdot \Delta t} \tag{4.21}$$

The Real and Imaginary components can then be extracted from equation (4.20):

$$z_i = e^{-\zeta_i \cdot \omega_i \cdot \Delta t} \cdot \left[\cos\left(\omega \cdot \sqrt{1-\zeta_i^2} \cdot \Delta t\right) + j \cdot \sin\left(\omega \cdot \sqrt{1-\zeta^2} \cdot \Delta t\right)\right]$$

$$z_i = e^{-\zeta_i \cdot \omega_i \cdot \Delta t} \cdot \cos\left(\omega \cdot \sqrt{1-\zeta_i^2} \cdot \Delta t\right) + e^{-\zeta_i \cdot \omega_i \cdot \Delta t} \cdot j \cdot \sin\left(\omega \cdot \sqrt{1-\zeta^2} \cdot \Delta t\right)$$

where the term on the left is the Real and the term on the write is the Imaginary term. Remembering from complex algebra that:

$$\sqrt{z_i \cdot z_i^*} = \sqrt{\text{Real}^2 + \text{Imag}^2} = e^{-\zeta_i \cdot \omega_i \cdot \Delta t} \tag{4.22}$$

Using the above relation, the damping ratio for each of the natural frequencies can

be determined. Equation (4.22) is decomposed into the variables used in the above MATLAB function. The physical meaning of the first of these variables is:

$$\text{alpha1} = \zeta_i \cdot \omega_i \tag{4.23}$$

Further manipulating equation (4.22) results in:

$$\frac{\text{Imag}}{\text{Real}} = \frac{\sin\left(\omega_i \cdot \sqrt{1-\zeta_i^2} \cdot \Delta t\right)}{\cos\left(\omega_i \cdot \sqrt{1-\zeta_i^2} \cdot \Delta t\right)} = \tan\left(\omega_i \cdot \sqrt{1-\zeta_i^2} \cdot \Delta t\right) \tag{4.24}$$

As a result:

$$\text{atan}\left(\frac{\text{Imag}}{\text{Real}}\right) = \omega_i \cdot \sqrt{1-\zeta_i^2} \cdot \Delta t \tag{4.25}$$

The corresponding variable in the MATLAB code is

$$\text{beta1} = \frac{\text{atan}\left(\frac{\text{Imag}}{\text{Real}}\right)}{\Delta t} = \omega_i \cdot \sqrt{1-\zeta_i^2} \tag{4.26}$$

Equations (4.23) and (4.24) can now be used to solve for the natural frequencies and the damping ratios. A tabulation of the damping ratios and natural frequencies developed from the adapted ERA method is displayed in Table 9. The resultant data shows interesting results. Three of the natural frequencies (13.113, 29.688, and 182.570 Hz) show damping ratios that are abnormally high. These higher than normal damping ratios could be a result of an inadequate data collection. Since the relevant damping ratios for the bare truss (HP-35655A) data were on in the order of 0-5%, additional tests should be conducted and the results analyzed to verify whether these ratios are realistic properties of the system.

Comparing the tabulated frequencies of Table 9 with the magnitude of the frequency response (Figure 36), it is evident that the final frequency, 199.333 Hz, is not present in the FRF plot. This is an effect of analyzing the data over a range of 200 Hz. At 200 Hz, the data of the impulse response trails off with the result that the analysis program perceives this as another modal frequency when in reality it is a manifestation of

the data analysis.

Frequency (Hz)	Damping Ratio (%)
13.113	11.050
17.125	4.050
29.688	14.620
72.075	0.330
89.371	0.580
96.153	1.000
103.046	0.470
110.338	0.590
135.820	0.130
140.448	0.260
175.789	0.160
180.874	1.390
182.570	20.430
192.966	0.200
199.333	1.440

Table 12. Natural Frequencies and Damping Ratios of Actuator/Sensor System

In addition to the natural frequencies and damping ratios, the ERA gives us the necessary elements to determine the state-space representation of the sensor-actuator system. Knowledge of the state, observability, and controllability matrices completely defines our system. By utilizing the MATLAB system identification toolbox (not available in the NPS SRDC) the state-space representation can be developed as follows:

$$sys = \mathrm{ss}(a, b, c, d) \tag{4.27}$$

where a, b, and c are the singular value optimizations of the state, observability, and controllability matrices and d is the initial time-response value. The variable, *sys,* is the state-space representation of the sensor-actuator system. By utilizing the MATLAB control systems toolbox this representation can be manipulated to obtain the transfer function, pole-zero model (Figure 47), or root-locus model (Figure 48) of the open-loop system. The above development has been included in the *active.m* MATLAB code of Appendix P. By combining this with a state-space representation of our control system it is now possible to develop an analytical model of the closed-loop transfer function.

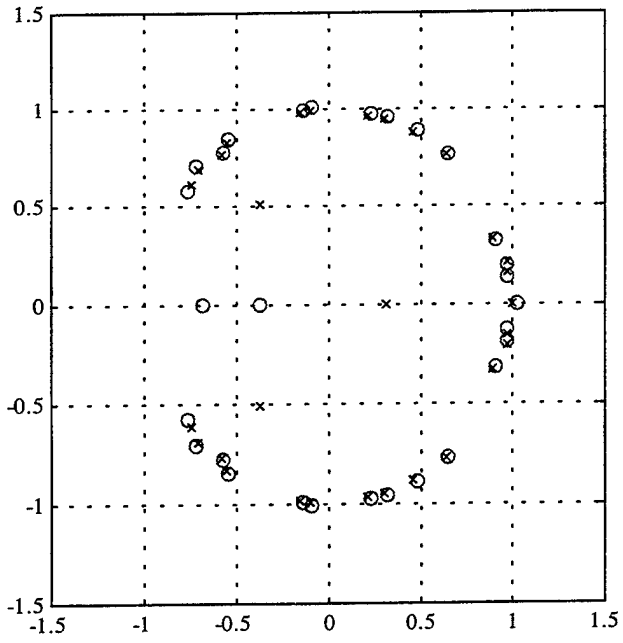

Figure 47. Actuator-Sensor Open-Loop Transfer Function Pole-Zero Plot

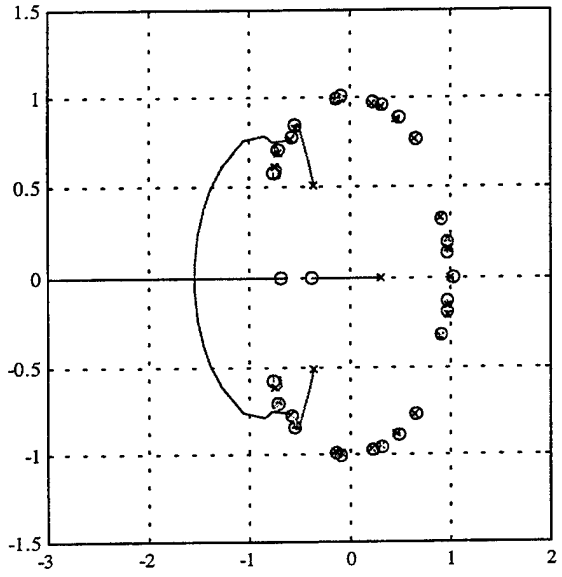

Figure 48. Actuator-Sensor Open-Loop Transfer Function Root Locus

V. CONCLUSIONS AND RECOMMENDATIONS

A. MODAL ANALYSIS

Impact modal testing of the NPS Space Truss was completed in order to identify the dynamic characteristics of the truss. The system input was provided from a PCB Impulse hammer and the system response was measured with Kistler tri-axis accelerometers. Two data acquisition/analysis systems were employed, dSPACE and the HP-35665A two-channel signal analyzer. After reviewing the testing data obtained using both systems, the conclusion was made that the results are inaccurate due to hardware limitations and further testing should be pursued to obtain an accurate set of data.

The research conducted in this thesis did identify potential improvements. The data acquisition system, dSPACE, was determined to be an inadequate data collection tool if used for modal testing and compelled further investigation into alternate data analysis systems. The dSPACE system at NPS possesses limited memory for data storage and manipulating the data files into the proper format to be used with the X-Modal modal analysis software is difficult and complex.

Use of a multi-channel signal analyzer is ideally suited for modal testing. The Hewlett Packard 35665A two-channel spectrum analyzer was employed for modal testing. Using only a two-channel analyzer, however, is time consuming and laborious. The HP-35665A however did produce higher quality data and in saved the data in the format compatible with X-Modal.

In the future, refinement of the existing NRL FEM should also be pursued. After confirming that the testing data is accurate, the FEM can be validated against the testing data using the Modal Assurance Criterion (MAC). MAC is a mechanism used to validate the correctness of mode shapes by verifying that the mode shapes are orthogonal. To obtain a set of high quality modal data for the NPS truss two possibilities are available. The first option is to use a more capable (multi-channel) signal analyzer, this will significantly reduce the number of test required and therefore minimize the error

associated with conducting multiple test. The second option is to out-source the truss to a contractor or other laboratory with adequate equipment for modal testing.

B. ACTIVE VIBRATION CONTROL

The active vibration control experiments, using a single piezoelectric strut, validated the use of integral plus double-integral force feedback as a means of actively suppressing the vibration on the NPS space truss using one active strut. The maximum response power reduction for the controlled versus uncontrolled case was 14.817 dB. The average reduction was on the order of 11-14 dB at various gain settings. The optimal frequency to operate the controller was determined to be 16.85 Hz, the second mode.

Damage to the second active strut did not allow us to target the first and second modal frequencies of the truss simultaneously. A second piezoceramic stack is currently on order. Upon arrival, the second stack should be integrated into the space truss using the preexisting interfaces that have already been constructed. With the installation of the second strut, the frequency response of both struts will have to be reevaluated and the two-strut controller should be implemented.

With the installation of the second strut, this active control configuration will be completed. The state-space representation of the open-loop transfer function should be combined with the state-space representation on the controller in order to develop a closed-loop transfer function of the system that can be to analytically model controller design. In the future, multiple sensor and actuator control of the space truss should be investigated. Two LPACTs and two piezoceramic stacks can be used as actuators along with accelerometers, fiber-optic devices, and force sensors to implement a variety of control options. There are numerous potential research opportunities involving the NPS space truss in the area of active control of spacecraft structures.

LIST OF REFERENCES

1. McClelland, Robert, Lim, Tae W., Bosse, Albert B., and Fisher, Shalom, "Implementation and Feedback Controllers for Vibration Suppression of a Truss Using Active Struts," *Proceedings of the International Society of Optical Engineering*, pp. 452-461, 1996.

2. Won, C. C., Sulla, L., Sparks, D. W., and Belvin, W. K., "Application of Piezoelectric Devices to Vibration Suppression," *Journal of Guidance, Control, and Dynamics,* Vol. 17 No. 6, November-December 1994, pp. 1333-1338.

3. Preumont, A., Dufour, J. P., and Malikian, C., "Active Damping by Local Force Feedback with Piezoelectric Actuators," *Journal of Guidance, Control, and Dynamics,* Vol. 15 No. 2, March-April 1992, pp. 390-395.

4. Fanson, J. L., Blackwok, G. H., and Chu, C-C., "Active Member Control of Precision Structures," *Proceedings of the AIAA Structures, Structural Dynamics, and Materials Conference,* pp. 1480-1494, 1989.

5. Andberg, Brent K., "*Modal Testing and Analysis of the NPS Space Truss,*" Naval Postgraduate School, September 1997.

6. Newsom, J. R., Layman, W. E., Waites, H. B., and Hayduk, R. J., "*The NASA Controls Structure Integration Technology Program,*" IAF-90-290, October 1990.

7. Smith-Taylor, R., and Tanner, S. E., "*Controls Structures Interaction Guest Investigator Program: Overview and Phase I Experimental Results and Future Plans.*" NASA Technical Memorandum 4412, Langley Research Center, February 1993.

8. Gronet, M. J., Davis, D. A., Kintis, D. H., Brillhart, R. D., and Atkins, E. M., *"Design, Analysis, and Testing of the Phase 1 CSI Evolutionary Model Erectable Truss."* NASA Contractor Report 4461, 1992.

9. Lim, T., W., and Waner, R. C., *"System Identification, Control and Health Monitoring of the NRL Space Truss Structure,"* Final Report KU-FRL-1159-1, Flight Research Laboratory, Univ. of Kansas Center for Research, Lawrence, Kansas, August 1995.

10. *LPACT and Electronics User Manual*, Planning Systems Incorporated, Melbourne Controls Group, Melbourne, FL, 1997.

11. Jaffe, B., Roth, R. S. and Marzullo, S., "Piezoelectric Properties of Lead Zirconate – Lead Titanate Solid Solution Ceramics," *Journal of Applied Physics*, Vol. 25, 1954, ps. 809-810.

12. *Piezo Performance Test Procedures and Documents (Technical Note TN 59E/2),* Physik Instrumente, Waldbronn, Germany, 12 February 1997.

13. *Kaman KD-2300.5SU Instruction Manual,* Kaman Instrumentation Corporation, Colorado Springs, CO, 1996.

14. *ICP Force Sensor Operating Manual,* PCB Piezotronics, Inc., Depew, NY, April 1996.

15. *Products for Micropositioning,* Physik Instrumente, Catalog 111.

16. Ewins, D. J., *Modal Testing: Theory and Practice*, Research Studies Press Ltd., John Wiley & Sons, New York, NY, 1984.

17. *MATLAB Signal Processing Toolbox*, The Math Works, Inc., Natick, MS, February 1994.

18. *Newport Vibration Control System Instruction Manual,* Newport Corp., Irvine, CA, 1991.

19. *Kistler Operating Instructions*, PiezoBEAM® Accelerometers, Kistler Instrument Corporation, Amherst, NY, 1997.

20. *Operating Instructions for the PCB Impact Hammer,* PCB Piezotronics, Inc., Depew, NY, April 1996.

21. White, R. G., and Pennington, R. J., "Practical Application of the Rapid Frequency Sweep Technique for Structural Frequency Response Measurement," *Aeronautical Journal*, May 1982.

22. *Kistler Operating Instructions*, Model 5124A Multi-Channel Couplers, Kistler Instrument Corporation, Amherst NY, April 1989.

23. *HP-35665A Dynamic Signal Analyzer Concept's Guide*, Hewlett Packard Company, Everett WA, June 1995. Krauss, T.P., Shure, L., and Little, J.N.,

24. *HP-35665A Dynamic Signal Analyzer Operator's Guide*, Hewlett Packard Company, Everett WA, June 1995. Krauss, T.P., Shure, L., and Little, J.N.,

25. Ho, B. L. and Kaman, R. E., "Effective Construction of Linear State-Variable Models from Input/Output Data," *Proceedings of the Third Annual Allerton Conference on Circuit and System Theory,* 1965, pp. 449-459.

26. Juang, J.-N. and Pappa, R. S., "An Eigensystem Realization Algorithm for Modal Parameter Identification and Model Reduction," *Journal of Guidance, Control, and Dynamics,* Vol. 8 No. 5, September-October 1985, pp. 620-627.

27. Juang, Jer-Nan, *Applied System Identification*, PTR Prentice Hall Inc, Englewood Cliffs NJ, 1994.

28. Ljung, Lennart, *System Identification: Theory For The User,* PTR Prentice Hall Inc, Englewood Cliffs NJ, 1987.

29. *MATLAB: High Performance Numeric Computation and Visualization Software Reference Guide,* The Math Works Inc, Natick MA, April 1995.

APPENDIX A. NPS SPACE TRUSS PROPERTIES

The following appendix is a conglomeration of data that represents some of the physical properties of the NPS space truss that have been determined through testing conducted in this and prior theses. The data is referenced according to its source and is provided as background to the reader and as a quick reference for future researchers.

Stiffness [Ref. 5]:

Battens/Longerons						
Number	**Serial #**	**f** (Hz)	ω (rad/sec)	**keff** (N/m)	**keff** (lb/in)	**ksta** (lb/in)
1	1-C-003	374.0	2349.911	5.19E+06	29609	29589
2	11-E-185	373.0	2343.628	5.16E+06	29451	29227
3	11-K-191	372.0	2337.345	5.13E+06	29293	32872
4	11-D-184	374.0	2349.911	5.19E+06	29609	30451
5	11-F-186	373.0	2343.628	5.16E+06	29451	28956
			average =	5.16E+06	29482	30219
			std. dev. =	2.31E+04	132	1587
			std. dev./ave. =	0.45%	0.45%	5.25%

Table 13. Batten/Longeron Effective Stiffness

Diagonal Elements						
Number	**Serial #**	**f** (Hz)	ω (rad/sec)	**keff** (N/m)	**keff** (lb/in)	**ksta** (lb/in)
1	10-R-177	301.5	1894.380	3.38E+06	19280	17852
2	6-N-089	303.0	1903.805	3.41E+06	19472	18866
3	10-S-178	304.0	1910.088	3.43E+06	19601	18334
4	10-T-179	303.5	1906.947	3.42E+06	19537	19277
5	10-P-175	300.0	1884.956	3.34E+06	19089	18041
			average =	3.40E+06	19396	18474
			std. dev. =	3.67E+04	210	590
			std. dev./ave. =	1.08%	1.08%	3.19%

Table 14. Diagonal Effective Stiffness

Natural Frequencies [Ref. 1 and 5]:

Mode Number	ω_n (rad/s)	Frequency (Hz)
1.00	92.01	14.64
2.00	102.14	16.26
3.00	191.06	30.41
4.00	213.44	33.97
5.00	395.40	62.93
6.00	468.36	74.54
7.00	506.79	80.66
8.00	634.66	101.01
9.00	793.12	126.23
10.00	854.35	135.97
11.00	885.68	140.96
12.00	1246.87	198.44
13.00	1305.21	207.73
14.00	1442.56	229.59
15.00	1461.82	232.66
16.00	1616.49	257.27
17.00	1762.29	280.48
18.00	1788.50	284.65
19.00	1970.66	313.64
20.00	2206.76	351.22

Table 15. NPS Space Truss Natural Frequencies

Mode Number	ω_n (rad/s)	Frequency (Hz)
1.00	79.24	12.61
2.00	88.65	14.11
3.00	166.23	26.46
4.00	185.71	29.56
5.00	343.14	54.61
6.00	404.34	64.35
7.00	435.82	69.36
8.00	549.16	87.40
9.00	689.26	109.70
10.00	742.51	118.17
11.00	769.08	122.40
12.00	1079.80	171.88
13.00	1139.06	181.29
14.00	1246.46	198.38
15.00	1255.79	199.87
16.00	1404.31	223.50
17.00	1527.16	243.06
18.00	1548.37	246.49
19.00	1704.14	271.22
20.00	1902.63	302.81

Table 16. NRL Space Truss Natural Frequencies

Mass Properties of the Bare and Modified Truss:

Part Name	Quant. In Bare Truss	Quant. In Mod Truss	Component Masses (kg)	Mass Bare Truss (kg)	Mass Mod. Truss (kg)
Node Balls	52	52	0.0663	3.445	3.445
Longerons	100	100	0.0448	4.475	4.475
Diagonals	61	58	0.0522	3.181	3.025
LPAC Strut	0	1	2.2760	0.000	2.276
Act. Strut #1	0	1	0.2900	0.000	0.290
Act. Strut #2	0	1	0.2724	0.000	0.272
Screw	322	322	0.0019	0.607	0.607
Total Mass Truss				11.708	14.390

Table 17. Mass Properties of Bare and Modified Truss

APPENDIX B. ELECTRONIC HARDWARE DOCUMENTATION

The following appendix provides a condensed summary of the specific characteristics of equipment used throughout the course of this research project. All manufacture's purchasing data is included as well as calibration characteristics for certain pieces. The data contained herein is referenced throughout this thesis and is integral to the analysis of the modal test and active control data sets of the NPS Space Truss. Additionally, information is included on instrumentation that can be used for future research applications.

Kistler Instrument Corp. Accelerometers:
(Note: g = 9.807 m/s^2)
Sensitivity at 100 Hz, 3 g rms

Type	Serial Number	+ x-axis	+ y-axis	+ z-axis	
8690C50	C112865	98.7	101.6	97.7	mV/g
8690C50	C112866	101.1	100.3	96.7	mV/g
8690C50	C112867	98.9	99.8	99.7	mV/g
8960C50	C112868	99.2	99.5	99.1	mV/g
8690C10	C112398	495	490	494	mV/g
8690C10	C112399	487	490	490	mV/g
8690C10	C112400	499	500	494	mV/g
8690C10	C112401	497	491	505	mV/g

Kistler Instrument Corp. Signal Conditioners (Multi-Channel Couplers):

Type	Serial Number
5124A (twelve channel)	C74930
5124A (twelve channel)	C74929

PCB® Piezotronics Impulse Force Hammer:

Type	Serial Number	Notes
086B01	4144	Hard (White), Soft (Red) and Very Soft (Black) plastic tips used for different testing. Tip used is annotated in test procedures.

PCB® Piezotronics Axial Force Sensor:

Type	Serial Number	Notes
Model 208B02	15022	Installed in with Active Strut #1
Model 208B02	15023	Active Strut #2

PCB® Piezotronics Signal Conditioner:

Type	Serial Number	Notes
484B	2086	Set CPLG to DC & Bias to 6 V
484B	2087	Set CPLG to DC & Bias to 6 V

Trek Voltage Amplifier:

Type	Serial Number	Notes
Trek 50/750	none	Requires calibration on 10 September 1998. Two channels that can be used with both active struts. Alternative models: Burleigh Model XXXX

Kaman Eddy Current Sensor:

Type	Serial Number	Notes
KD2300-.5SU	S9721761-01-01	Calibration Data from Reference 13 and included below.

Displacement (MILS)	Output (Volts)	Least Squares Fit (Volts)	Non-Linearity % FSO
0.00	0	-0.010	0.20
1.00	0.49	0.492	-0.04
2.00	0.988	0.994	-0.12
3.00	1.487	1.496	-0.18
4.00	1.996	1.998	-0.03
5.00	2.499	2.500	-0.01
6.00	3.005	3.001	0.07
7.00	3.507	3.503	0.07
8.00	4.011	4.005	0.12
9.00	4.511	4.507	0.08
10.00	5.001	5.009	-0.16

Table 18. Kaman Eddy Sensor Calibration Data

Polytec PI Piezoceramic Actuators:

Signal [Volts]	Expansion [Microns]	Contraction [Microns]	Hysteresis [Microns]	Hysteresis [Percent]
0.00	0.00	0.00	0.00	0.00
1.00	3.48	6.43	2.94	5.98
2.00	7.58	12.55	4.97	10.12
3.00	12.16	18.38	6.21	12.64
4.00	17.20	23.86	6.66	13.56
5.00	22.53	29.06	6.53	13.28
6.00	27.96	33.90	5.95	12.10
7.00	33.44	38.38	4.94	10.05
8.00	38.83	42.43	3.61	7.34
9.00	44.05	46.07	2.02	4.11
10.00	49.14	49.14	0.00	0.00

Table 19. Expansion and Contraction Data for Model P-843.30

Planning Systems LPACT [Ref. 10]:

Type	Serial Number	Notes
LPACT	CML-030-020-1	Reference 10 for instructions.

Item	Value
Force Constant (K_f)	5.5 lb/amp
Max. Current	1 amp
Coil Resistance	9 ohms
Flexure Natural Frequency (ω_n)	8 to 10 Hz
Flexure Modal Damping(ξ)	~3 % (or critical) without force loop, up to >100% with force loop on
Stroke	±0.2 inches
Stroke at 10 Hz for 3 lbs. output force	0.1 inches
Gravity Offset Spring Rate	2.4 lb/in
Allowable Strut Diameter	1.000 ± 0.01"
LPACT Envelope	3.8" OD x 4.86" height (including strut clamp and accelerometers)
LPACT Total Weight	4.0 lb.
LPACT Proof Mass Weight	2.9 LB

LPACT Model (low frequency) (refer to Figure 2 for measured FRF from current to force of LPACT)	$\frac{Output\,Force(lb)}{Current\ \text{Command}(amp)} = \frac{K_f s^2}{s^2 + 2\xi\omega_n s + \omega_n}$
Servo Amp Model	$\frac{\text{Current (amp)}}{\text{Servo Command (V)}} = K_a = 0.1\ \frac{\text{amp}}{\text{V}}$
Force Loop Model (see section 3.3 for definition of terms)	$\frac{\text{Servo Amp Voltage Command (volts)}}{\text{Pr oof Mass Accel (g)}} = \frac{K_{pre}\ K_{rt} K_{force} s^2}{(s + w_{pre})(s + w_{rt})^2}$
Rate Loop Model (see section 3.3 for definition of terms)	$\frac{Servo\ \text{Amp Voltage Command (volts)}}{\text{Primary Accel}(g)} = \frac{K_{pre} K_{rt} K_{rate} w_{rate} S_r\ s^2}{(s + w_{pre})(s + w_{rt})^2 (s + w_{rate})}$

Table 20. LPACT Characteristics

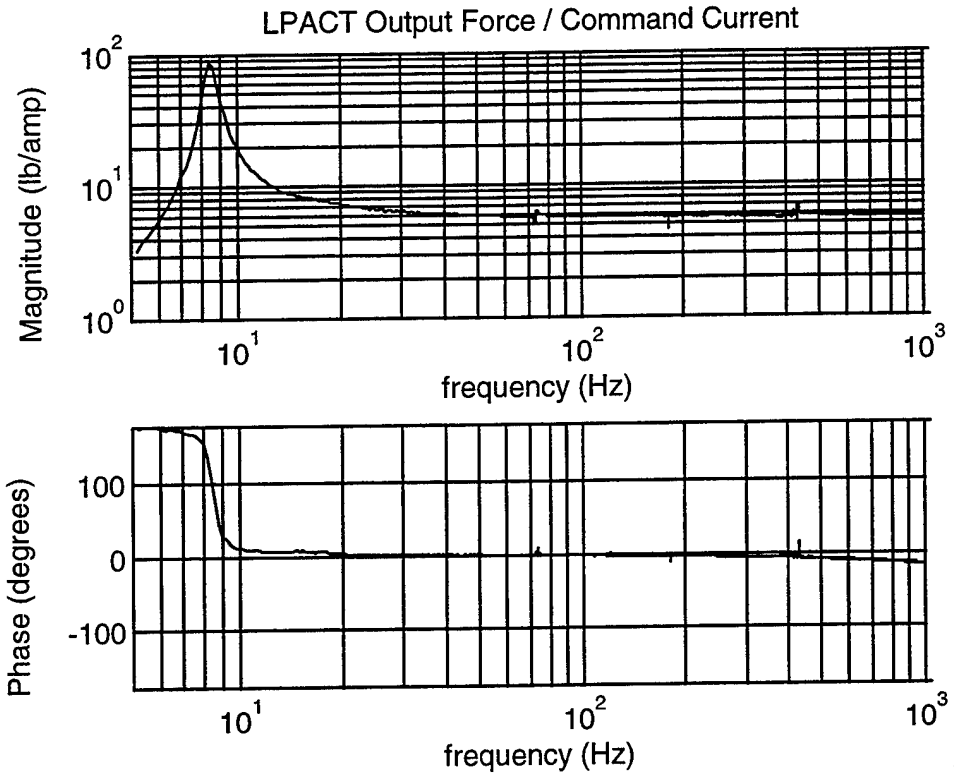

Figure 49. Measured Force/Current Transfer Function of LPACT (force loop off)

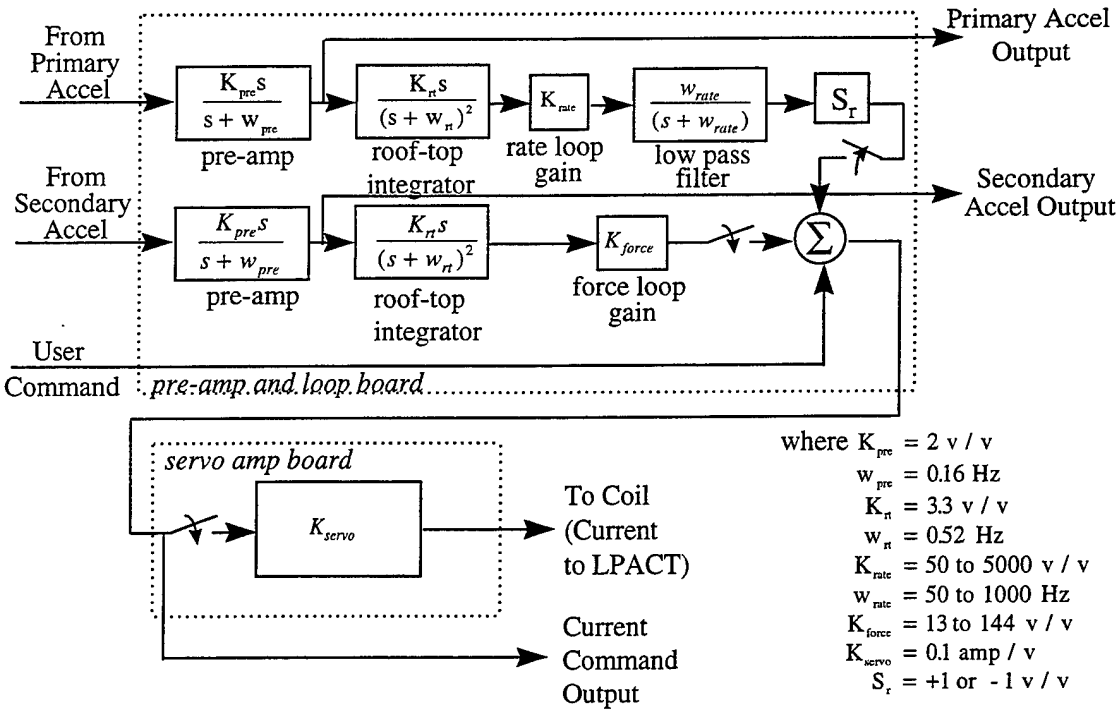

Figure 50. Block Diagram of Electronics

APPENDIX C. ENGINEERING DESIGN DRAWINGS

The following section contains a series of engineering drawings that were generated for the craftsmen in the Aeronautical Engineering, Mechanical Engineering and Space System Academic Group shops in order to cut and manufacture the interface struts that allowed incorporation of the LPACT and piezoceramic stacks into the space truss. The drawings use standard engineering drawing conventions and were generated using the TURBOCAD 2D and 3D software in the Space Dynamics and Research Laboratory.

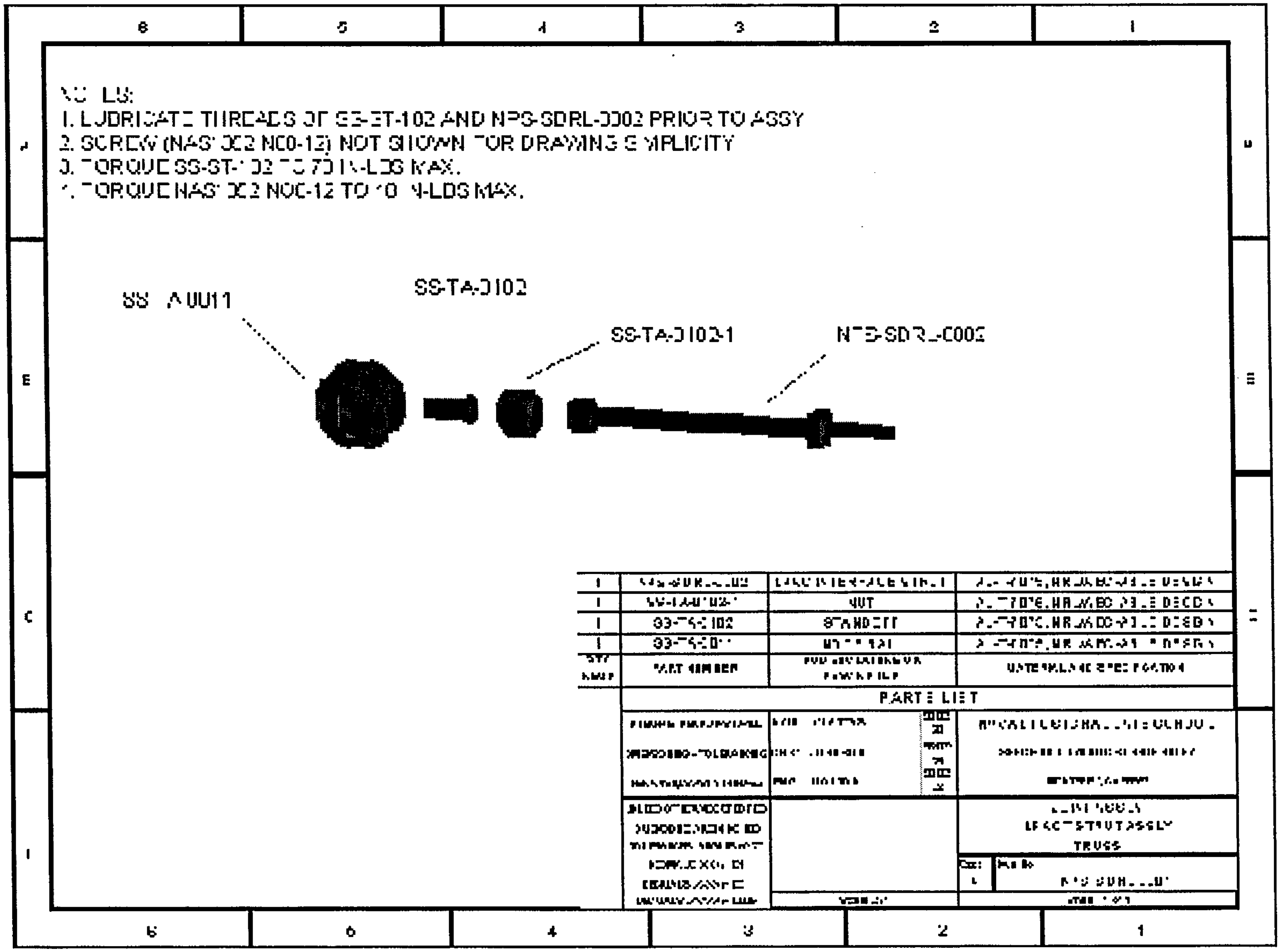
NOTES:
1. LUBRICATE THREADS OF SS-ST-102 AND NPS-SDRL-0002 PRIOR TO ASSY
2. SCREW (NAS1352 N08-12) NOT SHOWN FOR DRAWING SIMPLICITY
3. TORQUE SS-ST-102 TO 70 IN-LBS MAX.
4. TORQUE NAS1352 N08-12 TO 10 IN-LBS MAX.
SS-TA-0102
SS-TA-0102-1
NPS-SDRL-0002
NUT
STANDOFF
PART NUMBER
PARTS LIST
TRUSS

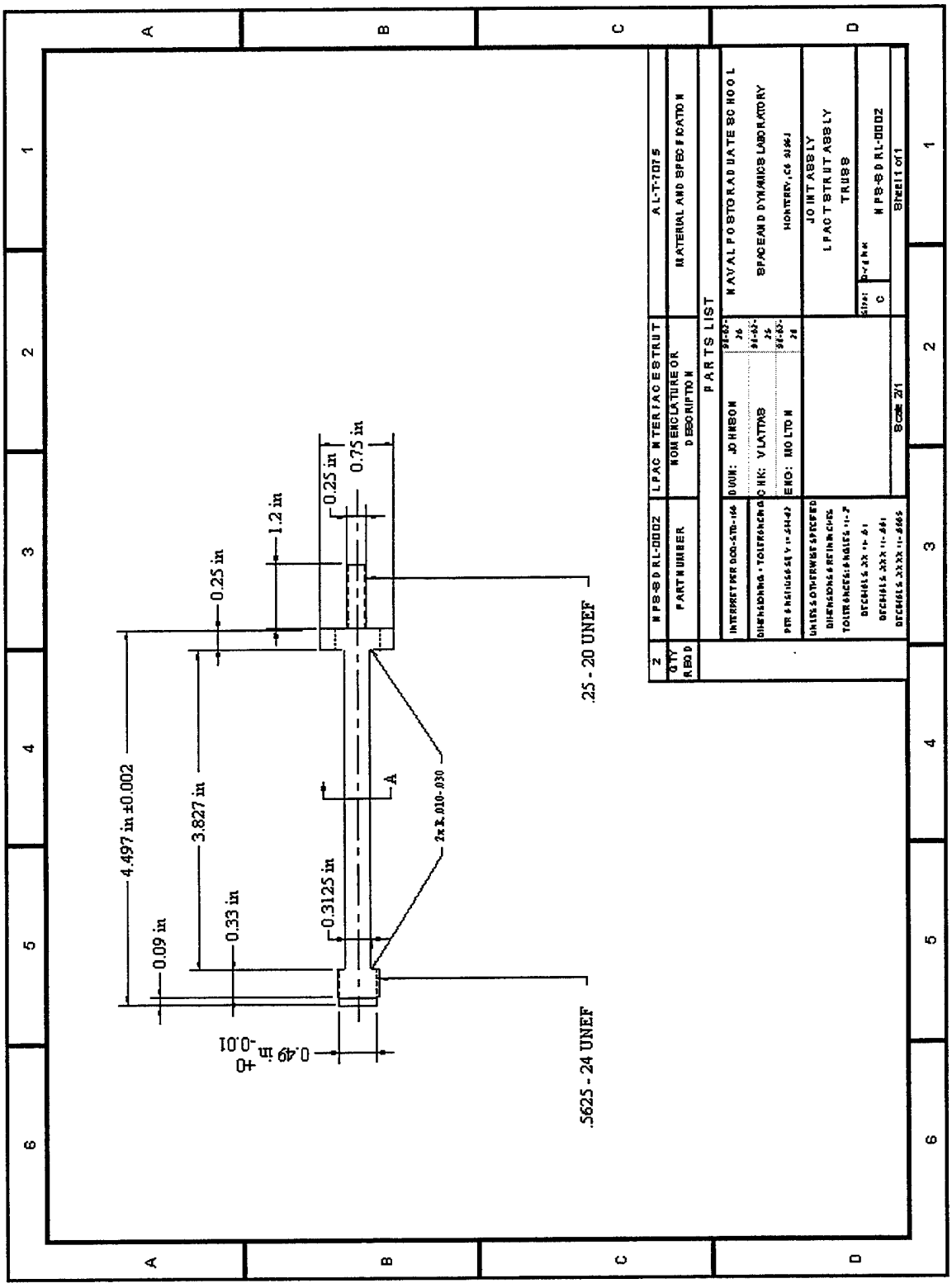
4.497 in ±0.002
3.827 in
0.09 in
0.33 in
0.3125 in
0.25 in
1.2 in
0.25 in
0.75 in
0.49 in +0 -0.01
2x R.010-.030
A
.25 - 20 UNEF
.5625 - 24 UNEF
A
B
C
D
1
2
3
4
5
6
PARTS LIST
NAVAL POSTGRADUATE SCHOOL
SPACE AND DYNAMICS LABORATORY
MONTEREY, CA 93943
JOINT ASSLY
LPAC STRUT ASSLY
TRUSS
MPS-BDRL-0002
Sheet 1 of 1
Scale: 2/1

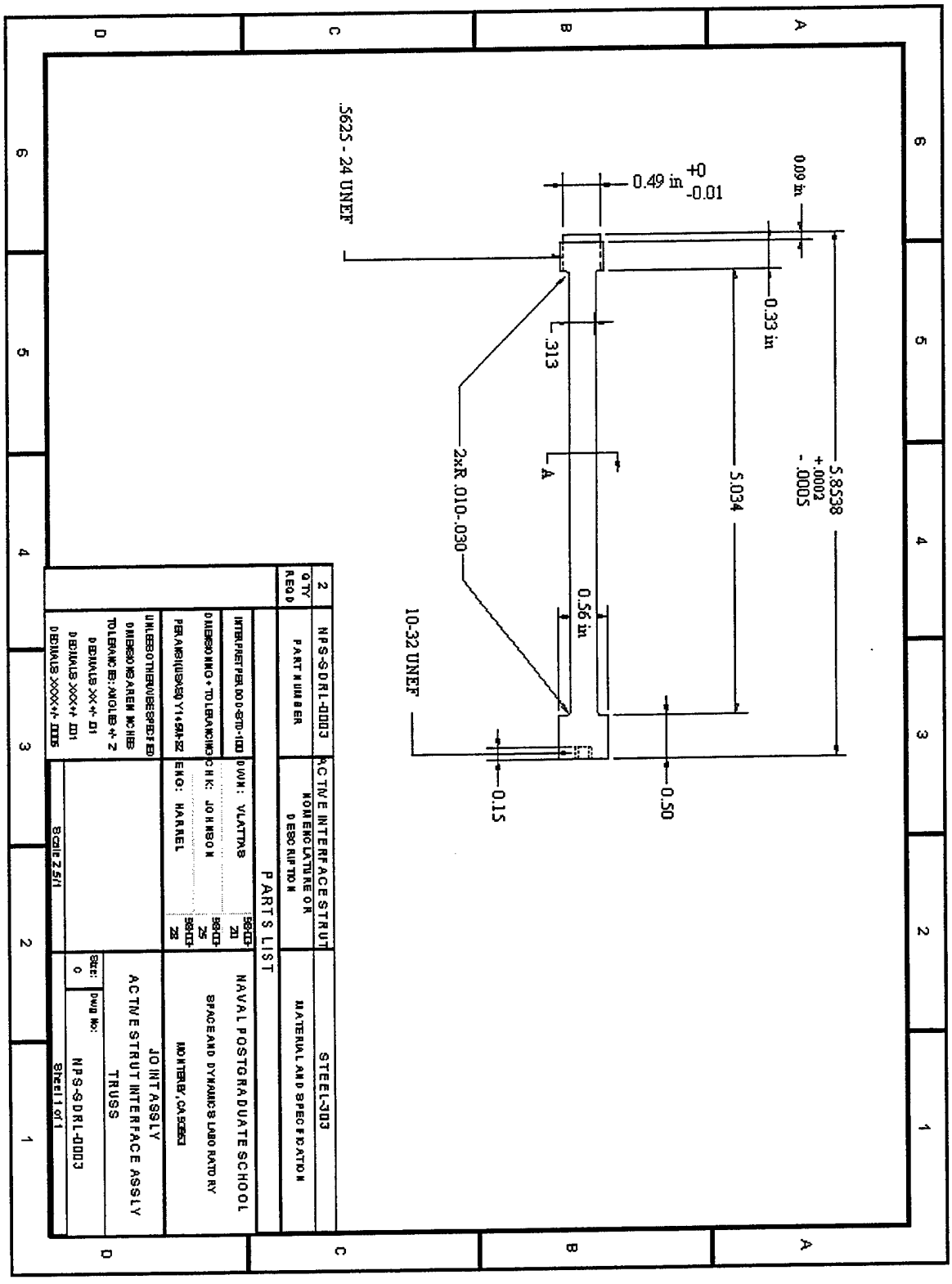
.5625 - 24 UNEF
0.49 in +0 -0.01
0.09 in
0.33 in
.313
A
2xR .010-.030
0.56 in
10-32 UNEF
5.8538 +.0002 -.0005
5.034
0.15
0.50
PARTS LIST
NPS-SDRL-0003
ACTIVE INTERFACE STRUT
STEEL-303
NAVAL POSTGRADUATE SCHOOL
SPACE AND DYNAMICS LABORATORY
MONTEREY, CA 93943
JOINT ASSLY
ACTIVE STRUT INTERFACE ASSLY
TRUSS
NPS-SDRL-0003
Scale 2.5/1
Sheet 1 of 1

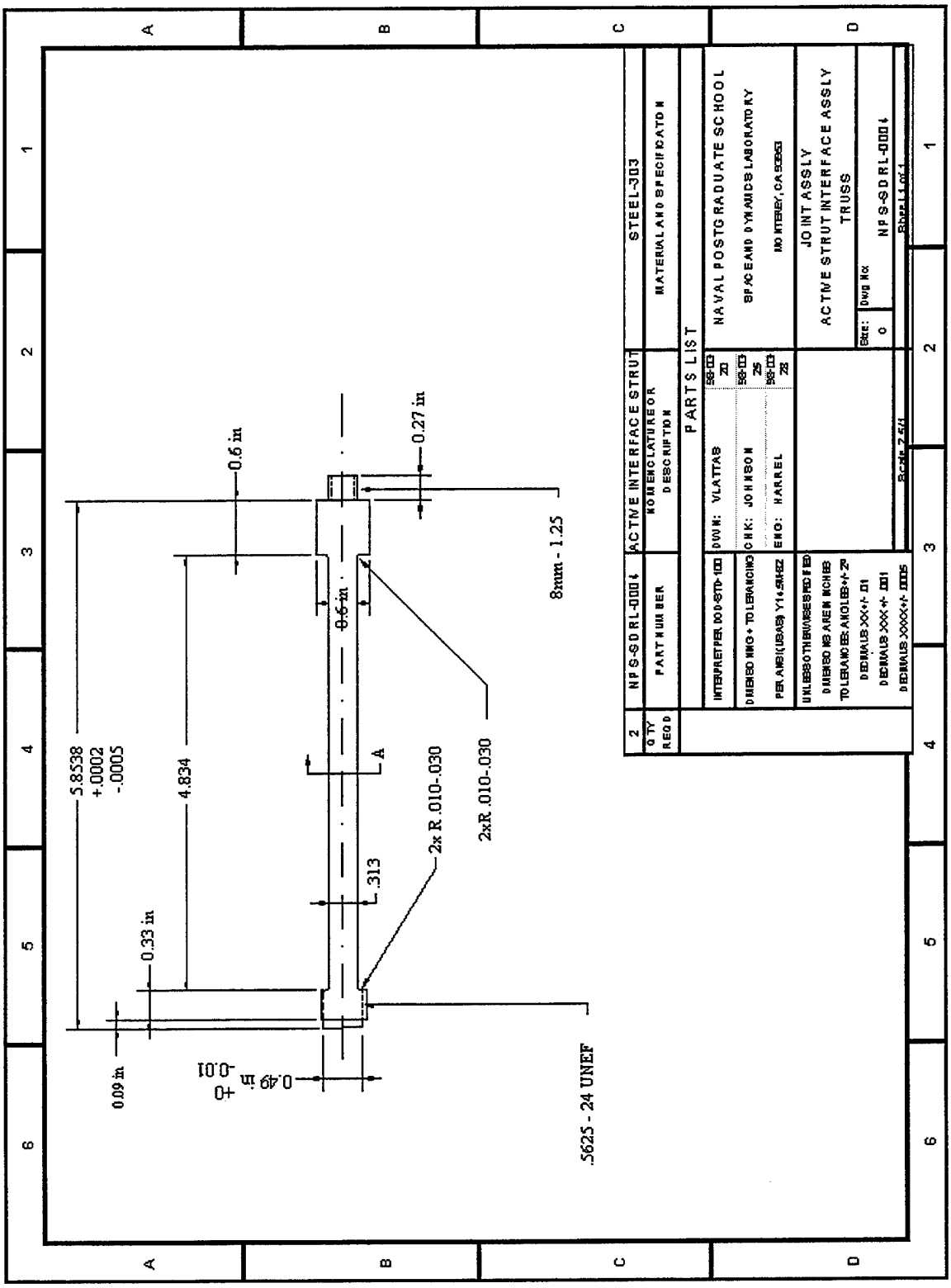
5.8538
+.0002
-.0005
4.834
0.6 in
0.27 in
0.33 in
0.09 in
0.49 in +0 -0.01
.313
2x R .010-.030
2xR .010-.030
8mm - 1.25
.5625 - 24 UNEF
A
STEEL-303
ACTIVE INTERFACE STRUT
NPS-SDRL-0004
PARTS LIST
NAVAL POSTGRADUATE SCHOOL
SPACE AND DYNAMICS LABORATORY
MONTEREY, CA 93943
JOINT ASSLY
ACTIVE STRUT INTERFACE ASSLY
TRUSS
NPS-SDRL-0004

APPENDIX D. PIEZO.M - MATLAB ANALYSIS CODE

```
%  PIEZO.M - MATLAB Analysis Code
%  This program plots the piezo calibration data by converting the
%  expansion data from a voltage reading to a physical displacement
%  using  calibration data provided by the manufacturer.
%  Experiments conducted 10 Mar 98

%  Program written by LT John Vlattas and LT Scott Johnson

clear all

volt=[0 1:10].*10;              % Load Applied Voltage Vector

% Manufacturer's Expansion Data

expand1 = [0 3.48 7.58 12.16 17.2 22.53 27.96 33.44 38.83 44.05 49.14];
expand2  =  [0  6.43  12.55  18.38  23.86  29.06  33.90  38.38  42.43  46.07
49.14];

% Experimental Expansion and Contraction For Piezo #1 and Piezo #2
% Data Entry - Table #3

p1exp1=[2.505  2.407  2.282  2.124  1.988  1.850  1.693  1.558  1.428  1.3
1.175];
p1cont1=[1.175  1.229  1.3  1.38  1.461  1.552  1.657  1.767  1.891  2.016
2.157];
p1exp2=[2.159  2.09  2.001  1.905  1.805  1.682  1.569  1.455  1.342  1.222
1.117];
p1cont2=[1.117  1.168  1.237  1.319  1.403  1.490  1.594  1.696  1.824  1.942
2.077];
p1exp3=[2.107  2.034  1.948  1.864  1.753  1.644  1.526  1.417  1.300  1.188
1.087];
p1cont3=[1.087  1.138  1.205  1.285  1.373  1.462  1.560  1.668  1.785  1.907
2.034];
p2exp1=[2.010  1.951  1.867  1.772  1.660  1.534  1.402  1.280  1.156  1.045
.937];
p2cont1=[.937  .997  1.060  1.140  1.228  1.319  1.416  1.534  1.652  1.771
1.898];
p2exp2=[1.892  1.830  1.752  1.655  1.553  1.438  1.325  1.220  1.105  1.002
.901];
p2cont2=[.901  .956  1.028  1.100  1.187  1.280  1.382  1.494  1.605  1.733
1.866];
p2exp3=[1.866 1.8 1.717 1.619 1.525 1.405 1.299 1.190 1.075 .975 .870];
p2cont3=[.870 .928 1 1.073 1.16 1.252 1.353 1.46 1.58 1.702 1.825];


% Extracts Data from Piezo#1 Expansion and Contraction Vectors

for n=1:3
      h=ones(size(eval(['p1exp' num2str(n)])));  %Generates Ones Vector
      x=(eval(['p1exp' num2str(n)]));
      y=x(1:1);                                  %Takes First Voltage Reading
      z=h*y;                                          %Generates Vector
      a=abs(eval(['p1exp' num2str(n)])-z);
```

```
      c=abs(eval(['p1cont' num2str(n)])-z);
      d=fliplr(c);                                    %Flips       Contraction
Matrix
      b=((a*2)*1000)*2.54e-2;
      e=((d*2)*1000)*2.54e-2;
      eval(['M' num2str(n) ' = b']);
      eval(['P' num2str(n) ' = e']);
end

% Extracts Data from Piezo#2 Expansion and Contraction Vectors

for n=1:3
      h=ones(size(eval(['p2exp' num2str(n)])));
      x=(eval(['p2exp' num2str(n)]));
      y=x(1:1);
      z=h*y;
      a=abs(eval(['p2exp' num2str(n)])-z);
      c=abs(eval(['p2cont' num2str(n)])-z);
      d=fliplr(c);                                    %Flips       Contraction
Matrix
      b=((a*2)*1000)*2.54e-2;
      e=((d*2)*1000)*2.54e-2;
      eval(['N' num2str(n) ' = b']);
      eval(['Q' num2str(n) ' = e']);
end

% Averages the three trials per piezo for graphing

exp1=(M1 + M2 + M3)./3;
exp2=(N1 + N2 + N3)./3;
cont1=(P1 + P2 + P3)./3;
cont2=(Q1 + Q2 + Q3)./3;

% Plot of Expansion and Contraction Curves Versus Manufacturer's Data

figure(1)

%  Plot of Expansion Data (Done for Legend Purposes)

plot(volt,expand1,'r--')
hold on
plot(volt,exp1,'b-.')
plot(volt,exp2,'g:')

%  Plot of Contraction Data

plot(volt,cont1,'b-.')
plot(volt,expand2,'r--')
plot(volt,cont2,'g:')

axis([0 105 0 60])
title('Expansion Characteristics of Model P-843.30 Piezo')
xlabel('Volts (V)')
ylabel('Expansion (microns)')
grid on
legend('r--','Manufacturers Data','b-.','Piezo #1','g:','Piezo #2')
```

APPENDIX E. dSPACE MODAL EXPERIMENTATION TEST LOG

This Appendix contains all relevant information for carrying out the dSPACE modal testing. Included within are the necessary cable arrangements and connections along with impact hammer, force magnitude data that were taken in order to aid in the analysis. In the general notes is some testing specific information that will aid in the reproduction of the results.

General Notes:

(a) A test series refers to a complete set of modal experiments for a given accelerometer setup. In general, for each test the truss will be impacted at two nodes (#41 and #24). The "a" in the file name refers to impact node 41 data and "b" refers to impact node 24 data. Dummy masses were attached to all nodes not being tested.

(b) Two tables are presented for each set of tests. The first table identifies the nodes, the associated accelerometers, the channel numbers, and the axes tested. The second table lists the true impact magnitudes read from the oscilloscope during dSPACE testing.

(c) During all testing the Newport table was floated.

(d) The sampling frequency was 10 kHz, and the test duration was 3.0 seconds. TRACE software was used for data collection.

Test No.: 1
Testing date: 14 March 1998, 1500
Data Storage Location: C:\Andberg\dSpace\Impact Test\

Experimental Setup: Test 1				
Node Tested	Accel Serial #	Line #	Channel # Signal Cond.	Axis
3	C112865	5	7	x
			8	y
			9	z
15	C112867	6	10	x
			11	y
			12	z
29	C112866	1	1	x
			2	y
			3	z
41	C112860	2	4	x
			5	y
			6	z

Table 21. dSpace Experimental Setup – Test 1.

Data Set: 1					
Test #	Magnitude dSpace (V)	Magnitude Oscilloscope (V)	Test #	Magnitude dSpace (V)	Magnitude Oscilloscope (V)
Test1-1a	0.065	3.750	Test1-1b	0.375	3.594
Test1-2a	0.200	3.300	Test1-2b	0.035	3.594
Test1-3a	0.300	4.100	Test1-3b	0.165	3.531
Test1-4a	0.120	3.500	Test1-4b	0.100	3.125
Test1-5a	0.180	2.500	Test1-5b	0.130	2.500
Test1-6a	0.050	3.813	Test1-6b	0.145	2.938
Test1-7a	0.025	2.500	Test1-7b	0.090	2.625
Test1-8a	0.070	3.158	Test1-8b	0.185	2.531
Test1-9a	0.150	1.812	Test1-9b	0.090	2.906
Test1-10a	0.100	4.000	Test1-10b	0.140	3.688

Table 22. dSpace Impact Testing Force Hammer Magnitudes - Test 1.

Test No.: 2
Testing date: 16 March 1998, 1200
Data Storage Location: C:\Andberg\dSpace\Impact Test\

Experimental Setup: Test 2				
Node Tested	Accel Serial #	Line #	Channel # Signal Cond.	Axis
4	C112865	5	7	x
			8	y
			9	z
16	C112867	6	10	x
			11	y
			12	z
30	C112866	1	1	x
			2	y
			3	z
42	C112860	2	4	x
			5	y
			6	z

Table 23. dSpace Experimental Setup – Test 2.

Data Set: 2					
Test #	Magnitude dSpace (V)	Magnitude Oscilloscope (V)	Test #	Magnitude dSpace (V)	Magnitude Oscilloscope (V)
Test2-1a	0.225	2.250	Test2-1b	0.095	5.750
Test2-2a	0.285	3.156	Test2-2b	0.135	4.187
Test2-3a	0.105	2.563	Test2-3b	0.030	5.000
Test2-4a	0.215	3.813	Test2-4b	0.090	4.437
Test2-5a	0.040	3.688	Test2-5b	0.150	3.000
Test2-6a	0.235	4.687	Test2-6b	0.050	3.625
Test2-7a	0.200	3.188	Test2-7b	0.025	3.625
Test2-8a	0.115	3.188	Test2-8b	0.140	3.313
Test2-9a	0.270	4.062	Test2-9b	0.400	4.062
Test2-10a	0.075	3.750	Test2-10b	0.270	3.750

Table 24. dSpace Impact Testing Force Hammer Magnitudes - Test 2.

Test No.: 3
Testing date: 16 March 1998, 1325
Data Storage Location: C:\Andberg\dSpace\Impact Test\

Experimental Setup: Test 3				
Node Tested	Accel Serial #	Line #	Channel # Signal Cond.	Axis
5	C112865	5	7	x
			8	y
			9	z
17	C112867	6	10	x
			11	y
			12	z
31	C112866	1	1	x
			2	y
			3	z
43	C112860	2	4	x
			5	y
			6	z

Table 25. dSpace Experimental Setup – Test 3.

Data Set: 3					
Test #	Magnitude dSpace (V)	Magnitude Oscilloscope (V)	Test #	Magnitude dSpace (V)	Magnitude Oscilloscope (V)
Test3-1a	0.220	3.563	Test3-1b	0.095	3.250
Test3-2a	0.070	3.563	Test3-2b	0.270	3.313
Test3-3a	0.070	4.562	Test3-3b	0.360	3.688
Test3-4a	0.240	4.562	Test3-4b	0.350	3.625
Test3-5a	0.265	3.375	Test3-5b	0.060	4.312
Test3-6a	0.230	3.938	Test3-6b	0.160	3.875
Test3-7a	0.080	3.750	Test3-7b	0.310	3.500
Test3-8a	0.140	3.750	Test3-8b	0.250	3.563
Test3-9a	0.250	4.062	Test3-9b	0.130	3.625
Test3-10a	0.200	3.625	Test3-10b	0.140	4.437

Table 26. dSpace Impact Testing Force Hammer Magnitudes - Test 3.

Test No.: 4
Testing date: 16 March 1998, 1415
Data Storage Location: C:\Andberg\dSpace\Impact Test\

Experimental Setup: Test 4				
Node Tested	Accel Serial #	Line #	Channel # Signal Cond.	Axis
6	C112865	5	7	x
			8	y
			9	z
18	C112867	6	10	x
			11	y
			12	z
32	C112866	1	1	x
			2	y
			3	z
44	C112860	2	4	x
			5	y
			6	z

Table 27. dSpace Experimental Setup – Test 4.

Data Set: 4					
Test #	Magnitude dSpace (V)	Magnitude Oscilloscope (V)	Test #	Magnitude dSpace (V)	Magnitude Oscilloscope (V)
Test4-1a	0.235	3.750	Test4-1b	0.280	4.000
Test4-2a	0.145	4.125	Test4-2b	0.085	3.063
Test4-3a	0.280	3.625	Test4-3b	0.255	3.563
Test4-4a	0.360	4.125	Test4-4b	0.125	3.688
Test4-5a	0.085	3.250	Test4-5b	0.320	4.312
Test4-6a	0.355	4.000	Test4-6b	0.135	4.187
Test4-7a	0.095	3.438	Test4-7b	0.330	3.750
Test4-8a	0.270	4.375	Test4-8b	0.150	4.062
Test4-9a	0.320	4.000	Test4-9b	0.290	4.062
Test4-10a	0.385	4.187	Test4-10b	0.150	3.375

Table 28. dSpace Impact Testing Force Hammer Magnitudes - Test 4.

Test No.: 5
Testing date: 17 March 1998, 1005
Data Storage Location: C:\Andberg\dSpace\Impact Test\

Experimental Setup: Test 5				
Node Tested	Accel Serial #	Line #	Channel # Signal Cond.	Axis
7	C112865	5	7	x
			8	y
			9	z
19	C112867	6	10	x
			11	y
			12	z
33	C112866	1	1	x
			2	y
			3	z
45	C112860	2	4	x
			5	y
			6	z

Table 29. dSpace Experimental Setup – Test 5.

Data Set: 5					
Test #	Magnitude dSpace (V)	Magnitude Oscilloscope (V)	Test #	Magnitude dSpace (V)	Magnitude Oscilloscope (V)
Test5-1a	0.1810	3.563	Test5-1b	0.3100	3.375
Test5-2a	0.3050	3.438	Test5-2b	0.3930	4.250
Test5-3a	0.3210	3.500	Test5-3b	0.0650	3.875
Test5-4a	0.2835	3.563	Test5-4b	0.3670	3.875
Test5-5a	0.0923	4.125	Test5-5b	0.0870	3.500
Test5-6a	0.7400	4.187	Test5-6b	0.2070	4.250
Test5-7a	0.2860	4.000	Test5-7b	0.2510	4.500
Test5-8a	0.2086	3.875	Test5-8b	0.1860	4.062
Test5-9a	0.1294	3.875	Test5-9b	0.4450	4.750
Test5-10a	0.2968	3.313	Test5-10b	0.3700	3.250

Table 30. dSpace Impact Testing Force Hammer Magnitudes - Test 5.

Test No.: 6
Testing date: 17 March 1998, 1145
Data Storage Location: C:\Andberg\dSpace\Impact Test\

Experimental Setup: Test 6				
Node Tested	Accel Serial #	Line #	Channel # Signal Cond.	Axis
8	C112865	5	7	x
			8	y
			9	z
20	C112867	6	10	x
			11	y
			12	z
34	C112866	1	1	x
			2	y
			3	z
46	C112860	2	4	x
			5	y
			6	z

Table 31. dSpace Experimental Setup – Test 6.

Data Set: 6					
Test #	Magnitude dSpace (V)	Magnitude Oscilloscope (V)	Test #	Magnitude dSpace (V)	Magnitude Oscilloscope (V)
Test6-1a	0.2069	3.813	Test6-1b	0.0900	3.813
Test6-2a	0.3210	3.938	Test6-2b	0.0577	4.250
Test6-3a	0.3026	4.000	Test6-3b	0.3539	4.125
Test6-4a	0.0767	3.688	Test6-4b	0.1400	3.750
Test6-5a	0.3553	3.750	Test6-5b	0.1978	3.938
Test6-6a	0.3724	4.000	Test6-6b	0.1130	3.938
Test6-7a	0.2161	4.312	Test6-7b	0.2800	3.875
Test6-8a	0.3559	4.125	Test6-8b	0.1303	3.688
Test6-9a	0.1482	3.000	Test6-9b	0.2369	3.250
Test6-10a	0.1130	4.562	Test6-10b	0.1500	3.500

Table 32. dSpace Impact Testing Force Hammer Magnitudes - Test 6.

Test No.: 7
Testing date: 17 March 1998, 1230
Data Storage Location: C:\Andberg\dSpace\Impact Test\

Experimental Setup: Test 7				
Node Tested	Accel Serial #	Line #	Channel # Signal Cond.	Axis
9	C112865	5	7	x
			8	y
			9	z
21	C112867	6	10	x
			11	y
			12	z
35	C112866	1	1	x
			2	y
			3	z
47	C112860	2	4	x
			5	y
			6	z

Table 33. dSpace Experimental Setup – Test 7.

Data Set: 7					
Test #	Magnitude dSpace (V)	Magnitude Oscilloscope (V)	Test #	Magnitude dSpace (V)	Magnitude Oscilloscope (V)
Test7-1a	0.2181	4.687	Test7-1b	0.3666	4.187
Test7-2a	0.2182	4.187	Test7-2b	0.2517	3.750
Test7-3a	0.2012	3.375	Test7-3b	0.0962	3.500
Test7-4a	0.2811	3.875	Test7-4b	0.3588	3.813
Test7-5a	0.2351	3.500	Test7-5b	0.2050	3.938
Test7-6a	0.2389	4.125	Test7-6b	0.1124	4.062
Test7-7a	0.1009	3.625	Test7-7b	0.3473	3.438
Test7-8a	0.2853	3.625	Test7-8b	0.1307	3.125
Test7-9a	0.2798	3.438	Test7-9b	0.2728	3.375
Test7-10a	0.2172	3.625	Test7-10b	0.2710	3.688

Table 34. dSpace Impact Testing Force Hammer Magnitudes - Test 7.

Test No.: 8
Testing date: 17 March 1998, 1330
Data Storage Location: C:\Andberg\dSpace\Impact Test\

Experimental Setup: Test 8				
Node Tested	Accel Serial #	Line #	Channel # Signal Cond.	Axis
10	C112865	5	7	x
			8	y
			9	z
22	C112867	6	10	x
			11	y
			12	z
36	C112866	1	1	x
			2	y
			3	z
48	C112860	2	4	x
			5	y
			6	z

Table 35. dSpace Experimental Setup – Test 8.

Data Set: 8					
Test #	Magnitude dSpace (V)	Magnitude Oscilloscope (V)	Test #	Magnitude dSpace (V)	Magnitude Oscilloscope (V)
Test8-1a	0.2654	4.312	Test8-1b	0.0962	4.062
Test8-2a	0.3351	3.750	Test8-2b	0.2829	4.000
Test8-3a	0.3036	4.062	Test8-3b	0.2312	3.375
Test8-4a	0.2358	3.313	Test8-4b	0.3982	4.000
Test8-5a	0.1334	3.750	Test8-5b	0.3329	3.813
Test8-6a	0.1846	3.563	Test8-6b	0.2728	3.500
Test8-7a	0.3186	3.250	Test8-7b	0.2819	3.500
Test8-8a	0.2446	3.375	Test8-8b	0.1073	3.625
Test8-9a	0.1963	3.438	Test8-9b	0.3168	3.750
Test8-10a	0.3926	4.250	Test8-10b	0.2231	4.312

Table 36. dSpace Impact Testing Force Hammer Magnitudes - Test 8.

Test No.: 9
Testing date: 18 March 1998, 0930
Data Storage Location: C:\Andberg\dSpace\Impact Test\

Experimental Setup: Test 9				
Node Tested	Accel Serial #	Line #	Channel # Signal Cond.	Axis
11	C112865	5	7	x
			8	y
			9	z
23	C112867	6	10	x
			11	y
			12	z
37	C112866	1	1	x
			2	y
			3	z
49	C112860	2	4	x
			5	y
			6	z

Table 37. dSpace Experimental Setup – Test 9.

Data Set: 9					
Test #	Magnitude dSpace (V)	Magnitude Oscilloscope (V)	Test #	Magnitude dSpace (V)	Magnitude Oscilloscope (V)
Test9-1a	0.1942	4.687	Test9-1b	0.1972	4.437
Test9-2a	0.2021	4.375	Test9-2b	0.3939	4.375
Test9-3a	0.1664	4.750	Test9-3b	0.3109	4.750
Test9-4a	0.2043	4.812	Test9-4b	0.3618	4.062
Test9-5a	0.0922	3.000	Test9-5b	0.2917	4.062
Test9-6a	0.2465	3.000	Test9-6b	0.0974	4.062
Test9-7a	0.1745	3.500	Test9-7b	0.1747	4.062
Test9-8a	0.3034	4.125	Test9-8b	0.4188	4.687
Test9-9a	0.2834	4.312	Test9-9b	0.3896	4.000
Test9-10a	0.3804	3.938	Test9-10b	0.2300	3.313

Table 38. dSpace Impact Testing Force Hammer Magnitudes - Test 9.

Test No.: 10
Testing date: 18 March 1998, 1040
Data Storage Location: C:\Andberg\dSpace\Impact Test\

Experimental Setup: Test 10				
Node Tested	Accel Serial #	Line #	Channel # Signal Cond.	Axis
12	C112865	5	7	x
			8	y
			9	z
24	C112867	6	10	x
			11	y
			12	z
38	C112866	1	1	x
			2	y
			3	z
50	C112860	2	4	x
			5	y
			6	z

Table 39. dSpace Experimental Setup – Test 10.

Data Set: 10					
Test #	Magnitude dSpace (V)	Magnitude Oscilloscope (V)	Test #	Magnitude dSpace (V)	Magnitude Oscilloscope (V)
Test10-1a	0.1309	5.062	Test10-1b	0.1318	3.125
Test10-2a	0.3145	4.000	Test10-2b	0.3352	3.500
Test10-3a	0.2216	5.000	Test10-3b	0.1746	3.625
Test10-4a	0.2824	5.875	Test10-4b	0.3128	3.375
Test10-5a	0.1238	5.375	Test10-5b	0.2071	4.125
Test10-6a	0.1686	6.312	Test10-6b	0.2774	4.625
Test10-7a	0.2168	4.750	Test10-7b	0.2533	3.188
Test10-8a	0.2534	5.187	Test10-8b	0.3024	3.313
Test10-9a	0.4648	6.250	Test10-9b	0.3663	4.375
Test10-10a	0.1046	5.500	Test10-10b	0.3226	4.062

Table 40. dSpace Impact Testing Force Hammer Magnitudes - Test 10.

Test No.: 11
Testing date: 18 March 1998, 1150
Data Storage Location: C:\Andberg\dSpace\Impact Test\

Experimental Setup: Test 11				
Node Tested	Accel Serial #	Line #	Channel # Signal Cond.	Axis
13	C112865	5	7	x
			8	y
			9	z
25	C112867	6	10	x
			11	y
			12	z
39	C112866	1	1	x
			2	y
			3	z
51	C112860	2	4	x
			5	y
			6	z

Table 41. dSpace Experimental Setup – Test 11.

Data Set: 11					
Test #	Magnitude dSpace (V)	Magnitude Oscilloscope (V)	Test #	Magnitude dSpace (V)	Magnitude Oscilloscope (V)
Test11-1a	0.1917	3.625	Test11-1b	0.1417	3.375
Test11-2a	0.3253	4.437	Test11-2b	0.1034	3.250
Test11-3a	0.2931	4.437	Test11-3b	0.1442	3.938
Test11-4a	0.2128	3.688	Test11-4b	0.3621	3.813
Test11-5a	0.1257	3.688	Test11-5b	0.1037	4.812
Test11-6a	0.3285	4.375	Test11-6b	0.2016	4.187
Test11-7a	0.1392	4.312	Test11-7b	0.4564	4.625
Test11-8a	0.1424	3.813	Test11-8b	0.1024	3.750
Test11-9a	0.1208	3.813	Test11-9b	0.1015	3.750
Test11-10a	0.4478	5.125	Test11-10b	0.3150	3.188

Table 42. dSpace Impact Testing Force Hammer Magnitudes - Test 11.

Test No.: 12
Testing date: 18 March 1998, 1225
Data Storage Location: C:\Andberg\dSpace\Impact Test\

Experimental Setup: Test 12				
Node Tested	Accel Serial #	Line #	Channel # Signal Cond.	Axis
14	C112865	5	7	x
			8	y
			9	z
26	C112867	6	10	x
			11	y
			12	z
40	C112866	1	1	x
			2	y
			3	z
52	C112860	2	4	x
			5	y
			6	z

Table 43. dSpace Experimental Setup – Test 12.

Data Set: 12					
Test #	Magnitude dSpace (V)	Magnitude Oscilloscope (V)	Test #	Magnitude dSpace (V)	Magnitude Oscilloscope (V)
Test12-1a	0.2968	4.000	Test12-1b	0.1243	3.938
Test12-2a	0.4297	3.125	Test12-2b	0.1568	3.250
Test12-3a	0.2265	4.812	Test12-3b	0.2843	4.812
Test12-4a	0.4946	5.187	Test12-4b	0.2113	3.938
Test12-5a	0.1363	5.000	Test12-5b	0.3241	4.312
Test12-6a	0.3546	5.937	Test12-6b	0.2154	3.813
Test12-7a	0.4554	5.312	Test12-7b	0.3032	3.063
Test12-8a	0.1186	5.437	Test12-8b	0.3447	5.062
Test12-9a	0.4464	5.187	Test12-9b	0.2047	3.938
Test12-10a	0.2035	5.500	Test12-10b	0.4324	4.812

Table 44. dSpace Impact Testing Force Hammer Magnitudes - Test 12.

APPENDIX F. HAMMER.M – MATLAB ANALYSIS CODE

```
% HAMMER.M - MATLAB Analysis Code
% This file loads all hammer calibration test data and verifies the
% impulse hammer calibration.

% Written by LT Scott E Johnson and LT John Vlattas
% Testing conducted 3,4,5 March 1998
% Last modified: 5 March 1998

      clear all
      cal=[];

      for n=1:50

                        % before running, load 'fname.mat' file
                        % containing all
                        % calibration values
                        % trace_y, column 1 should be hammer values
                        % trace_y, column 2 should be accelerometer
                        % values

      datafile=['cal' int2str(n)];
      eval(['load ' datafile]);

      ka = 0.0987;      % ka is accelerometer sensitivity (x-axis),
                        % units: [v/g]
                        % ka is given in accelerometer spec. sheet
                        % x-axis sens. for Kistler accel:
                        % model# 8690C50, S/N C112865

      kaprime = 1/ka;   % units: [g/v]
                        % m is mass of test mass (Al block) & accel.

      m = 0.7674;       % combined units: [kg]


                        %kf is force (hammer) sensitivity (calculated)
      kf = m*kaprime*max(abs(trace_y(2,:)))/max(abs(trace_y(1,:)));
      cal(n)=kf;
      end

            % Find overall Mean kf and standard deviation

                  KFMEAN=mean(cal)
                  KFSTD=std(cal)
                  cal
```

APPENDIX G. TFEAVG.M – MATLAB ANALYSIS CODE

```
% TFEAVG.M - MATLAB Analysis Code
% This program loads the dSPACE test data and performs the Transfer
% Funcion Estimate between the impact and accelerometers. The TFE
% function computes the PSD of the data therefor allowing the 10 subtest
% for each test configuration to be averaged.

% Progran developed by LT Scott E. Johnson and LT John Vlattas
% Last modified: 16 April 1998

clear all

tic

%  Oscilloscope Impact Magnitude Test Data

t1a = [3.75 3.30 4.10 3.50 2.50 3.813 2.5 3.158 1.812 4];
t1b = [3.594 3.594 3.531 3.125 2.5 2.938 2.625 2.531 2.906 3.688];
t2a = [2.250 3.156 2.563 3.813 3.688 4.687 3.188 3.188 4.062 3.750];
t2b = [5.750 4.187 5.000 4.437 3.000 3.625 3.625 3.313 4.062 3.750];
t3a = [3.563 3.563 4.562 4.562 3.375 3.938 3.750 3.750 4.062 3.625];
t3b = [3.250 3.313 3.688 3.625 4.312 3.875 3.500 3.563 3.625 4.437];
t4a = [3.750 4.125 3.625 4.125 3.250 4.000 3.438 4.375 4.000 4.187];
t4b = [4.000 3.063 3.563 3.688 4.312 4.187 3.750 4.062 4.062 3.375];
t5a = [3.563 3.438 3.500 3.563 4.125 4.187 4.000 3.875 3.875 3.313];
t5b = [3.375 4.250 3.875 3.875 3.500 4.250 4.500 4.062 4.750 3.250];
t6a = [3.813 3.938 4.000 3.688 3.750 4.000 4.312 4.125 3.000 4.562];
t6b = [3.813 4.250 4.125 3.750 3.938 3.938 3.875 3.688 3.250 3.500];
t7a = [4.687 4.187 3.375 3.875 3.500 4.125 3.625 3.625 3.438 3.625];
t7b = [4.187 3.750 3.500 3.813 3.938 4.062 3.438 3.125 3.375 3.688];
t8a = [4.312 3.750 4.062 3.313 3.750 3.563 3.250 3.375 3.438 4.250];
t8b = [4.062 4.000 3.375 4.000 3.813 3.500 3.500 3.625 3.750 4.312];
t9a = [4.687 4.375 4.750 4.812 3.000 3.000 3.500 4.125 4.312 3.938];
t9b = [4.437 4.375 4.750 4.062 4.062 4.062 4.062 4.687 4.000 3.313];
t10a = [5.062 4.000 5.000 5.875 5.375 6.312 4.750 5.187 6.250 5.500];
t10b = [3.125 3.500 3.625 3.375 4.125 4.625 3.188 3.313 4.375 4.062];
t11a = [3.625 4.437 4.437 3.688 3.688 4.375 4.312 3.813 3.813 5.125];
t11b = [3.375 3.250 3.938 3.813 4.812 4.187 4.625 3.750 3.750 3.188];
t12a = [4.000 3.125 4.812 5.187 5.000 5.937 5.312 5.437 5.187 5.500];
t12b = [3.938 3.250 4.812 3.938 4.312 3.813 3.063 5.062 3.938 4.812];

t1aa = t1a';
t1bb = t1b';
t2aa = t2a';
t2bb = t2b';
t3aa = t3a';
t3bb = t3b';
t4aa = t4a';
t4bb = t4b';
t5aa = t5a';
t5bb = t5b';
t6aa = t6a';
t6bb = t6b';
t7aa = t7a';
```

```
t7bb = t7b';
t8aa = t8a';
t8bb = t8b';
t9aa = t9a';
t9bb = t9b';
t10aa = t10a';
t10bb = t10b';
t11aa = t11a';
t11bb = t11b';
t12aa = t12a';
t12bb = t12b';

% put magnitudes in colomn matrix form
maga=[t1aa t2aa t3aa t4aa t5aa t6aa t7aa t8aa t9aa t10aa t11aa t12aa];
magb=[t1bb t2bb t3bb t4bb t5bb t6bb t7bb t8bb t9bb t10bb t11bb t12bb];

% Main Body of Program

tstno=input('Enter Test Congiguration Number:');% test configuration

%accelerometer sensitivitys channels 1 thru 12 see appendix
%used for scaling in tfe function
accelsen=[101.1 100.3 96.7 99.2 99.5 99.1 98.8 101.6 97.7 98.9 99.8
99.7];

for nochan = 1:12                    % loop thru 12 axis of the four
accelerometers

Txy=[0];

      for   subtstno=1:10            % loop that loads all 10 sub-test
for eac test config
            %subtstno                % Display loop count to screen


            datafile=['t' num2str(tstno) '_' num2str(subtstno) 'a'];
            eval(['load ' datafile]);

            % replace dspace impulse magnitude with o-scope magnitude
            n=find(trace_y(13,:)==max(trace_y(13,:)));
            impact=zeros(1,length(trace_y(13,:)));    % window impact
for dirac input
            impact(n)=maga(subtstno,tstno);           % replace wiht
true impact magnitude
            %trace_y(13,n)=maga(subtstno,tstno);

            % Compute Transfer function estimate for each subtest
            %[txy,f]=tfe(.707*impact,trace_y(nochan,:),12000,5000);

[txy,f]=tfe((.707*impact),((1/.1)*accelsen(nochan)*trace_y(nochan,:)),12
000,5000,HAMMING(8192));

            Txy=Txy+txy;      % compute sum to find average

      end

Txyavg=Txy/10;
```

```
if nochan==1

      figure(1)
      %subplot(3,1,nochan)
      plot(f,20*log10(abs(Txyavg)),'r'), grid, hold on
      axis([0 200 -5 70])
      xlabel('Frequency (Hz)'),
      ylabel('Tranfer Function Estimate (dB)');
      %title(['Test Configuration ', int2str(tstno)])
      zoom on

elseif nochan==2

      figure(1)
      %subplot(3,1,nochan)
      plot(f,20*log10(abs(Txyavg)),'-.m')
      %axis([0 200 -5 70])
      %xlabel('Frequency (Hz)'),
      ylabel('Tranfer Function Estimate (dB)');
      %title(['Test Configuration ', int2str(tstno)])
      zoom on

elseif nochan==3

      figure(1)
      %subplot(3,1,nochan)
      plot(f,20*log10(abs(Txyavg)),'--b')
      %axis([0 200 -5 70])
      %xlabel('Frequency (Hz)'),
      ylabel('Tranfer Function Estimate (dB)');
      %title(['Test Configuration ', int2str(tstno)])
      zoom on
      legend('X','Y','Z');

elseif nochan==4

      figure(2)
      %subplot(3,1,nochan)
      plot(f,20*log10(abs(Txyavg)),'r'), grid, hold on
      axis([0 200 -5 70])
      xlabel('Frequency (Hz)'),
      ylabel('Tranfer Function Estimate (dB)');
      %title(['Test Configuration ', int2str(tstno)])
      zoom on

elseif nochan==5

      figure(2)
      %subplot(3,1,nochan)
      plot(f,20*log10(abs(Txyavg)),'-.m')
      %axis([0 200 -5 70])
      %xlabel('Frequency (Hz)'),
      ylabel('Tranfer Function Estimate (dB)');
      %title(['Test Configuration ', int2str(tstno)])
      zoom on
```

```
elseif nochan==6

      figure(2)
      %subplot(3,1,nochan)
      plot(f,20*log10(abs(Txyavg)),'--b')
      %axis([0 200 -5 70])
      %xlabel('Frequency (Hz)'),
      ylabel('Tranfer Function Estimate (dB)');
      %title(['Test Configuration ', int2str(tstno)])
      zoom on
      legend('X','Y','Z');


elseif nochan==7

      figure(3)
      %subplot(3,1,nochan)
      plot(f,20*log10(abs(Txyavg)),'r'), grid, hold on
      axis([0 200 -5 70])
      xlabel('Frequency (Hz)'),
      ylabel('Tranfer Function Estimate (dB)');
      %title(['Test Configuration ', int2str(tstno)])
      zoom on

elseif nochan==8

      figure(3)
      %subplot(3,1,nochan)
      plot(f,20*log10(abs(Txyavg)),'-.m')
      %axis([0 200 -5 70])
      %xlabel('Frequency (Hz)'),
      ylabel('Tranfer Function Estimate (dB)');
      %title(['Test Configuration ', int2str(tstno)])
      zoom on

elseif nochan==9

      figure(3)
      %subplot(3,1,nochan)
      plot(f,20*log10(abs(Txyavg)),'--b')
      %axis([0 200 -5 70])
      %xlabel('Frequency (Hz)'),
      ylabel('Tranfer Function Estimate (dB)');
      %title(['Test Configuration ', int2str(tstno)])
      zoom on
      legend('X','Y','Z');


elseif nochan==10

      figure(4)
      %subplot(3,1,nochan)
      plot(f,20*log10(abs(Txyavg)),'r'), grid on, hold on
      axis([0 200 -5 70])
      xlabel('Frequency (Hz)'),
      ylabel('Tranfer Function Estimate (dB)');
      %title(['Test Configuration ', int2str(tstno)])
```

```
            zoom on

        elseif nochan==11

            figure(4)
            %subplot(3,1,nochan)
            plot(f,20*log10(abs(Txyavg)),'-.m')
            %axis([0 200 -5 70])
            %xlabel('Frequency (Hz)'),
            ylabel('Tranfer Function Estimate (dB)');
            %title(['Test Configuration ', int2str(tstno)])
            zoom on


        else

            figure(4)
            %subplot(3,1,(nochan-9))
            plot(f,20*log10(abs(Txyavg)),'--b')
            %axis([0 200 -5 70])
            %xlabel('Frequency (Hz)'),
            ylabel('Tranfer Function Estimate(dB)');
            zoom on
            legend('X','Y','Z');


        end   % end plot if branch

end           % end nochan loop


t=toc
```

APPENDIX H. dSPACE EXPERIMENTAL RESULTS

This Appendix contains typical results of the dSPACE data after analysis using the TFEAVG.M MATLAB code. The nodes analyzed are 15, 40, 44, and 51. Below is a legend for the graphs in this section.

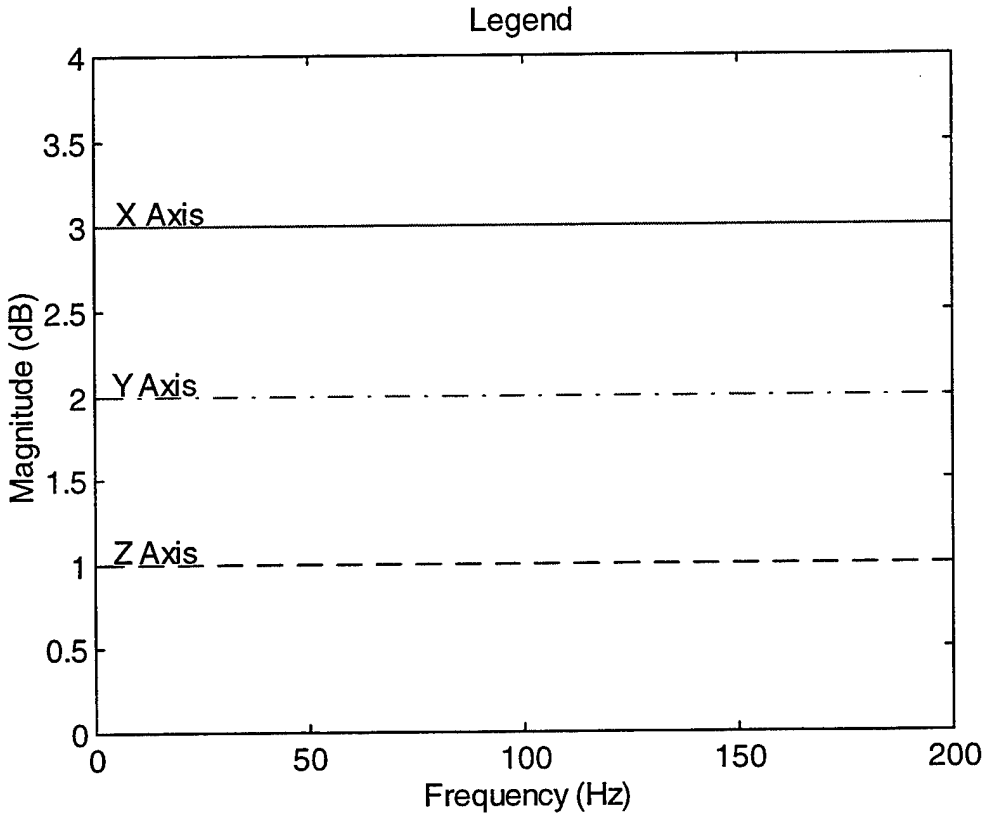

Figure 51. Legend for dSPACE Results

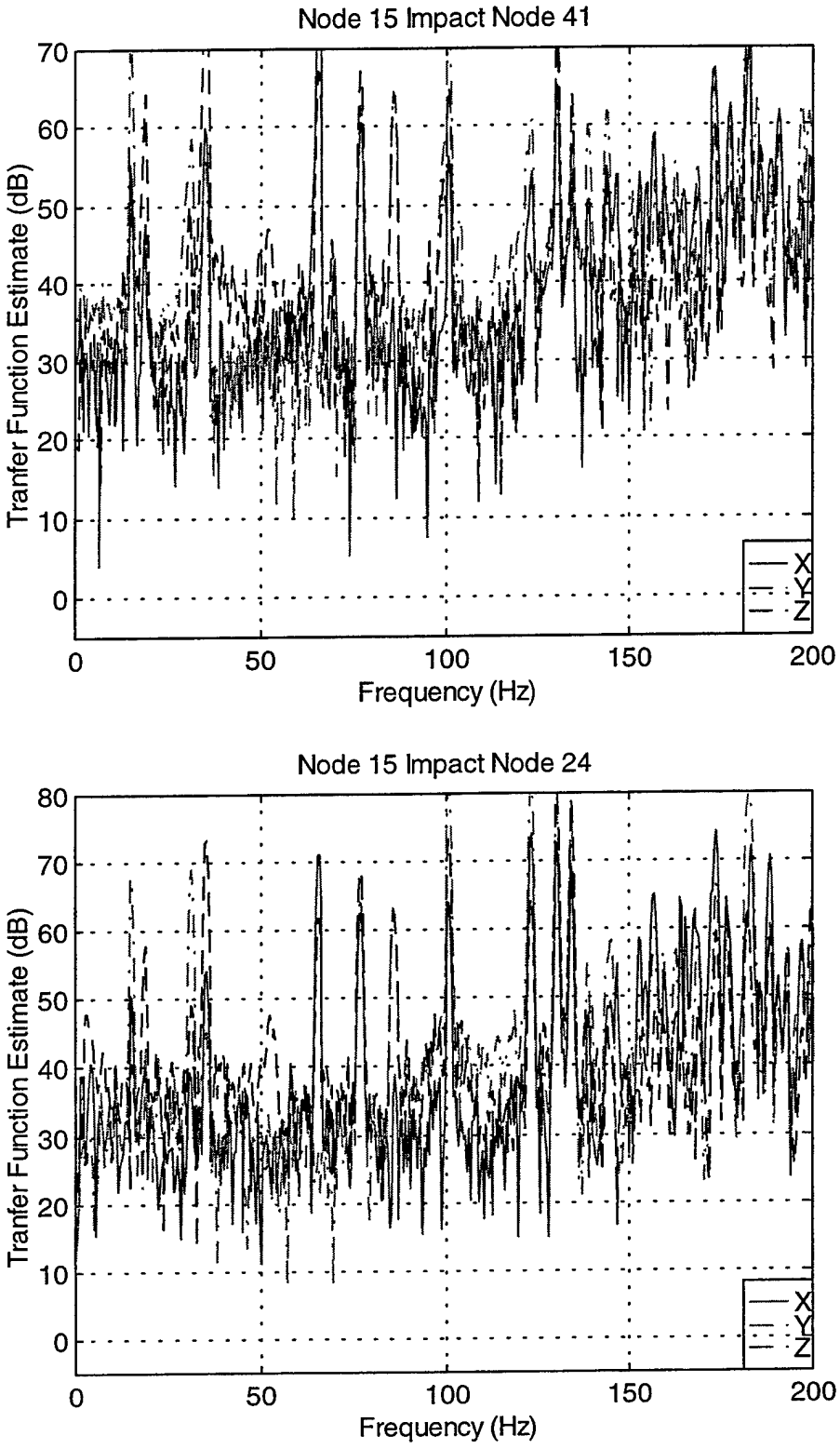

Figure 52. dSPACE Node 15 Test Data

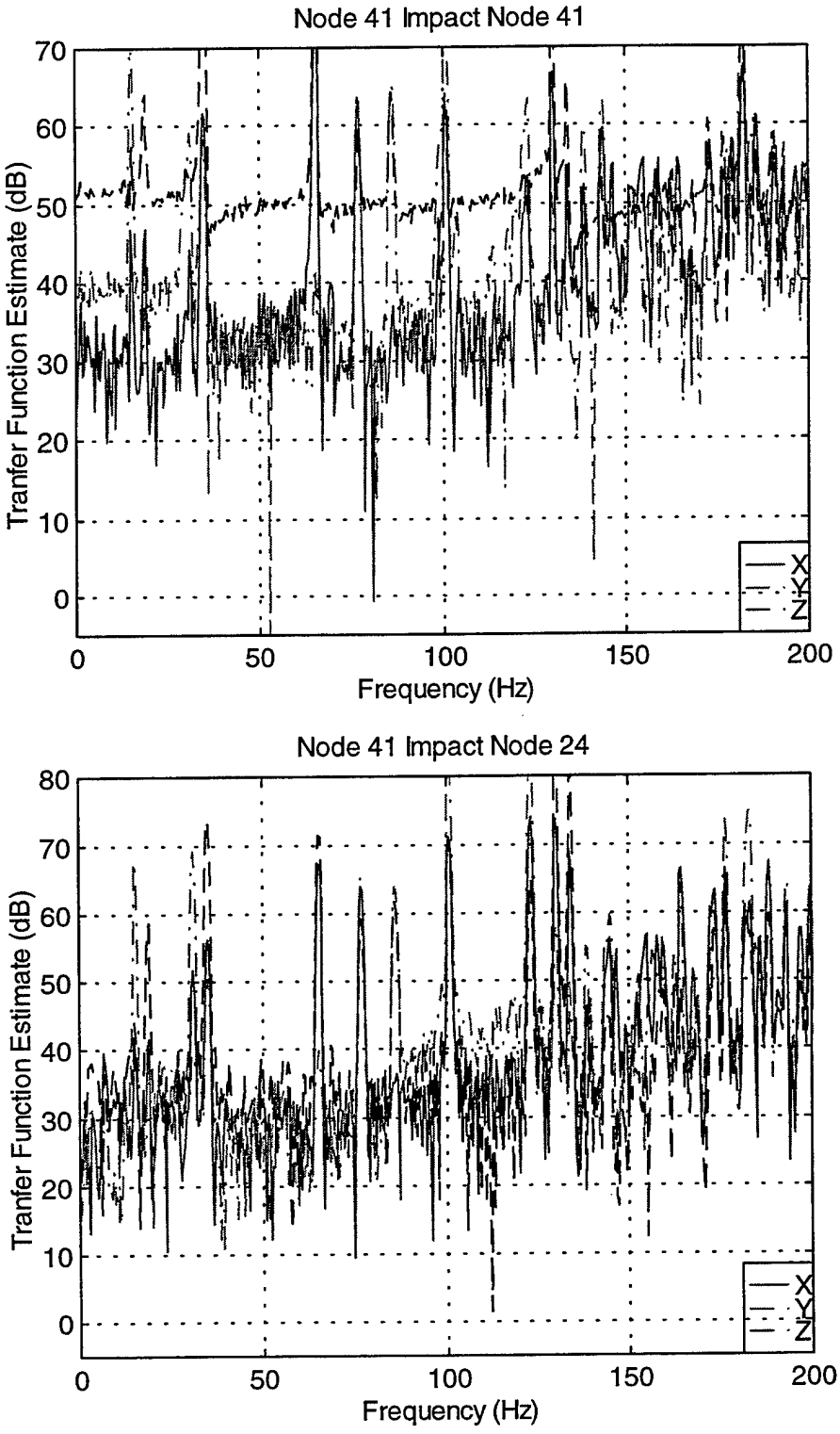

Figure 53. dSPACE Node 40 Test Data

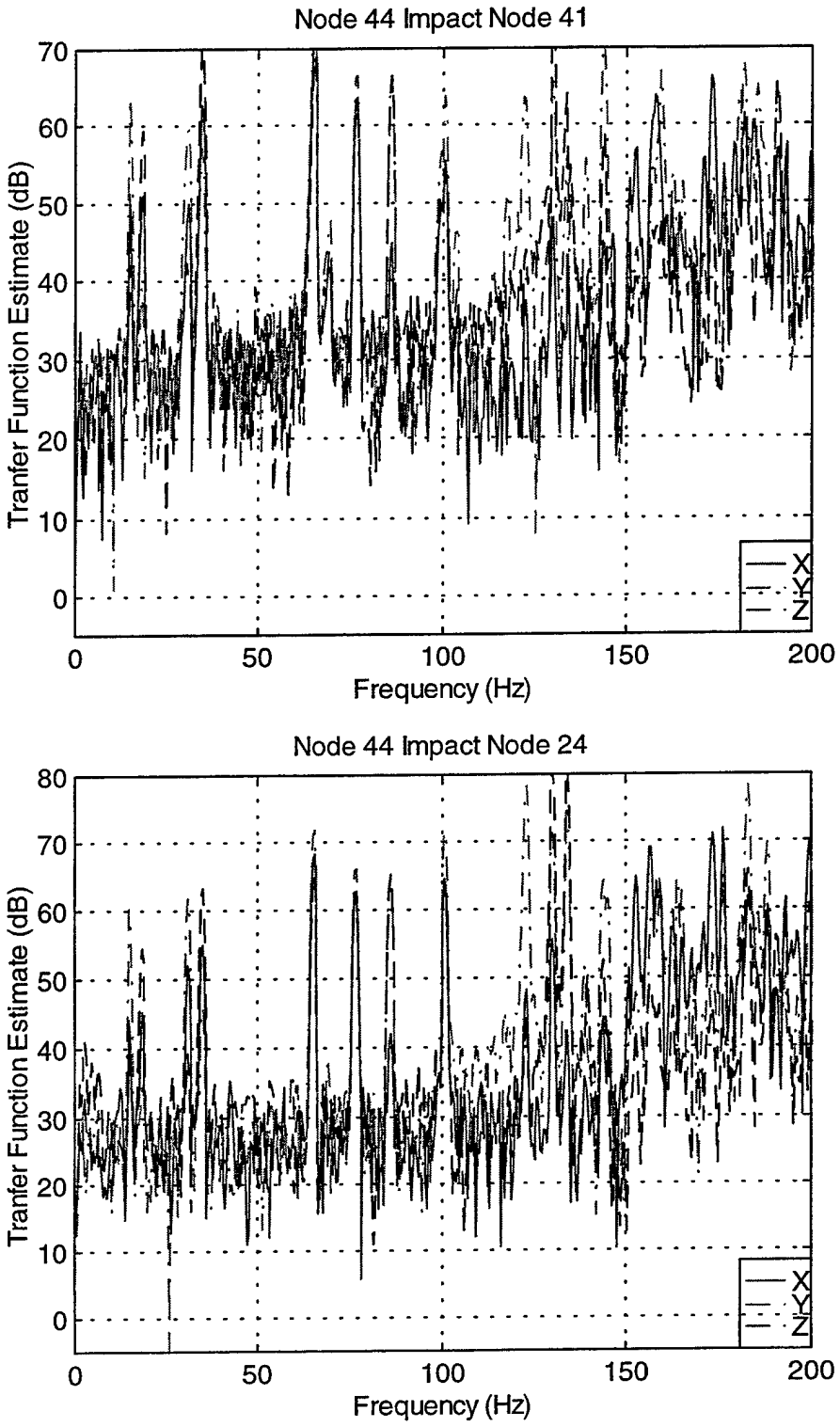

Figure 54. dSPACE Node 44 Test Data

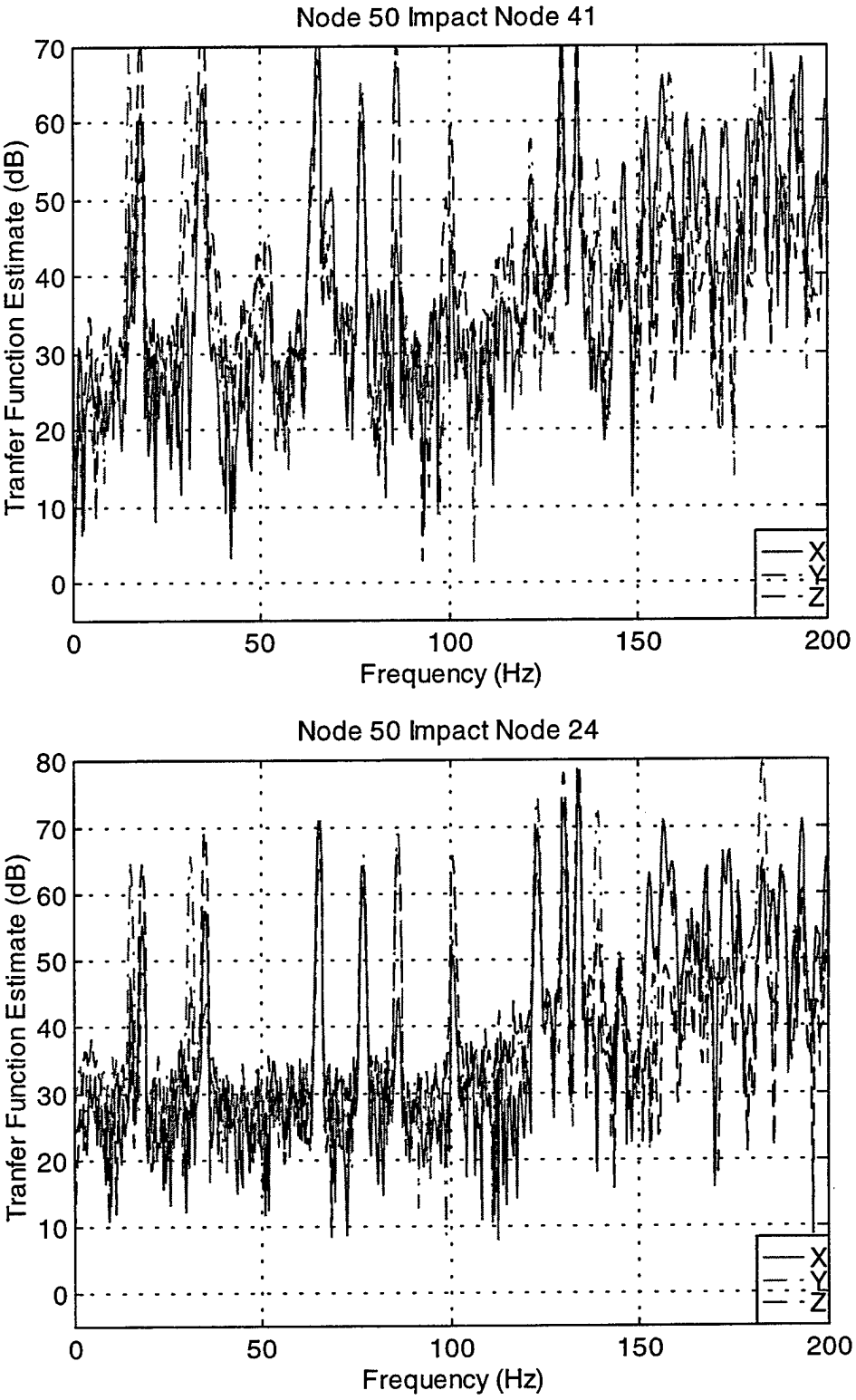

Figure 55. dSPACE Node 50 Test Data

APPENDIX I. HP-35665A SIGNAL ANALYZER EXPERIMENTAL RESULTS

This Appendix contains typical results of the HP-35665A data after analysis. The nodes presented are 15, 40, 44, and 51. Below is a detailed listing of all the data file names and a legend for the graphs in this section. During all testing the Newport table was floated. The HP-35665A configuration is prescribed in Chapter III.

HP-35665A Data File Names					
Directory: c:\truss_data\sdf_data					
i3xa.dat	i3ya.dat	i3za.dat	i3xb.dat	i3yb.dat	i3zb.dat
i4xa.dat	i4ya.dat	i4za.dat	i4xb.dat	i4yb.dat	i4zb.dat
i5xa.dat	i5ya.dat	i5za.dat	i5xb.dat	i5yb.dat	i5zb.dat
i6xa.dat	i6ya.dat	i6za.dat	i6xb.dat	i6yb.dat	i6zb.dat
i7xa.dat	i7ya.dat	i7za.dat	i7xb.dat	i7yb.dat	i7zb.dat
i8xa.dat	i8ya.dat	i8za.dat	i8xb.dat	i8yb.dat	i8zb.dat
i9xa.dat	i9ya.dat	i9za.dat	i9xb.dat	i9yb.dat	i9zb.dat
i10xa.dat	i10ya.dat	i10za.dat	i10xb.dat	i10yb.dat	i10zb.dat
i11xa.dat	i11ya.dat	i11za.dat	i11xb.dat	i11yb.dat	i11zb.dat
i12xa.dat	i12ya.dat	i12za.dat	i12xb.dat	i12yb.dat	i12zb.dat
i13xa.dat	i13ya.dat	i13za.dat	i13xb.dat	i13yb.dat	i13zb.dat
i14xa.dat	i14ya.dat	i14za.dat	i14xb.dat	i14yb.dat	i14zb.dat
i15xa.dat	i15ya.dat	i15za.dat	i15xb.dat	i15yb.dat	i15zb.dat
i16xa.dat	i16ya.dat	i16za.dat	i16xb.dat	i16yb.dat	i16zb.dat
i17xa.dat	i17ya.dat	i17za.dat	i17xb.dat	i17yb.dat	i17zb.dat
i18xa.dat	i18ya.dat	i18za.dat	i18xb.dat	i18yb.dat	i18zb.dat
i19xa.dat	i19ya.dat	i19za.dat	i19xb.dat	i19yb.dat	i19zb.dat
i20xa.dat	i20ya.dat	i20za.dat	i20xb.dat	i20yb.dat	i20zb.dat
i21xa.dat	i21ya.dat	i21za.dat	i21xb.dat	i21yb.dat	i21zb.dat
i22xa.dat	i22ya.dat	i22za.dat	i22xb.dat	i22yb.dat	i22zb.dat
i23xa.dat	i23ya.dat	i23za.dat	i23xb.dat	i23yb.dat	i23zb.dat
i24xa.dat	i24ya.dat	i24za.dat	i24xb.dat	i24yb.dat	i24zb.dat
i25xa.dat	i25ya.dat	i25za.dat	i25xb.dat	i25yb.dat	i25zb.dat
i26xa.dat	i26ya.dat	i26za.dat	i26xb.dat	i26yb.dat	i26zb.dat
i29xa.dat	i29ya.dat	i29za.dat	i29xb.dat	i29yb.dat	i29zb.dat
i30xa.dat	i30ya.dat	i30za.dat	i30xb.dat	i30yb.dat	i30zb.dat
i31xa.dat	i31ya.dat	i31za.dat	i31xb.dat	i31yb.dat	i31zb.dat
i32xa.dat	i32ya.dat	i32za.dat	i32xb.dat	i32yb.dat	i32zb.dat
i33xa.dat	i33ya.dat	i33za.dat	i33xb.dat	i33yb.dat	i33zb.dat
i34xa.dat	i34ya.dat	i34za.dat	i34xb.dat	i34yb.dat	i34zb.dat
i35xa.dat	i35ya.dat	i35za.dat	i35xb.dat	i35yb.dat	i35zb.dat

i36xa.dat	i36ya.dat	i36za.dat	i36xb.dat	i36yb.dat	i36zb.dat
i37xa.dat	i37ya.dat	i37za.dat	i37xb.dat	i37yb.dat	i37zb.dat
i38xa.dat	i38ya.dat	i38za.dat	i38xb.dat	i38yb.dat	i38zb.dat
i39xa.dat	i39ya.dat	i39za.dat	i39xb.dat	i39yb.dat	i39zb.dat
i40xa.dat	i40ya.dat	i40za.dat	i40xb.dat	i40yb.dat	i40zb.dat
i41xa.dat	i41ya.dat	i41za.dat	i41xb.dat	i41yb.dat	i41zb.dat
i42xa.dat	i42ya.dat	i42za.dat	i42xb.dat	i42yb.dat	i42zb.dat
i43xa.dat	i43ya.dat	i43za.dat	i43xb.dat	i43yb.dat	i43zb.dat
i44xa.dat	i44ya.dat	i44za.dat	i44xb.dat	i44yb.dat	i44zb.dat
i45xa.dat	i45ya.dat	i45za.dat	i45xb.dat	i45yb.dat	i45zb.dat
i46xa.dat	i46ya.dat	i46za.dat	i46xb.dat	i46yb.dat	i46zb.dat
i47xa.dat	i47ya.dat	i47za.dat	i47xb.dat	i47yb.dat	i47zb.dat
i48xa.dat	i48ya.dat	i48za.dat	i48xb.dat	i48yb.dat	i48zb.dat
i49xa.dat	i49ya.dat	i49za.dat	i49xb.dat	i49yb.dat	i49zb.dat
i50xa.dat	i50ya.dat	i50za.dat	i50xb.dat	i50yb.dat	i50zb.dat
i51xa.dat	i51ya.dat	i51za.dat	i51xb.dat	i51yb.dat	i51zb.dat
i52xa.dat	i52ya.dat	i52za.dat	i52xb.dat	i52yb.dat	i52zb.dat

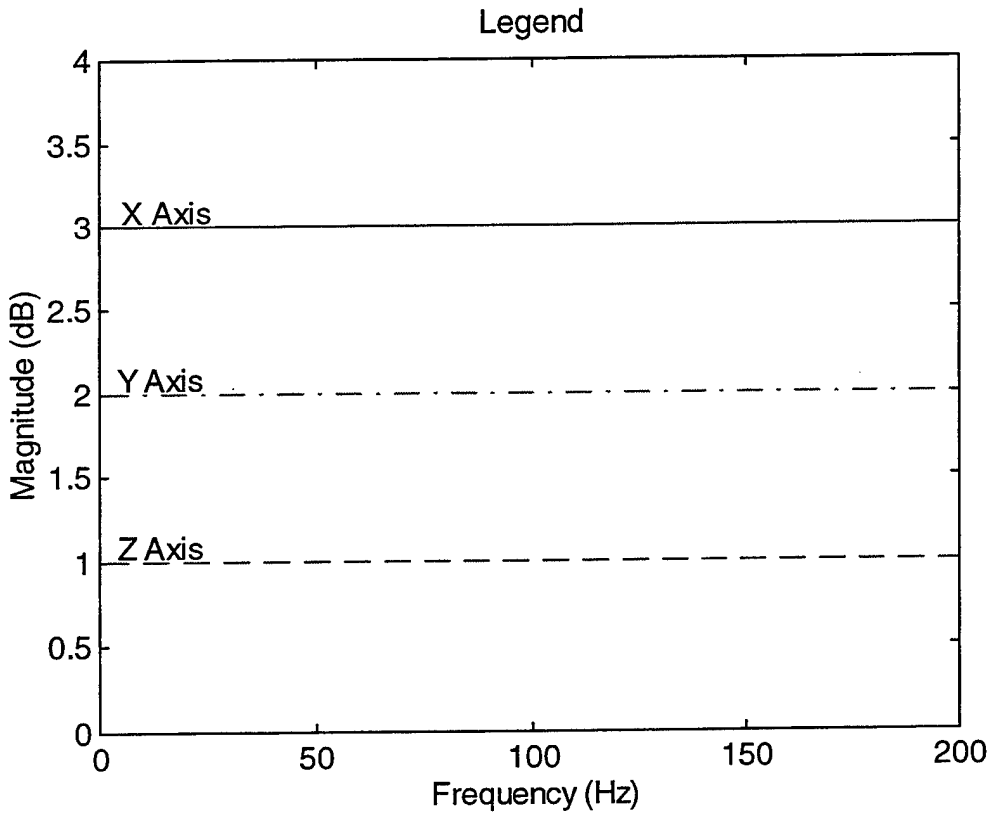

Figure 56. Legend for HP-35655A Signal Analyzer Results

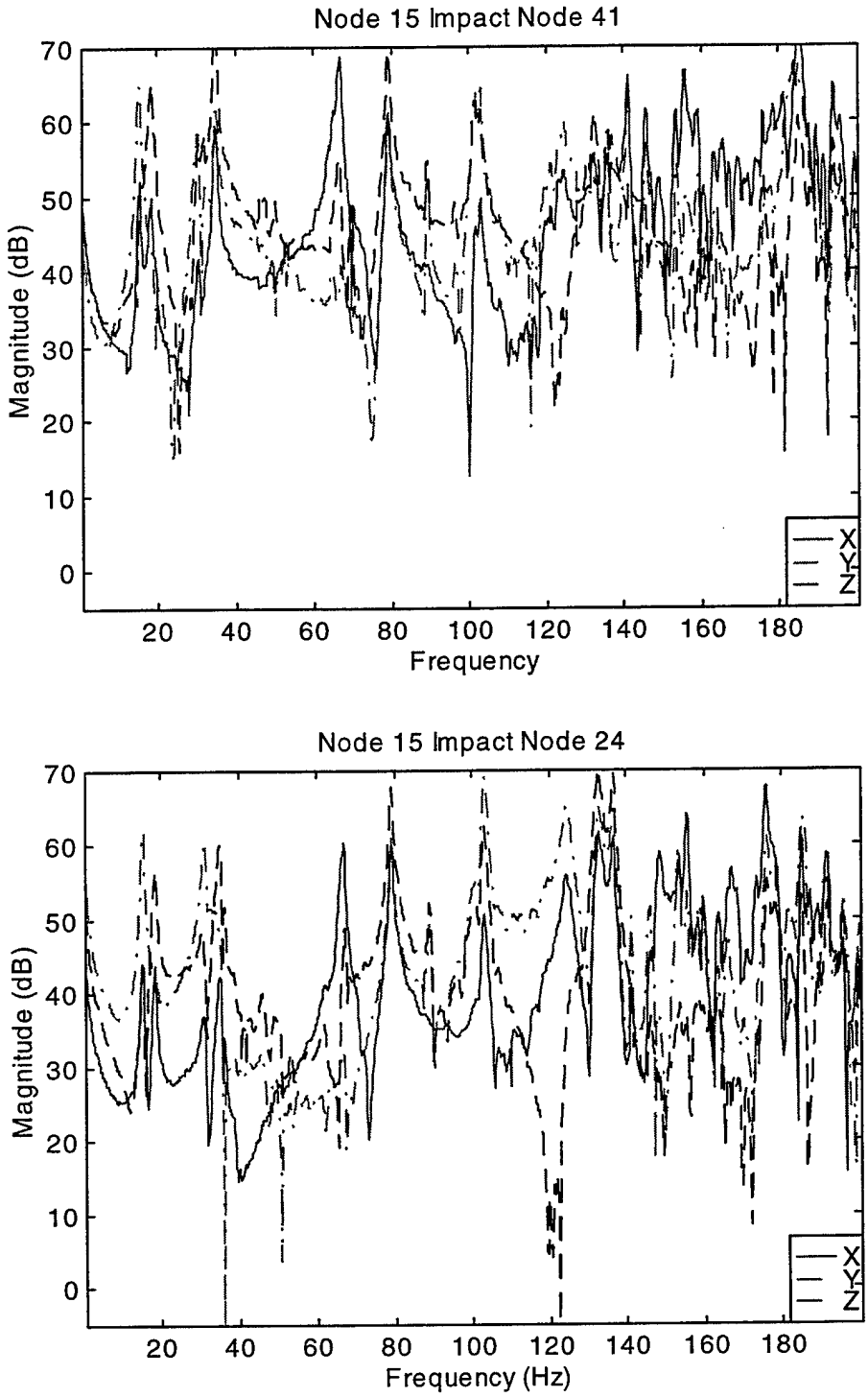

Figure 57. HP-35655A Node 15 Test Data.

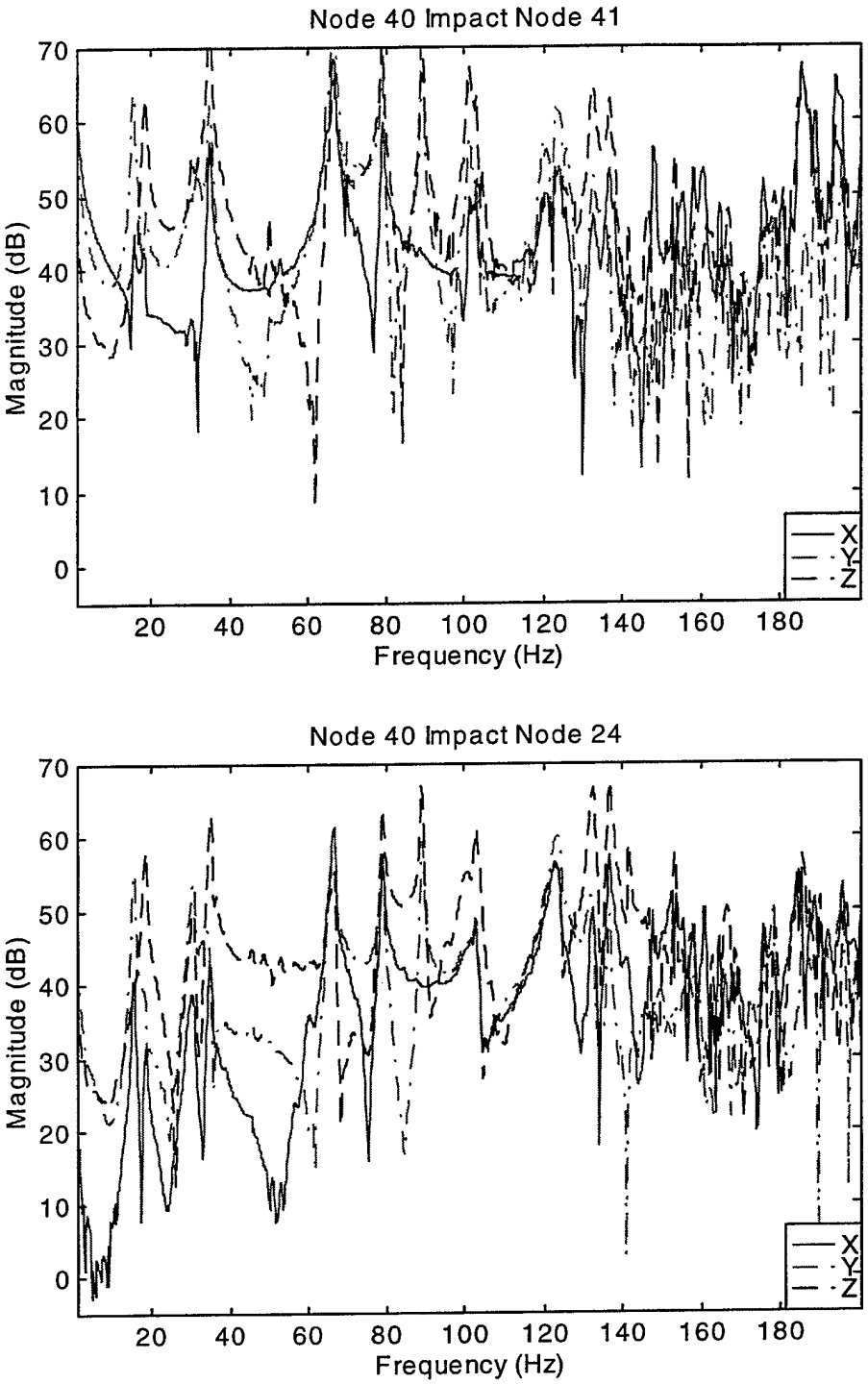

Figure 58. HP-35655A Node 40 Test Data.

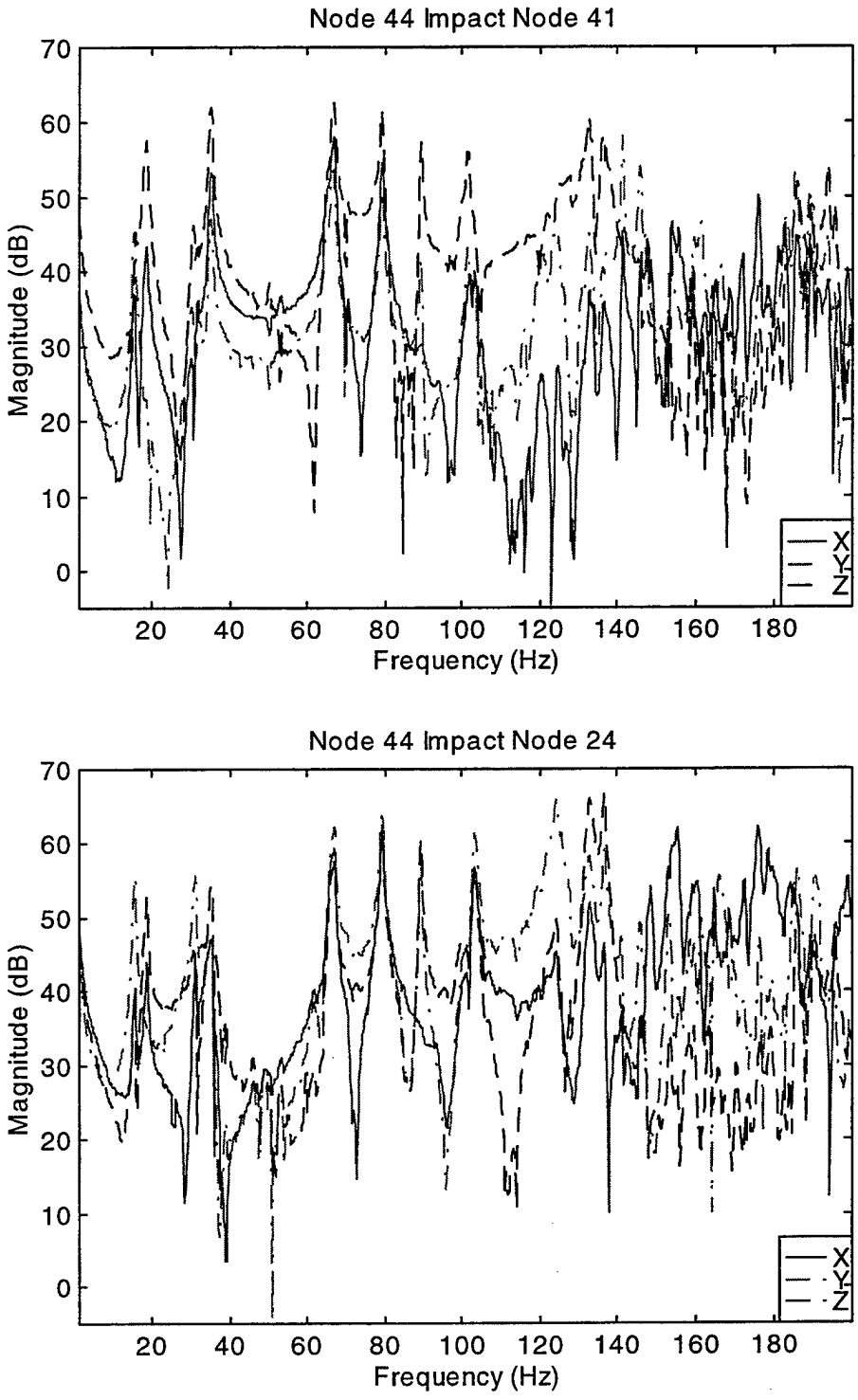

Figure 59. HP-35655A Node 44 Test Data.

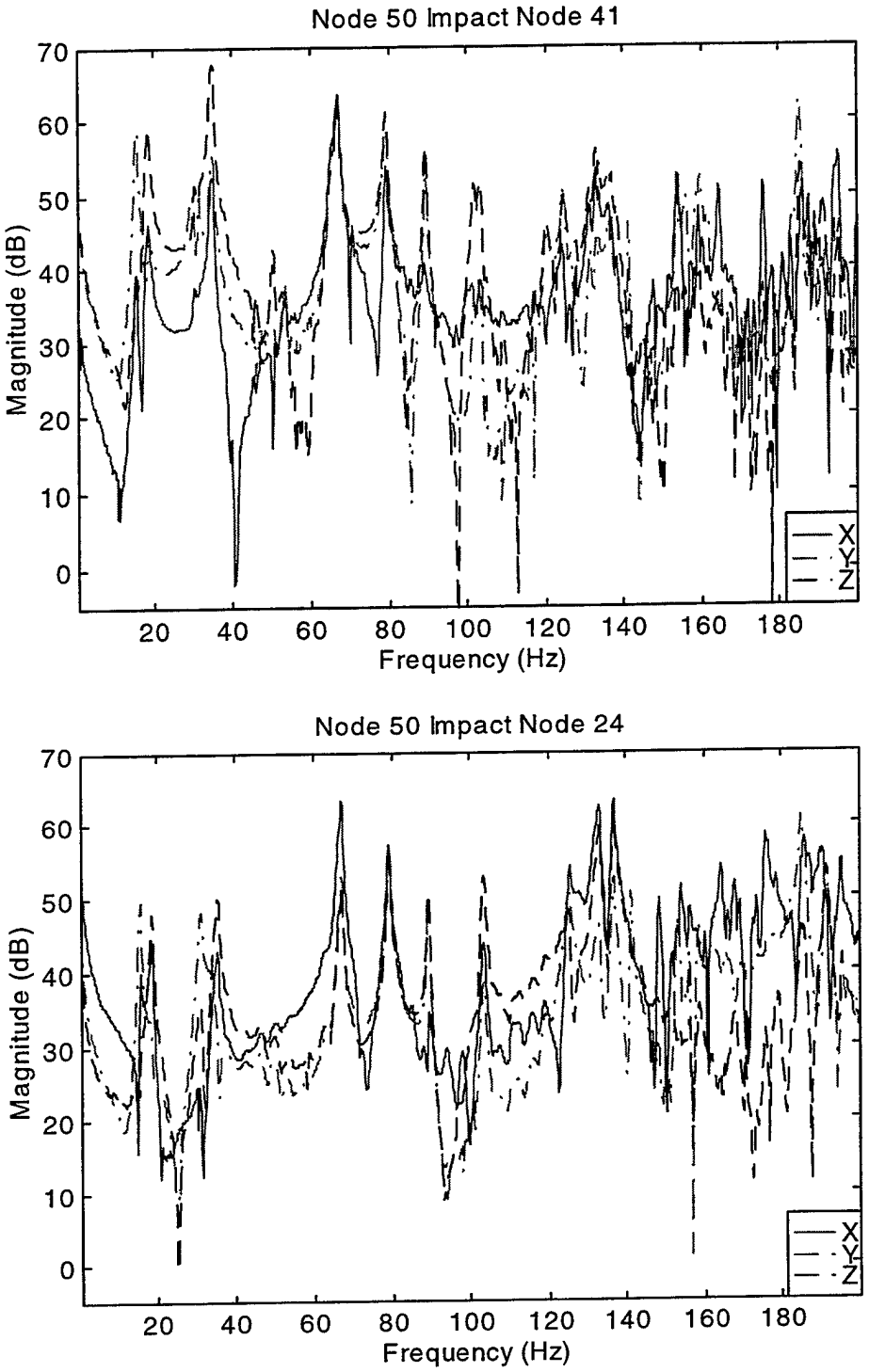

Figure 60. HP-35655A Node 50 Test Data.

APPENDIX J. SDFCONV.M – MATLAB ANALYSIS CODE

```
%  SDFCONV.M - MATLAB Analysis Code
%  This program converts data collected on HP 35665A signal anlayzer
%  from Standard Data Format to MATLAB .mat files and to UNV58 formatted
%  files.

%  Written by LT Scott E. Johnson and LT. John Vlattas
%  Last Modified: 15 April 1998


clear all

for node=3:26           % loop that loads nodes 3 thru 26


            %  Impact Node 41 "a.dat"

            dfilex=['sdftoml i' num2str(node) 'xa.dat  i' num2str(node)
'xa.mat /x']; % convert sdf to matlab
            eval('dos(dfilex)')
            %eval(['load ' datafile]);

            dfilex=['sdfto58 i' num2str(node) 'xa.dat  i' num2str(node)
'xa.unv']; % convert sdf to unv58
            eval('dos(dfilex)')
            %eval(['load ' datafile]);

            dfiley=['sdftoml i' num2str(node) 'ya.dat  i' num2str(node)
'ya.mat /x']; % convert sdf to matlab
            eval('dos(dfiley)')
            %eval(['load ' datafile]);

            dfiley=['sdfto58 i' num2str(node) 'ya.dat  i' num2str(node)
'ya.unv']; % convert sdf to unv58
            eval('dos(dfiley)')
            %eval(['load ' datafile]);

            dfilez=['sdftoml i' num2str(node) 'za.dat  i' num2str(node)
'za.mat /x']; % convert sdf to matlab
            eval('dos(dfilez)')
            %eval(['load ' datafile]);

            dfilez=['sdfto58 i' num2str(node) 'za.dat  i' num2str(node)
'za.unv']; % convert sdf to unv58
            eval('dos(dfilez)')
            %eval(['load ' datafile])



            %  Impact Node 24 "b.dat"

            dfilex=['sdftoml i' num2str(node) 'xb.dat  i' num2str(node)
'xb.mat /x']; % convert sdf to matlab
            eval('dos(dfilex)')
```

```
            %eval(['load ' datafile]);

            dfilex=['sdfto58 i' num2str(node) 'xb.dat  i' num2str(node)
'xb.unv']; % convert sdf to unv58
            eval('dos(dfilex)')
            %eval(['load ' datafile]);

            dfiley=['sdftoml i' num2str(node) 'yb.dat  i' num2str(node)
'yb.mat /x']; % convert sdf to matlab
            eval('dos(dfiley)')
            %eval(['load ' datafile]);

            dfiley=['sdfto58 i' num2str(node) 'yb.dat  i' num2str(node)
'yb.unv']; % convert sdf to unv58
            eval('dos(dfiley)')
            %eval(['load ' datafile]);

            dfilez=['sdftoml i' num2str(node) 'zb.dat  i' num2str(node)
'zb.mat /x']; % convert sdf to matlab
            eval('dos(dfilez)')
            %eval(['load ' datafile]);

            dfilez=['sdfto58 i' num2str(node) 'zb.dat  i' num2str(node)
'zb.unv']; % convert sdf to unv58
            eval('dos(dfilez)')
            %eval(['load ' datafile])

end   % end loop nodes 3 thru 26



for   node=29:52        % loop that loads nodes 3 thru 26

            node

            %  Impact Node 41 "a.dat"

            dfilex=['sdftoml i' num2str(node) 'xa.dat  i' num2str(node)
'xa.mat /x']; % convert sdf to matlab
            eval('dos(dfilex)')
            %eval(['load ' datafile]);

            dfilex=['sdfto58 i' num2str(node) 'xa.dat  i' num2str(node)
'xa.unv']; % convert sdf to unv58
            eval('dos(dfilex)')
            %eval(['load ' datafile]);

            dfiley=['sdftoml i' num2str(node) 'ya.dat  i' num2str(node)
'ya.mat /x']; % convert sdf to matlab
            eval('dos(dfiley)')
            %eval(['load ' datafile]);

            dfiley=['sdfto58 i' num2str(node) 'ya.dat  i' num2str(node)
'ya.unv']; % convert sdf to unv58
            eval('dos(dfiley)')
            %eval(['load ' datafile]);
```

```
dfilez=['sdftoml i' num2str(node) 'za.dat  i' num2str(node) 'za.mat/x'];
                        % convert sdf to matlab
eval('dos(dfilez)')
%eval(['load ' datafile]);


dfilez=['sdfto58 i' num2str(node) 'za.dat  i' num2str(node) 'za.unv'];
                        % convert sdf to unv58
eval('dos(dfilez)')
%eval(['load ' datafile])



          %  Impact Node 24 "b.dat"

dfilex=['sdftoml i' num2str(node) 'xb.dat  i' num2str(node) 'xb.mat/x'];
                        % convert sdf to matlab
eval('dos(dfilex)')
%eval(['load ' datafile]);

dfilex=['sdfto58 i' num2str(node) 'xb.dat  i' num2str(node) 'xb.unv'];
                        % convert sdf to unv58
eval('dos(dfilex)')
%eval(['load ' datafile]);


dfiley=['sdftoml i' num2str(node) 'yb.dat  i' num2str(node) 'yb.mat/x'];
                        % convert sdf to matlab
eval('dos(dfiley)')
%eval(['load ' datafile]);


dfiley=['sdfto58 i' num2str(node) 'yb.dat  i' num2str(node) 'yb.unv'];
                        % convert sdf to unv58
eval('dos(dfiley)')
%eval(['load ' datafile]);


dfilez=['sdftoml i' num2str(node) 'zb.dat  i' num2str(node) 'zb.mat/x'];
                        % convert sdf to matlab
eval('dos(dfilez)')
%eval(['load ' datafile]);


dfilez=['sdfto58 i' num2str(node) 'zb.dat  i' num2str(node) 'zb.unv'];
                        % convert sdf to unv58
eval('dos(dfilez)')
%eval(['load ' datafile])


end                     % end loop nodes 29 thru 52
```

APPENDIX K. MAT_PLOT.M – MATLAB ANALYSIS CODE

```
% MAT_PLOT.M - MATLAB Analysis Code
% This program loads the HP-35665A test data and plots the magnitude
% (dB) of each file

% Program developed by LT Scott E. Johnson and LT John Vlattas
% Last modified: 16 April 1998

clear all

      % Magnitude (dB) Plot .mat data nodes 3 thru 26

      for node=3:26           % loop that loads nodes 3 thru 26
            figure(node)
            datafile=['i' num2str(node) 'xb.mat'];
            eval(['load ' datafile]);
            plot(o2i1x,20.*log10(abs(o2i1)), 'r')
            grid
            axis([1 200 -5 70])
            xlabel('Frequency (Hz)'), ylabel('Magnitude (dB)');
            title(['Node ', int2str(node), ' Impact Node 24'])

            hold on

            datafile=['i' num2str(node) 'yb.mat'];
            eval(['load ' datafile]);
            plot(o2i1x,20.*log10(abs(o2i1)), '-.m')

            hold on

            datafile=['i' num2str(node) 'zb.mat'];
            eval(['load ' datafile]);
            plot(o2i1x,20.*log10(abs(o2i1)), '--b')
            %legend('X','Y','Z')


      end

      % Magnitude (dB) Plot .mat data nodes 29 thru 52
      % data not collected on nodes 27 or 28

      for node=29:52          % loop that loads nodes 29 thru 52
            figure(node)
            datafile=['i' num2str(node) 'xb.mat'];
            eval(['load ' datafile]);
            plot(o2i1x,20.*log10(abs(o2i1)), 'r')
            grid
            axis([1 200 -5 70])
            xlabel('Frequency (Hz)'), ylabel('Magnitude (dB)');
            title(['Node ', int2str(node), ' Impact Node 24'])

            hold on

            datafile=['i' num2str(node) 'yb.mat'];
```

```
eval(['load ' datafile]);
plot(o2i1x,20.*log10(abs(o2i1)), '-.m')

hold on

datafile=['i' num2str(node) 'zb.mat'];
eval(['load ' datafile]);
plot(o2i1x,20.*log10(abs(o2i1)), '--b')

%legend('X','Y','Z')


end
```

APPENDIX L. MACPLOT.M – MODAL ASSURANCE CRITERIA AND ASSOCIATED CODE

```
% MACPLOT.M - MATLAB Analysis Code
% Does MAC (Modal Assurance Criterion) plot using a set
% of modeshapes

% Written by Dr. Albert Bosse, NRL 2/27/98
% Modified by LT Scott E. Johnson and LT John Vlattas
% Last Modified: 10 May 1998

global U55param U55shape U55nodes U55id1 U55id2 U55id3 U55id4 U55id5
nDOF
fid=fopen('nrl_heal.unv');
unv(fid)
testshapes=U55shape;
FEMshapes=U55shape;
% Reorder DOF if necessary

% Normalize test shapes
[m,n]=size(U55shape);
for i=1:n
   testshapes(:,i)=testshapes(:,i)/norm(testshapes(:,i));
end
% Normalize FEM shapes
[m,n]=size(FEMshapes);
for i=1:n
  FEMshapes(:,i)=FEMshapes(:,i)/norm(FEMshapes(:,i));
end
mesh(testshapes.'*FEMshapes)
title('MAC Plot for NRL Healthy Truss Data')
fclose(fid);

function unv55(fid,U55);
% Usage: function unv55(fid,U55);
% 950401 Date last modified by Al Bosse at NRL
%
% This function will read in a Universal Type 55 record.
%
% This program will return a parameter matrix, a mode shape matrix
% and a nodes matrix as global variables.
%
%    U55param= [ [ Freq1, Mmass1, VDamp1, HDamp1 ]
%              [ Freq2, Mmass2, Vdamp2, HDamp2 ] ]
%
%       if it is a complex mode, then the following applies...
%           Freq1  ==> Complex Eigenvalue
%           Mmass1 ==> Complex Modal A
%           Vdamp1 ==> Complex Modal B
%           HDamp1 ==> -1 as a flag value
%
%    U55shape= [ [1_1x 1_1y 1_1z 1_2x 1_2y 1_2z]
%                [2_1x 2_1y 2_1z 2_2x 2_2y 2_2z] ]
%             where 1_2x is node 2, direction x of mode shape one.
```

```
%
%    U55nodes= [ [Mode# 1_N1 1_N2 1_N3]
%                [Mode# 2_n1 2_N2 2_N3] ]
%
%    U55id1..U55id4 = ID Lines 1 to 4.
%
global U55param U55shape U55nodes U55id1 U55id2 U55id3 U55id4 U55id5
nDOF

ID1=fgetl(fid);
if strcmp(ID1,'NONE')
  ID1=' ';
end
ID2=fgetl(fid);
if strcmp(ID2,'NONE')
  ID2=' ';
end
ID3=fgetl(fid);
if strcmp(ID3,'NONE')
  ID3=' ';
end
ID4=fgetl(fid);
if strcmp(ID4, 'NONE')
  ID4=' ';
end
ID5=fgetl(fid);
if strcmp(ID5,'NONE')
  ID5=' ';
end
Lin=fgetl(fid);
R6=sscanf(Lin,'%d');
if (R6(2) == 2)
  Nrml_Mode=1;
elseif (R6(2) == 3)
  Nrml_Mode=0;
else
  disp('Unknown Mode Type...bad data');
end
Lin=fgetl(fid);
R7=sscanf(Lin,'%d');
Mnodes(1)=R7(4);     %Record Mode Number Label
%disp(['Reading Label: ',num2str(Mnodes(1))]);
Lin=fgetl(fid);
R8=sscanf(Lin,'%e');
if Nrml_Mode==1
  Mparam(1:4)=R8(1:4);     %Store Modal Parameters: Frq, Mmass, Vdamp,
Hdamp
elseif Nrml_Mode==0
  Mparam(1)=R8(1)+R8(2)*i; %Complex Eigenvalue
  Mparam(2)=R8(3)+R8(4)*i; %Complex Modal A
  Mparam(3)=R8(5)+R8(6)*i; %Complex Modal B
  Mparam(4)=-1;             %Space Holder & Flag
else
  Mparam(1:4)=[-1,-1,-1,-2];
end
Nindex=1;
index2=1;
```

```
nDOF=R6(6);     %# of DOF's in shape record, usually 3 (x,y,z)
NEOF=1;
while (NEOF==1)
  Lin=fgetl(fid);
  R9=sscanf(Lin,'%d');
  if (R9 ~= -1)
    Mnodes(index2)=R9;
    Lin=fgetl(fid);
    R10=sscanf(Lin,'%e');
    if Nrml_Mode == 1
      Mshape(Nindex:Nindex+2)=R10(1:3);
    elseif Nrml_Mode == 0
      Mshape(Nindex)   = R10(1)+R10(2)*i;
      Mshape(Nindex+1) = R10(3)+R10(4)*i;
      Mshape(Nindex+2) = R10(5)+R10(6)*i;
    else
      Mshape(Nindex:Nindex+nDOF-1)=[-1,-1,-1];
    end
    Nindex=Nindex+nDOF;
    index2=index2+1;
  else
    NEOF=0;
  end
end
U55param(:,U55)=Mparam(:);
U55shape(:,U55)=Mshape(:);
U55nodes(:,U55)=Mnodes(:);
if length(U55id1) == 0
  U55id1(:,1)=ID1';
  U55id2(:,1)=ID2';
  U55id3(:,1)=ID3';
  U55id4(:,1)=ID4';
  U55id5(:,1)=ID5';
else
  U55id1=str2mat(U55id1',ID1)';
  U55id2=str2mat(U55id2',ID2)';
  U55id3=str2mat(U55id3',ID3)';
  U55id4=str2mat(U55id4',ID4)';
  U55id5=str2mat(U55id5',ID5)';
end

return


function Stat=NegOne(fid)
%Searches forward in file handle for the next -1
  Stat=0;
  LinIn=fgetl(fid);
  if (LinIn == -1)
    Stat = -4;
  else
    while (sscanf(LinIn,'%d',1) ~= -1)
      LinIn=fgetl(fid);
      if (LinIn == -1)
        Stat = -4;
        LinIn='-1';
      end
```

```
    end
  end
return
```

APPENDIX M. ACTIVE CONTROL EXPERIMENTAL RESULTS

This Appendix contains the results for the active control testing of the NPS space truss. Time response data for each trial is plotted for nodes 26 and 49, which are the end nodes of the truss and have the largest amplitudes during excitation. The power spectral density for each the controlled versus uncontrolled parts of each trial to get a quantitative estimate of how much reduction in vibration has occurred for each test case. All trials are annotated with a legend delineating the settings of the gain parameters and the targeted frequency.

Trial Number: 1
Gain Parameter: (Uncontrolled Case)
Iigain = 0
Igain = 0
System Gain = 0
Targeted Frequency = 0
Power Reduction = 0

(No Power Spectral Density for this Case)

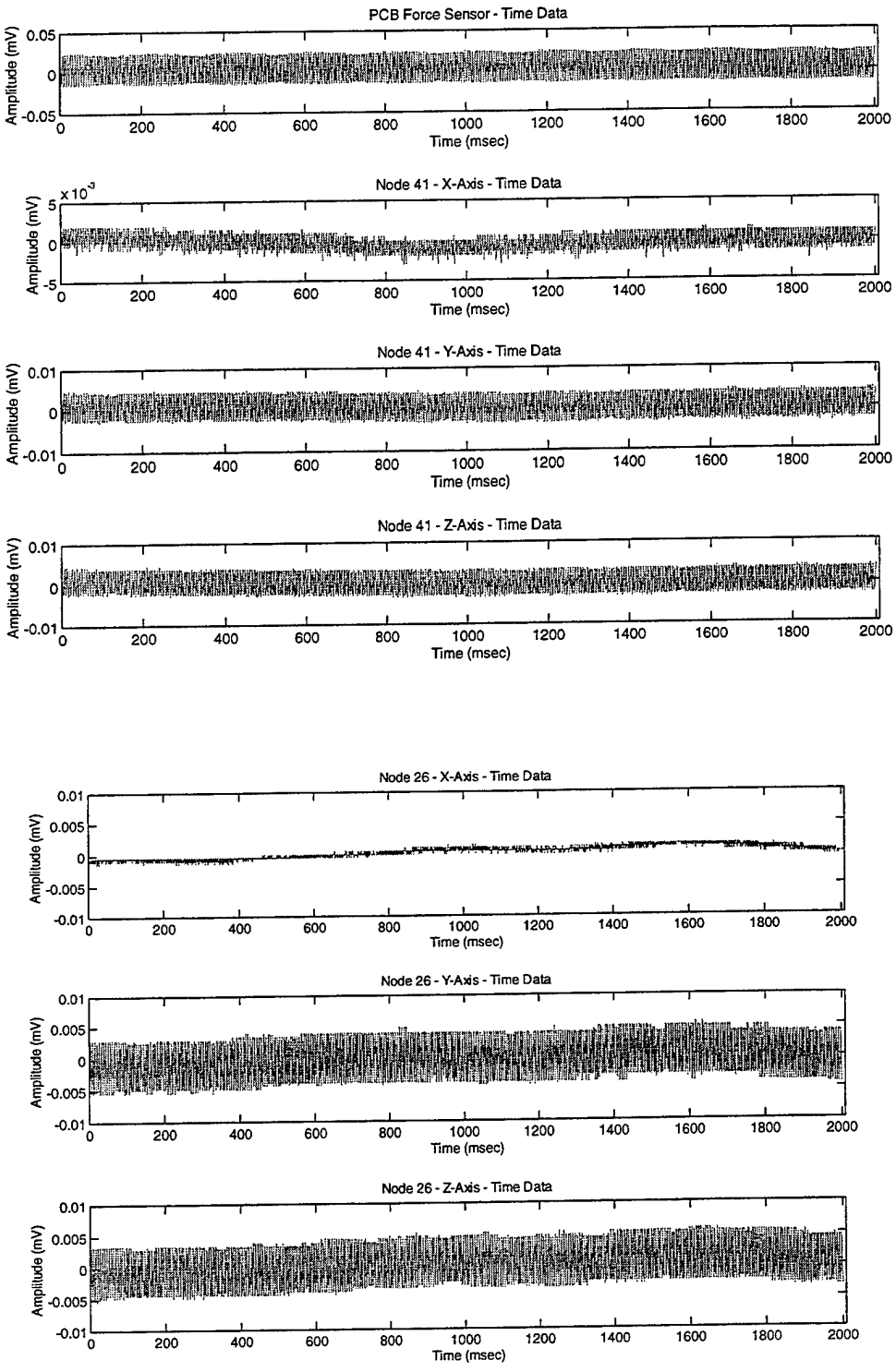

Figure 61. Active Control Testing - Trial 1 - Node 26 and 41 Response

Trial Number: 2

Gain Parameters:

Iigain = 0

Igain = 300

System Gain = 1.75

Targeted Frequency = 16.75

Power Reduction = 11.6091

Notes:

(a) In all subsequent case the controller is activated 5 seconds after the start of the test. Test duration is 20 seconds.

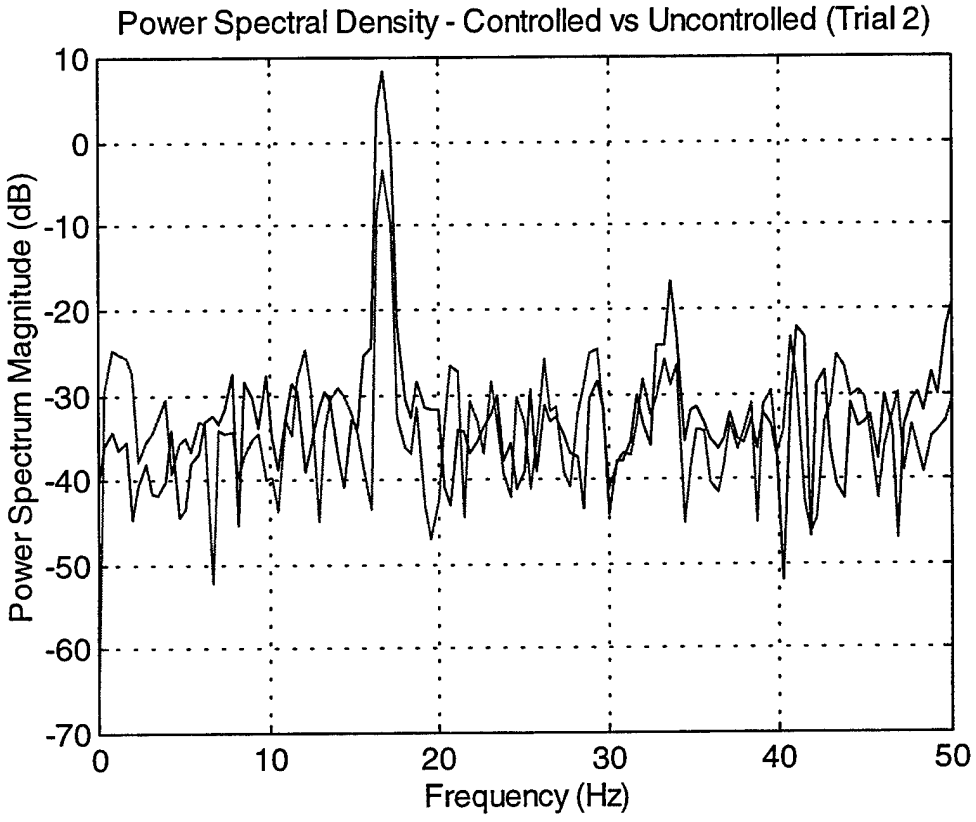

Figure 62. Active Control Testing – Trial 2 – Power Spectral Density

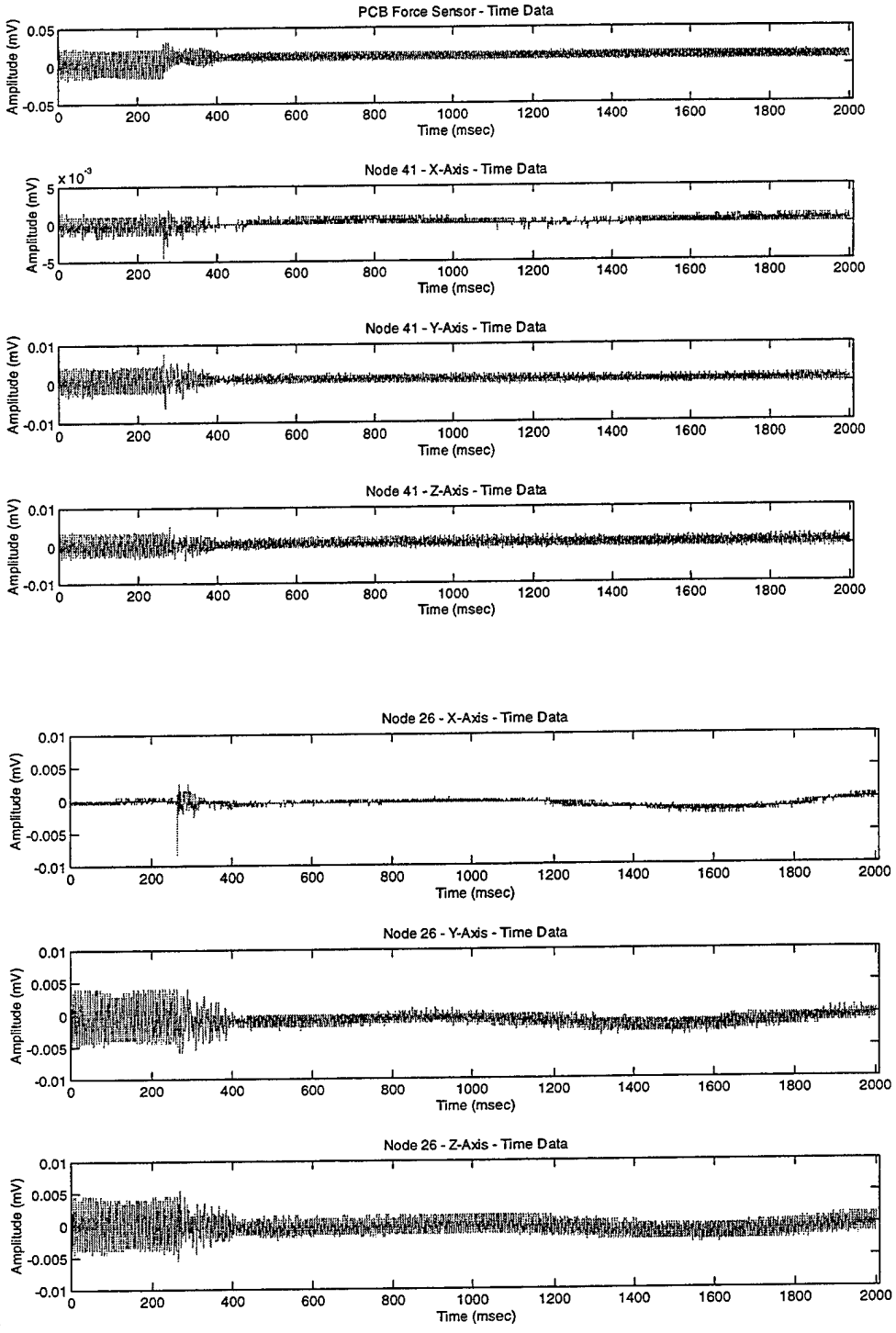

Figure 63. Active Control Testing – Trial 2 – Node 26 and 41 Response

Trial Number: 3

Gain Parameters:

Iigain = 0

Igain = 200

System Gain = 1.75

Targeted Frequency = 16.75

Power Reduction = 8.7463

Notes:

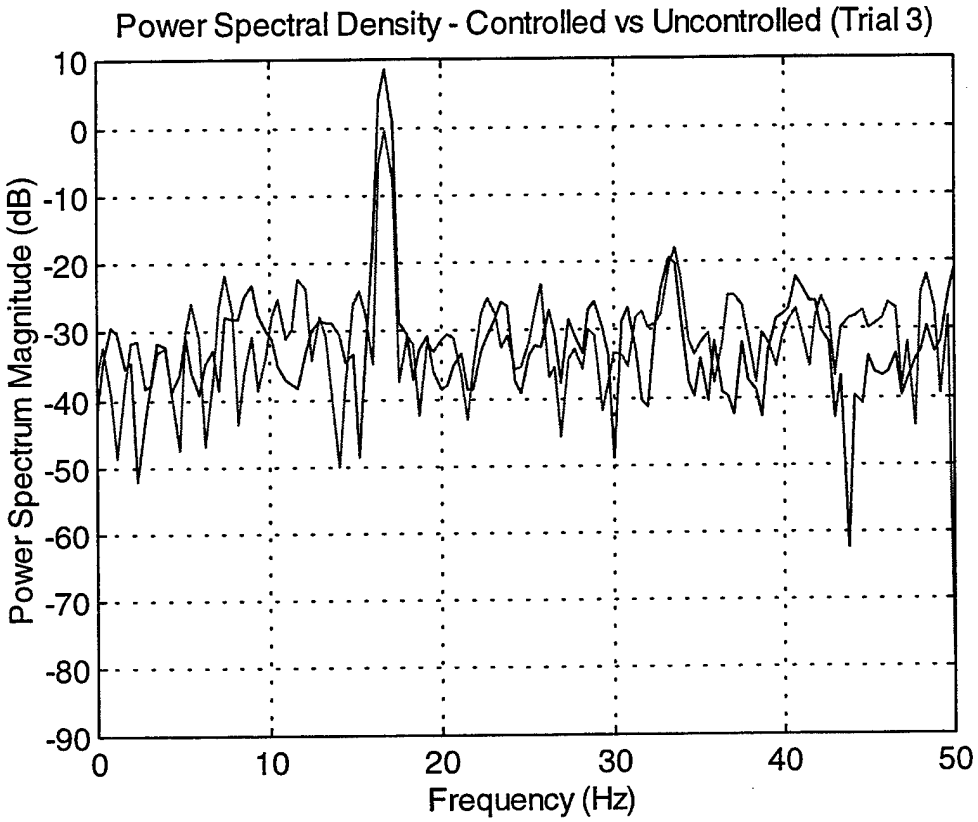

Figure 64. Active Control Testing – Trial 3 – Power Spectral Density

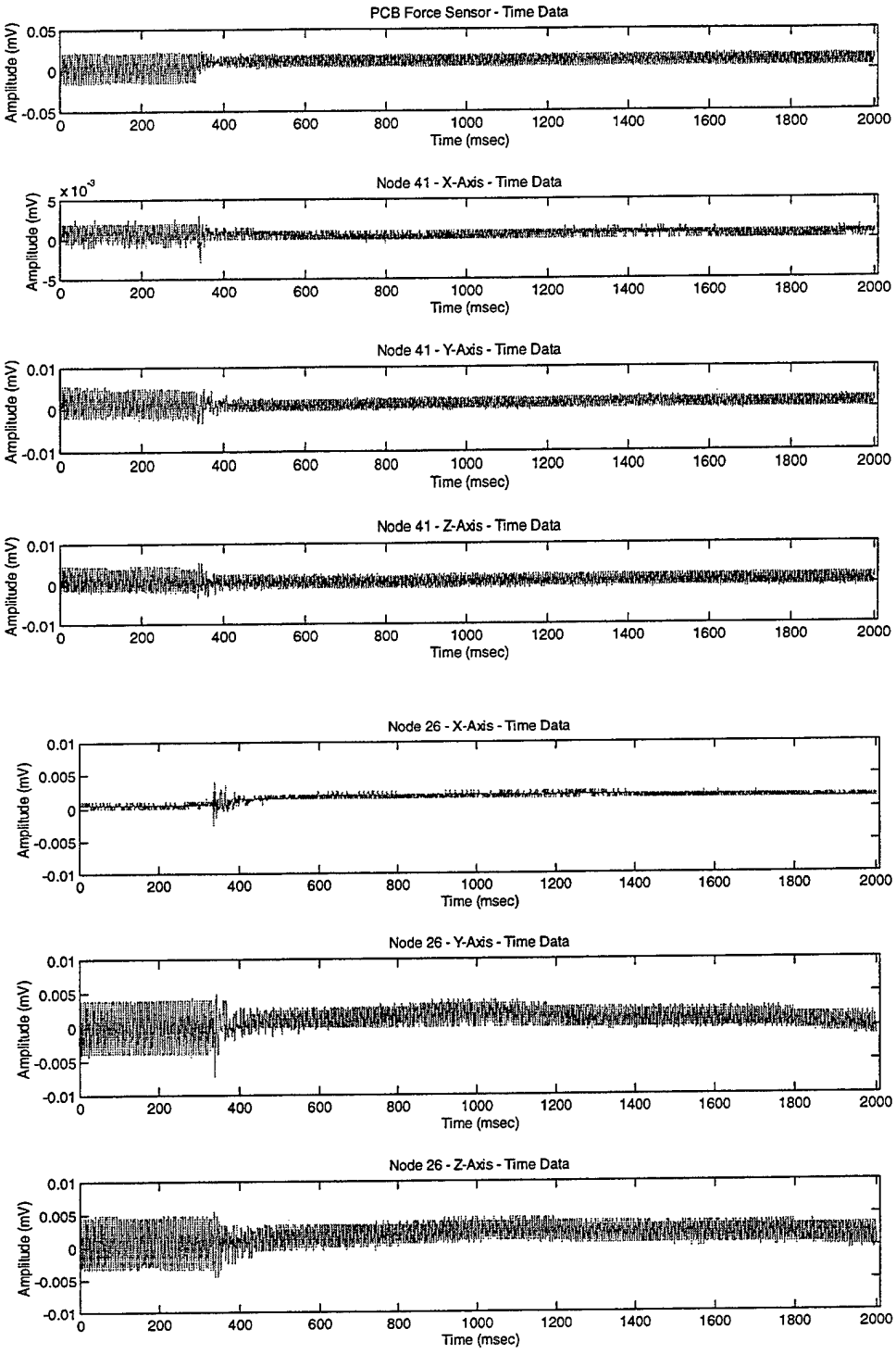

Figure 65. Active Control Testing – Trial 3 – Node 26 and 41 Response

Trial Number: 4

Gain Parameters:

Iigain = 0

Igain = 100

System Gain = 1.75

Targeted Frequency = 16.75

Power Reduction = 5.3681

Notes:

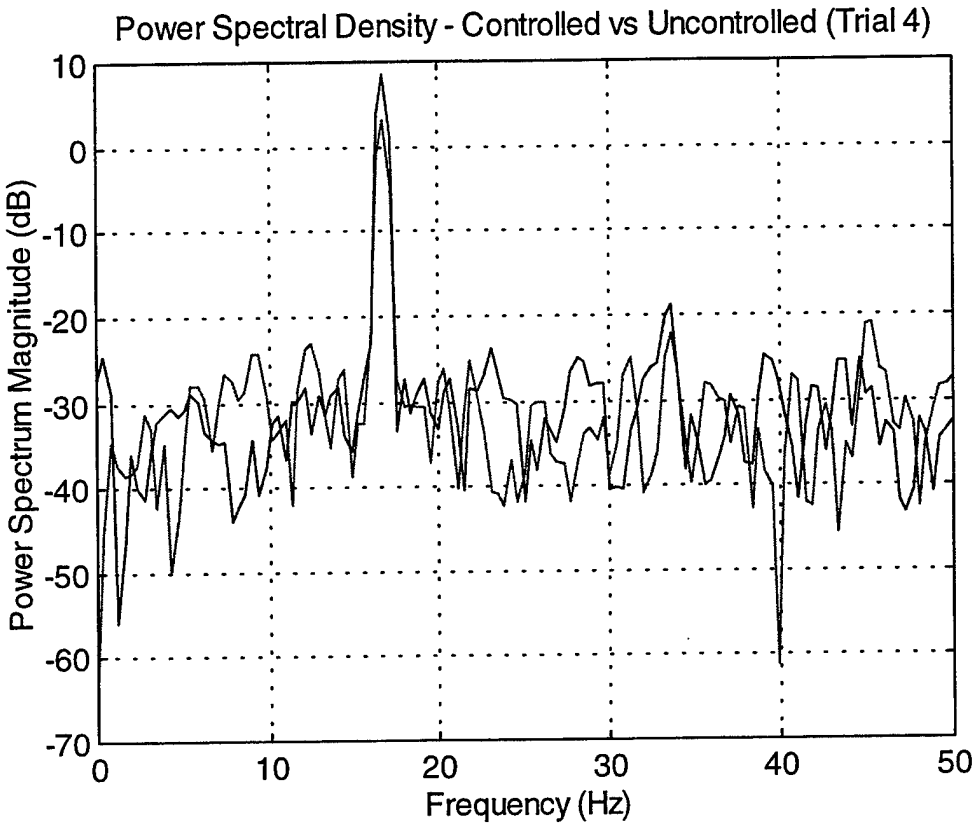

Figure 66. Active Control Testing – Trial 4 – Power Spectral Density

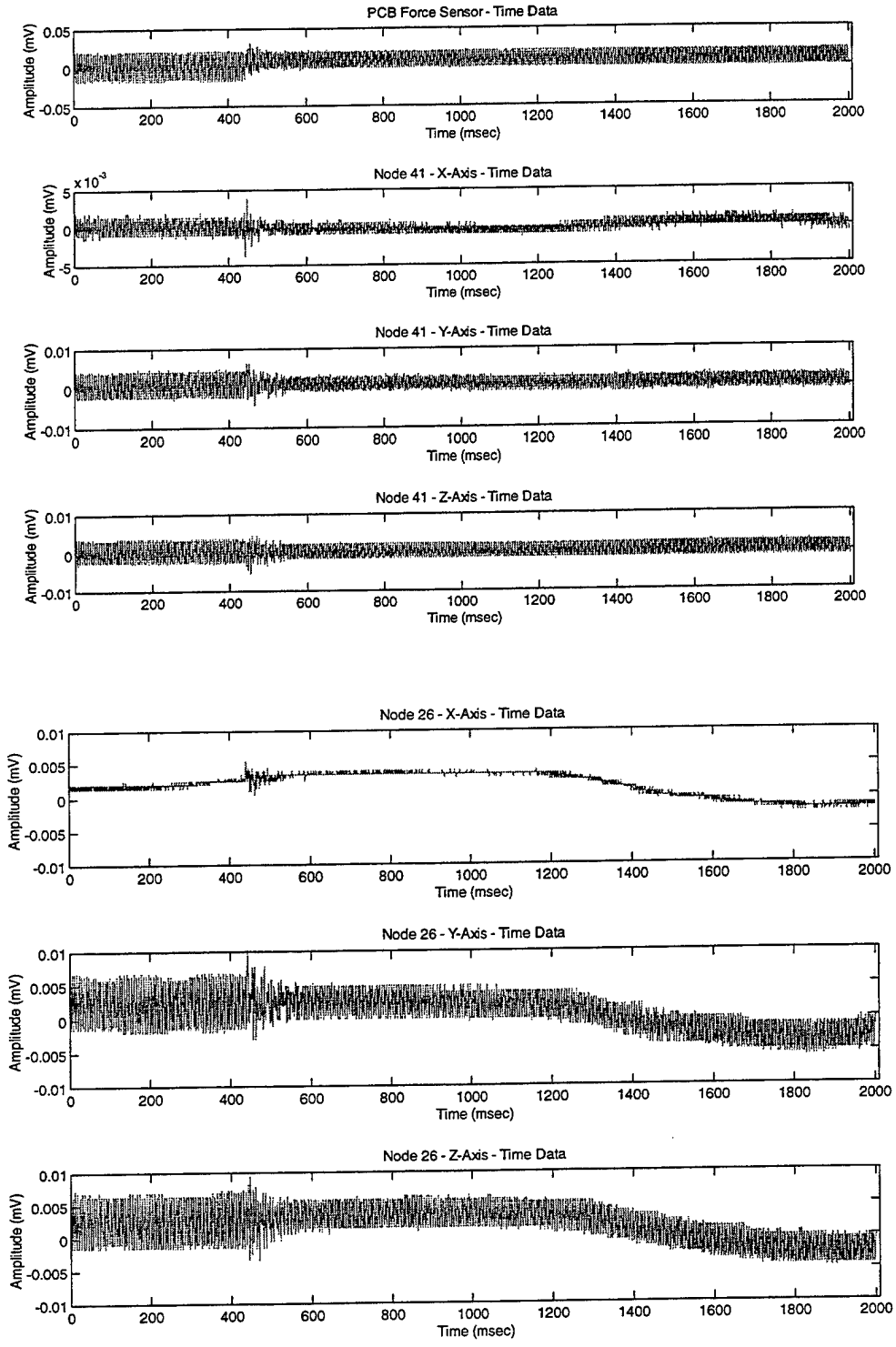

Figure 67. Active Control Testing – Trial 4 – Node 26 and 41 Response

Trial Number: 5

Gain Parameters:

Iigain = 100

Igain = 0

System Gain = 1.75

Targeted Frequency = 16.75

Power Reduction (dB) = .3228

Notes:

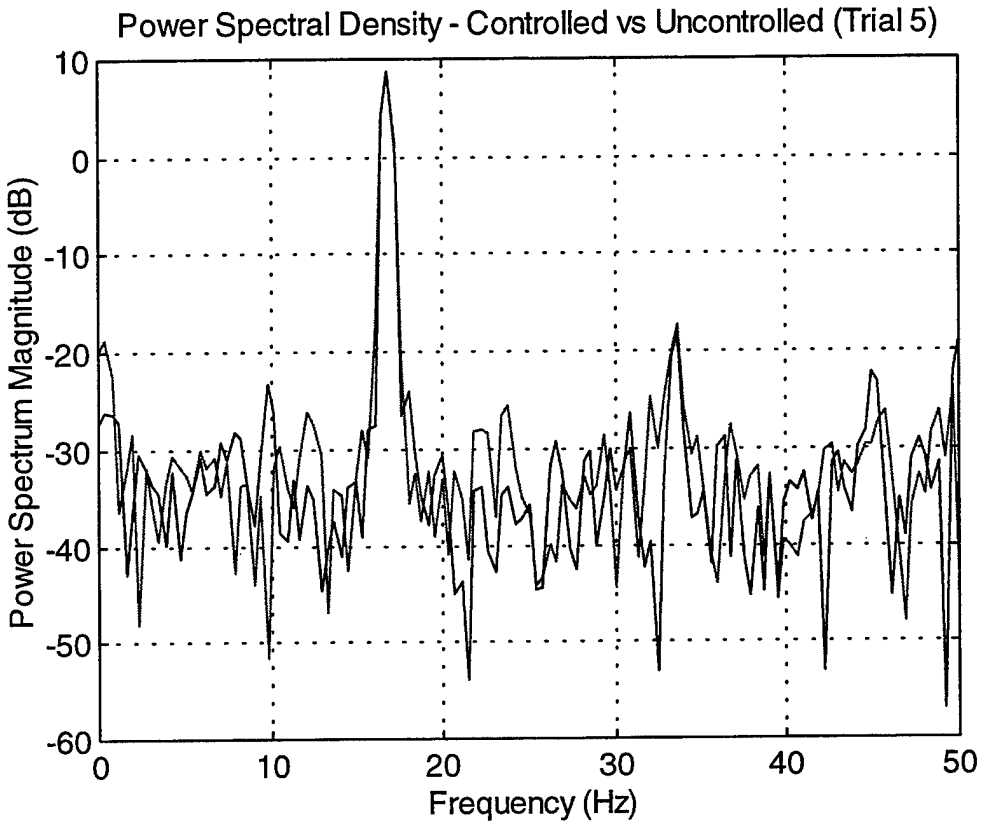

Figure 68. Active Control Testing – Trial 5 – Power Spectral Density

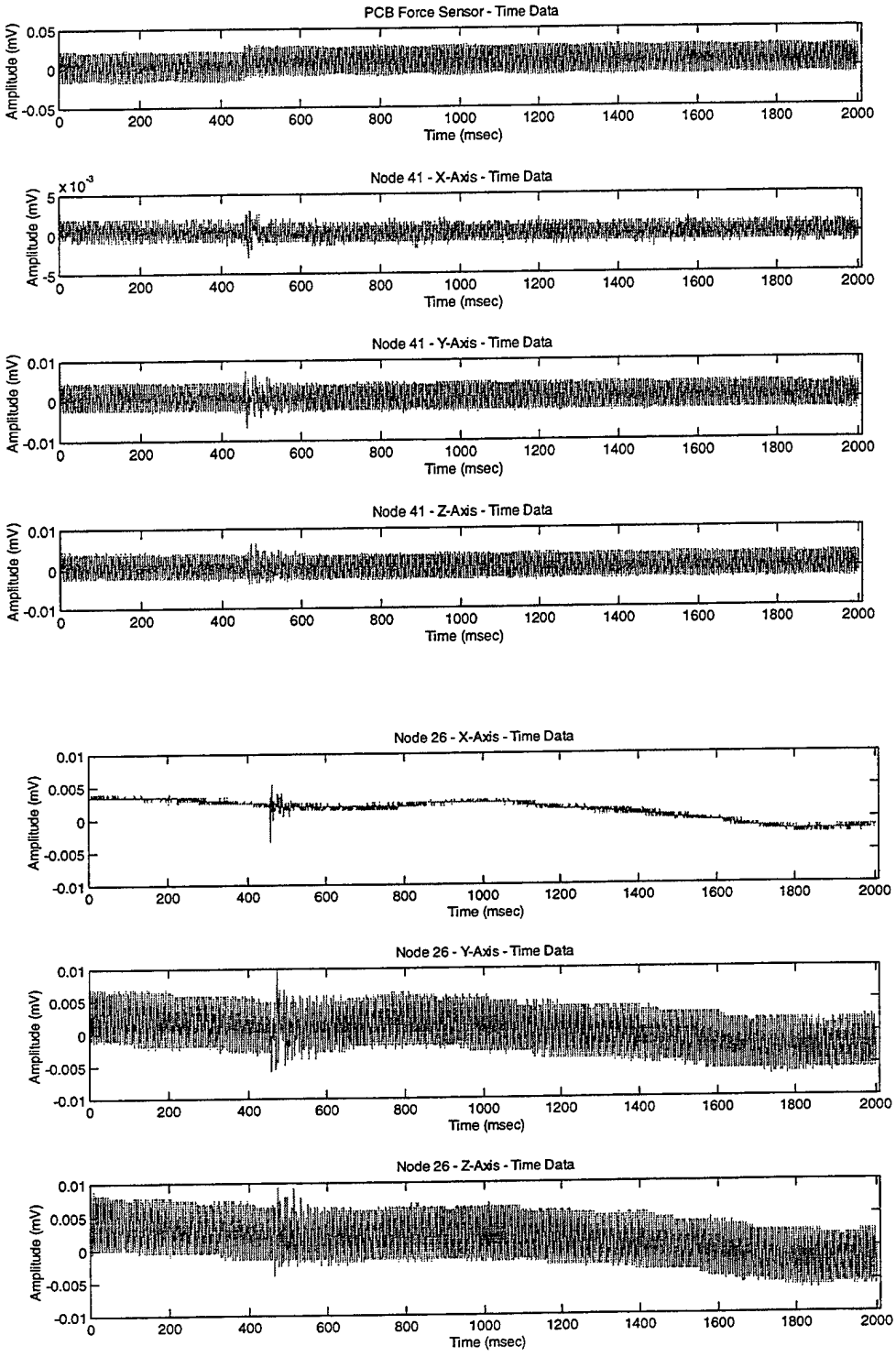

Figure 69. Active Control Testing – Trial 5 – Node 26 and 41 Response

Trial Number: 6

Gain Parameters:

Iigain = 250

Igain = 0

System Gain = 1.75

Targeted Frequency = 16.75

Power Reduction (dB) = 0

Notes:

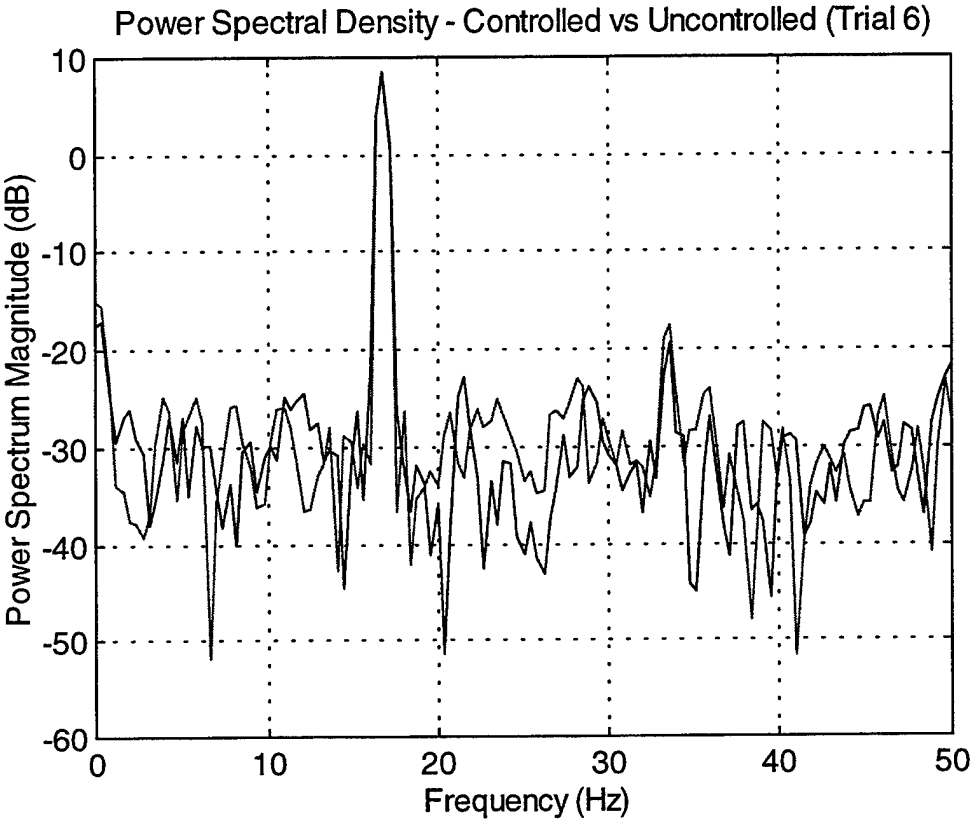

Figure 70. Active Control Testing – Trial 6 – Power Spectral Density

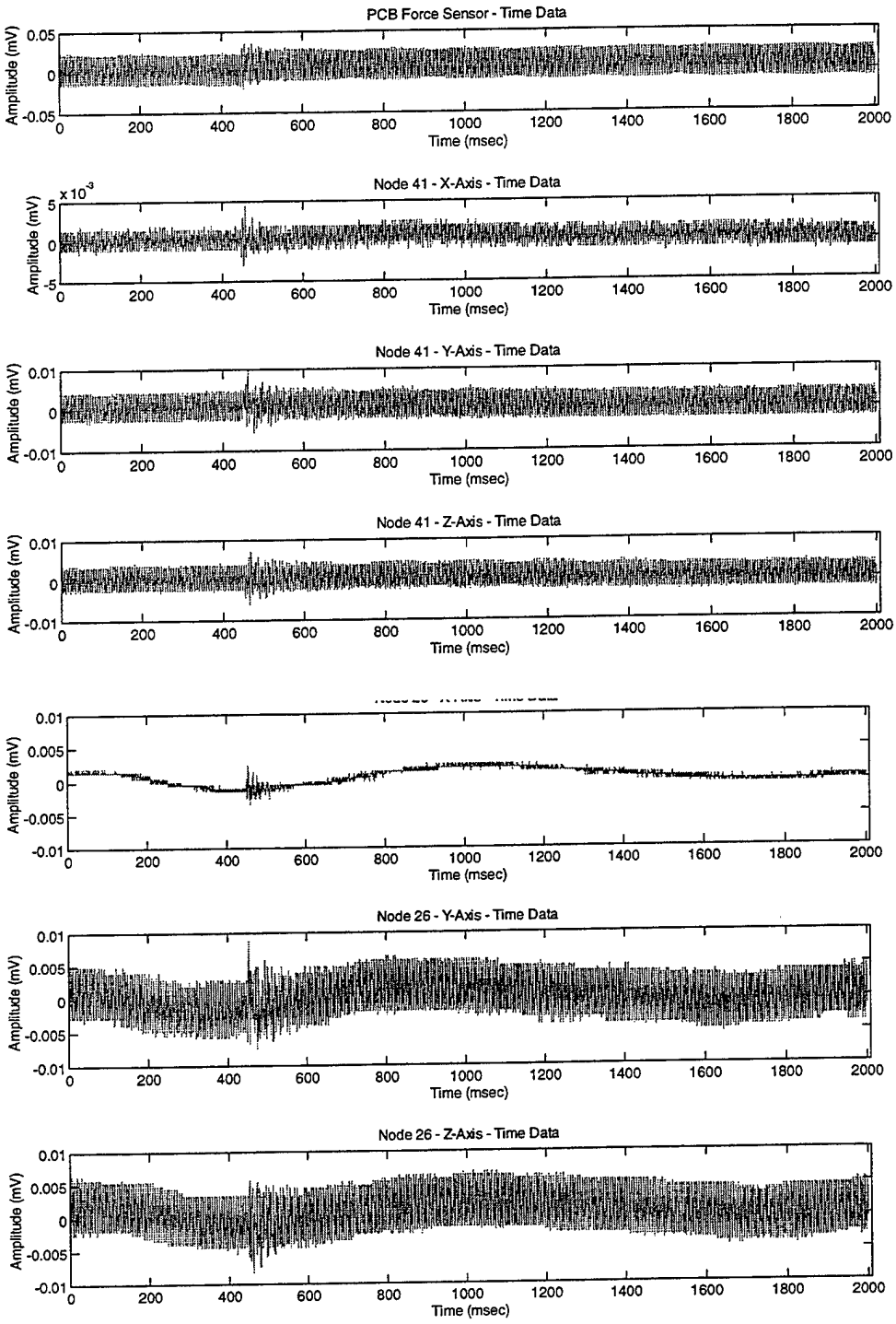

Figure 71. Active Control Testing – Trial 6 – Node 26 and 41 Response

Trial Number: 7

Gain Parameters:

Iigain = 300

Igain = 100

System Gain = 1.75

Targeted Frequency = 16.75

Power Reduction (dB) = 11.3974

Notes:

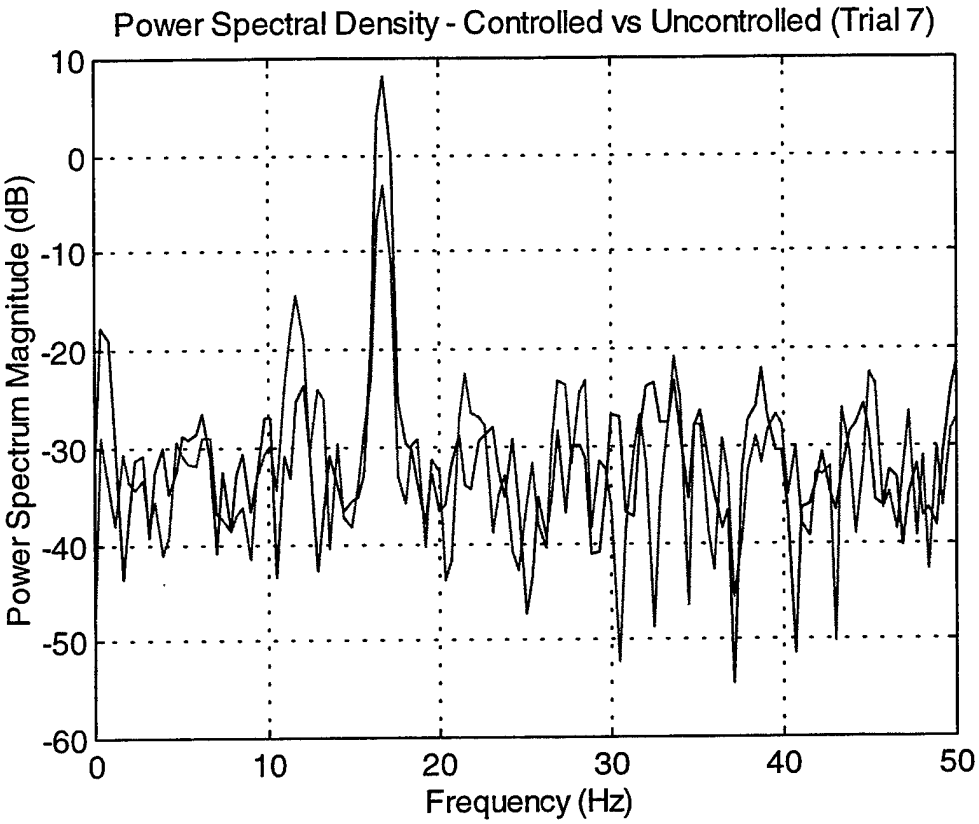

Figure 72. Active Control Testing – Trial 7 – Power Spectral Density

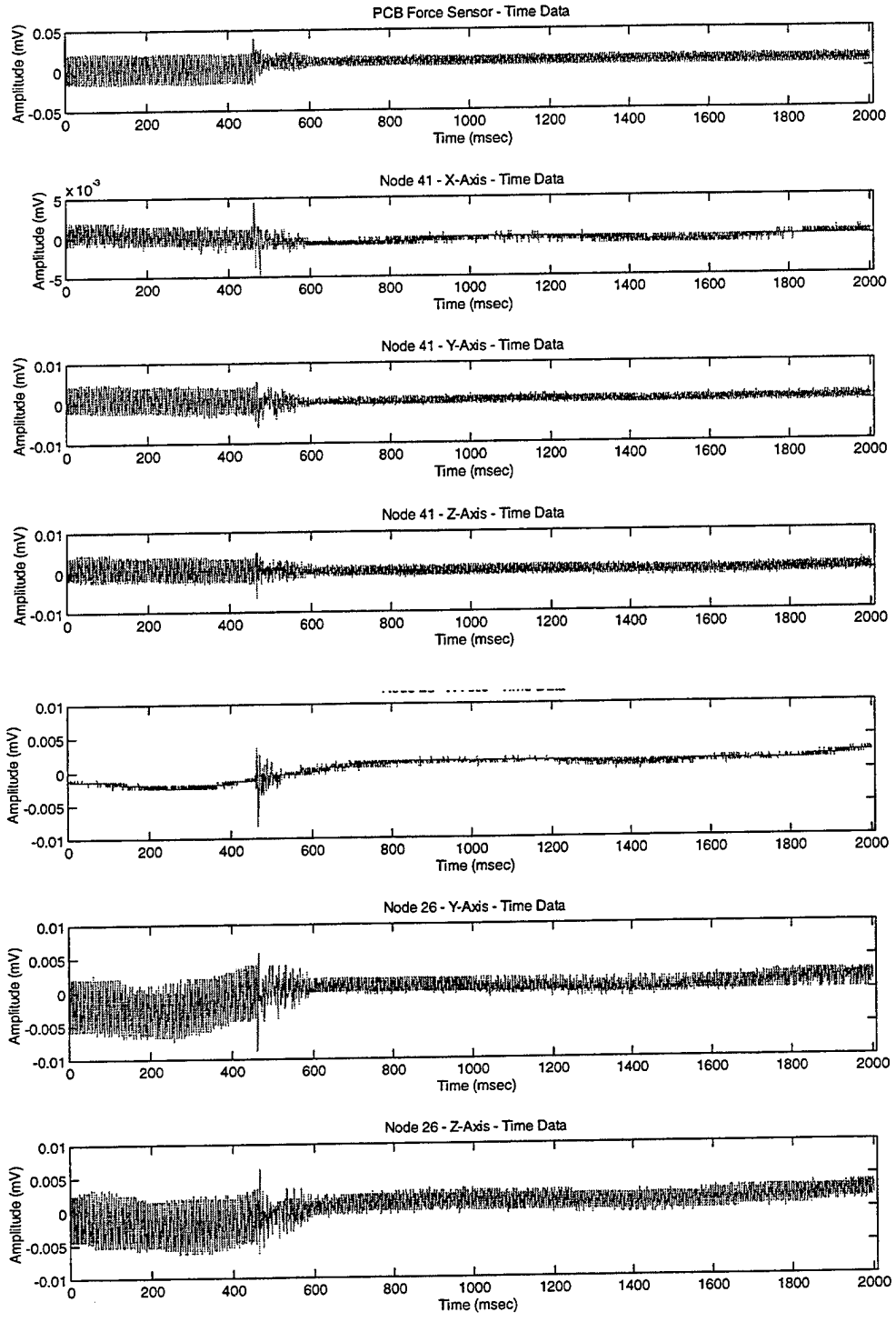

Figure 73. Active Control Testing – Trial 7 – Node 26 and 41 Response

Trial Number: 8

Gain Parameters:

Iigain = 300

Igain = 100

System Gain = 2

Targeted Frequency = 16.75

Power Reduction (dB) = 13.8544

Notes:

(a) System was disturbed after controller reached steady-state to evaluate stability. System remained stable.

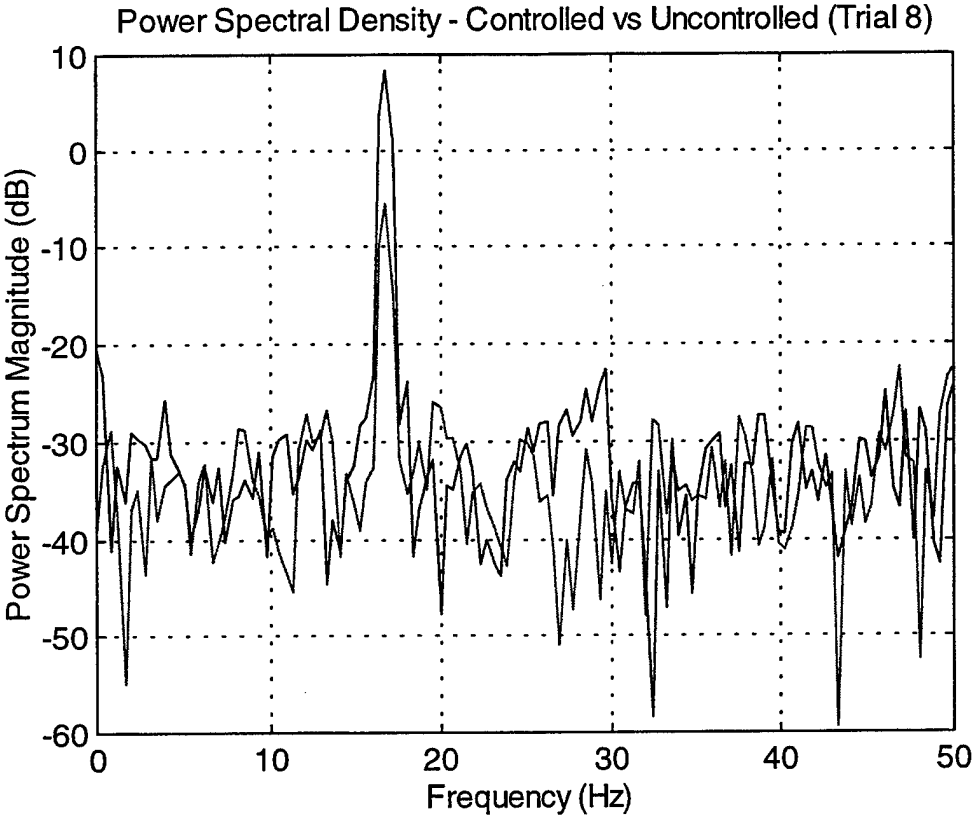

Figure 74. Active Control Testing – Trial 8 – Power Spectral Density

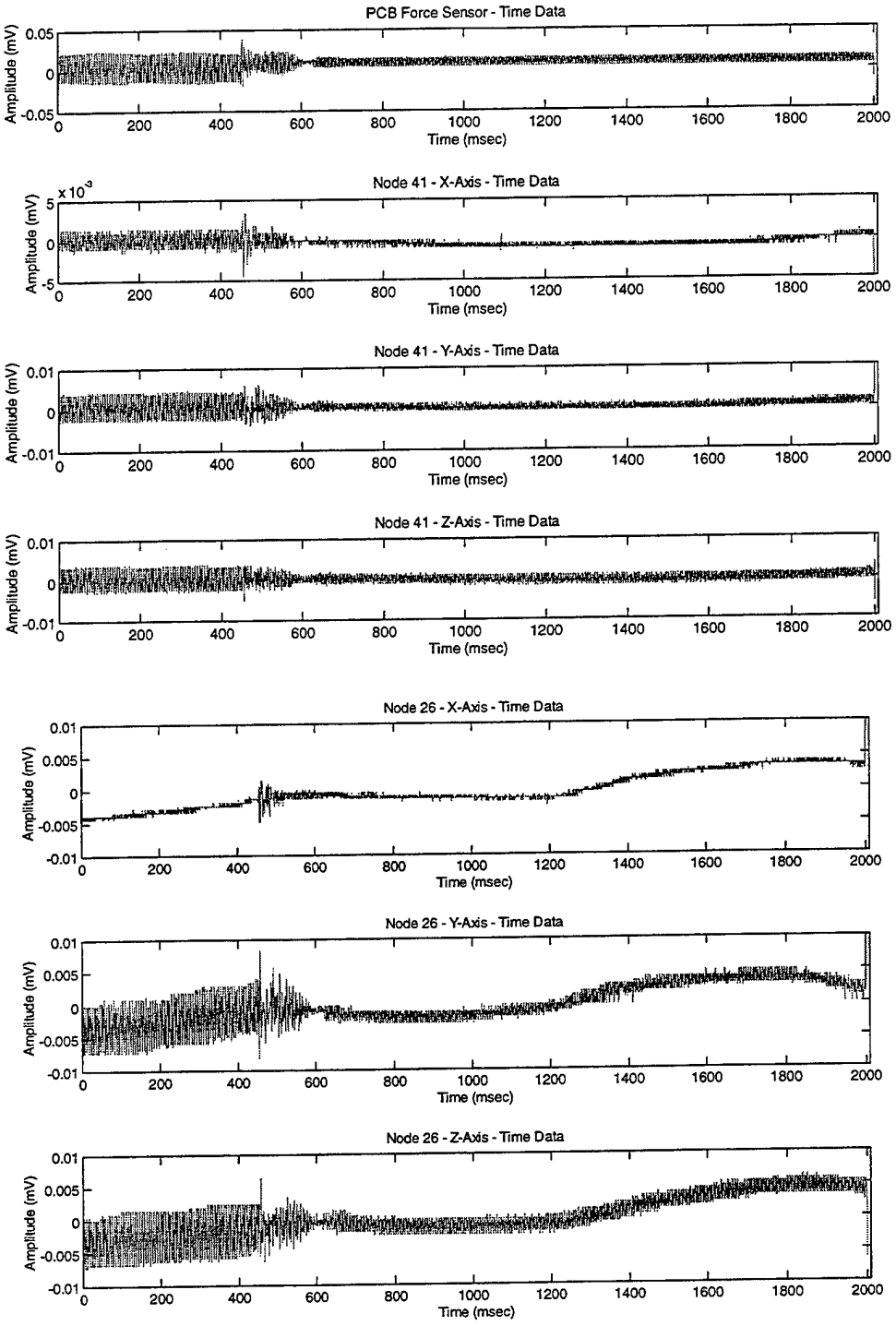

Figure 75. Active Control Testing – Trial 8 – Node 26 and 41 Response

Trial Number: 9

Gain Parameters:

Iigain = 300

Igain = 100

System Gain = 2.25

Targeted Frequency = 16.75

Power Reduction (dB) = 12.9382

Notes:

(a) System was disturbed after controller reached steady-state to evaluate stability. System remained stable. Indications of instability in time history.

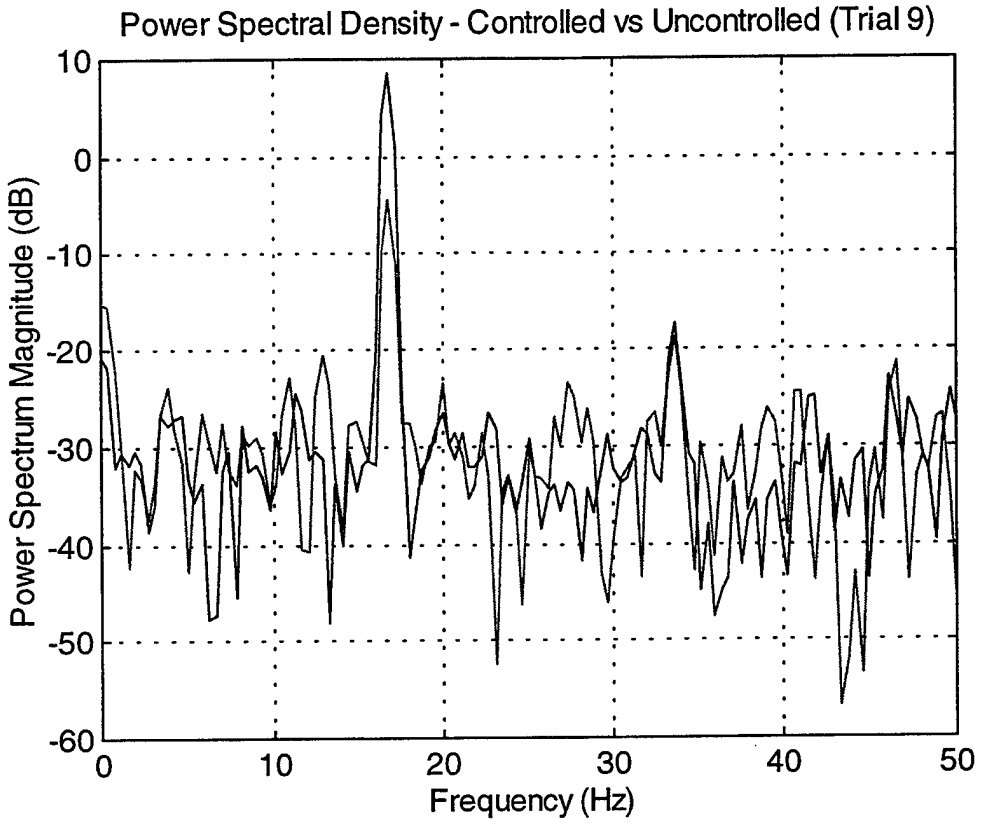

Figure 76. Active Control Testing – Trial 9 – Power Spectral Density

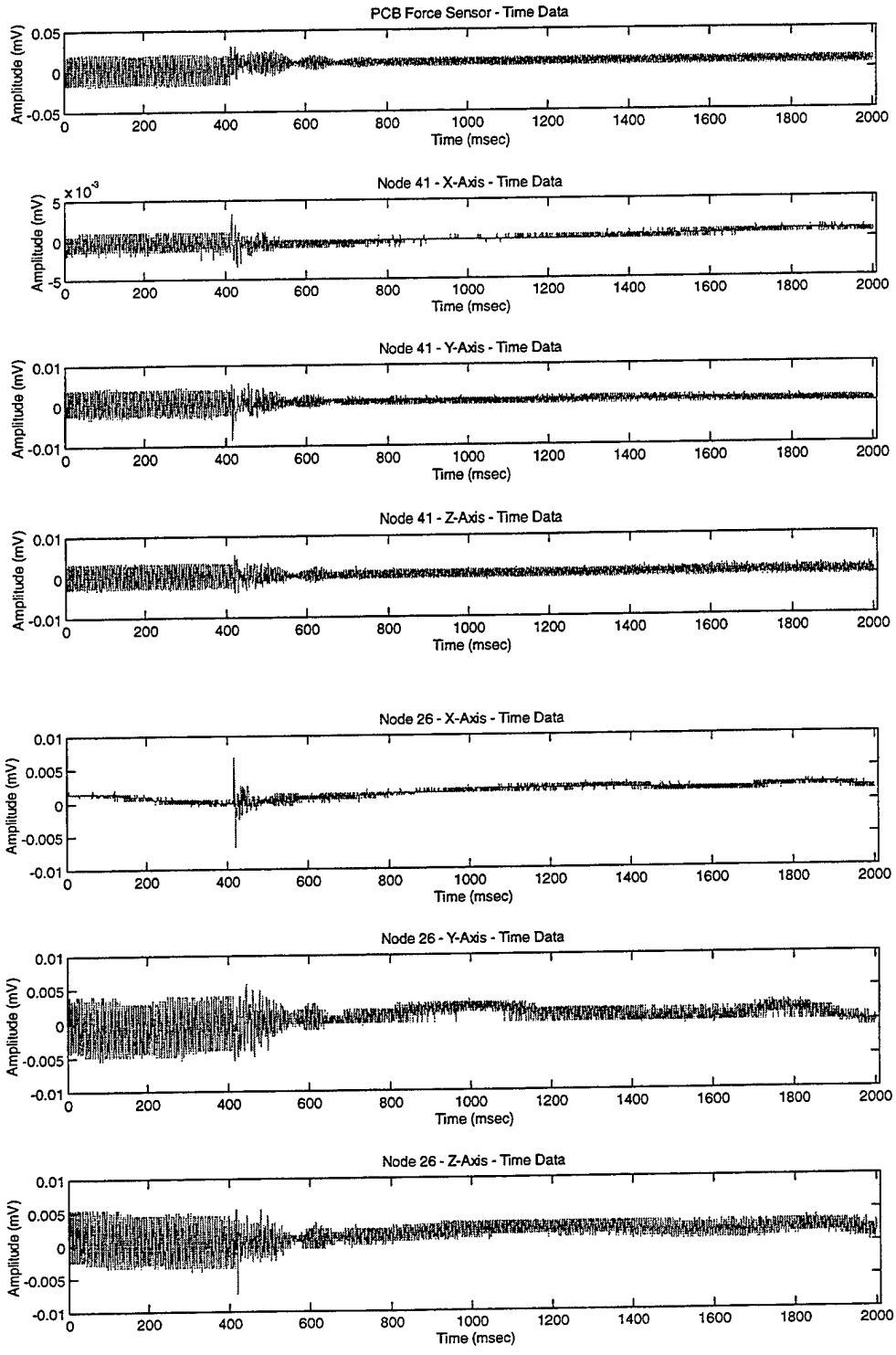

Figure 77. Active Control Testing – Trial 9 – Node 26 and 41 Response

Trial Number: 10

Gain Parameters:

Iigain = 300

Igain = 100

System Gain = 2.5

Targeted Frequency = 16.75

Power Reduction (dB) = 14.8166

Notes:

(a) System was disturbed after controller reached steady-state to evaluate stability. System remained stable. Strong indication of potential instability in graph of actuating signal (Channel 4) (below).

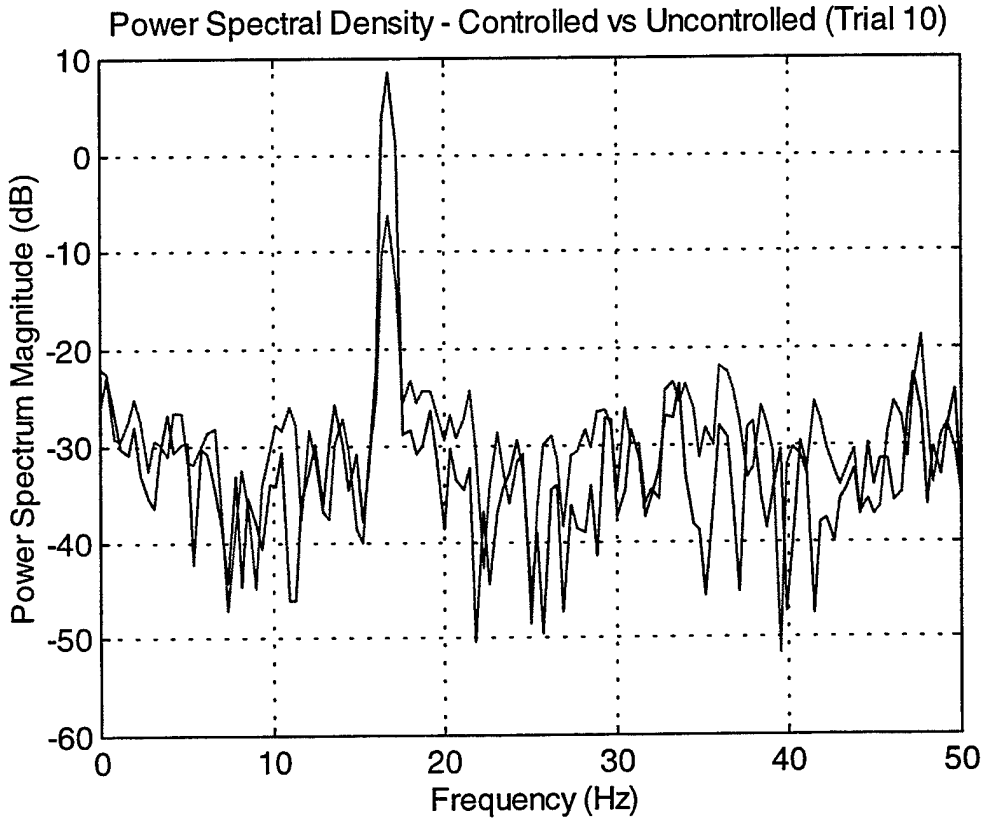

Figure 78. Active Control Testing – Trial 10 – Power Spectral Density

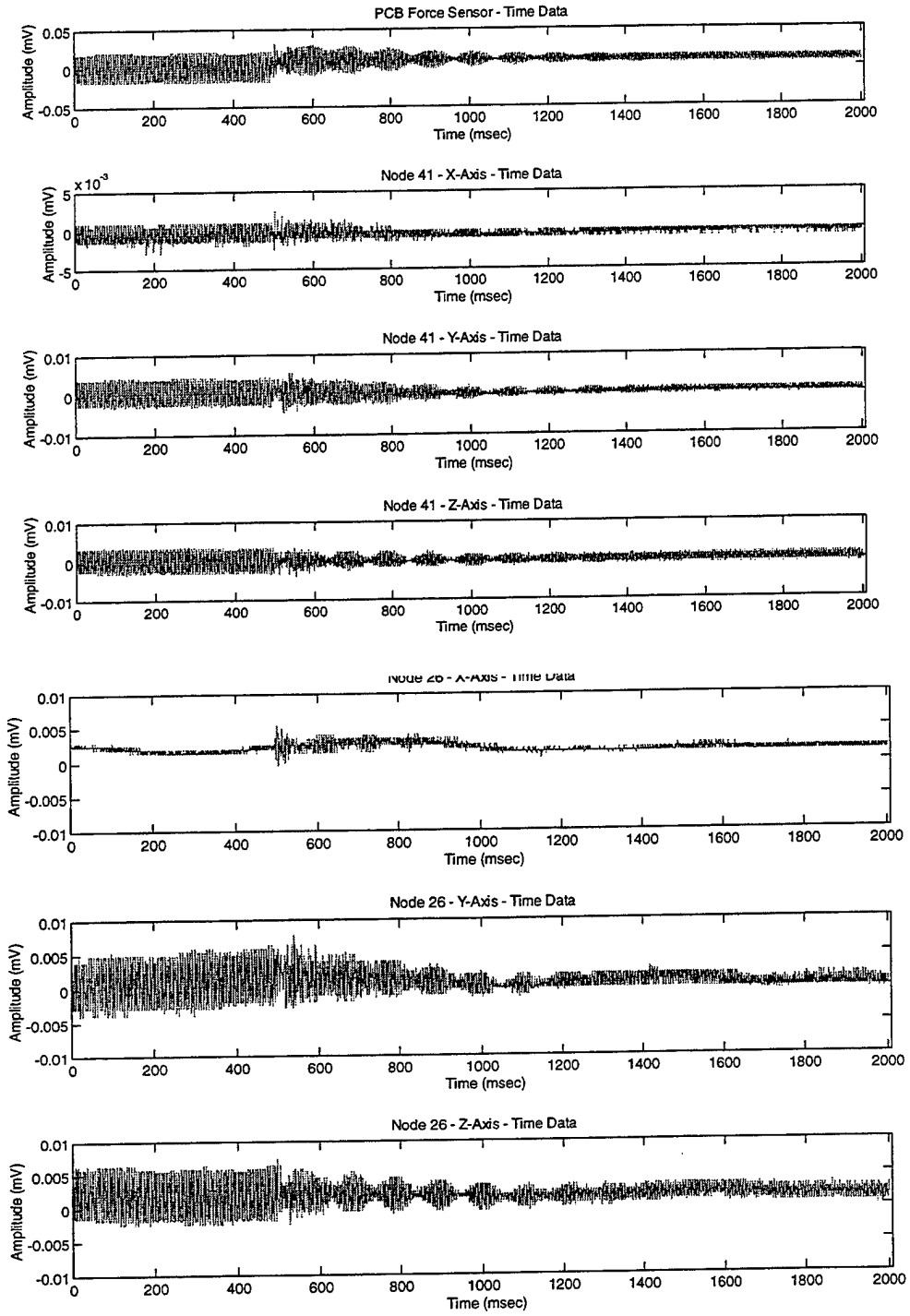

Figure 79. Active Control Testing – Trial 10 – Node 26 and 41 Response

Trial Number: 11

Gain Parameters:

Iigain = 300

Igain = 100

System Gain = 1.75

Targeted Frequency = 17.0

Power Reduction (dB) = 8.8336

Notes:

(a) Testing frequencies for all subsequent tests.

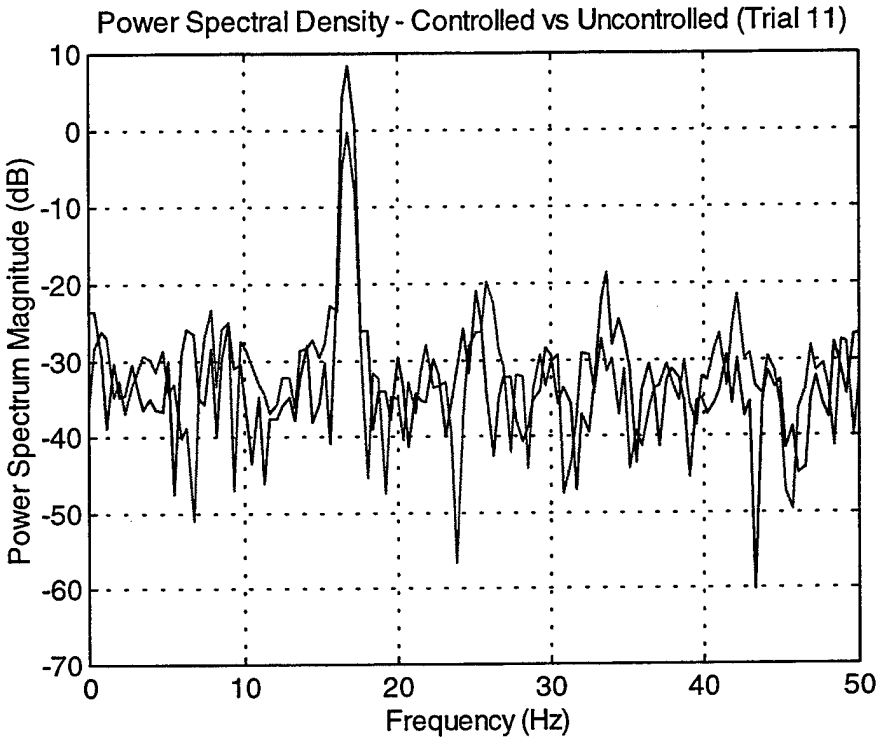

(b)

Figure 80. Active Control Testing – Trial 11 – Power Spectral Density

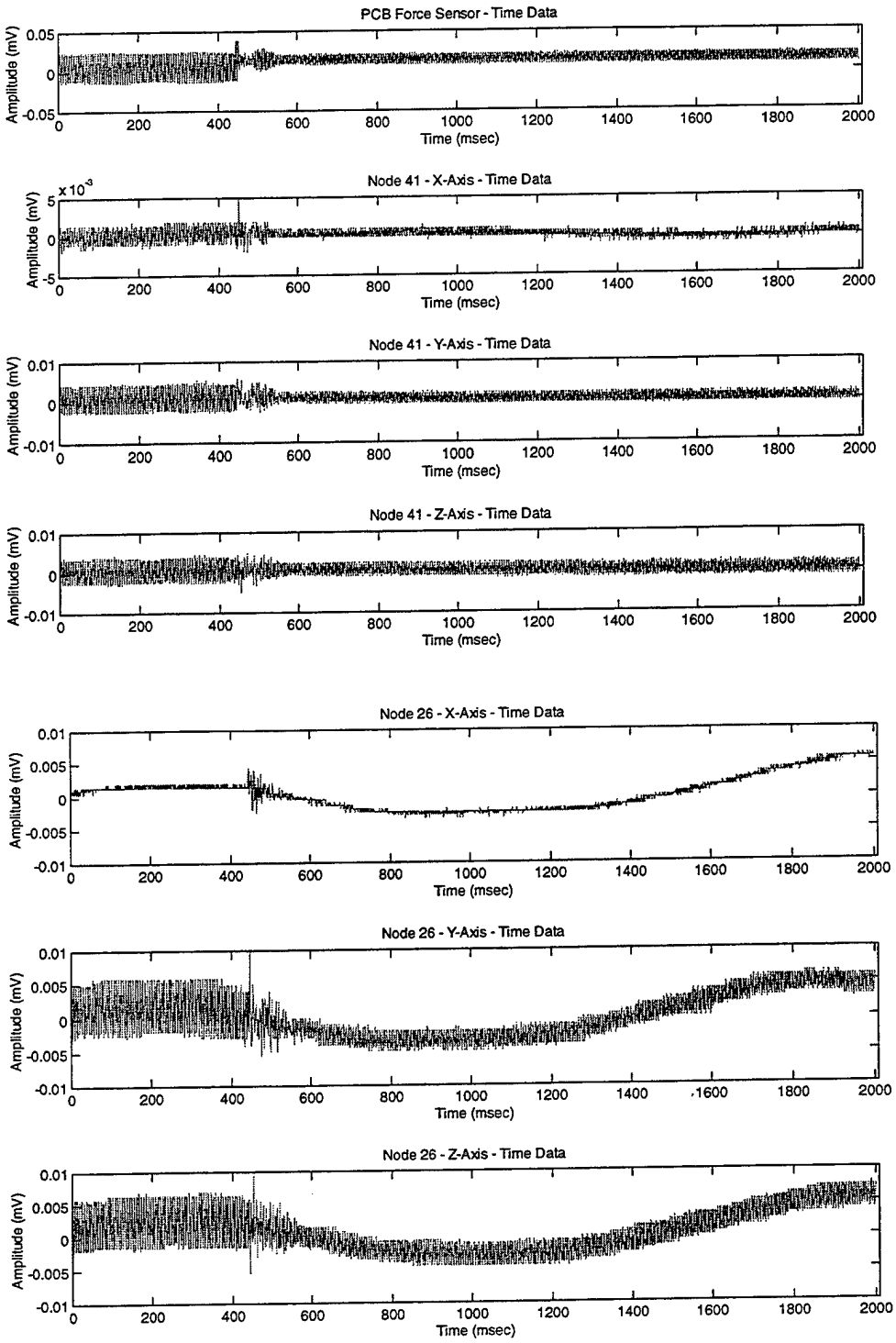

Figure 81. Active Control Testing – Trial 11 – Node 26 and 41 Response

Trial Number: 12

Gain Parameters:

Iigain = 300

Igain = 100

System Gain = 1.75

Targeted Frequency = 17.25

Power Reduction (dB) = 6.6519

Notes:

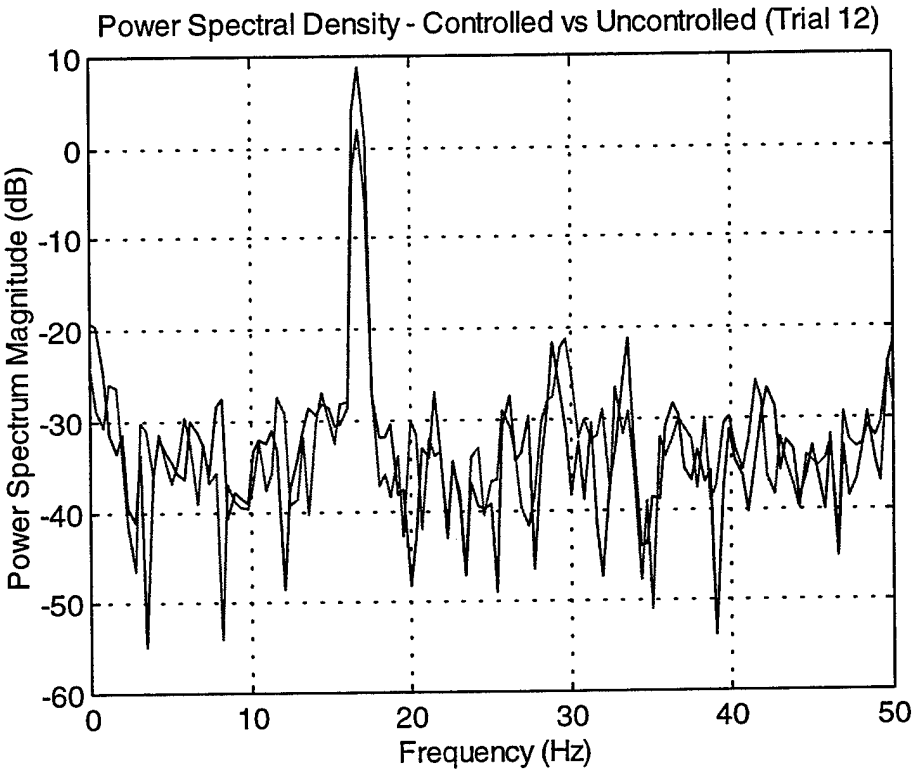

Figure 82. Active Control Testing – Trial 12 – Power Spectral Density

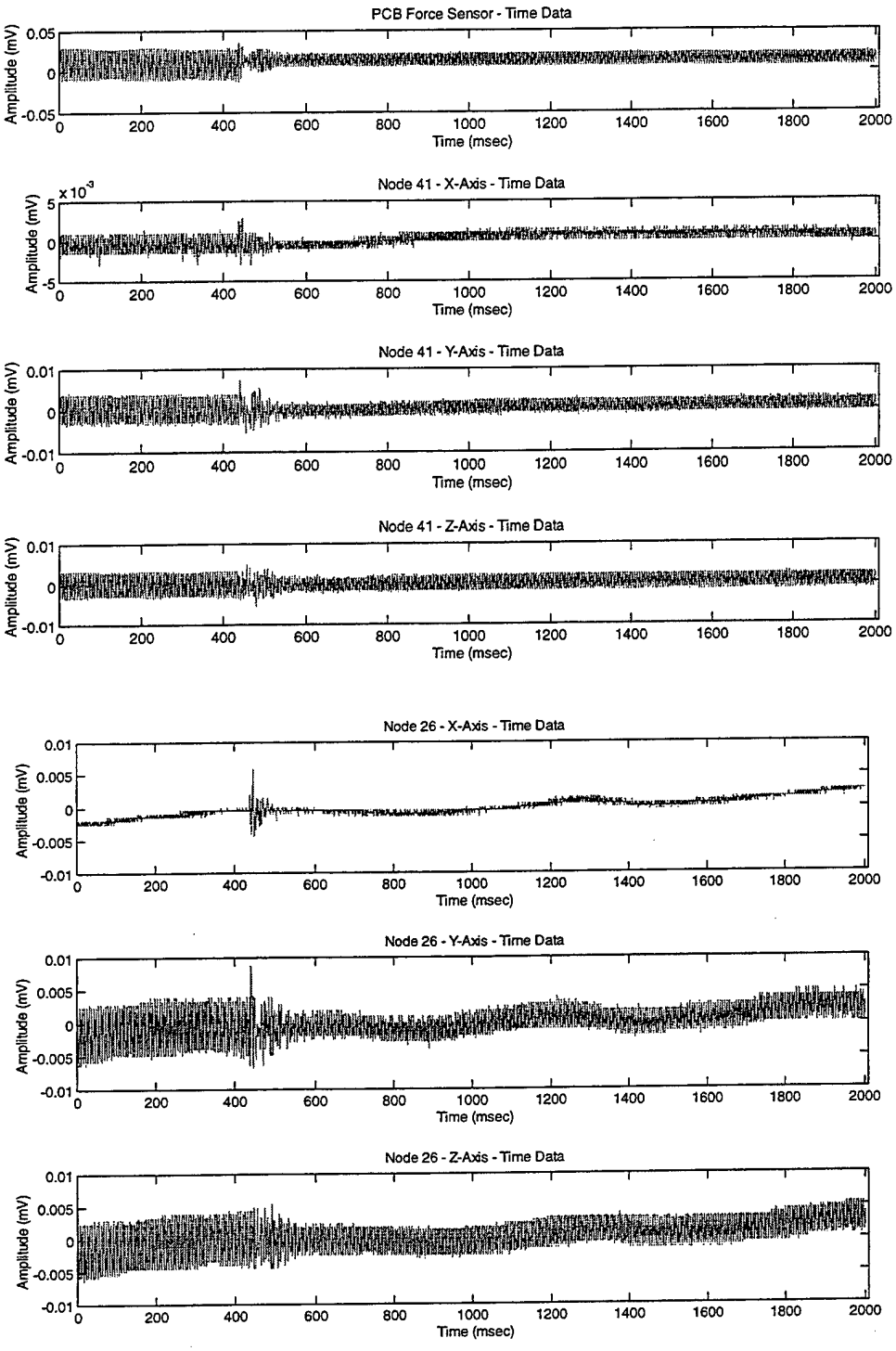

Figure 83. Active Control Testing – Trial 12 – Node 26 and 41 Response

Trial Number: 13

Gain Parameters:

Iigain = 300

Igain = 100

System Gain = 1.75

Targeted Frequency = 17.5

Power Reduction (dB) = 5.1781

Notes:

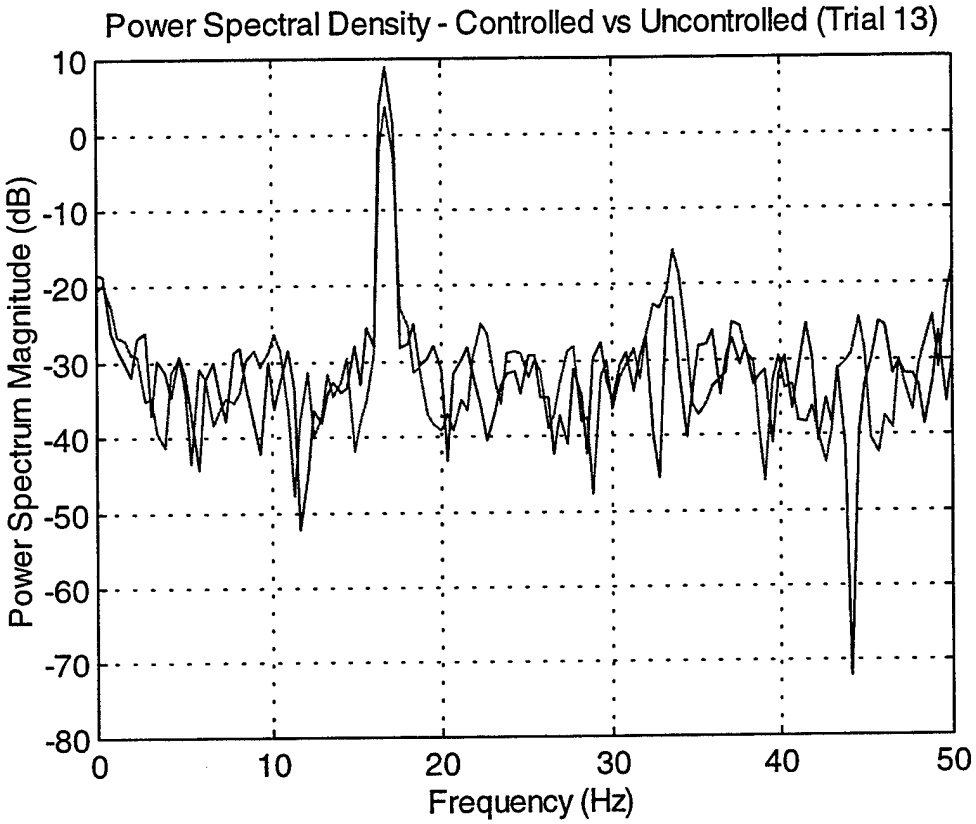

Figure 84. Active Control Testing – Trial 13 – Power Spectral Density

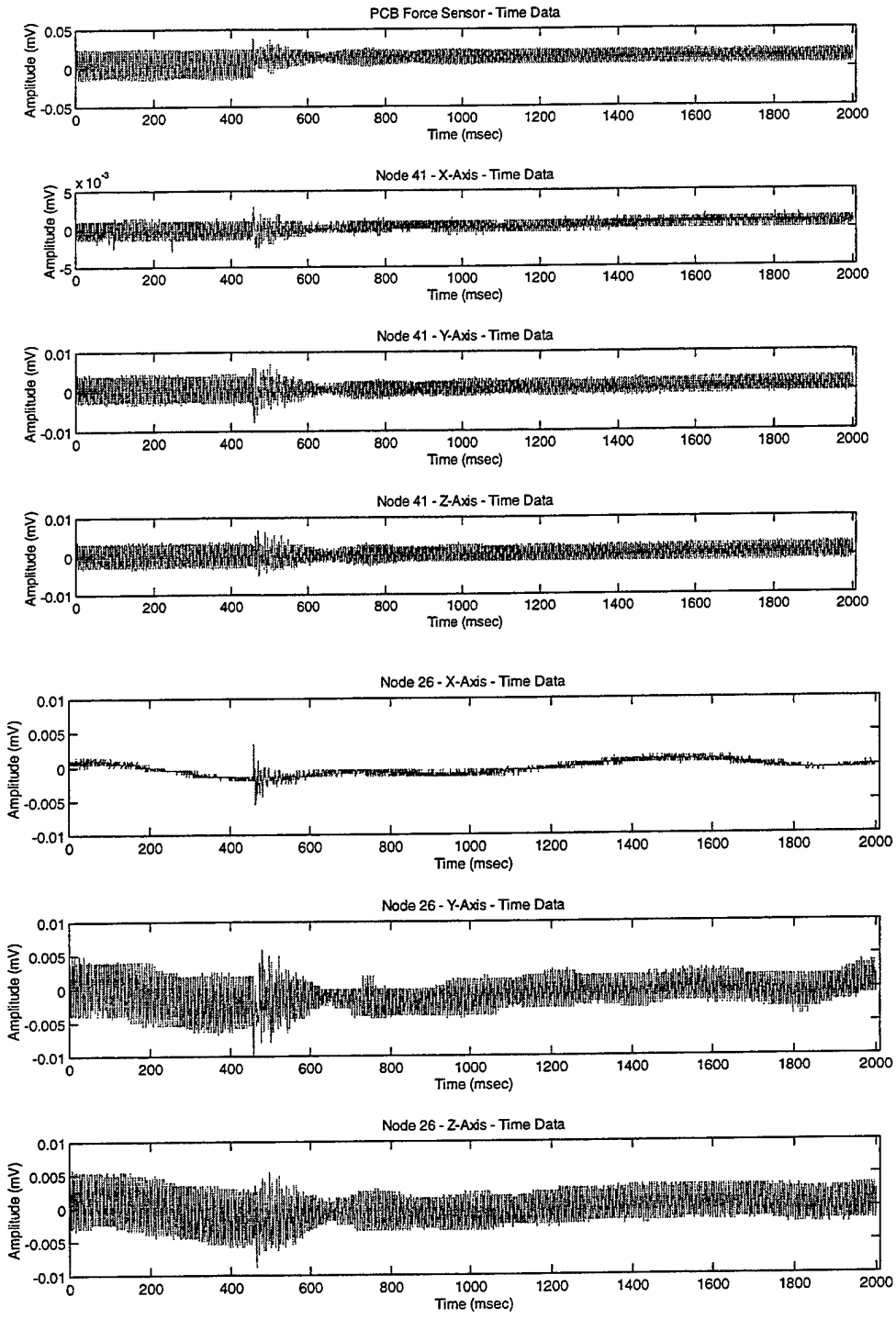

Figure 85. Active Control Testing – Trial 13 – Node 26 and 41 Response

Trial Number: 14

Gain Parameters:

Iigain = 300

Igain = 100

System Gain = 1.75

Targeted Frequency = 16.5

Power Reduction (dB) = 12.2648

Notes:

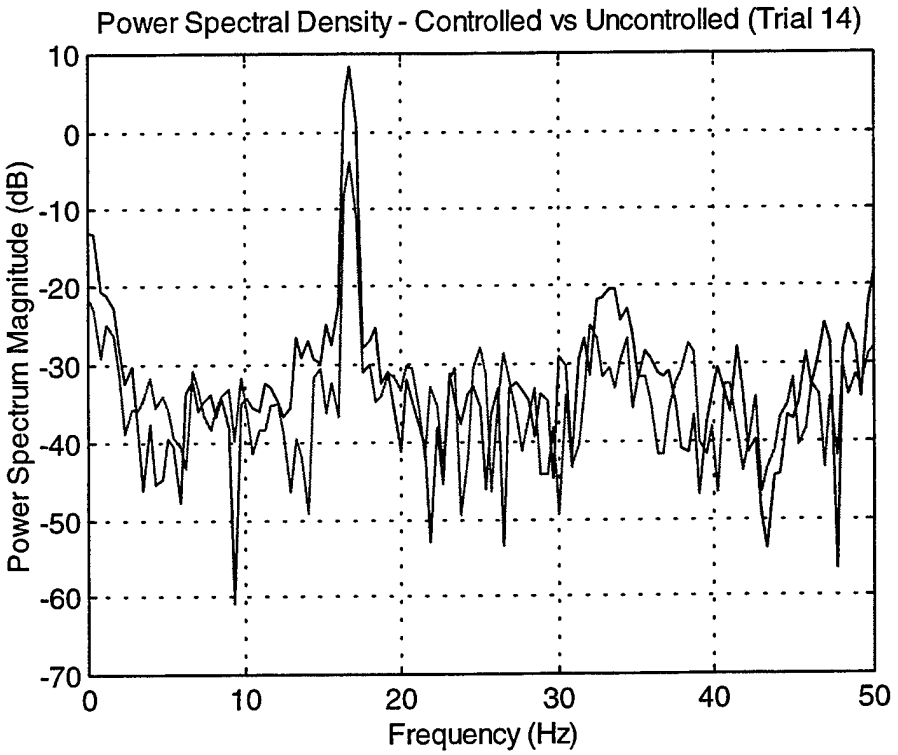

Figure 86. Active Control Testing – Trial 14 – Power Spectral Density

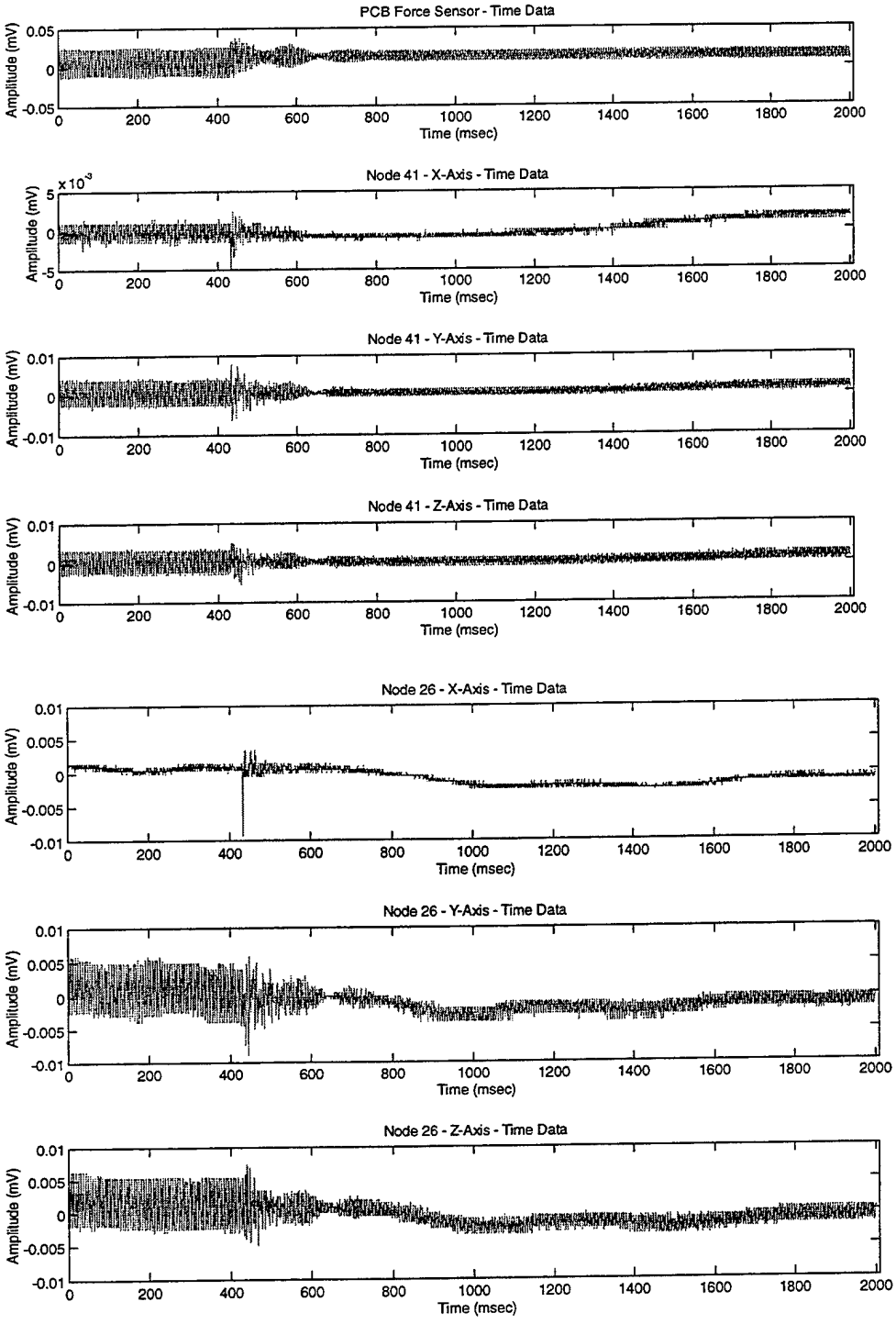

Figure 87. Active Control Testing – Trial 14 – Node 26 and 41 Response

Trial Number: 15

Gain Parameters:

Iigain = 300

Igain = 100

System Gain = 1.75

Targeted Frequency = 16.25

Power Reduction (dB) = 7.0241

Notes:

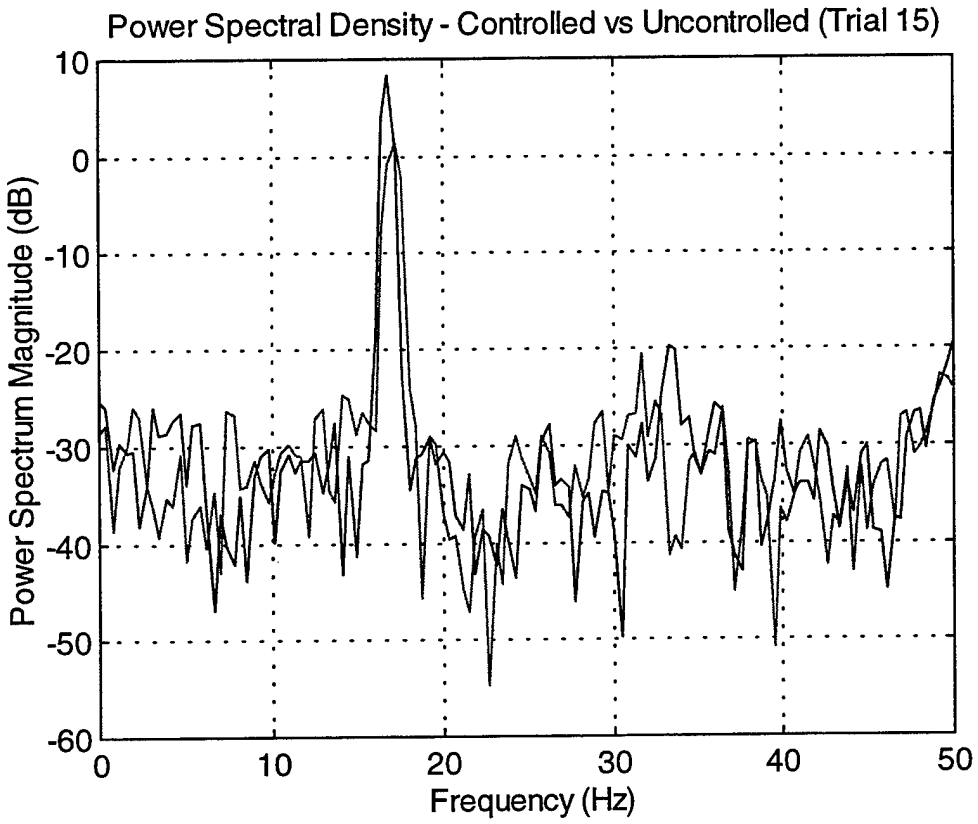

Figure 88. Active Control Testing – Trial 15 – Power Spectral Density

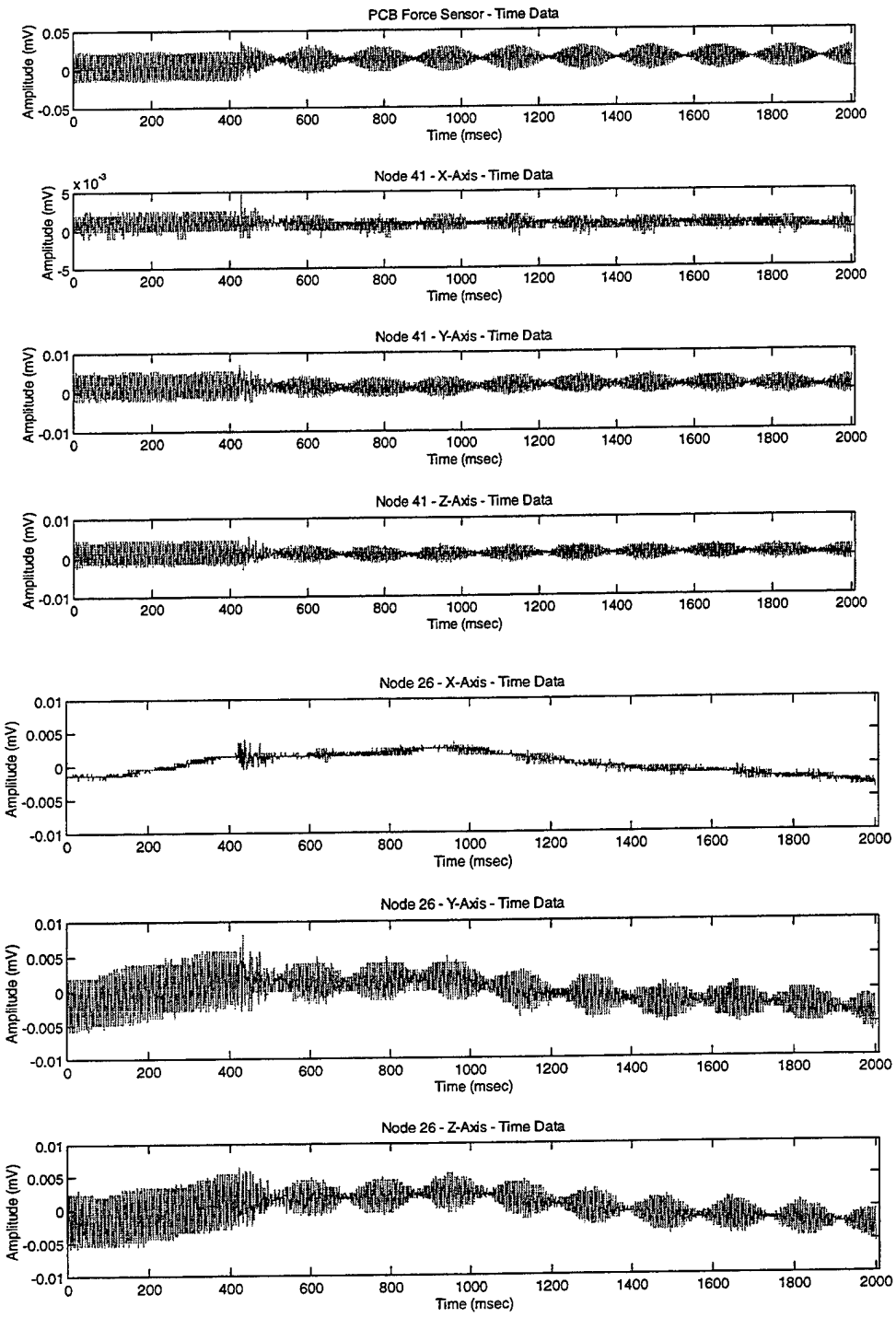

Figure 89. Active Control Testing – Trial 15 – Node 26 and 41 Response

Trial Number: 16

Gain Parameters:

Iigain = 300

Igain = 100

System Gain = 1.75

Targeted Frequency = 16.0

Power Reduction (dB) = 0

Notes:

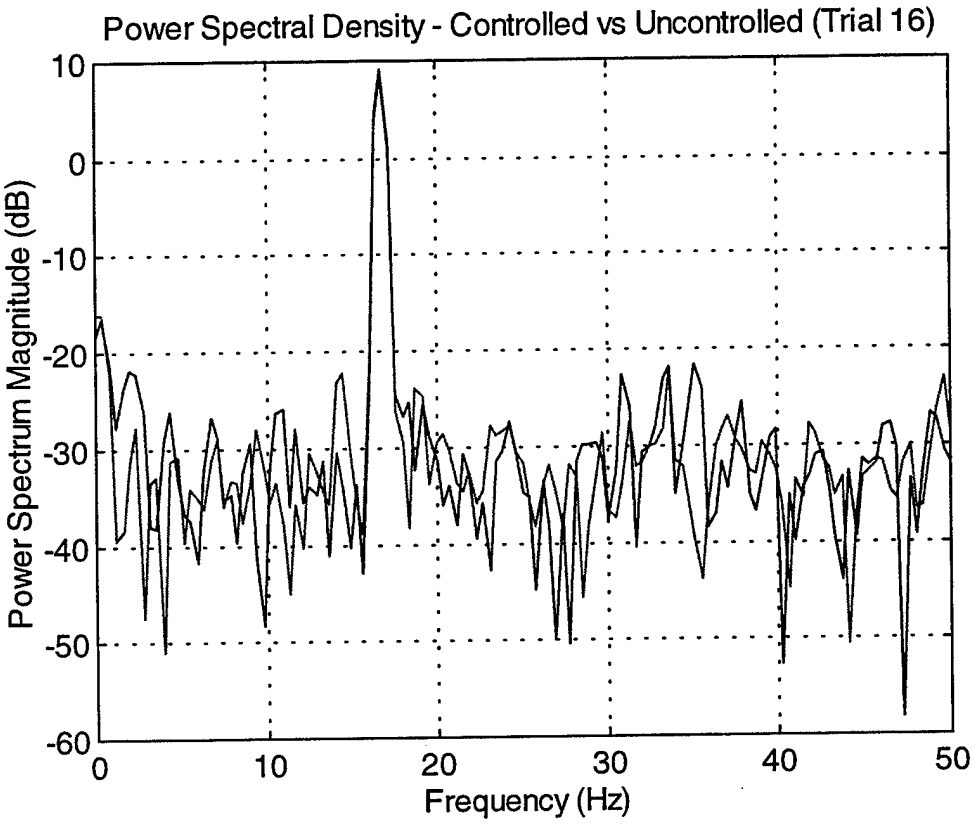

Figure 90. Active Control Testing – Trial 16 – Power Spectral Density

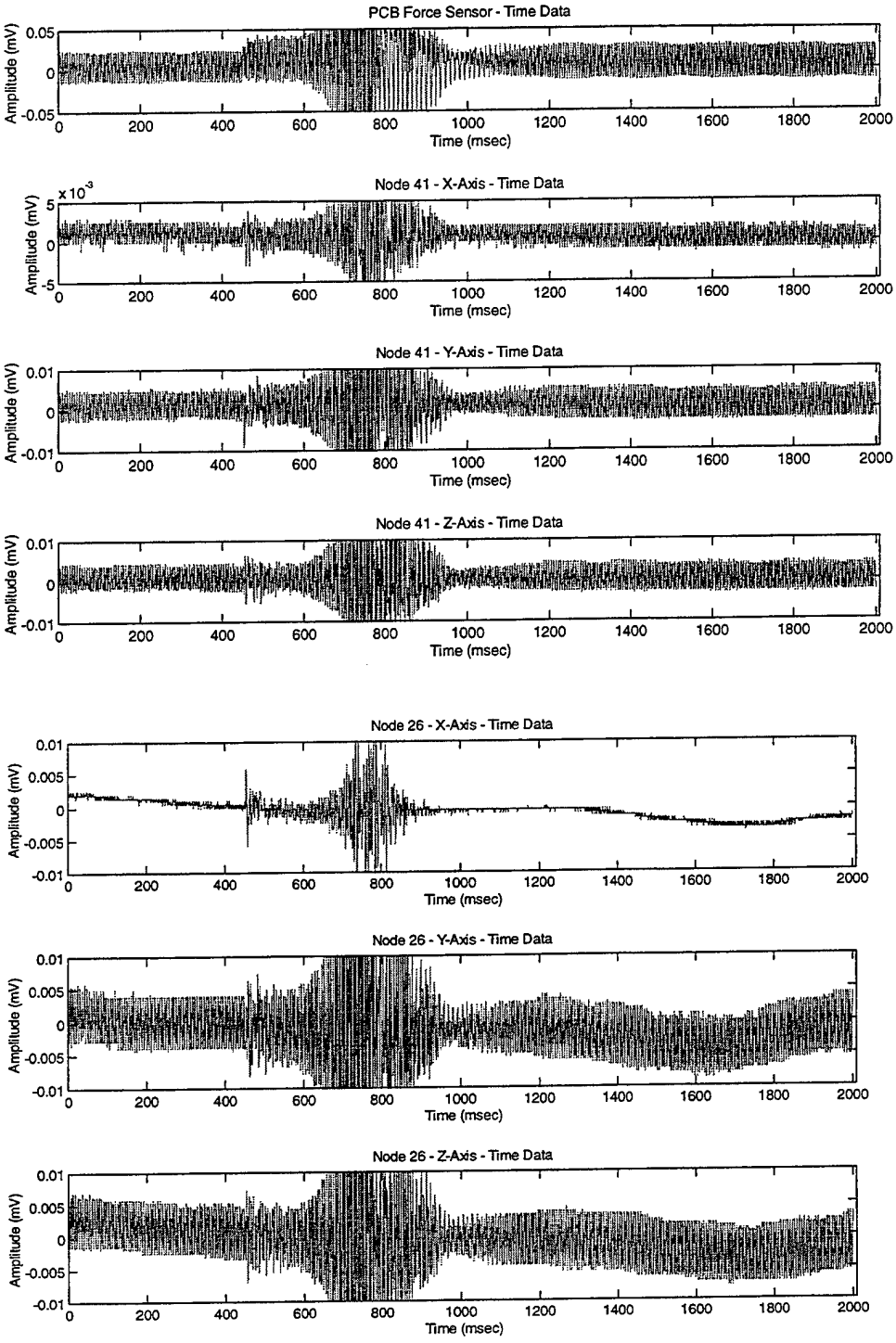

Figure 91. Active Control Testing – Trial 16 – Node 26 and 41 Response

Trial Number: 17

Gain Parameters:

Iigain = 300

Igain = 100

System Gain = 1.75

Targeted Frequency = 16.65

Power Reduction (dB) = 12.5126

Notes:

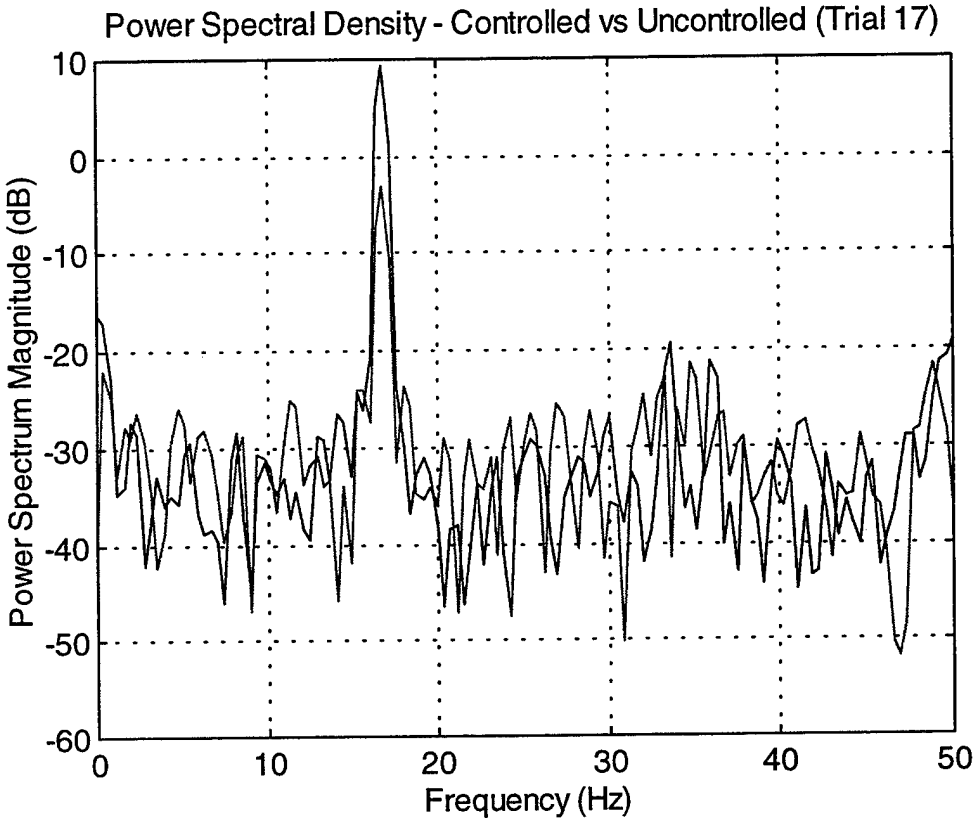

Figure 92. Active Control Testing – Trial 17 – Power Spectral Density

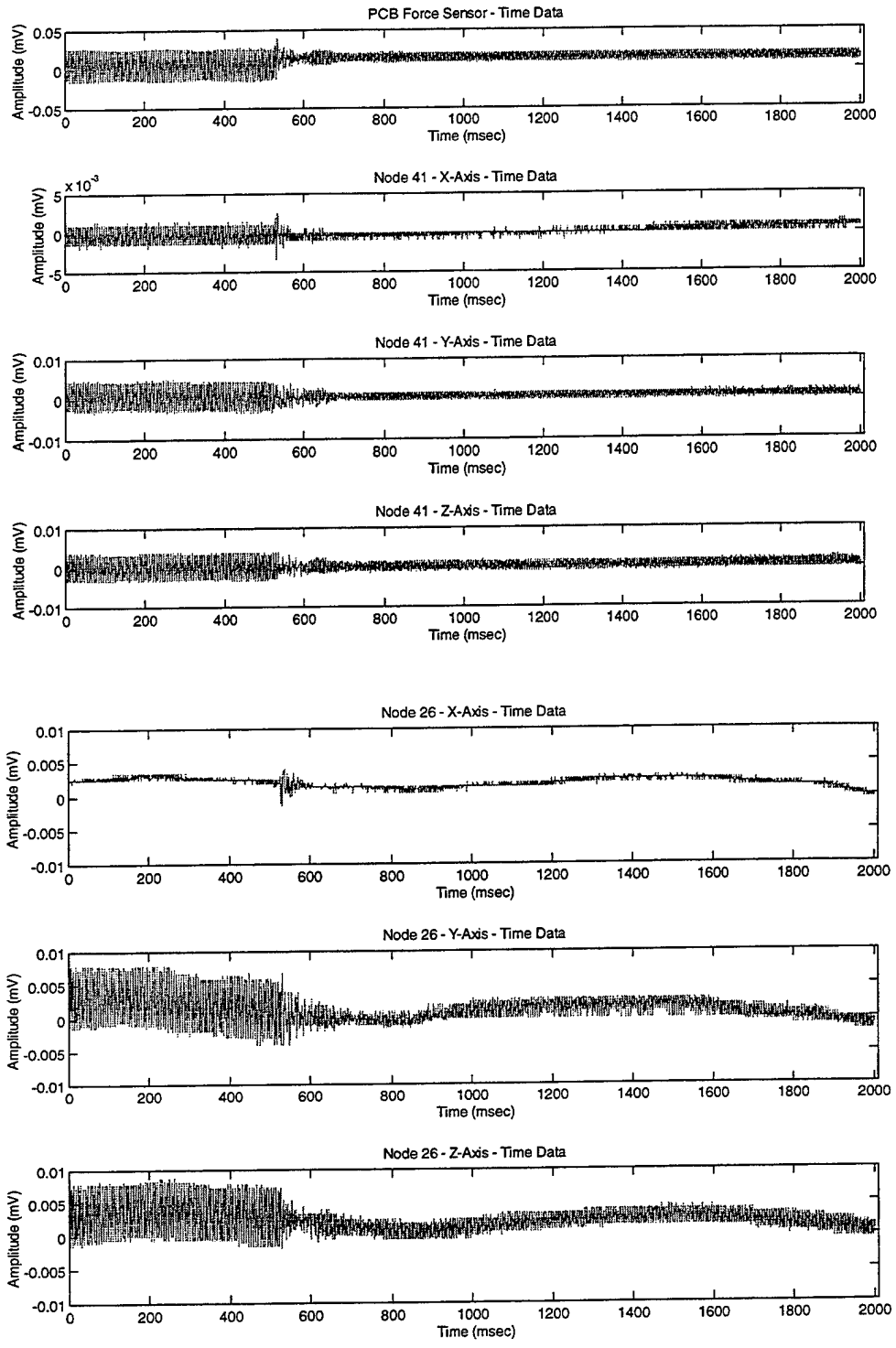

Figure 93. Active Control Testing – Trial 17 – Node 26 and 41 Response

Trial Number: 18

Gain Parameters:

Iigain = 300

Igain = 100

System Gain = 1.75

Targeted Frequency = 16.85

Power Reduction (dB) = 12.766

Notes:

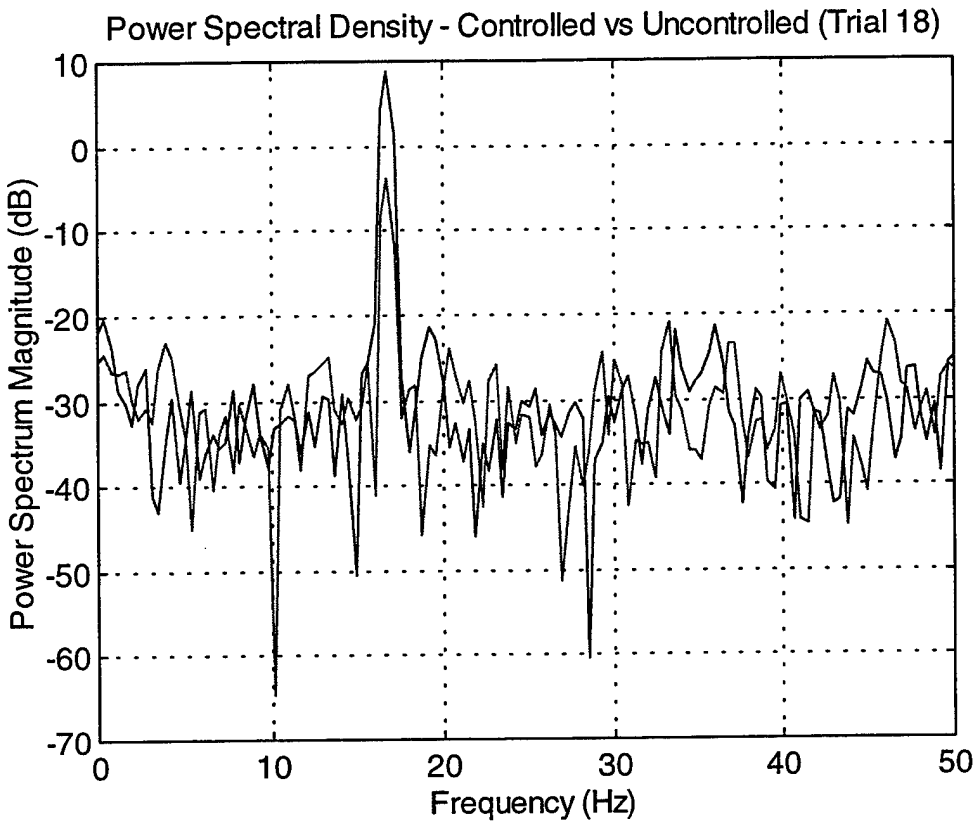

Figure 94. Active Control Testing – Trial 18 – Power Spectral Density

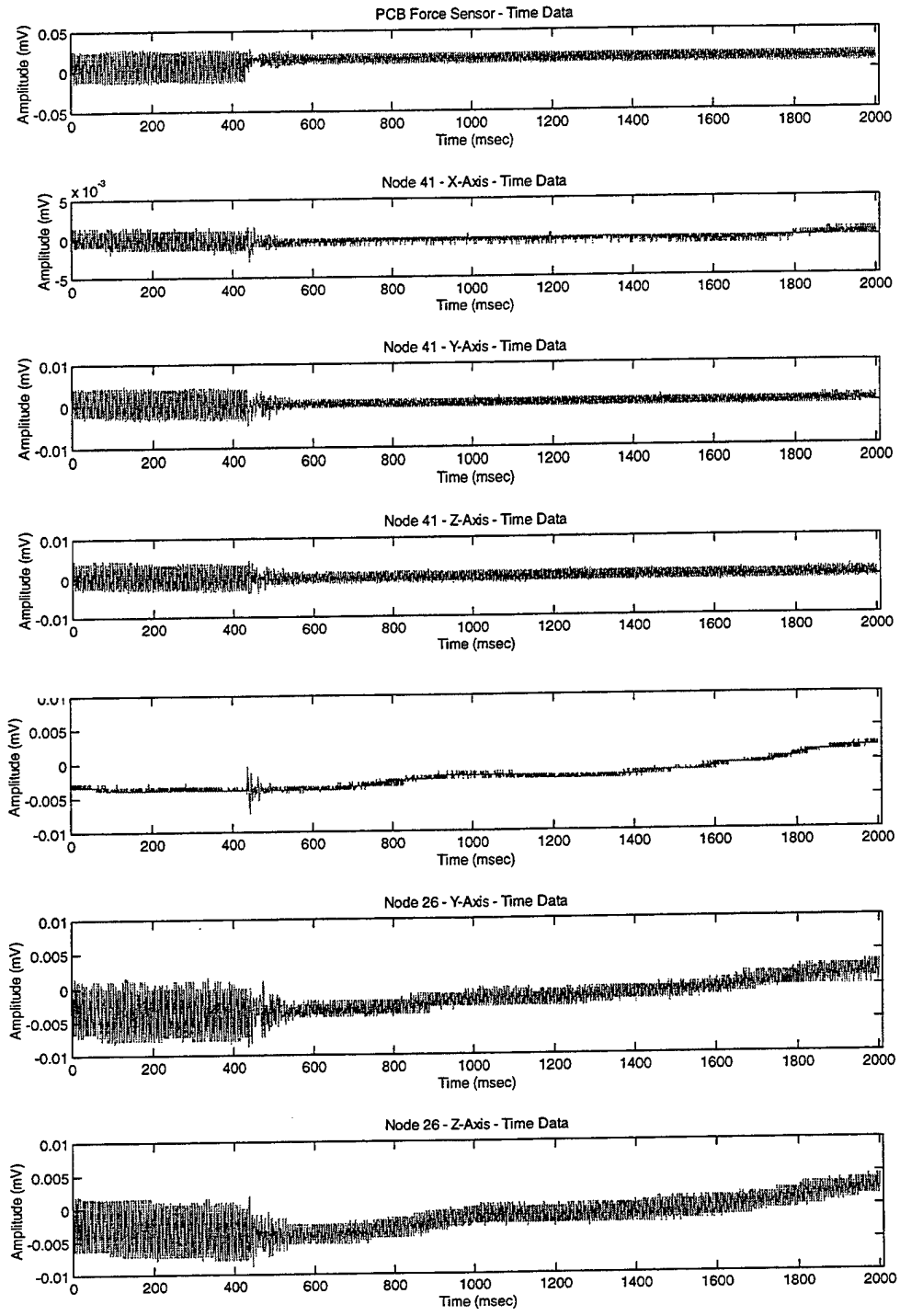

Figure 95. Active Control Testing – Trial 18 – Node 26 and 41 Response

APPENDIX N. GRAPH.M – MATLAB ANALYSIS CODE

```
%  GRAPH.M - MATLAB Analysis Code
%  Analysis of Active Control Data  - Continuous Response
%  Plots Data In The Designated Vector.

%  Written by LT John Vlattas and LT Scott E. Johnson
%  Last Modified: 10 May 1998

clear all
load trial18                    % Loads Specific Case


%     Takes all data that is in the dSPACE collection vector and
seperates it out into individual
%     vectors.


for n = 1:16
      eval(['Y' num2str(n) ' = trace_y(n,:);']);  % Seperates Data

%  Plots the output of the Chebychev Filters and Output response of the
%  Controller on the first plot.
      if n < 4
            figure(1)
            subplot(3,1,n)
                  if n == 1
                        plot(eval(['Y' num2str(n)]))
                        title('Chebychev Type BP Filter - Time Data')
                        xlabel('Time (msec)')
                        ylabel('Amplitude (mV)')
                        axis([0 2010 -.05 .05])
                  elseif n == 2
                        plot(eval(['Y' num2str(n)]))
                        title('Chebychev Type BP Filter1 - Time Data')
                        xlabel('Time (msec)')
                        ylabel('Amplitude (mV)')
                        axis([0 2010 -1e-5 1e-5])
                  elseif n == 3
                        plot(eval(['Y' num2str(n)]))
                        title('Output of Controller - Time Data')
                        xlabel('Time (msec)')
                        ylabel('Amplitude (mV)')
                        axis([0 2010 0 3e-5])
                  end
            orient tall
      elseif n < 8
            figure(2)
            subplot(4,1,(n-3))
                  if n == 4
                        plot(eval(['Y' num2str(n)]),'m')
                        title('PCB Force Sensor - Time Data')
                        xlabel('Time (msec)')
                        ylabel('Amplitude (mV)')
                        axis([0 2010 -.05 .05])
```

```
            elseif n == 5
                  plot(eval(['Y' num2str(n)]),'m')
                  title('Node 41 - X-Axis - Time Data')
                  xlabel('Time (msec)')
                  ylabel('Amplitude (mV)')
                  axis([0 2010 -.005 .005])
            elseif n == 6
                  plot(eval(['Y' num2str(n)]),'m')
                  title('Node 41 - Y-Axis - Time Data')
                  xlabel('Time (msec)')
                  ylabel('Amplitude (mV)')
                  axis([0 2010 -.01 .01])
            elseif n == 7
                  plot(eval(['Y' num2str(n)]),'m')
                  title('Node 41 - Z-Axis - Time Data')
                  xlabel('Time (msec)')
                  ylabel('Amplitude (mV)')
                  axis([0 2010 -.01 .01])
            end
      orient tall
elseif n < 11
      figure(3)
      subplot(3,1,(n-7))
            if n == 8
                  plot(eval(['Y' num2str(n)]),'m')
                  title('Node 18 - X-Axis - Time Data')
                  xlabel('Time (msec)')
                  ylabel('Amplitude (mV)')
                  axis([0 2010 -.01 .01])
            elseif n == 9
                  plot(eval(['Y' num2str(n)]),'m')
                  title('Node 18 - Y-Axis - Time Data')
                  xlabel('Time (msec)')
                  ylabel('Amplitude (mV)')
                  axis([0 2010 -.01 .01])
            elseif n == 10
                  plot(eval(['Y' num2str(n)]),'m')
                  title('Node 18 - Z-Axis - Time Data')
                  xlabel('Time (msec)')
                  ylabel('Amplitude (mV)')
                  axis([0 2010 -.01 .01])
            end
      orient tall
elseif n < 14
      figure(4)
      subplot(3,1,(n-10))
            if n == 11
                  plot(eval(['Y' num2str(n)]),'m')
                  title('Node 49 - X-Axis - Time Data')
                  xlabel('Time (msec)')
                  ylabel('Amplitude (mV)')
                  axis([0 2010 -.01 .01])
            elseif n == 12
                  plot(eval(['Y' num2str(n)]),'m')
                  title('Node 49 - Y-Axis - Time Data')
                  xlabel('Time (msec)')
                  ylabel('Amplitude (mV)')
```

```
                        axis([0 2010 -.01 .01])
                  elseif n == 13
                        plot(eval(['Y' num2str(n)]),'m')
                        title('Node 49 - Z-Axis - Time Data')
                        xlabel('Time (msec)')
                        ylabel('Amplitude (mV)')
                        axis([0 2010 -.01 .01])
                  end
            orient tall
      elseif n < 17
            figure(5)
            subplot(3,1,(n-13))
                  if n == 14
                        plot(eval(['Y' num2str(n)]),'m')
                        title('Node 26 - X-Axis - Time Data')
                        xlabel('Time (msec)')
                        ylabel('Amplitude (mV)')
                        axis([0 2010 -.01 .01])
                  elseif n == 15
                        plot(eval(['Y' num2str(n)]),'m')
                        title('Node 26 - Y-Axis - Time Data')
                        xlabel('Time (msec)')
                        ylabel('Amplitude (mV)')
                        axis([0 2010 -.01 .01])
                  elseif n == 16
                        plot(eval(['Y' num2str(n)]),'m')
                        title('Node 26 - Z-Axis - Time Data')
                        xlabel('Time (msec)')
                        ylabel('Amplitude (mV)')
                        axis([0 2010 -.01 .01])
                  end
            orient tall
      end
end
end

load trial9
for n = 1:16
      eval(['M' num2str(n) ' = trace_y(n,:);']);                    %
Seperates Data
      if n > 13
            figure(6)
            subplot(3,1,(n-13))
                  if n == 14
                        plot(eval(['M' num2str(n)]),'m')
                        title('Node 26 - X-Axis - Time Data')
                        xlabel('Time (msec)')
                        ylabel('Amplitude (mV)')
                        axis([0 2010 -.01 .01])
                  elseif n == 15
                        plot(eval(['M' num2str(n)]),'m')
                        title('Node 26 - Y-Axis - Time Data')
                        xlabel('Time (msec)')
                        ylabel('Amplitude (mV)')
                        axis([0 2010 -.01 .01])
                  elseif n == 16
                        plot(eval(['M' num2str(n)]),'m')
```

```
                        title('Node 26 - Z-Axis - Time Data')
                        xlabel('Time (msec)')
                        ylabel('Amplitude (mV)')
                        axis([0 2010 -.01 .01])
                    end
                orient tall
        else
        end
end

[Pxx1,F1] = psd(Y15,512,100);
[Pxx2,F2] = psd(Y15,512,100);
```

APPENDIX O. PSDPLOT.M - MATLAB ANALYSIS CODE

```
%  PSDPLOT.M - MATLAB Analysis Code
%  Analysis of Active Control Data  - Continuous Response
%  Plots Power Spectral Density of Data In The Designated Vectors.
%  Compares the Controlled Versus Uncontrolled Data for Each Trial
%  and Computes the dB Reduction Due to Control.

%  Written by LT John Vlattas and LT Scott E. Johnson
%  Last Modified: 15 May 1998

clear all
load trial1                                              % Loads Data
Uncontrolled Case

for n = 1:16
      eval(['Y' num2str(n) ' = trace_y(n,:);']);         % Seperates Data
end

load trial3                                              % Loads Data Trial
for n = 1:16
      eval(['M' num2str(n) ' = trace_y(n,:);']);         % Seperates Data
end


%  Takes Power Spectral Density of Given Vectors For Comparison

[Pxx1,F1] = psd(100*Y15(:,1500:2000),256,100);
[Pxx2,F2] = psd(100*M15(:,1500:2000),256,100);
[Pxx3,F3] = psd(100*M15(:,1:500),256,100);

%  Finds Maximum Value of the Power Spectral Density For Trial In
Question
u = max(10*log10(Pxx3));
c = max(10*log10(Pxx2));
diff = u - c                                             % dB reduction due
to control


%  Comparison to Max dB Reduction for Trials 11 - 18
MaxdB = 11.3974;
P = 100 - ((diff/MaxdB) * 100)                           % Percentage
Difference from Max

figure(7)
% plot(F1,10*log(Pxx1),'r',F2,20*log(Pxx2),'g',F3,20*log(Pxx3),'y')
plot(F2,10*log10(Pxx2),'r',F3,10*log10(Pxx3),'b')
grid
title('Power Spectral Density - Controlled vs Uncontrolled (Trial 3)')
ylabel('Power Spectrum Magnitude (dB)')
xlabel('Frequency (Hz)')
```

APPENDIX P. ACTIVE.M – MATLAB ANALYSIS CODE

```
% ACTIVE.M - MATLAB Analysis Code
% This MATLAB takes the frequency response data of the active controller and derives the
% the state-space representation of the system using the Eigensystem Realization Algorithm.
% The ERA, derived from Reference 25 has been converted into MATLAB code for the user.


% Written by LT John Vlattas and LT Scott Johnson
% Last Revised: 18 May 1998

load frf3i.dat                  % Loads frequency response data of interest


% Next command generates a matrix of size 2048 since HP aliasing eliminates points.
% We add zeros for the missing data and then reflect the remainder of the data to make
% it symmetric for the IFFT command

o2i1b = [o2i1(1:801);zeros(446,1);flipud(conj([o2i1(1:801)]))];

size(o2i1b)                     % Verifies size of matrix too ensure 2048 pts.

imp = ifft(o2i1b)               % IFFT generates complex time response data

figure(1)                               % Plot of the impulse response for evaluation
plot([1/512:1/512:2048/512],real(imp))  % Time Increment = .002 sec, Duration = 4 sec
grid
title('Impulse Response')
ylabel('Magnitude')
xlabel('Time (s)')

% Take real parts of the impulse response to define the Markov parameters and generate the
% reduced hankel matrix. 200 points are selected by evaluating Figure (1) to see up to where there
% is data. This is an arbitrary number developed through some trial and error

impr = real(imp)
y = hankel(impr(1:120), impr(120:199));   % Reduced Hankel matrix
[u,s,v] = svd(y);                         % Singular Value Decomp of hankel matrix

% u =  observability matrix
% v = controllability matrix
% s = singular values

figure(2)                       % Plot of singular values to determine "significant' modes
plot(diag(s))
semilogy(diag (s))
plot(diag(s),'*')
grid
title('Singular Values')
xlabel('Number')
```

```
ylabel('Magnitude')

% Solving for the system matrix A

a = pinv(u(1:119,1:30))*u(2:120,1:30);

ev = eig(a)                                   % Eigenvalues of the State Matrix

% Call function eig_fr to find Natural Frequencies and Damping Ratios of  A
% See eig_fr Code

[fre,dam] = eig_fr(ev, 1/512)

% Use observability and controllability matrices to construct state space representation of
% Sensor Actuator system

b=v(1,1:30)';
c=u(1,1:30);
d=impr(1:1);                                  % Initial Value = First Value of Impulse Response

sys = ss(a,b,c,d,1/512);                      % sys = state space representation

% Now use functions from the control systems toolbox (i.e pzmap and rlocus)
```

APPENDIX Q. IMPORTANT POINTS OF CONTACT

The follow points of contact are worth listing as they are able to provide valuable support in regards to the purchase, operation, and maintenance of the NPS Space Truss and test equipment.

Name	Association	Phone Number
Albert Bosse, Ph.D.	Naval Research Lab	(202) 404 2724 (lab) (202) 404 8341 (office) (202) 767 9339 (FAX)
Fred Tasker, Ph.D.	Naval Research Lab	(202) 404 2721
David Steinberg	Physik Instrumente	(714) 850 1835 (office)
Scott Greely	Planning System Inc.	(407) 768 6500 (office)
Paul Smith	Gould Instrumentation	(216) 328 7000 (office)
James Borkowski	Kistler Instrument Corp.	(716) 691 5100 (office)

INITIAL DISTRIBUTION LIST

1. Defense Technical Information Center..... 2
   8725 John J. Kingman Rd., STE 0944
   Ft. Belvoir, Virginia 22060-6218

2. Dudley Knox Library..... 2
   Naval Postgraduate School
   411 Dyer Rd.
   Monterey, California 93943-5101

3. Professor Lindsey, Chairman,Code AA..... 1
   Department of Aeronautics and Astronautics
   Naval Postgraduate School
   Monterey, California 93943

4. Professor Brij N. Agrawal, Code AA/Ag 2
   Department of Aeronautics and Astronautics
   Naval Postgraduate School
   Monterey, California 93943

5. Dr. Gangbing Song, Code AA/Sb.....2
   Department of Aeronautics and Astronautics
   Naval Postgraduate School
   Monterey, California 93943

6. Space Design Research Center..... 2
   Department of Aeronautics and Astronautics
   Naval Postgraduate School
   Monterey, California 93943

7. LT Scott Johnson.....2
1809 Parkview Drive
Friendswood, TX 77546

8. LT John Vlattas.....2
131 Butler Pkwy
Summit, New Jersey 07901